Optimality of Electroless Plating Processes for Dense Metal Ceramic Composite Membrane Fabrication

Thesis submitted in partial fulfillment of the requirements for the degree of

DOCTOR OF PHILOSOPHY

by

Amrita Agarwal

Department of Chemical Engineering

Indian Institute of Technology, Guwahati

Guwahati - 781039, India

OPTIMALITY OF ELECTROLESS PLATING PROCESSES FOR DENSE METAL CERAMIC COMPOSITE MEMBRANE FABRICATION

Amrita Agarwal

Optimality of Electroless Plating Processes for Dense Metal Ceramic Composite Membrane Fabrication

Thesis submitted in partial fulfillment of the

requirements for the degree of

DOCTOR OF PHILOSOPHY

by

Amrita Agarwal
Roll No.: 10610717

Department of Chemical Engineering

Indian Institute of Technology Guwahati

Guwahati - 781039, India

July, 2014

Dedicated to

my grandparents, parents, family, supervisors & friends

for whom I have become what I am today.

Department of Chemical Engineering
Indian Institute of Technology Guwahati
Guwahati - 781039, India

CERTIFICATE

This is to certify that the thesis entitled **"Optimality of Electroless Plating Processes for Dense Metal Ceramic Composite Membrane Fabrication"** being submitted by ***Amrita Agarwal*** for the award of PhD degree has been carried out under our guidance and supervision. The work documented in this thesis has not been submitted to any other University or Institute for the award of any degree or diploma.

(Dr. Ramgopal V. S. Uppaluri)
Professor
Department of Chemical Engineering
Indian Institute of Technology Guwahati
Guwahati - 781039, India.

(Dr. Anil Verma)
Associate Professor
Department of Chemical Engineering,
Indian Institute of Technology Guwahati
Guwahati - 781039, India.

Acknowledgements

I would like to express my gratitude to all those who in different ways helped me in completing this research work within the time span of four years directly or indirectly. Foremost, I would like to express my gratitude to my supervisors, **Prof. Ramgopal V. S. Uppaluri** and **Dr. Anil Verma**, for providing me continuous inspiration and guidance throughout the entire course of work. I am indebted to both of them for their useful suggestions and constant encouragement throughout the entire period.

I am grateful to **Dr. Ramgopal V. S. Uppaluri** for his continuous support, interesting discussions and giving me freedom in choosing how to approach different issues. I appreciate very much his expertise in analyzing the experimental data points to model them suitably. His uncompromising approach to complete the experimental, data analysis, writing manuscripts as well as thesis within stipulated time period helped me a lot in completing my research work in this much shorter span of time. The numerous brain storming sessions during the project meetings with him were very useful in enriching my analytical power. It has been an amazing experience working with Prof. Uppaluri, which will help me a lot in my future life to complete work within stipulated time without compromising upon the quality of work.

I would like to express my sincere gratitude to **Dr. Anil Verma** for his meticulous research planning to get an idea on how to perform the research work. I appreciate very much his flexibility and openness in dealing with the specific and general needs of this research work. He taught me how to write and improve the quality of a journal paper and the thesis. I thank him for his patience and amicable nature. It has been a great privilege to work with him.

I must also thank my doctoral committee members **Dr. Vimal Katiyar, Dr. Nanda Kishore** Department of Chemical Engineering, **Dr. Mohd. Qureshi,** Chemistry Department for their valuable suggestions and contributions towards my research work.

I must also thank the faculty members of the Department of Chemical Engineering for their kind cooperation during my stay in the department. I am also thankful to all present and ex-staff

members and scientific officers of the Chemical Engineering Department for their genuine help during my entire research period.

I am thankful to the **Central Instruments Facility** of IIT Guwahati for allowing me to carry out **Field Emission Scanning Electron Microscopy** analysis on my own**,** which has been very important in this research work. In this regard, I should acknowledge **Mr. Madhurjya Borah** the Junior Technical Superintendent, Central Instruments Facility, IIT Guwahati. He taught me how to use the FESEM instruments, and take images at various critical conditions of the sample. Special thanks to **Dibjyoti Saloi** who worked as project assistant and helped me in fabrication of my supports.

I was fortunate enough to get excellent mates like **Sri Harsha Emami, Murali Pujari, China Malakondaiah Kaniganti, Yennam Rajesh, Bandi Chandra Sekhar, Ruhit Jyoti Konwar, Richa Sharma, Chitrita Kundu** for their friendly support and timely assistance whenever needed. I am also thankful to my senior research scholar, **Dr. Aparajita Goswami** for her help and co-operation in my research work.

Most of all, I would like to express my deepest sense of gratitude to all my family members, my parents. Their love, care, sacrifices and encouragement have made it possible for me to come so far. I appreciate the courage, understanding and dedicated support shown by all of them despite many testing times at their end.

Amrita Agarwal

Abstract

Dense metal ceramic composite membranes such as nickel-ceramic and palladium-ceramic membranes have several functional applications including media for XRD studies, separation of dust particles from gaseous streams, hydrogen separation, membrane reformers, insitu hydrogen production etc. Typically, dense Pd-ceramic and nickel-ceramic composite membranes are fabricated with magnetron sputtering and electroless plating techniques respectively. Considering the issues of scalability and process simplicity, electroless plating can be considered to be the most viable technology for the inexpensive fabrication of dense metal ceramic composite membranes.

Research in the field of metal ceramic composite membrane shall target (a) cheaper and stable porous ceramic supports using inexpensive precursors such as kaolin (b) deployment of electroless plating with optimal combinations of process conditions and operating parameters and (c) supplementing the electroless plating technique with scalable rate enhancement techniques to enhance plating rates without jeopardizing upon the quality of plating.

With process-product optimality as the central research theme, this work addresses a conceptual research methodology that systematically targets the optimality of electroless plating processes for dense Ni-ceramic and Pd-ceramic composite membrane fabrication. Rigorous and extensive experimental investigations have been targeted for the inexpensive nickel precursors to gain substantial insights with respect to the performance characteristics of various electroless plating processes. Finally, with the obtained insights, deploying the optimal choices of the plating processes, dense Pd-ceramic composite membrane fabrication research has been targeted to

achieve low cost dense Pd composite membranes. Throughout the thesis, combinatorial plating characteristics have been considered as suitable benchmarks for the screening and scoping of alternate electroless plating processes. Various combinatorial plating characteristics considered include process (plating and transport efficiency) and membrane (percent pore densification (PPD), metal film thickness and plating rate) variables.

Invariably, during metal-ceramic composite membrane fabrication, the selection of an appropriate ceramic support would often influence the optimality of electroless plating processes. Therefore, early research focused upon the development of inexpensive porous ceramic support using which process optimality could be explored. Firstly, an inexpensive ceramic precursor formulation has been identified to achieve porous ceramic supports possessing lower average pore size of 50 - 70 nm. Using these supports, various electroless plating processes were investigated for nickel ceramic membrane fabrication. These include conventional electroless plating (CEP), surfactant induced electroless plating (SIEP) and sonication induced electroless plating (SOEP). The surface and physical characterization was conducted using LPSA, BET, FTIR, XRD, FESEM and nitrogen permeation techniques. It has been evaluated that prior to nickel electroless plating, sonication of the membrane support in alkaline conditions enormously enhanced corrosion resistance of the support and made it compatible for prolonged nickel ELP. The alkali treated ceramic supports possessed an average pore size of 90 – 120 nm. Among various processes, it was evaluated that SIEP and SOEP processes provided highest plating rates to achieve an average theoretical metal film thickness of 18.3 and 24.6 μm respectively for a total plating time of 24 h. Correspondingly, it was also analyzed that the ratio of percent pore densification (PPD) to metal film thickness (δ) i.e. $\frac{PPD}{\delta}$ varied from 11.2 – 5.35 and 3.5 – 4.7

for SIEP and SOEP baths respectively for a variation in total plating time from 8 - 24 h. Thereby, the preliminary research investigations indicated that SIEP possessed maximum potential towards dense metal ceramic composite membrane fabrication in the context of maximum *PPD* with minimal metal film thickness as compared to CEP and SOEP baths.

Further deliberating upon the process modifications for SIEP baths, the thesis eventually addressed the optimality of precursor concentrations and contacting pattern of the reducing agent to achieve dense Ni-ceramic composite membranes. In these experimental investigations, firstly, the optimality of the reducing agent contacting pattern was studied for an initial Ni solution concentration of 0.08 mol/L and 100% excess hydrazine (reducing agent) concentrations. It was evaluated that for bulk addition of reducing agent, the PPD was 84.5% which increased to 89.3% for drop wise addition strategy of the reducing agent. Eventually, for the identified optimal reducing agent contacting pattern, the optimality of reducing agent concentrations (50 – 200 % excess) was investigated. For a Ni solution concentration of 0.08 mol/L, 100% excess reducing agent concentration was the optimal choice. Finally, the optimality of Ni solution concentration (0.08 – 0.24 mol/L) was investigated for varying reducing agent concentration (50 - 200% excess) with drop wise addition strategy. From all such hierarchical experimental investigations, it was identified that a Ni solution concentration of 0.08 mol/L, 100% excess hydrazine reducing agent concentration with drop wise addition strategy provided optimal combinational plating characteristics. For a variation in total plating time from 4 – 12h, these correspond to a variation in plating efficiency, average plating rate, theoretical metal film thickness and PPD from 53.2 – 47.8%, 11.2 – 5.5 $\times 10^{-5}$ mol/m^2.s, 10.6 – 15.7 μm and 57.4 – 89.3 % respectively.

To further enhance the combinatorial plating characteristics of the electroless plating process, the role of sonication for the optimal fabrication of nickel ceramic composite membranes using

electroless plating was investigated. The combined mode of surfactant and sonication induced electroless plating (SSOEP) was targeted with optimal reducing agent contacting pattern. Further, the optimal surfactant contacting strategy (dropwise and bulk) was also studied. For comparison purpose, SIEP baths were also investigated. Rigorous experimental investigations indicated that the combination of ultrasound (in degas mode), surfactant and reducing agent pattern had a profound influence in altering the combinatorial plating characteristics as compared to SIEP baths. These novel insights consolidate newer research horizons for the role of ultrasound to achieve dense metal ceramic composite membranes in a shorter span of total plating time. For SSOEP baths, with dropwise reducing agent and bulk surfactant, the PPD and metal film thickness values were 73.4% and 8.4μm. Compared to this process, the corresponding values for SSOEP baths with dropwise reducing agent and dropwise surfactant were 66.9 % and 13.3μm respectively. Further, it has also been analyzed that the SSOEP baths provided maximum ratio of percent pore densification per unit metal film thickness $\left(\frac{PPD}{\delta}\right)$ as compared to SIEP baths and thus holds the key for further fine tuning of the associated degrees of freedom. For a variation in total plating time from 2 – 8h, the optimal combinatorial characteristics for SSOEP Ni ELP baths correspond to a variation in plating efficiency, average plating rate, theoretical metal film thickness and PPD from 77.2 - 89.8% , 11- 4.4 × 10^{-5} mol/m^2.s , 5.2 – 8.4 μm and 54.6 -73.4 % respectively.

Further elaborating upon the role of surfactant type, this work also addressed the combinatorial plating characteristics for the fabrication of nickel ceramic composite membranes using SSOEP baths supplemented with drop wise addition of the reducing agent and bulk mode of surfactant addition. The experimental investigations were targeted to evaluate the optimality of solution concentrations of CTAB (cationic) and SDS (anionic) surfactants during SSOEP based Ni ELP.

For a variation in CTAB solution concentration from 1 – 6 CMC and a total plating time of 2 - 8 h, it was evaluated that the pore densification, metal film thickness, plating efficiency varied from 47.6 – 64.4%, 7.6 – 10.8μm, 40.1 – 59.9% respectively. Amongst both surfactants, CTAB (cationic) surfactant with a solution concentration of 4 CMC provided optimal combinations of pore densification (73.4%), metal film thickness (8.4 μm) and plating efficiency (89.9%). These experimental observations confirm upon the larger role of the various degrees of freedom for surfactant and sonication induced electroless plating baths towards metal ceramic composite membrane fabrication.

With identified process, reducing agent and surfactant contacting pattern optimality for Ni ELP baths, the last section of the thesis is dovetailed towards targeting the low cost fabrication of dense palladium-ceramic composite membranes with minimal Pd precursor utilization and total plating time. While SIEP and SSOEP processes are of particular interest for the Pd ELP baths, other processes such as CEP and SOEP have also been considered for comparative assessment purpose. The experimental investigations were also targeted to evaluate the optimality of Pd solution concentrations (0.005 – 0.015 mol/L) for SSOEP baths. Also, this work critically targeted the cost analysis of the fabricated dense Pd ceramic composite membranes with a comparative assessment of the cost of other similar membranes reported in the literature. Amongst all processes, it has been identified that the SSOEP process is the optimal choice to achieve low cost dense Pd-ceramic composite membrane. For the said process, optimal combinatorial plating characteristics correspond to a variation in plating efficiencies, transport efficiencies, plating rates from 95.9 – 60.6%, 41.3-21.7 % and 1.50 – 0.79 x 10^{-4} mol/m^2.s respectively. Optimal parametric choice for SSOEP process are 0.01mol/L Pd solution concentration, 2 CMC CTAB solution concentration, 10.5h total plating time and 99.7% PPD.

Further, the fabricated membrane is highly cost effective (18.75 $/m^2) even on a retail basis i.e. 51.6% cost effective in comparison with dense Pd-alumina composite membrane fabricated with SIEP process; 58.2% cost effective in comparison with dense Pd-alumina membrane fabricated with CEP; 83.8% cost effective in comparison with dense Pd-stainless membrane fabricated with CEP and 70.6% cost effective in comparison with dense Pd-stainless steel composite membrane fabricated with SIEP process. The lowest cost of the fabricated Pd-ceramic composite membrane is due to the simultaneous optimality of process (SSOEP), product (kaolin based ceramic support) and associated process parameters. Based on obtained results, an effort has been carried out finally to compare and contrast Ni and Pd plating baths to provide a conceptual research methodology road map for the systematic targeting of inexpensive dense Pd ceramic composite membrane fabrication by rigorous experimental investigations with Ni ELP baths.

In summary, the Ph.D. thesis summarizes the following research findings from the perspective of novelty and innovation:

a) Identification of low cost inorganic precursor formulation to achieve a compatible porous ceramic support with an average pore size of 150 - 250 nm.

b) Optimality of sonication and surfactant as scalable rate enhancement techniques for dense metal ceramic composite membrane fabrication.

c) Optimality of metal and reducing agent concentration and reducing agent contacting pattern for SIEP process for dense Ni ceramic composite membrane fabrication.

d) Optimality of surfactant contacting pattern (bulk for SSOEP and dropwise for SIEP) and concentration for SIEP and SSOEP processes to fabricate dense Ni ceramic composite membrane fabrication.

e) Process and parametric optimality for the inexpensive fabrication of dense Pd-ceramic composite membrane fabrication.

f) A framework for the comparative assessment of optimal ELP processes and associated parameters for dense Ni and Pd ceramic composite membrane fabrication.

These research findings are anticipated to substantially accelerate the large scale fabrication of dense ceramic composite membranes using the electroless plating process and its variants.

Contents

List of Tables

List of Figures

Nomenclature

Abbreviations

PPD	Percent pore densification, %
ELP	Electroless Plating
CEP	Conventional Electroless Plating
SIEP	Surfactant Induced Electroless Plating
SOEP	Sonication Induced Electroless Plating
SSOEP	Coupled Surfactant and Sonication Induced Electroless Plating
CEP–BR	Conventional Electroless Plating – bulk reducing agent
SOEP-BR	Sonication Induced Electroless Plating -bulk reducing agent
SIEP-BR-BS	Surfactant Induced Electroless Plating -bulk reducing agent- bulk surfactant
SIEP-DWR-BS	Surfactant Induced Electroless Plating–drop-wise reducing agent- bulk surfactant
SIEP-DWR-DWS	Surfactant Induced Electroless Plating–drop-wise reducing agent- drop-wise surfactant
SSOEP-DWR-BS	Coupled Surfactant and Sonication Induced Electroless Plating–drop-wise reducing agent- bulk surfactant
SSOEP-DWR-DWS	Coupled Surfactant and Sonication Induced Electroless Plating–drop-wise reducing agent- drop-wise surfactant

Notations

A_m	Permeable area of the membrane, m^2
Q	Volumetric flow rate, $\frac{m^3}{s}$
P_2	Membrane pressure at permeate side, Pa
ΔP	Trans-membrane pressure drop, Pa
d_p	Average pore size, μm
$\left(\frac{\varepsilon}{q^2}\right)$	Effective porosity
$\overline{P}$	Average pressure on the membrane, Pa
v	Molecular mean velocity of the gas, $\frac{m}{s}$
l	Pore length, m
q	Tortuosity

η	Viscosity of gas, $Pa.s$
K	Effective permeability factor, $\frac{m}{s}$
J	Flux through the membrane, $\frac{mol}{m^2 s}$
$\bar{J}$	Average flux through the membrane, $\frac{mol}{m^2 s}$
i	Hour of nickel plating(as exponent)
$\bar{J}_0$	Average flux through the support, $\frac{mol}{m^2 s}$
$\bar{J}_i$	Average flux through the membrane after ith hour of nickel plating, $\frac{mol}{m^2 s}$
C_i	Initial concentration of Ni^{+2} in the plating solution, $\frac{mol}{L}$
C_f	Average Ni^{+2} solution concentration after plating, $\frac{mol}{L}$
x	Conversion
η	Plating efficiency, %
w_0	Dry weight of the membrane before plating, g
w_i	Dry weight of the membrane after ith hour of plating , g
w	Total amount of nickel originally available in the plating bath, g
n	Number of plating cycles
V_0	volume of plating solution in each plating cycle ,L
M_{Ni}	Molecular weight of nickel metal $\frac{g}{mol}$
ρ_{Ni}	Density of nickel metal, $\frac{g}{cm^3}$
$\bar{r}_i$	Plating rate , $\frac{mol}{L.s}$
t_i	Time of plating for the ith hour, h

Chapter 1

Introduction and Literature Review

This chapter presents a brief summary of the fabrication engineering aspects associated to dense metal ceramic membranes. State of the art on the methods associated to dense metal ceramic composite membrane has been elaborately discussed. Based on the state of the art, the scope for further research has been identified. Following this, the aim of the present work has been summarized. Finally, the organization of the thesis has been presented.

1.1 Background

Membrane based separation processes offer several advantages such as compact operation, low cost and lower energy consumption (Ward and Dao, 1999). Broadly, based on the materials used, membranes can be categorized into two types: (i) Organic (Polymer) and (ii) Inorganic (Ceramic and Metal). Amongst organic and inorganic/metal membranes, the latter are highly promising towards various industrial schemes that involve higher processing temperatures and corrosive environments. Inorganic/metal membranes have been further classified into porous and dense composite membranes. Typically, alumina, carbon or stainless steel are commonly used supports or support materials for metal composite membranes (Kishore et al., 2003; Kitiwan and Atong, 2010; Mabande et al., 2004; Silva et al., 2012). Amongst these, sintered stainless steel membranes have received attention due to higher durability as a filter medium for superior separations and consistent performance under extreme process conditions and high operating temperatures. However, large scale applications of stainless steel membranes are highly expensive when compared to ceramic membranes and fabrication research is also equally focused towards utilizing ceramic membrane supports (Potdar et al., 2002).

Presently, metal ceramic composite membranes have been suggested for several applications including TiO_2 recovery from waste water streams (Jha and Rubow, 1999), production of ultrapure gases for special applications (Ryi et al., 2007), bacteriostatic treatment (Vasanth et al., 2011), asymmetric supports for dense palladium (Pd) composite membranes (Lin et al., 2010) and hydrogen separation (Ernst et al., 2007). Today, several companies produce and sell metal composite membranes citing several commercial applications (Table 1.1). Typically, amongst ceramics, α-alumina supports are used for Pd composite membrane fabrication. However, α-alumina being relatively expensive, its large scale application for metal composite membranes is also bound to contribute relatively higher costs for the composite membrane and hence there is a need for research in low cost ceramic supports for dense metal ceramic membrane fabrication.

To fabricate Pd/Ni composite membranes with good combinations of hydrogen permeability, and separation efficiency at a lower cost, several deposition methods have been reported.

1.2 Fabrication techniques for metal composite membranes

Table 1.1: A summary of commercial metal membranes and their applications.

S No.	Corporate firm	Membrane type	Support used	Applications
1.	Mott Corporation [WL1]	Pure porous nickel membrane	No support used	• Liquid filters • Removal and recovery of TiO_2 from waste streams
2.	Mykrons [WL2]	Sintered porous nickel membrane	No support used	• Separation of dust particles from air • Supports for palladium membranes
3.	Entegris [WL3]	Porous nickel composite membrane	Stainless steel	• Hydrogen Purification • X-ray diffraction media
4.	Johnson Matthey [WL4]	Palladium composite membrane	Porous stainless steel	• Hydrogen generators • Steam reforming
5.	ECN Netherlands [WL5]	Palladium composite membrane	Commercially available ceramic supports	• Membrane reactors • Fuel cell applications

These include physical vapor deposition (PVD) (Jayraman and Lin, 1995), chemical vapor deposition (CVD) (Gielens et al., 2002), magnetron sputtering (Brien et al., 2001), electroless plating (Cheng and Yeung, 2001; Yeung et al., 1999), electro-plating (Tong et al., 2005) and their combinations.

These well-known deposition methods have several advantages as well as disadvantages. Physical vapor deposition (PVD) process involves the deposition of metal films by vapor condensation on a support. Typically, PVD processes have poor deposition characteristics and hence require thicker films to produce surface defects. In chemical vapor deposition (CVD), the support is placed inside a reactor to which a number of gases are supplied. The fundamental principle of the process is that a chemical reaction takes place between the source gases. The product of that reaction is a vapor that eventually condenses on all surfaces inside the reactor. Thereby the desired metal is deposited on the target. A good rule of thumb for the CVD is that higher process temperature yields a composite material with better quality. However, owing to greater controls, CVD requires careful design of the experimental setup and is expensive when compared to the PVD. In the sputtering process, the material to be deposited is released from the source at much lower temperature than the temperature required for evaporation. The support is placed in a vacuum chamber with the source material, named a target, and an inert gas (such as argon) is introduced at low pressure. The ions are accelerated towards the surface of the target thereby causing atoms of the source material to break off from the target in vapor form and condense on all surfaces including the support. Electrodeposition also known as "electroplating" is typically restricted to electrically conductive materials. In the electroplating process, a chemical redox process is driven by the electrical power source and thus results in the formation of a layer of metal material on the support. The electrodeposition process is well suited to deposit films of metals such as copper, gold, palladium, silver and nickel. The films can be made within the range of ~1μm

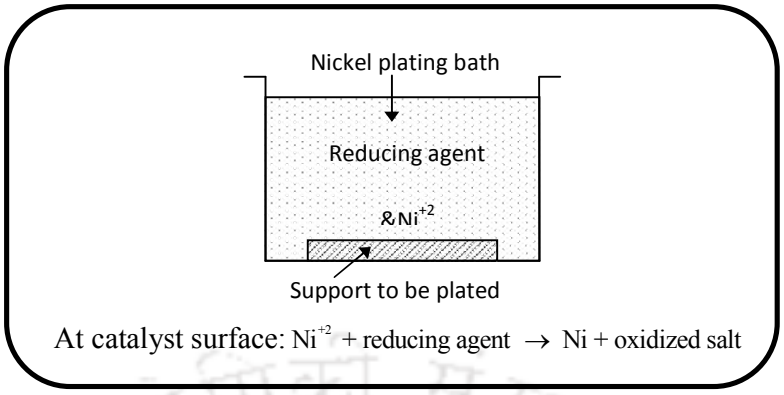

Fig 1.1: Schematic of Ni ELP bath.

to 100 μm thickness. The deposition is best controlled with the external electrical potential. However, the process requires electrical contact to the support upon immersion in the liquid bath. However, they suffer with the major disadvantage of current polarization and inability to deposit on non-conducting surfaces etc.

Electroless plating, also known as chemical or auto-catalytic plating, is a non-galvanic type of plating method that involves several simultaneous reactions in an aqueous solution, which occur without the use of external electrical power. Fig. 1.1 depicts a schematic representation of the method for Ni electroless plating. In the electroless plating process, a more complex chemical solution is used and deposition occurs spontaneously on any surface which possesses a sufficiently higher electrochemical potential than the solution.

1.2.1 A summary of fabrication variables that effect fabrication parameters

An important issue for metal membrane fabrication is to allow maximum flexibility in fabrication variables so as to obtain metal films with desired characteristics. While temperature plays a key role in the CVD technique, vacuum (pressure) plays a greater role in the sputtering process. Similarly, electro-plated membranes are largely influenced by the current density and solution concentration. On the other hand, electroless plating provides maximum flexibility in terms of fabrication variables. These include concentration of metal

precursors (palladium/nickel/silver ion concentration in the solution), selection of reducing agent concentrations, scheduling of reducing agent addition to the bath, loading ratio (defined as volume of solution used per unit area of membrane surface subjected to the plating), pH, temperature and coupled rate enhancement supplements (sonication, surfactant, vacuum, stirring, hydrothermal, pulsation etc.) to the process.

Therefore, from fabrication perspective, it is herewith inferred that electroless plating process offers maximum advantages when compared to the other deposition processes. These include flexibility in various operational variables in addition to other advantages such as ease of deposition, simple experimental set up, ability to deposit on non-conducting surfaces and ability to ensure uniform deposition even on complex surfaces.

1.2.2 Characteristic features of ELP

Electroless plating process does not require any external electrical potential and therefore, does not induce electrical stresses in the system. However, it is more difficult to control the electroless plating process with regards to film thickness and uniformity. A striking advantage of the electroless plating process is with respect to the ability to deposit metals on non – conducting surfaces such as plastics and ceramics. Also, the electroless technique require less expensive equipments and have the potential for the cost effective production of the membranes on an industrial scale (Bunshah, 1994).

- In electroless plating process, the reduction reactions are favored at high pH values. Therefore a buffering agent is used to keep the pH above 8.0. Moreover reducing agents often react with the bath thus resulting in slower deposition rates and poorer deposit quality and the plating bath solution is also subjected to spontaneous decomposition. This requires the addition of some stabilizers. Although extremely

similar to electroplating, electroless operations feature some distinctive characteristics.

- Electroless plating demand much tighter control over process parameters than electroplating. Critical parameters include metal concentration, reducing agent concentration, pH, temperature, agitation, and contamination control. Improper control over these process variables can result in increased plating inefficiencies, metal nucleation in the solution and hence higher production of waste in the bath.

- Chemical reactions in electroless process bath cause plate-out in which everything coming into contact with the process solution, including the tank itself, is coated with the plating material. This is due to significant metal nucleation in the plating solution and on vessel surface. To treat plate-out, the plating line must be taken off-line and stripped. In the case of electroless nickel, stripping is accomplished with nitric acid. The nitric acid stripping process can cause significant air releases of nitrous oxides (NO_x) if the stripping solution is too dilute. Thus to avoid these, there is a need to control the addition of the reducing agent and dispersing agent so that the ELP bath does not get decompose and plate-out is avoided.

- The autocatalytic metal (nickel) electroless plating process suffers with the basic disadvantage of lower rates of deposition (1.5μm/h) and hence rate enhancement techniques are required to supplement the conventional electroless plating process.

1.2.3 Scalability perspective of electroless plating process coupled with rate enhancement techniques

Several plating rate enhancement techniques include agitation (in the form of either solution stirring or membrane stirring (Ayturk and Ma, 2009) or gas sparging (Altinisik et al., 2005)),

vacuum (Nam and Lee, 2000), hydrothermal (Bulasara et al., 2012), osmosis (Li et al., 1999), sonication (Haas and Gedanken, 2006) and surfactant assisted electroless plating baths (Chen et al., 2002). However, amongst these techniques, agitation is scalable but suffers with the major disadvantage of poor plating efficiency (< 40%). Agitation may contribute to metal plating inefficiencies due to additional stresses caused by agitation for loosely bounded metal adhering to the support surface (Bulasara et al., 2011a) and therefore might not be recommended for industrial practice. This is especially important for dense metal composites where metal pitting from the surface is an important problem that cannot be ignored. On the other hand, vacuum as a rate enhancement technique is very efficient in operation but is unsuitable for scaleup. Vacuum electrodeposition requires usage of compatible seals (Nam and Lee, 2000) and induce additional stresses on the ceramic support. Similarly, hydrothermal rate enhancement technique involves simple process but suffers with the major disadvantage of poor operatibilty and poor scale up capabilities. Hydrothermal assisted ELP involves complicated loading and unloading operations and sealing of the ELP reactor during operation (Bulasara et al., 2012). While osmosis is scalable, it needs careful design of experimental process so that the salt solution does not leach and disturb the electroless plating bath stability (Li et al., 1999). Also, intermittent membrane cleaning is required to facilitate salt removal from the Pd metal surface. Therefore, osmosis is not advantageous from operational perspective, considering the fact that dense membranes are achieved only after 10-12h of continuous ELP.

On the other hand, surfactant induced electroless plating have significant number of features. The usage of surfactant is advantageous in two ways – firstly surfactant reduces the interfacial tension of the support-solution interface and therefore enables the generation of smaller bubbles on the surface. This minimizes the pitting effect. Secondly, since smaller gas bubbles are removed at a faster pace, the redox reaction shifts to the forward direction and

therefore metal plating is enhanced (Chen et al., 2002). During sonication assisted ELP, ultrasonic waves contributes to increase mass transport, interfacial cleaning and thermal effects (Haas and Gedanken, 2006). Thus, from the perspectives of scalability, combinatorial plating characteristics and ease of operation, sonication and surfactant remained attractive, as industrial scale sonication baths are available and surfactant assisted electroless plating could be scaled up easily. This is not the case for other rate enhancement techniques such as agitation (or stirring), vacuum and hydrothermal supplements.

1.3 State of the art

Several literatures are available in the field of metal ceramic composite membranes and associated fabrication technique optimality. The available state of the art is presented in three subsections namely (a) Effect of support morphology on metal film deposition characteristics, (b) Electroless plating process characteristics, (c) Metal deposition coupled with rate enhancement techniques etc.

1.3.1 Effect of support morphology on metal film deposition characteristics

Several literatures indicate that support morphology affects strongly the metal (Pd/Ni) plating characteristics and performance of the metal composite membranes.

Changrong et al. (2001) prepared microfiltration nickel membranes on porous alumina supports by electroless plating using sol–gel process to activate the alumina supports. They observed that the membrane thickness and amount of nickel increased with plating time and the pore size decreased greatly as electroless coating time enhanced to 15 min after which the pore size decreased slightly. The authors obtained a thickness of 4.5 μm in 90 min with a narrow distribution of pores. The mean pore radius was about 0.13 μm for the metal which did not possess cracks or pinholes.

Zheng and Wu (2000) reported upon the effectiveness for palladium electroless plating under hydrothermal conditions. The authors observed that using a support of nominal pore size 800 nm, the average membrane pore size was reduced to about 360 nm in a single electroless plating deposition step. This corresponds to a pore densification of about 79.75% in only 2 h of Pd electroless plating. However, process inefficiency and selective conversion have not been reported by the authors.

Ryi et al. (2007) prepared symmetric nickel membranes with a nominal pore size of 33 nm from nickel powder using compression (333 MPa) and sintering (650°C) technique. They found that the porous nickel support had very small pores with uniformity and smooth surface. These are good features of the support for the dense Pd membrane fabrication. Later, the same authors (Ryi et al., 2006a; Ryi et al., 2006b) prepared Pd–Cu–Ni alloy membrane of 4 μm thick on porous nickel support (33 nm) by multi-target sputtering and Cu-reflow technique. They observed that the nickel support was very stable and a very high H_2/N_2 separation factor (∞) was obtained. However, flexibility to vary the surface pore size and average porosity has not been addressed by the authors. In addition, fabrication technique used i.e., sputtering is not highly scalable.

Bulasara et al. (2011b) used a ceramic support with a nominal pore size of 700 nm to study the effect of support surface roughness along with various mass transfer enhancement techniques. The plating characteristics were investigated for three different roughness values, stirrer speeds (0–300 rpm) at a loading ratio (defined as membrane area per unit volume of plating solution) value of 196 cm^2/L. Their work concluded that the membrane pore size reduced to 100 nm and 130 nm respectively with stirring and sonication as rate enhancement techniques. Also, it has been inferred that both rate enhancement techniques normalized the role of variant surface roughness during nickel ELP.

Table 1.2: A summary of support morphological parameters for Ni-ceramic membrane fabrication.

Author	Support	Average pore size (µm) / Porosity (%)	Critical Observations
Xue et al.	Ni–B alloy/ Commercial alpha alumina tubes	0.3 / 40	High hydrogen permeability and high separation efficiency
Bulasara et al.	Ni/ceramic composite membranes	0.275 / 40	Pore size of 0. 128 –0.090 µm and PPD in the range of 78– 90% were obtained.
Changrong et al.	Ni/alpha alumina supports	0.43 / -	Pore radius of 0.13µm and metal film thickness of 4.5 µm were obtained.
Bulasara et al.	Ni/ceramic composite membranes	0.700 / -	Reduction in average membrane pore size by 0.100 µm for stirring and 0.130 µm for sonication

In a similar study, Vichaphund and Atong (2010) prepared nickel–alumina membranes using both powder and bulk impregnation methods for hydrogen separation. In this study as well, various important issues such as controlling film pore size, thickness and average effective porosity have not been addressed which influence to a significant extent the permeation characteristics of the membrane.

Table 1.2 presents a summary of the effect of support morphological parameters on metal ceramic composite fabrication. In summary, the effect of support morphology and support pore size has not been emphasized in a systematic framework. There is no systematic insight that provides suitable guidelines for best possible support. For example, a support with a narrow pore size distribution results in less metal film thickness but poor adhesion strength of the metal film. On the other hand, for a support with a rough surface, the film adhesion is stronger but higher metal film thickness is required to achieve dense metal membranes. Thus there is no clear research emphasis towards the optimality of support morphological parameters. In addition, the time dependency of process and membrane parameters was also targeted by the authors. All the literatures reported distinct combinations of support and plating process parameters whose further optimality has not been examined.

1.3.2 Electroless plating process characteristics

Yeung et al. (1999) fabricated Pd composite membranes using ELP on Vycor glass tubular supports. The authors emphasized on plating kinetics for hydrazine based Pd plating baths. The authors studied the variation of deposition rate and film thickness with several plating parameters and developed an empirical correlation between grain size, initial plating rate and plating time. Their work enabled towards the dependence of film micro-structure (i.e. thickness and morphology) on plating parameters such as concentrations of Pd^{2+}, N_2H_4, NH_4OH and plating temperature.

Mardilovich et al. (2002) systematically studied the effect of metal film thickness on the hydrogen permeance of Pd-PSS membrane. The minimum ratio of 3: 1 for Pd layer thickness and size of the largest pores in the support, that was originally reported by Ma et al. (2001) was corroborated by the authors for a large number of membrane samples using three different support morphologies. They further compared the actual Pd layer thickness with the predictions of the required Pd layer thickness based on 3 times the maximum pore size (rule of thumb). The authors found that a support grade of size 0.1 μm with a maximum pore size of 4-5 μm required a minimal dense Pd layer thickness in the range of 11.7-14.3 μm. These values are close to predicted thickness values in the range of 12-15 μm. Similar results were reported for supports with nominal pore sizes of grade 0.2 and 0.5 μm.

Haag et al. (2006) fabricated a nickel/ceramic composite membrane by electroless plating. The Ni film had a thickness of 1-1.5 μm thickness. Eventually, the authors identified the optimal conditions to prepare a homogeneous, pure nickel deposit on alumina. These are temperature of 75 °C, pH=9.6, $[Ni(AC)_2]$=0.12 mol L^{-1} and $[N_2H_4]$=0.4 mol L^{-1}.The thermal stability of the Ni film was not studied elaborately but their results indicated that the

mechanism of hydrogen transport is related to the Knudsen diffusion mechanism. Their work also presented few results associated to the plating characteristics as functions of time by targeting Ni solution concentration in the Ni ELP baths.

In summary, in the presented literature, electroless plating research for metal composite membranes has been primarily targeted from a product quality oriented perspective, but not from process engineering perspectives. Combinatorial plating characteristics involve the simultaneous assessment of plating process parameters (such as conversion, efficiency and plating rate) and product parameters (such as metal film thickness, average pore size and percent pore densification). This is an important area of research that can drive the efficacy of both manufacturing processes and materials. The state of the art scarcely addresses this approach.

1.3.3 Metal deposition coupled with rate enhancement techniques

Ayturk et al. (2009) coupled bath agitation with conventional ELP for the synthesis of composite Pd and Pd/Ag membranes. In their work, the process parameters i.e the initial metal ion concentrations for Pd and Ag were varied over a range of 8.2–24.5 mM and 3.1–12.5 mM, respectively and the plating temperature was varied between 20–60°C and the initial hydrazine concentration was varied between 1.8–5.4 mM. For a constant-volume batch reactor, the integrated rate law was solved to calculate the conversion and the reactant concentrations as a function of plating time. The authors carried out long-term hydrogen permeance testing of the Pd/Ag membranes in the temperature range of 300–500°C over a total period of 1200 h. It was further concluded that the H_2 permeance for the 4.7 μm thick pure-Pd membrane at 400°C was as high as 63 m^3/ m^2-h-$atm^{0.5}$ after a total testing period of 690 h.

Li et al. (1999) investigated upon the combinatorial effect of electroless plating with osmosis for the fabrication of Pd based membranes. They inferred that the defects in the Pd film are due to non-uniform activation of the support which can be eliminated by coupling osmosis with the ELP. The authors evaluated that the membrane with an initial H_2/N_2 permeation ratio of 10 could be repaired to enhance the ratio to 1000 using the osmosis coupled electroless plating technique.

Xue and Deng (2001) prepared a new amorphous Ni–B alloy/ceramic composite membrane by vacuum assisted electroless plating technique by driving away the gases trapped in the porous ceramic support and the metal film with the application of vacuum on the opposite side of the membrane along with rigorous stirring in the plating bath. The resultant composite membrane exhibited not only high permeability, but also high separation efficiency while the membrane prepared by the conventional plating method suffered from defects and low separation efficiency.

Zhao et al. (2000) employed electroless plating and magnetron sputtering for the fabrication of Pd and Pd–Ag alloy composite membrane. The authors coated ceramic membrane with γ-Al_2O_3 layer by the sol–gel method and used it as a support for the Pd and Pd–Ag alloy film. Both membranes provided He gas-tight performance at room temperature with a thickness of <1 μm. The authors reported a H_2/N_2 permselectivity of about 60.

Nam et al. (2000) prepared thin but dense palladium/nickel composite membrane with a thickness less than 2 μm on mesoporous stainless steel (SUS) support using vacuum electrodeposition technique. Smaller grain size and higher Pd content films were achieved using lower current density conditions. Not only this, higher hydrogen permeance and greater hydrogen/nitrogen selectivity were also evaluated for membranes fabricated at lower current density. The authors reported that the optimal current density, hydrogen permeance and

hydrogen/nitrogen (H_2/N_2) selectivity are 6.5 mA/cm^2, 2×10^{-2} cm^3/cm^2 .cm Hg. s and 3000 respectively at a temperature of 723 K.

In summary, there is lack of emphasis in the literature on a comparative technical assessment on the possible role of rate enhancement techniques in metal composite membranes from the perspective of combinatorial process as well as membrane characteristics. Moreover, issues like scalability, repeatability, low cost remain central themes before adapting rate enhancement techniques. But the literatures as mentioned seem to be more oriented towards trial and error methodologies using techniques that may or may not be systematic. Thus, the literature indicates the lack of systematic approach towards adopting a scalable rate enhancement technique that suits from both membrane and process perspective.

1.3.3.1 Metal deposition facilitated with surfactant induced electroless plating (SIEP)

Elansezhian et al. (2009) indicated a new approach and studied upon the addition of surfactants to conventional Ni ELP process. The authors used sodium hypophosphite as a reducing agent and investigated upon various features such as surface finish, microhardness, phosphorus content and micro structure. It was observed that the addition of two surfactants namely SDS and CTAB during deposition of Ni–P enabled enhancement in phosphorus content and corrosion resistance of the deposited film. With the addition of SDS, the improvement in the hardness of the coated layer was 52% and with CTAB it was 50%. The authors further evaluated that for a surfactant concentration lower than 0.6 g/L, the surface finish of the film was poor. Smoother surface finish of the deposited layers was obtained with the addition of SDS as compared to CTAB. Further, it was also reported that at lower surfactant concentrations, the average surface roughness value is higher and when concentration reaches to 0.6 g/L and above, the roughness value gets stabilized and it varied between 1.569 -2.557 μm (average value of 2.238 μm) for CTAB and 1.579 - 1.884 μm for

SDS (average value of 1.796 μm).These average roughness values are lower than the average roughness value (1.885 μm) of Ni–P deposits obtained without surfactant addition. Elansezhian et al. (2008) also studied the effect of the surfactants (SDS and CTAB) on the surface morphology and surface topography of the electroless Ni -P coatings and concluded that higher concentrations (above 0.6 g/L) of surfactants resulted in smoother and more uniform deposition.

Islam et al. (2012) compared surfactant induced electroless plating (SIEP) to the conventional electroless plating (CEP) for the fabrication of a Pd - Cu composite membranes on microporous stainless steel support. The authors used DTAB, a cationic surfactant in their investigations. Compared to the CEP, SIEP provided better combinations of metal grain structures and grain agglomeration. Further, dense and thinner films of Pd - Cu were achieved with shorter deposition time using SIEP process. The authors also observed that the alloying of Pd - Cu at an annealing temperature of 773 K under hydrogen environment was complete. Finally, it was inferred that under thermal cycling (573 - 873 K), the SIEP Pd - Cu membrane was stable and retained hydrogen permeation characteristics for over three months of operation.

Nwosu et al. (2011) reported on the efficacy of addition of an anionic surfactant SDS on the composition of nickel-yttria stabilized zirconia (YSZ) electroless co-deposition (ECD) on composite materials. The authors reported that the addition of SDS to electroless nickel bath containing YSZ concentration of 50 g/L provided an enhancement of more than 60 % in the YSZ coating volume. However, a major limitation has been identified. It was observed that with increasing SDS content, plating thickness reduced from 14 μm to about 2 μm and the coatings became incoherent. These indicates that surfactant addition reduces reduces film

thickness. Further studies revealed that the surface roughness also increased with SDS concentration.

Ilias et al. (2012) investigated Pd-ELP bath characteristics using three different surfactants. These were polyethylene glycol ter-octaphenylether (nonionic) surfactant, dodecyltetramethylammonium bromide (cationic) surfactant and dodecylbenzenesulfonic acid sodium salt (anionic) surfactant. The authors concluded that the addition of a suitable cationic surfactant could ensure the better removal of evolved gases such as NH_3, N_2 and this would in turn increase the rate of Pd deposition and thereby improve the Pd-film morphology significantly.

Bulasara et al. (2011c) fabricated nickel ceramic composite membranes so as to visualize the effect of surfactant concentration on the performance characteristics of the electroless plating baths using sodium hypophosphite as the reducing agent. They opted for SDS (anionic surfactant) with a concentration varying between 0 and 1.5 gL^{-1} and CTAB (cationic surfactant) with a concentration varying between 0 and 1.8 gL^{-1}. With an increase in concentration, it was evaluated that the conversion increased from 19 to 25% for SDS and from 19 to 27.5% for CTAB. With SDS and CTAB, the overall plating rates increased by 32% and 45% respectively. Thereby the authors inferred that CTAB provided higher bath conversions and was more effective in reducing the pore size than SDS for membrane perspective.

Further, Mafi et al. (2011) studied the effect of three different types of surfactant (cationic, anionic and non-ionic) at different concentrations in the plating bath on the deposition rate, PTFE content and surface morphology of electroless Ni–P/PTFE composite coatings. The authors inferred that cationic and non-ionic surfactants created a uniform distribution of

PTFE particles in the coatings. Further the effect of surfactant type and concentration on the corrosion properties of Ni–P/PTFE coatings were also investigated.

Chen et al. (2002) emphasized upon the role of surfactant in nickel-phosphorus (Ni-P) deposits on brass supports using ELP baths. The authors inferred that the addition of suitable amounts of surfactants can increase the deposition rate up to 25% and reduce the formation of the pores on the surface of Ni−P alloys. Further, surfactant addition also enhances the corrosion resistance of the deposits.

Table 1.3 presents a summary of SIEP processes for metal composite membrane fabrication. It can be observed that SIEP studies towards nickel composite membranes have not been addressed for a ceramic support. Such studies are also required from a processing perspective as well, given the fact that stainless steel membranes are significantly expensive than ceramic membranes. Thus the utilization of low cost ceramic membranes with SIEP metal depositional process could pave the way for faster research commercialization and scale up. This is also true due to the fact that SIEP reduces metal film thickness (enhances flux), enhances plating rates and promotes utilization of lower solution concentrations. Also, SIEP processes were not investigated for Pd-ceramic membranes and have been studied in a limited context for Ni-ceramic membranes. The time dependency of process and membrane characteristics was not studied as well.

1.3.3.2 Metal deposition facilitated with sonication induced electroless plating (SOEP)

There aren't many literatures that address sonication induced electroless metal plating for porous and dense metal composite membrane fabrication. Sonication facilitates rigorous agitation that can enhance plating rate. Therefore few additional literatures have been included to obtain good insights in the mechanism and quality of deposition for sonication induced electroless plating. Many of these do not target membrane fabrication.

Bulsara et al. (2012) addressed sonication as an additional degree of freedom to the conventional electroless plating process and evaluated the relationship between morphology of metallic skin layer and process parameters of hydrazine-based electroless plating baths during the fabrication of nickel-ceramic microfiltration membranes. The authors inferred that the selective conversion was enhanced by more than 50% and about 50–100% excess nickel plating rate was obtained with ultrasound as compared to other cases. Finally, it was concluded that SOEP baths provided the best combination of both process as well as performance characteristics in comparison with the base case and membrane stirred cases. However, membrane pore densification was not significant for SIEP baths.

Jiang et al. (2007) indicated that sonication assisted electroless plating can provide efficient deposition of nickel even at 40°C, a temperature which is considered to be very inefficient for the conventional nickel electroless plating baths due to extremely low reaction rates.

Wu et al. (2009) deposited nickel nanoparticles on metal oxides by a modified electroless nickel-plating method. The authors evaluated that the dispersion of nickel nanoparticles was dependent on the interfacial reaction between the metal oxide and the plating solution or the active metal and the plating solution. The Ag loading and acidity of the metal oxide mainly

Table 1.3: Literature data summary for SIEP based Ni and Pd composite membrane fabrication.

Plating parameters and Variables							Membrane parameters and Variables						
S no.	Type of membrane & support	Type of surfactant	Surfactant conc. (g/L)	Reducing agent	Activation energy (kJ/mol)	Selectivity (H_2flux/N_2 flux)	Film Thickness (μm)	Avg pore size(nm)	Porosity / PPD (%)	Metal conc (mol/L)	Plating Rate Increment (%)	Avg. H_2 Flux (mol/m^2.s)	References
1	Pd - MPSS	Triton X-100 (nonionic)	-	Hydrazine	9.7	312 (40psig) 230 (100psig)	8.5	-	-	0.081	-	0.34 (40psig) 0..72 (100psig))	Ilias et al
		DTAB (cationic)											
	Pd/Ag-MPSS	SDBS (anionic)			8.9	120 (40psig) 73 (100psig)	12.54					0.33 (40psig) 0..80 (100psig)	
2	N-P- MPSS	SDS (anionic)	0.15-.15	Sodium hypophosphite	-		-	-	-	0.231	-	-	Elansezhi-an et al*.
		CTAB (cationic)	0.15-1.8										
3	Pd – Cu-MPSS	DTAB (cationic)	-	Hydrazine	9.4	84.1	16.73	-	-	Pd 0.013 Cu 0.0048	-	0.0922 (573K)	Islam et al.
												0.13357 (873K)	
4	Ni -Ceramic	SDS (anionic)	0-1.5	Sodium hypophosphite	-	-	12.2-14.3	92	0.74 88.8	0.216	32	-	Bulasara et al.
		CTAB (cationic)	0-1.8				13-15.7	82	0.82 91.1		45		

* For stainless steel rods as support

affected the interfacial reaction to change the dispersion of nickel nanoparticles. It was concluded that the use of ultrasonic waves and microwaves and selection of ethylene glycol solvent instead of water in electroless plating could affect the dispersion and size of nickel nanoparticles.

Lu (2010) found that ultrasonic assistance during electroless copper plating generates a specific agitation due to cavitation phenomenon. This results in high quality metal coating. Touyeras et al. (2005) also showed that ultrasound irradiation improves deposit adhesion strength by decreasing internal stress.

Further, few researchers also stated that ultrasonic waves in sonication induced electroless plating enhances the speed of electroless plating due to the cavitation of ultrasound which accounts for increased mass transport, interfacial cleaning and thermal effects (Soloviev and Gedanken, 2011; Wu et al., 2009).

1.4 Possible scope for further research

In the following subsections, a critical insight is provided for possible research in metal membrane morphology, rate enhancement techniques, optimum metal concentrations on ELP baths and the role of surfactant addition on the combinatorial performance characteristics. The following sub-sections address the possible scope for research in metal ELP baths for composite membrane fabrication. The identified gaps in literatures are anticipated to be the central themes for the research that needs to be addressed in this work.

1.4.1 Development of low cost ceramic supports for efficient metal ELP

Process engineering studies towards materials fabrication need to first address compatibility of support materials towards the desired application. The consistent performance of ceramic membranes to serve as functional supports for dense Pd and porous Ni membranes needs to ensure their compatibility from several perspectives. Firstly, membranes with lower pore size, good porosity and narrow pore size distribution are required so as to reduce the critical film thickness of Pd required for the realization of dense membrane. Secondly, the membrane shall possess excellent corrosion resistance to withstand conditions during nickel electroless plating under basic pH conditions. Thirdly, the support shall enable continuous enhancement in pore densification during sequential metal deposition using electroless plating. Fourthly, the metal film shall provide lower gas flux when compared to the support flux and therefore the support morphological parameters need to be fine-tuned during fabrication research. Further, the cost of a composite membrane is a function of both metal film and the support and hence, cost reductions in support fabrication along with efficient metal film deposition would be relevant to drive economic competitiveness of the metal ceramic composite membranes. A critical review of literatures available for dense metal membranes research indicates the lack of integrated methodologies and approaches towards research in the functional supports (Kitiwan and Atong, 2010; Lin et al., 2010).

Bulasara et al. (2011d) concluded upon the efficacy of nickel hydrazine baths and suggested that an optimal condition of electroless plating for nickel membrane fabrication is about 0.08 mol/L and 393 cm^2/L. However, their work did not elaborate upon the following issues:

- A constant plating time of about 8 hours has been considered and time dependent variation of various process, membrane and depositional characteristics have not been studied.
- A ceramic porous support prepared using low cost inorganic precursors is used for the fabrication of the nickel composite membrane. The average pore size of the membrane is reported to be 275 nm. However the influence of support morphology on the depositional characteristics and the sensitivity of support morphological parameters (such as average pore size and porosity) on the performance characteristics were not addressed.

Considering these issues, it will be beneficial to exclusively focus upon the morphology related issues in the fabrication of nickel-ceramic composite membranes. It is evident that engineering research towards the design and development of good quality ceramic porous supports is highly beneficial to reduce the critical thickness required to achieve a dense membrane and eventually provide appropriate refinement in the guidelines available for the large scale fabrication of metal ceramic composite membranes.

Thus the role of support morphology to influence dense metal membrane depositional characteristics need to be studied. In this regard, the adhesion strength of the metal film to the support also needs to be considered, given the fact that the adhesion strength of the deposited metal film is a function of both support properties and film properties. The film properties are inturn functions of the electroless plating process parameters. In summary, a systematic study needs to be addressed that provides suitable guidelines for the selection of support morphological parameters towards metal electroless plating in terms of:

Process Optimality: Selection of scalable processes, Identification of optimal scalable process, Optimization of scalable and optimally scalable process parameters

Product Optimality: Selection of suitable support with optimal combinations of pore size and porosity, fabrication of composite membrane with minimal thickness, maximum PPD/delta etc.

1.4.2 Combinatorial performance characteristics of SIEP baths for dense Ni membrane fabrication

In recent years, researchers have studied anionic surfactant (SDS) because of its low cost (Nwosu et al., 2011; Zielinska et al., 2012). However, combinatorial plating characteristics (PPD, plating efficiency, metal film thickness) have not been targeted. Further, amongst cationic surfactants, DTAB has been studied in few literatures. Ilias et al. (2012) deposited a Pd-film on porous stainless steel using ELP and SIEP with DTAB as a surfactant and concluded that the same thickness can be obtained by reducing the plating time if a suitable surfactant is used during ELP. However, their results do not incorporate time dependent characteristics and therefore fall short of providing systematic insights with respect to the performance efficacy (total plating time, metal film thickness, transport efficiency and pore densification) of Pd electroless plating baths. Further, the work of Islam et al. (2012) compared SIEP to CEP with higher concentrations of metal (0.015M) and DTAB (4CMC) surfactant. Due to the higher solution concentrations and cost of the DTAB surfactant, the fabrication cost of the dense membranes is significantly high. This can be further reduced by targeting processes that utilize lower Pd solution concentrations and CTAB surfactant which is 40 time inexpensive than the DTAB surfactant. Also, CTAB surfactant possesses lower HLB value (Chen et al., 2002; Nwosu et al., 2012) than DTAB surfactant, which is a promising feature.

Bulasara et al. (2011c) carried out preliminary experimental investigations to infer that CTAB nickel SIEP is superior to agitation coupled ELP. However, the authors did not elaborate upon a detailed comparative assessment of various processes based on time dependent plating and process characteristics. Such studies could identify the optimal combinations of parameters and thereby infer upon the efficacy of surfactant in comparison with other metal ELP processes. Also, the authors studied the combinatorial plating characteristics for sodium hypophosphite reducing agent which is not as effective as hydrazine reducing agent. Thus, a comparative study of SIEP and CEP for various cases i.e. Ni-CTAB-hydrazine and Pd-CTAB-hydrazine for ceramic supports could provide significant insights with respect to various challenges associated to dense metal composite membrane fabrication. Also, the authors utilized a total plating of 8 h by deploying eight sequential plating steps with 1 h duration for each plating step at a loading ratio of 196 cm^2 L^{-1}. In summary, time dependent combinatorial plating characteristics for SIEP processes with ceramic supports could further extend the existing knowledge in the field of metal ceramic composite membrane fabrication using metal electroless plating.

Also it can be also observed in the literature that while SIEP has been studied for stainless steel supports (Islam et al., 2012) and alumina supports (Kitiwan and Atong, 2010) for Pd composite membranes, SIEP processes were not studied for nickel composite membranes which can serve as functional supports to achieve the palladium composite membranes. In addition, literatures are not available for Pd-ceramic composite membrane fabrication using SIEP Pd ELP process. Such studies are also required from a processing perspective as well, given the fact that stainless steel membranes are significantly expensive than ceramic membranes and the utilization of ceramic membrane could pave the way for faster research commercialization and scale up.

Additionally, it can be observed that a comparative study of different types of surfactants could be also beneficial from the perspective of the optimality of the type and concentration of a surfactant for dense metal composite membrane fabrication using SIEP process. While few literature are available for the application of SIEP towards products, other than membranes, the emphasis towards pore densification is an interesting area of research that needs to be thoroughly investigated in the context of the SIEP process. Specifically, the criticality of the surfactant type and concentration in inducing coupled rate enhancement without jeopardizing upon the quality of deposition needs to be targeted. The long term objective of such investigations is to achieve the simultaneous maximization of percent pore densification and minimization of metal film thickness on a ceramic support using the SIEP process.

1.4.3 Combinatorial performance characteristics of SOEP Ni ELP baths

There are very limited literature on sonication assisted electroless plating for fabrication of metal ceramic composites. Amongst the few literature, it was the work of Bulasara et al. (2012) that inferred that amongst various rate enhancement techniques, sonication coupled electroless plating (SOEP) provided maximum plating efficiency and selective conversion to achieve porous nickel-ceramic composite membranes. However, their work was focused towards porous metal composites and did not elaborate upon dense metal composites. Further, the authors compared SOEP and stirring assisted ELP. In other words, a comparative study of two scalable processes i.e. SIEP and SOEP were not addressed in the literature and needs to be examined in the context of effective pore densification to achieve dense metal composite membranes. Also, it can be analyzed that Bulasara et al. (2012) did not study the time dependent combinatorial plating characteristics for SOEP processes. Since 100% or near to 100% densification is the major

objective of this work, the number of sequential ELP steps needs to be enhanced from 8 to 16 or 24 to visualize upon the competence of the metal ELP process and its variants (SOEP, SIEP) to achieve higher pore densification values. The generated pore densification data trends are anticipated to be extremely useful for the engineering of efficient membrane supports and processes that facilitate the simultaneous maximization of pore densification and minimization of lower metal film thickness.

1.4.4 Performance characteristics of SSOEP Ni ELP baths

Till date, there are very few literatures that addressed the combined effect of two rate enhancement techniques coupled with ELP baths. Bulasara et al. (2012) studied a combination of hydrothermal and sonication for ELP baths and concluded that hydrothermal conditions are not favorable at higher metal solution concentrations for hydrazine baths. Also, hydrothermal assisted ELP involve complicated loading and unloading operations involving the regular sealing of the ELP reactor during operation and are not attractive from the perspective of process operability.

Till date, the literature is scarce on the coupled effect of two most scalable rate enhancement techniques namely surfactant and sonication for the fabrication of metal ceramic composite fabrication using ELP technique. In the field of metal membrane fabrication, researches have either explored surfactant (Chen et al., 2002; Elansezhian et al., 2008; Elansezhian et al., 2009; Nwosu et al., 2012; Zielinska et al., 2012) or sonication (Kathirgamanathan, 1994; Lu, 2010) rate enhancement techniques separately. The coupled effect of surfactant and sonication during metal ELP has been investigated for applications other than metal composite membrane fabrication. Yang et al. (2013) studied sonication-assisted dispersion of carbon nanotubes in anionic

surfactant SDBS containing aqueous solutions and concluded that sonication effectively promotes the dispersion of carbon nanotubes and accelerates their solubility. Similarly, other researchers (Haas and Gedanken, 2006) studied a coupled mechanism of electrochemistry with ultrasonic radiation for the preparation of nanosized copper particles by introducing different types of surfactants and unexpectedly obtained CuBr nanoparticles, instead of copper. Mizukoshi et al. (2001) investigated upon the role of different surfactants for the preparation of platinum nanoparticles using sonochemical reduction.

Bulasara et al. (2012) inferred that while sonication enhances plating rate, it does not effectively allow substantial enhancement of pore densification due to the layering of the metal instead of deposition in the porous structures. Also, in a recent work of Bulasara et al. (2011c), surfactant has been identified to allow effective impregnation of metal inside the pores by simultaneously reducing the pitting effect and enhancing the metal plating rate. However, surfactant induced electroless plating may not offer better plating rates and coupling sonication might be effective to further reduce the total plating time. In this regard, it shall be noted that electroless plating is a slow metal depositional process and reduction in total plating time to achieve a desired product specification is promising to reduce the fabrication cost. Given these few literature, it will be interesting to examine how sonication can be engineered with the utilization of a surfactant to promote faster plating rates and effective metal coverage in the porous structures. Such an approach is also beneficial from the scale up perspective as well, given the fact that both sonication and surfactant have been identified independently as scalable rate enhancement techniques to supplement the conventional metal electroless plating processes.

The lack of research interest to couple sonication as a potential rate enhancement technique during metal composite membrane fabrication with the metal ELP technique is due to the layering effect, which has been reported by Bulasara et al. (2012). Thus, it appears that sonication needs to be effectively engineering to achieve the desired functional characteristics of the metal ELP process namely successive enhancement in pore densification with increasing periods of plating time. Such investigations cannot be addressed unless one targets the time dependent plating and pore densification characteristics.

Hypothetically, the sonication and surfactant coupled metal electroless plating process (SSOEP) should provide maximum combinations of transport efficiency, plating rates, film growth rate, pore densification and minimal combinations of total plating time, metal solution concentrations and cost. The SSOEP process assumes paramount relevance in the context of highly dense metal composite membranes, as some of the limitations of both surfactant and sonication assisted ELP processes on their own could be nullified.

1.4.5 Effect of reducing agent contacting pattern and concentration on the combinatorial performance characteristics of SIEP Ni ELP baths

Plating efficiency and percent pore densification are two important combinatorial process characteristics of metal ELP baths. Plating efficiency can be defined as the ratio of the metal quantity plated on a membrane support to the quantity of the metal converted in the reaction. The PPD is a measure of the effective reduction in the pore sizes of the membrane and is essentially a function of the measured gas fluxes before and after plating. An efficient metal ELP process must have maximum combinations of PPD and plating efficiency. However, it is a fact that while PPD may increase, plating efficiency may reduce in ELP processes. This is primarily

due to the metal nucleation in the solution. Therefore, tradeoffs are required to achieve the desired combinations of PPD and plating efficiency and typically plating efficiency is ignored to achieve desired PPD for metal ceramic composite membranes.

Several rate enhancements have distinct combinations of PPD and plating efficiency characteristics. For instance, stirring improves PPD but significantly reduces plating efficiencies (Bulasara et al., 2011b). On the other hand, sonication enhances both PPD and plating efficiency but cannot bypass the layering effect due to which PPD values do not increase significantly beyond a particular value. Also, few literatures addressed the role of loading ratio to influence the combinatorial plating characteristics. Bulasara et al. (2011d) inferred that lower loading ratio (196 cm^2/L) enabled better pore densification than higher loading ratio (393 cm^2/L). However, plating rates enhanced without enhancing PPD. This is possibly due to the fact that larger amounts of plating solution (at lower loading ratio) enabled greater nucleation of nickel metal in the solution at higher solution concentrations and therefore maximizes nickel deposition in the solution than on the support.

A deeper insight into the electroless plating process indicates that while metal precursors, loading ratio, plating temperature invariably affect the combinatorial plating characteristics, it is the reducing agent which has a more fundamental role to influence these characteristics. This is due to the fact that the reducing agent undergoes oxidation on the metal nuclei (which may exist on the membrane surface or in the plating solution) to convert the metal ionic species to metallic species. Thus, controlling the time dependent concentrations of the reducing agent are very important to achieve higher plating efficiencies of metal ELP processes.

It is well known that reducing agents such as hydrazine are heat sensitive and disintegrate within a short span of time, when they are brought in contact with the hot plating solution (Cheng and Yeung, 2001). The addition of reducing agent to an electroless plating process is similar to the current density utilized in an electroplating process. Conceptually, the plating behavior of an efficient ELP process attempts to resemble that of the pulse electrodeposition technique, where the current density is highly programmed to achieve nano-structured metal deposition (Bryden and Ying, 1998). Considering the fact that electrodeposition techniques could not be efficiently applied for non-conducting surfaces, it is very important to conceive various process modifications to the surfactant/sonication enhanced electroless plating process to substantially improve both process and depositional characteristics.

Till date, there is only one literature that addressed the contacting pattern of the reducing agent and all other literatures addressed bulk addition of reducing agent for the fabrication of metal composite membranes. Yeung et al. (1999) reported that the formation of metal particles in the plating solution could be due to higher concentration of the reducing agent (hydrazine). Thereby, lower plating efficiencies and quality of deposition were evaluated. The authors recommended that the reducing agent shall be added in a semi-batch/phase wise mode so as to avoid bulk precipitation, achieve higher plating rates and obtain metal membranes with good morphological characteristics.

Along with these physical insights, it is important to conceive the optimality of the contacting pattern and concentration of the reducing agent. Conceptually, to overcome these issues a controlled (drop-wise) reducing agent addition strategy can be adopted during the entire duration of the plating process which is anticipated to alter the combinatorial plating characteristics substantially. Till date, among various process alternatives during SIEP/SOEP/SSOEP, the drop

wise addition of the hydrazine reducing agent to the metal ELP bath has not been explored in the literature and needs to be addressed for a comparative assessment with the familiar bulk mode of reducing agent addition.

1.4.6 Effect of surfactant type, concentration and contacting pattern on the combinatorial performance characteristics of SSOEP Ni ELP baths

Conceptually, a SIEP bath can be operated in several ways. As a first alternative, all the constituents can be mixed initially and plating could be initiated. As a second alterative, the reducing agent can be added in a phase wise or continuous mode to the mixture of surfactant and metal solution in an ELP bath as mentioned in the previous sub-section. As a third alternate, both reducing agent and surfactant can be added in a phase wise and continuous mode to the ELP baths. While these options may appear naïve for the general application of ELP, they may be of paramount relevance for dense metal composite membranes.

Till date there is no literature that elaborates upon the role of contacting pattern of the surfactant in electroless plating bath for dense composite membrane fabrication. In the field of dense metal membrane fabrication using electroless plating, only few literatures are available with respect to the applicability of different type of surfactants (Elansezhian et al., 2008; Elansezhian et al., 2009; Islam et al., 2012) and optimal concentration of surfactant (Islam et al., 2012). These literatures as well did not address upon the criticality of the contacting pattern of the reducing agent and surfactant. Thus, all relevant literatures addressed bulk addition of surfactant for metal deposition using electroless plating.

The bulk addition of surfactant encourages uneven deposition of metal composites which becomes increasingly disadvantageous in the final stages of fully dense metal composite membranes using SIEP. This is due to the adsorption of surfactant on the membrane surface which promotes uneven charge distributions on the surface (Chen et al., 2002). This encourages greater metal nucleation in the solution which is an undesired issue. Thus, with surfactant being an additional degree of freedom, its contacting pattern and concentration distributions can be also worth investigating as important research problems. Variation in the surfactant contacting pattern is hypothesized to promote better depositional characteristics and membrane pore densification due to lesser adsorption of surfactants on the support surface. Thus, to further enhance the plating efficacy of the ELP process, there is a need to focus upon the contacting pattern of the dispersing agent (surfactant).

1.4.7 Combinatorial plating characteristics of SIEP and SSOEP processes for dense Pd ceramic composite membrane fabrication

Till date, numerous literatures addressed the deposition of Pd on ceramic supports using conventional ELP technique. Collins et al. (1993) fabricated composite palladium-ceramic membranes using ELP and Seshimo et al. (2008) fabricated a Pd/γ-alumina/anodic alumina composite membrane by electroless plating. Further Hu et al. (2010) fabricated a highly permeable and selective Pd/pencil/Al_2O_3 composite membrane on a low-cost macroporous Al_2O_3 as a support by electroless plating.

Till date, coupling rate enhancement techniques for Pd-ceramic composite membrane did not receive much attention. Sari et al. (2013) studied the performance of a novel coating of palladium over an alumina ceramic membrane using a combined sol–gel process and an

electroless plating technique. Such a methodology is not feasible from the perspective of scalability and repeatability. Given the fact that ceramics are non-conducting surfaces and plating will be more challenging and difficult on such surfaces, it would be an interesting research problem to investigate upon the efficacy of various rate enhancement techniques for Pd ceramic composite membrane fabrication. In this regard, the efficacy of SSOEP process is highly relevant from the context of process operability, simplicity and scale up. Also, due to high cost of palladium, it is important to focus upon the role of inter-diffusion barrier such as Ni to achieve thin and dense Pd composite membranes. Such studies in an academic context will enable to obtain valuable insights towards the large scale fabrication of dense Pd composite membranes.

A critical observation of all relevant literatures indicates that the electroless plating research for dense palladium membranes is highly dovetailed towards membrane engineering (film thickness and densification) but not towards process engineering or a combinatorial process-product engineering perspective. In terms of the electroless plating process and product parameters, an efficient Pd electroless plating process for dense Pd composite membrane fabrication should offer maximum combinations of selective conversion, plating efficiency, plating rate and percent pore densification and minimal combinations of palladium solution concentration, plating time and metal film thickness. There is no emphasis towards such an approach in the literature.

Based on the important experimental findings, the following features can be outlined. Most of the experimental investigations were dedicated towards the membrane performance but not the process. However, it is a fact that palladium deposition using electroless plating cannot be restricted to the membrane performance characteristics only, as palladium is a rare metal and is as expensive as gold. Therefore, metal losses in due course of electroless plating due to process

Table 1.4: A summary of process and product parameters

Process Parameters	**Product Parameters**
Selection of scalable processes (CEP/SIEP/SOEP/SSOEP)	Optimal combinations of pore size and porosity
Identification of optimal surfactant contacting pattern (dropwise/bulk)	Achieve minimal metal film thickness
Identification of optimal reducing agent contacting pattern (dropwise/bulk)	Achieve maximum pore densification
	Achieve minimum time of plating

inefficiencies shall be identified and minimized without jeopardizing upon the quality of plating. Secondly, the combinatorial performance characteristics of electroless plating coupled with rate enhancement techniques for ceramic supports were not addressed. In summary, Table 1.4 explicitly conveys the process and product parameters/variables for membrane fabrication.

1.4.8 Summary

Conceptually, the consideration of the support with lower pore size and porosity and thereby lower surface area encourages research from the process optimization perspective. Essentially membranes with lower surface area undergo less activation and therefore the ability of the rate enhancement technique to rapidly contribute to pore densification is an interesting issue to explore. The long term goal of the Ph.D. thesis is to understand the intricacies involved in coupling rate enhancement with ELP process for dense palladium ceramic composite membrane fabrication. With Pd being expensive, it would be wise to first devote significant effort towards the deposition of an inexpensive metal on the ceramic support. In this regard, rigorous experimentation can be targeted with Ni ELP baths to gain insights with respect to the efficacy of both rate enhancement techniques and process parameters. Once the optimality of these parameters can be established for cheaper metal deposition (Ni) on ceramic supports, minimum number of plating experiments will be required to achieve dense Pd ceramic composite

membranes. In this work, Ni deposition on ceramic supports has been targeted extensively for dense metal ceramic composite membrane fabrication. It should always be kept in mind that the optimal parameters for Pd ELP baths could be different than those found for Ni ELP baths. Nonetheless, the optimality of rate enhancement techniques is believed to be applicable for both Ni & Pd baths. This is also due to the fact that Ni plating rates are lower than Pd plating rates and therefore optimizing the challenges involved in dense Ni membrane fabrication would be useful to achieve very easily a dense Pd composite membrane. In summary by adopting the above research strategy, minimum Pd precursor utilization for the fabrication related experimental research can be targeted.

1.5 Objectives of the work

1.5.1 Overview

The chemistry involving the interaction between surfactant, metal and reducing agent is highly complex. This work intends to provide a good number of insights with respect to possible modification to metal ELP processes for metal composite membrane fabrication. It specifically targets the process optimization of electroless plating process to fabricate nickel-ceramic composite membranes. Also the effect of support morphological parameters on the performance characteristics of nickel hydrazine baths will be addressed**.** This work also intends to compare and contrast the efficacy of several efficient rate enhancement techniques (surfactant, sonication etc.) on combinatorial performance characteristics of ELP baths. The role of rate enhancement techniques such as surfactant and sonication to enhance pore densification and achieve a defect free composite membrane with minimal metal film thickness will be as well addressed.

The main objective of this work will be to relate densification and metal film thickness with plating time which seems to be a missing issue in many studies. Moreover, this work also elaborates upon the performance characteristics of SIEP processes supplemented with controlled addition of the hydrazine as reducing agent along with the optimization of reducing agent and metal concentrations in an SIEP process for the optimal membrane fabrication. Similarly, research would also be dovetailed towards identifying the optimal performance characteristics of SIEP/SOEP/SSOEP processes supplemented with controlled addition of surfactant. Finally, the ultimate objective will be to study Pd deposition for ceramic supports on the optimized/modified electroless plating from the perspective of 100% pore densification. All these novel research works are anticipated to consolidate the fabrication research of metal composite membranes in the context of scalable rate enhanced metal electroless plating processes.

1.5.2 Details

Based on the existing gaps in the literatures that were thoroughly discussed in the previous section, the following objectives have been identified to be fulfilled in this thesis:

a) **Support engineering:** Firstly, a low cost ceramic support with lower combinations of pore size and porosity needs to be fabricated. Eventually, the membrane morphological properties namely average flux and film growth rate need to be analyzed for conventional metal electroless plating processes. Thereby, the role of support morphology to influence the combinatorial plating characteristics is the primary objective of the support engineering research. The combinatorial plating characteristics precisely refer to membrane characteristics (film thickness and percent pore densification) and process characteristics (plating and transport efficiency). The relevance of time dependent variation of these parameters in the context of minimizing total plating time for desired

pore densification is an important issue that can infer upon the optimality of rate enhanced electroless plating processes.

b) **SOEP and SIEP process characteristics:** Targeting maximum pore densification and minimal metal film thickness, combinatorial plating characteristics of rate enhanced (SOEP and SIEP) nickel ELP processes for metal composite membrane fabrication need to be assessed after optimizing the support morphology. Subsequently, a comparative assessment of these techniques with conventional ELP will be useful to infer upon the most favorable rate enhancement technique for metal composite membrane fabrication.

c) **Identification of optimal reducing agent contacting pattern and concentration during SIEP:** The specific objective refers to the identification of optimal combinations of reducing agent concentration and contacting pattern for SIEP nickel ELP baths. Thereby, the emphasis will be towards identifying both process as well as its parameters in the context of combinatorial plating characteristics for dense nickel ceramic composite membrane fabrication.

d) **Optimality of precursor concentrations:** For most promising rate enhanced nickel ELP, the objective of such studies is to evaluate upon the role of variant metal solution concentration and reducing agent concentration on the maximization of PPD, plating rate, plating efficiency and minimization of metal film thickness and plating time.

e) **Optimality of surfactant concentration and its contacting pattern:** For SIEP/SOEP/SSOEP baths, the optimality of surfactant type, solution concentration and its contacting pattern (bulk vs. drop wise) will be investigated towards fabricating metal composite membrane. The optimal surfactant solution concentration corresponds to its concentration expressed in terms of its critical micelle concentration (CMC).

Thus, objectives (a) – (e) involve a hierarchical approach that systematically explores nickel ceramic composite membrane fabrication with systematic emphasis towards:

- Support optimality
- Optimality of rate enhancement technique amongst SIEP,SOEP and SSOEP processes
- Optimality of reducing agent, its contacting pattern and metal solution concentration for most promising rate enhanced Ni ELP processes
- Optimality of precursor concentrations
- Optimality of surfactant concentration and contacting pattern for most promising rate enhanced Ni ELP processes

f) Dense Pd Ceramic Composite fabrication using SIEP and SSOEP processes: For most efficient contacting pattern of the reducing agent and surfactant, combinatorial plating characteristics will be investigated for Pd ceramic composite membranes using SIEP/SSOEP processes.

The insights gained from objectives (a – e) will be useful to conduct minimal experiments for the fabrication of Pd-ceramic composite membranes. The ultimate goal of the experimental investigations is to identify the best Pd ELP process that can provide maximum percent pore densification (PPD), plating rate ($\overline{r_i}$) and plating efficiency (η) and minimum metal film thickness (δ) with reference to rate enhancement techniques and optimal concentrations and contacting patterns of metal, reducing agent and surfactant respectively.

1.6 Organization of the Thesis

Chapter 1 presents a brief introduction of metal ceramic membranes along with the available literature and possible scope for research to identify an optimal and scalable rate enhanced ELP process for Ni/Pd ceramic composite membranes.

Chapter 2 presents details with respect to the preparation and characterization of low cost ceramic membrane supports and experimental procedures for various electroless plating process adopted in this study to achieve Ni and Pd composite membranes.

Chapter 3 addresses a broad research methodology for the development of low cost ceramics to serve as functional supports for dense metal composite membranes. Laboratory fabricated supports characterized with lower combinations of average pore size and lower effective porosity have been targeted for applicability in CEP/SIEP/SOEP baths.

Chapter 4 highlights novel method of reducing agent contacting pattern for Ni ELP plating baths supplemented with CTAB surfactant. Also, the optimality of reducing agent and metal concentration is as well addressed.

Chapter 5 elaborates upon the plating bath performance characteristics for bulk and drop wise contacting pattern of the surfactant along with drop wise addition of reducing agent for dense nickel composite membrane fabrication using SIEP and SSOEP baths.

Chapter 6 targets the optimality of surfactant type and concentration for dense nickel composite membrane fabrication using SSOEP baths.

Chapter 7 presents results obtained for the fabrication of dense palladium ceramic composite membranes using various ELP processes. Also, the optimality of Pd solution concentration is as well addressed.

Chapter 8 briefly summarizes various important conclusions drawn from this work followed with the extensions for future work.

Experimental Procedure

This chapter is divided into three sections. The first section addresses the preparation and fabrication of ceramic membrane supports. The circular disk shaped ceramic membranes were prepared with dry compaction method. The second section presents the techniques adopted surface and physical characterization. Third section summarizes the methodology adopted for electroless plating along with evaluation of various parameters for characterizing the electroless plating process as well as the membrane performance.

2.1 Support preparation and fabrication

2.1.1 Raw materials

The raw materials used for the fabrication of ceramic membrane supports are kaolin, feldspar, quartz, sodium carbonate, pyrophyllite, boric acid and sodium metasilicate. Kaolin was obtained from CDH Ltd., India; feldspar and pyrophyllite from National Chemicals, India; quartz from Research-lab Fine Chem Industries, India; sodium metasilicate from SD Fine-Chem Ltd., India. All other inorganic precursors (sodium carbonate and boric acid) were obtained from Merck Ltd., India. The composition of various above mentioned raw materials with their major functional attributes are listed in Table 2.1. The composition was identified based on a trial and error experimental approach.

2.1.2 Support fabrication

The circular ceramic supports were fabricated in the laboratory using the dry compaction method. The fabrication methodology consists of the following sequential steps: mixing of the raw materials, casting of the raw material mixture into circular moulds, drying of the raw discs at 373 K for 6 h, sintering of the discs at 1173 K with a controlled heating/cooling rate

Table 2.1: Inorganic precursor formulation and their functional attributes.

Material	Composition (Wt. %)	Functional Attributes
Kaolin	40	Low plasticity & High Refractory Properties
Feldspar	15	Improves chemical and physical stability
Quartz	15	Mechanical & Thermal Stability
Na_2CO_3	10	Pore forming agent & Colloidal Agent
Pyrophyllite	10	Increased fired strength & Reduced shrinkage
Boric Acid	5	Colloidal Agent & Increases mechanical strength
Sodium Metasilicate	5	Binding Agent

(1.5^oC /min) followed by polishing of the membrane and finally cleaning the supports in a sonicator bath.

To start with, all the raw materials were mixed in the composition mentioned in Table 2.1. They were initially manually mixed to make a uniform powder and then grinder thoroughly using a mixer grinder. These uniformly grinded mixture was weighed 10 g for each membrane and packeted. The mixture was then placed in circular stainless steel moulds to fabricate disk shaped ceramic supports. The circular moulds were then placed in a hydraulic press (Make – Velan Engineering) and operated at a pressure of 4.9 and 6.9 MPa using the dry compaction method. Eventually the circular raw disks were obtained. They were then dried in a muffle furnace at 373 K for 6 h to facilitate moisture removal. Subsequently, the disks were sintered at 1173 K with a controlled heating/cooling rate (1.5 ^oC/min). The sintering temperature was chosen based on the thermo gravimetric analysis (TGA) of the raw material mixture presented in the literature (Vasanth et al., 2011). The supports were then allowed to cool down to room temperature. The sintered supports were then polished using a silicon carbide abrasive paper (No. C – 220) to obtain a smoother surface finish. The ceramic

supports were then subjected to ultrasonic cleaning in a de – ionized water bath for 10 min to remove any loose particles adhering on the polished surface. After ultrasonic cleaning, the membranes were dried in a hot air oven to remove the moisture. Finally ceramic supports with a diameter of 36 mm and a thickness of 3.5 mm were obtained. Due to variation in fabrication pressure (4.9 and 6.9 MPa) supports with two different ranges of pore size particularly 50-70 nm and 150-250 nm were fabricated.

2.2 Support characterization

Surface and physical characterization were performed using several techniques. Laser particle size analysis (LPSA) (Make: Malvern; Model: Mastersizer 2000, UK) was carried out to evaluate the average particle size of the raw material. Fourier transform infrared spectroscopy (FTIR) analysis was conducted to record the characteristic peaks of various raw materials (Make: Shimadzu Corporation; Model:IR Affinity –1). The Brunauer–Emmett–Teller (BET) surface area and pore size of the support material was determined withN_2 adsorption desorption isotherm at 77K that was obtained with surface area analyzer (Make: Beckman-Coulter; Model: SA3100). X-Ray diffraction (XRD) analysis of the ceramic support was conducted to evaluate the extent of phase transformations before and after sintering (Make: Bruker; Model: D8 Advance). Field emission scanning electron microscopic (FESEM) study (Make: Oxford; Model: Leo 1430VP, UK) was carried out to analyze the presence of possible defects and estimate the membrane pore size. Room temperature nitrogen permeation experiments were conducted to quantify the extent of pore densification using the experimental setup adopted by Bulsara et al. (Bulasara et al., 2011b). For all permeation experiments, high purity N_2 (99.99% obtained from Assam Air Products Ltd., Guwahati) was used for an effective permeation area of $1.0173\times10^{-3}\ m^2$.

2.3 Electroless plating

Electroless plating, also known as chemical or auto-catalytic plating, is a non-galvanic type of plating method that involves several simultaneous reactions in an aqueous solution, which occur without the use of external electrical power. Prior to electroless plating, the supports were seeded with palladium seeds via a process which involved sequential steps of sensitization, activation and rinsing using baths of specific compositions presented in Table 2.2 (Bulasara et al., 2011a). The seeding process involved keeping the ceramic support in the sensitization bath ($SnCl_2$ solution) for 5 min, followed by rinsing with distilled water and subsequent placement of the support in the activation bath (dilute $PdCl_2$ solution) for 5 min. Finally the discs were placed in acidic bath (0.1N HCL) for 2 min. The mentioned sequential steps were repeated 10-12 times for ensuring the existence ofsmall Pd catalytic sites uniformly throughout the membrane surface. After seeding, the support was dried overnight in an oven at 393 K.

2.4 Nickel Electroless Plating

Considering nickel as the target plating metal, a conceptual research methodology has been outlined that systematically addresses the experimental and theoretical insights for the realization of metal composite membranes. The optimized conventional electroless Ni plating

Table 2.2: Composition of sensitization and activation baths.

Constituent	Amount used in each bath	
	Sensitization	Activation
$SnCl_2.2H_2O$ (g/L)	1.0	–
$PdCl_2$ (g/L)	–	0.1
35% HCl (ml/L)	1.0	0.5
pH	4-5	4-5

bath composition (as shown in Table 2.3 (Murali et al., 2014)) consists of nickel sulfate (as a source of nickel),hydrazine hydrate (as an electron source), trisodium citrate (as a stabilizer) and sodium hydroxide (as a pH maintaining agent). Plating characteristics were investigated at a loading ratio of $203\left(\frac{cm^2}{L}\right)$, plating bath temperature of 80°C, pH of 10-12 and 1h plating time for one metal depositional step.

Typically, the reduction of Ni^{2+} with hydrazine hydrate reducing agent during ELP involves the following three reactions (Li and Han, 2006)

$$2Ni^{2+} + N_2H_4 + 4OH^- \rightarrow 2Ni\downarrow + N_2\uparrow + 4H_2O \quad (2.1)$$

$$N_2H_4 \rightarrow N_2\uparrow + 2H_2 \quad (2.2)$$

$$3N_2H_4 \rightarrow N_2\uparrow + 4NH_3\uparrow \quad (2.3)$$

In the above three reactions, while reaction (1) occurs on the activated support surface and is desired, reactions (2) and (3) occurs in the plating solution and are undesired, as they deplete reducing agent concentration in the solution. In this regard, the electroless plating bath was modified and accompanied with different rate enhancement techniques along with different strategies for the reducing agent contacting pattern as mentioned in the sub-sections below.

Table 2.3: Composition of Ni ELP baths for Ni-ceramic membrane fabrication.

S. No.	Component	Formula	Amount
1.	Nickel Sulfate	$NiSO_4.7H_2O$	0.08 mol/L
2.	Hydrazine Hydrate	$H_2NNH_2.H_2O$	50,100, 200 % excess
3.	Trisodium Citrate	$Na_3C_6H_5O_7.2H_2O$	0.2mol/L
4.	Sodium Hydroxide	NaOH	10-12

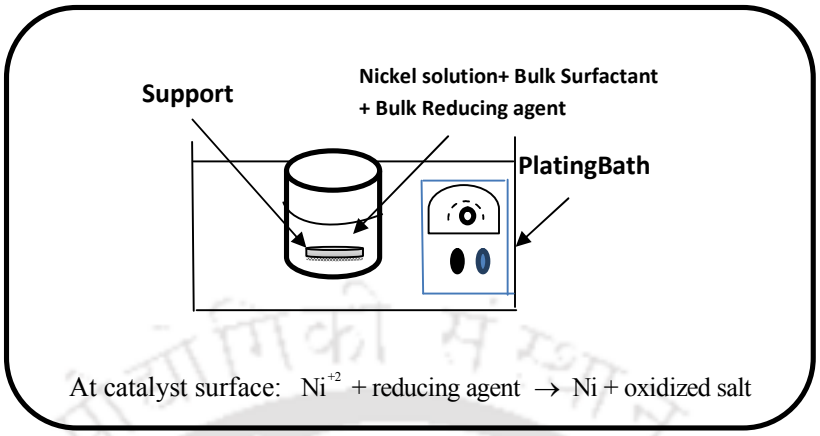

Fig. 2.1: Schematic of conventional Ni ELP bath (CEP-BR).

2.4.1 Conventional Electroless Plating (CEP)

Conventional electroless plating involves heating the plating solution in a water bath at a constant temperature of 80°C. The schematic of CEP is shown in Fig. 2.1. Once the plating temperature is achieved, the seeded support along with reducing agent is added in bulk mode.Since the process involves bulk addition of reducing agent, the CEP process is also referred to as CEP– BR (bulk reducing agent).

2.4.2 Surfactant Induced Electroless Plating (SIEP)

The electroless plating bath composition and plating parameters is similar to CEP as summarized in section 2.4.1. The only variation in the composition of bath is with respect to the addition of a cationic surfactant cetyltrimethylammonium bromide (CTAB) in an amount equivalent to 1.2g/L. This variation in CEP is termed as SIEP baths (as shown in Fig: 2.2). Since the process involves bulk addition of surfactant and reducing agent, the SIEP process is also referred to as SIEP-BR (bulk reducing agent)-BS (bulk surfactant). This is also due to the fact that for subsequent variants to the SIEP process, the SIEP-BR-BS will be regarded as the base case experimental set.

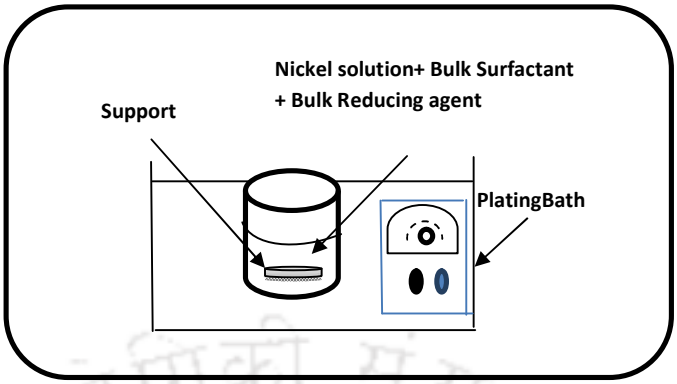

Fig. 2.2: Schematic of surfactant induced Ni ELP bath (SIEP-BR-BS).

2.4.3 Sonication Induced Electroless Plating (SOEP)

For the SOEP process, the bath composition and plating parameters are similar to those presented for CEP in section 2.4.1. The only variation is that the conventional plating bath is replaced by a sonicator bath (Elma S 30 H) that operated at a frequency of 37 kHZ with a power consumption of 280 W in degas mode.The inner dimensions of the rectangular cleaning bath are 240 mm (Length) x 137 mm (Width) x 100 mm (Height). The plating solution along with reducing agent and the seeded support was kept in the sonicator bath provided with an internal heater to maintain plating temperature. This variation in CEP baths is termed as SOEP bath (as shown in Fig: 2.3). Since the process involves bulk addition of reducing agent, the SOEP process is also referred to as SOEP-BR.

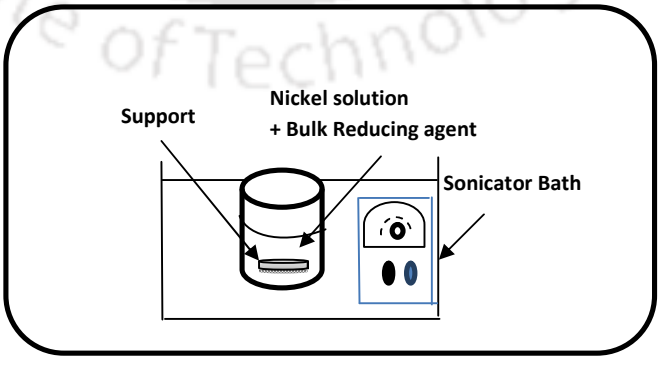

Fig. 2.3: Schematic of sonication induced Ni ELP bath (SOEP-BR).

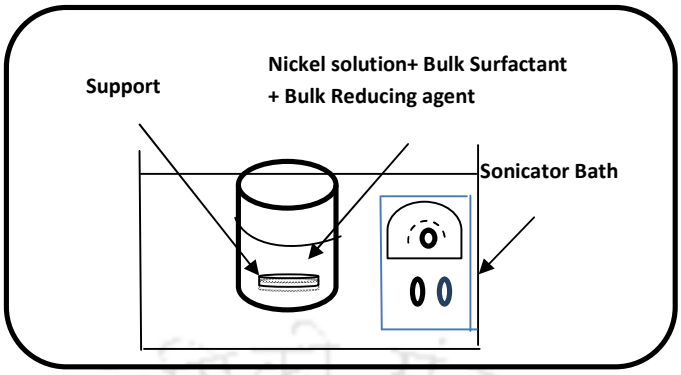

Fig. 2.4: Schematic of surfactant and sonication coupled Ni ELP bath (SSOEP-BR-BS).

2.4.4 Surfactant and Sonication Coupled Electroless plating (SSOEP)

For the SSOEP process, the bath composition and plating parameters are similar to those presented for CEP in section 2.4.1. The only variation for the case is that the conventional plating bath is replaced by a sonicator bath along with an addition of a suitable surfactant as mentioned in Fig. 2.4. This variation in CEP bath is termed as SSOEP baths. Since the process involves bulk addition of surfactant and reducing agent, the SSOEP process is also referred to as SSOEP–BR (bulk reducing agent)-BS (bulk surfactant). This is also due to the fact that for variants to the SSOEP process, the SSOEP-BR-BS will be regarded as the base case experimental set.

2.4.5 SIEP with process variants

The variants are classified as SIEP-DWR-BS and SIEP-DWR-DWS as shown in Fig. 2.5. The controls refer to the regular SIEP process i.e., SIEP-BR-BS. The variant SIEP-DWR-BS process refers to SIEP bath with dropwise addition of reducing agent and bulk addition of surfactant and SIEP-DWR-DWS refers to SIEP bath with dropwise addition of reducing agent and dropwise addition of surfactant.

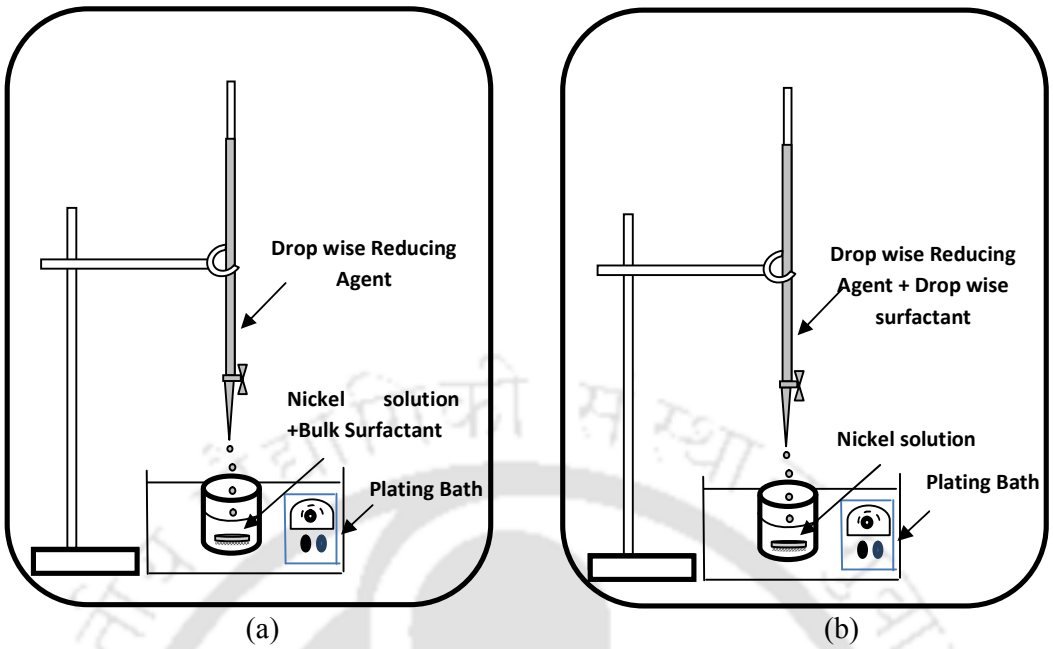

Fig. 2.5: Schematic of (a) SIEP-DWR-BS and (b) SIEP-DWR-DWS baths.

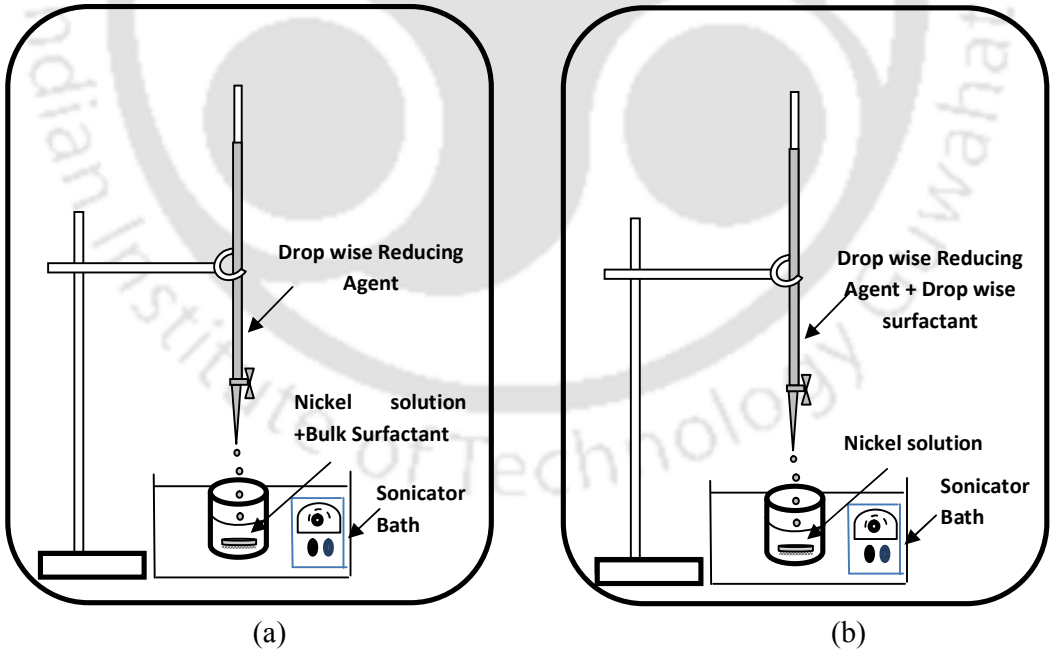

Fig. 2.6: Schematic of (a) SSOEP-DWR-BS and (b) SSOEP-DWR-DWS baths.

2.4.6 SSOEP with process variants

The variants are classified as SSOEP-DWR-BS and SSOEP-DWR-DWS as shown in Fig. 2.6. The controls refer to the regular SSOEP process which can be also classified as SSOEP-BR-BS. The variant SSOEP-DWR-BS refers to SSOEP bath with dropwise addition of reducing agent and bulk addition of surfactant and SSOEP-DWR-DWS refers to SSOEP bath with dropwise addition of reducing agent and dropwise addition of surfactant.

2.5 Palladium Electroless Plating

The optimized conventional electroless palladium plating bath composition (as shown in Table 2.4) consists of palladium chloride (as a source of palladium), hydrazine hydrate (as an electron source), ethylenediamine tetra acetic acid (as a stabilizer), and liquor ammonia (as a pH maintaining agent). Plating characteristics were investigated at a loading ratio of $203\left(\frac{cm^2}{L}\right)$, plating bath temperature of 60°C, pH of 10-12 and 20-25 min of plating time for one plating step. The electroless plating of palladium proceeds via the following reactions (Ilias et al. 2012):

$$2Pd(NH_3)_4^{2+} + 4e^- \rightarrow 2Pd\downarrow + 8NH_3\uparrow \quad (2.4)$$

$$N_2H_4 + 4OH^- \rightarrow N_2\uparrow + 2H_2O + 4e^- \quad (2.5)$$

Overall Reaction

$$2Pd(NH_3)_4^{2+} + N_2H_4 + 4OH^- \rightarrow 2Pd + N_2 + 8NH_3 + H_2.O \quad (2.6)$$

Prior to plating, the sensitization and activation stepswere followed whose procedures are similar to those mentioned for nickel electroless plating. A palladium solution concentration

Table 2.4: Composition of Pd ELP baths for Pd-ceramic membrane fabrication.

S. No.	Component	Formula	Amount	Amount	Amount
1.	Palladium Chloride	$PdCl_2$	0.005 mol/L	0.01 mol/L	0.015mol/L
2.	Hydrazine Hydrate	$H_2NNH_2.H_2O$	40% excess	40% excess	40% excess
3.	Ethylene di-amine tetra acetic acid	Na_2EDTA	14.89 g/L	29.78 g/L	44.67 g/L
4.	Liquor Ammonia	$NH_3.H_2O$ (25%)	110ml/L	220ml/L	330ml/L

of 0.005M - 0.015M for SSOEP-DWR-BS baths was used in the present study.

2.6 Evaluation of support performance

Parameters involved for the evaluation of porous ceramic support properties include flux (J), average trans-membrane flux $\overline{J}$, average pore diameter (d_p) and effective porosity $\left(\frac{\varepsilon}{q^2}\right)$.

The nitrogen flux through the membrane (J) at varying pressure was evaluated from the volumetric flow rate data

$$J = \frac{Q}{A_m} \tag{2.7}$$

Where Q represents the volumetric flow rate in LPM, A_m the permeable area of the membrane in m^2 and J the flux through the membrane in $\left(\frac{mol}{m^2 s}\right)$

$$\overline{J} = \frac{\int_{P1}^{P2} JdP}{(P_2 - P_1)} \tag{2.8}$$

where $\bar{J}$ represents the average flux through the membrane, $\int_{P1}^{P2} JdP$ corresponds to the area under the curve of a plot between the membrane flux $\left(\frac{mol}{m^2 s}\right)$ and pressure (psi).The term (P_2-P_1) corresponds to the trans–membrane pressure drop. The average flux $\bar{J}$ was evaluated

using trapezoidal rule with obtained experimental data of $\bar{J}$ and (P_2-P_1). In the above equation, the trans-membrane pressure differential shall remain constant (10-50 psi) to maintain consistency in evaluating the average membrane flux.

Based on the gas permeation data, average pore diameter (d_p) and effective porosity $\left(\frac{\varepsilon}{q^2}\right)$ can be estimated according to the following expression (Vichaphund and Atong, 2010).

$$K_i^{cal} = \left(\frac{2.133}{2}\frac{d_p v}{l}\left(\frac{\varepsilon}{q^2}\right) + \frac{1.6}{4}\frac{d_p{}^2}{l\eta}\left(\frac{\varepsilon}{q^2}\right)\bar{P}\right)\frac{\Delta P}{P_2} \qquad (2.9)$$

Here, $\bar{P}$ is the average pressure on the membrane, v (m/s) is the molecular mean velocity of the gas, l (m) is the pore length, q is the tortuosity, η (Pa.s) is the viscosity of gas, and K (m/s) the effective permeability factor. The average pressure corresponds to the average of the inlet and outlet pressures of the membrane. Appendix A summarizes the details with respect to the evaluation of (d_p) and $\left(\frac{\varepsilon}{q^2}\right)$.

2.7 Evaluation of combinatorial plating characteristics for Ni membranes

Parameters involved for evaluating the performance assessment of nickel ELP process include average trans-membrane flux $\left(\bar{J}\right)$, plating efficiency $\left(\eta\right)$, average plating rate ($\bar{r}_i$), metal film thickness (δ) percent pore densification $\left(PPD\right)$ and bath conversion $\left(x\right)$.

Flux and average trans-membrane flux calculations were similar to that described in section 2.6.

Pore densification was defined as the fractional volume of the pores covered by the deposited metal and it was expressed as follows:

$$PPD_i = \frac{\overline{J_0} - \overline{J_i}}{\overline{J_0}} \times 100 \qquad (2.10)$$

where $\overline{J}_0$ represents the average flux through the support and $\overline{J}_i$ represents the average flux through the membrane after ith hour of nickel plating.

The theoretical nickel film thickness (δ) was evaluated as follows:

$$\delta = \frac{w_2 - w_1}{\rho_{Ni} A_m} \qquad (2.11)$$

where $\rho_{Ni}\left(\frac{g}{cm^3}\right)$ represents the density of nickel metal and $A_m(m^2)$ the membrane surface area for nitrogen permeation experiments. The theoretical metal film thickness was estimated using the density of dense nickel film. During ELP, the metal film density varies from that of the porous support to that of the dense nickel film. Since we intend to achieve dense metal composite membranes, the theoretical film thickness was evaluated using metal density and hence the obtained thickness values before dense membranes were achieved would be lower than those that existed. This is due to the fact that dense metal film density is always greater than that of the porous support density.

The plating rate $\overline{r}_i\left(\frac{mol}{m^2.s}\right)$ was evaluated as follows:

$$\overline{r_i} = \frac{w_2 - w_1}{M_{Ni} \times A_m \times t_i} \qquad (2.12)$$

where t_i corresponds to the time of plating for the ith hour.

The plating efficiency $\eta(\%)$ defined as the ratio of amount of metal deposited on the ceramic support to the amount of metal converted during the reaction and is evaluated as follows:

$$\eta = \frac{w_2 - w_1}{w_0 x} \times 100 \qquad (2.13)$$

where x corresponds to the conversion in the plating bath. Further, the inefficiency of the plating process was evaluated using the expression:

%inefficiency = 100 - η

The plating bath conversion (x) is defined as the ratio of the amount of metal ion reacted during the plating process to the amount of metal present initially in the plating solution and is expressed as

$$x = \frac{V_i C_i - V_f C_f}{V_i C_i} \tag{2.14}$$

The initial and final Ni solution concentrations were determined using the titration method. Further, details w.r.t. the titration method is presented in Appendix B of the thesis. Further, sample calculations of various parameters for one nickel membrane are presented in Appendix C.

2.8 Evaluation of combinatorial plating characteristics for Pd membranes

Parameters involved for evaluating the performance assessment of palladium plating include average trans-membrane flux $(\bar{J})$, plating efficiency (η) , average plating rate ($\bar{r}_i$), metal film thickness (δ), percent pore densification (PPD), bath conversion (x) and transport efficiency .

Apart from transport efficiency, all other calculations are similar to that described in section 2.6 and 2.7 respectively.

Further transport efficiency is defined as the product of plating efficiency and conversion of the plating bath expressed as:

Transport efficiency = η × x (2.15)

The initial and final Pd solution concentrations were determined using the atomic absorption spectroscopy (Make: M/S Varian BV, Model: Spectra AA 220FS) in the flame mode with a Pd lamp of wavelength 247.6 Å (Merdivan, 1997). A calibration curve was used to determine the unknown concentration of an element in a solution. Also, details w.r.t. the measurement is presented in Appendix D of the thesis. Further, sample calculations of various parameters for one palladiummembrane are presented in Appendix E.

2.9 Summary

The following sub-sections highlight a summary of identified and literature related compositions etc., that were adopted for the carried out research.

Support: The compositions were identified based on trial and error basis based on composition available in literature (Nandi et al., 2009; Vasanth et al., 2011)

Ni-CEP/SOEP/SIEP/SSOEP: Nickel and surfactant concentration were taken similar to that available in the literature (Bulasara et al., 2011a), reducing agent concentration (50-200% excess) were identified based on trial and error basis based on composition available in literature (Ilias et al., 2012 & Islam et al., 2012). Contacting patterns of surfactant and reducing agent (drop, bulk) were partly based on literature (Yeung et al., 1999) and partly from physical insights.

Pd-CEP/SIEP/SOEP/SSOEP: Palladium concentration lower than that reported in the literature (Islam et al.,2012) were taken , surfactant concentration based on literature (Islam et al.,2012; Chen et al., 2002), reducing agent concentration taken from literature contributed from our own research group (Pujari et al., 2014). Contacting patterns of surfactant and reducing agent (drop, bulk) were partly based on literature and partly from physical insights.

Based on extensive experimental investiations, membranes with diverse morphological properties and chemical constitution (Ni/Pd) were obtained. Table 2.5 presents a detailed summary of various cases considered in the carried out research study.

Table 2.5: A summary of various cases investigated in the thesis.

Membrane No.	Process	Metal		Reducing agent concentration (% excess)	Surfactant	
		Type	concentration (mol/L)		Type	concentration (CMC)
M_1	CEP-BR	Ni	0.08	100	CTAB	4
M_2	SOEP-BR	Ni	0.08	100	CTAB	4
M_3	SIEP-BR-BS	Ni	0.08	100	CTAB	4
M_4	SIEP-BR-BS + NaOH	Ni	0.08	100	CTAB	4
M_5	SOEP-BR + NaOH	Ni	0.08	100	CTAB	4
SM_1	SIEP-BR-BS	Ni	0.08	100	CTAB	4
SM_2	SIEP-DWR-BS	Ni	0.08	100	CTAB	4
SM_3	SIEP-DWR-BS	Ni	0.08	50	CTAB	4
SM_4	SIEP-DWR-BS	Ni	0.08	200	CTAB	4
SM_5	SIEP-DWR-BS	Ni	0.16	50	CTAB	4
SM_6	SIEP-DWR-BS	Ni	0.16	100	CTAB	4
SM_7	SIEP-DWR-BS	Ni	0.24	50	CTAB	4
SM_8	SIEP-DWR-BS	Ni	0.24	100	CTAB	4
SM_9	SIEP-DWR-DWS	Ni	0.08	100	CTAB	4
SSM_1	SSOEP-DWR-BS	Ni	0.08	100	CTAB	4
SSM_2	SSOEP-DWR-DWS	Ni	0.08	100	CTAB	4
SSM_3	SSOEP-DWR-BS	Ni	0.08	100	CTAB	1
SSM_4	SSOEP-DWR-BS	Ni	0.08	100	CTAB	2
SSM_5	SSOEP-DWR-BS	Ni	0.08	100	CTAB	6
SSM_6	SSOEP-DWR-BS	Ni	0.08	100	SDS	1
SSM_7	SSOEP-DWR-BS	Ni	0.08	100	SDS	2
SSM_8	SSOEP-DWR-BS	Ni	0.08	100	SDS	4
SSM_9	SSOEP-DWR-BS	Ni	0.08	100	SDS	6
PM_1	CEP-DWR	Pd	0.01	40	CTAB	2
PM_2	SOEP-DWR	Pd	0.01	40	CTAB	2
PM_3	SIEP-DWR-DWS	Pd	0.01	40	CTAB	2
PM_4	SSOEP-DWR-BS	Pd	0.01	40	CTAB	2
PM_5	SSOEP-DWR-BS	Pd	0.005	40	CTAB	2
PM_6	SSOEP-DWR-BS	Pd	0.015	40	CTAB	2

Combinatorial Performance Characteristics of Conventional, Surfactant and Sonication Induced Electroless Plating Baths

The results in this chapter are presented in various sections. Section 3.2 refers to the technical justification for the identified support pore morphology (50-70 nm). Section 3.3 elaborates on the surface treatment and surface characterization. Section 3.4 presents the optimal plating rate enhancement techniques for the fabrication of dense nickel composites. Finally the conclusions are presented in section 3.5.

3.1 Introduction

Considering nickel as the target plating metal, a conceptual research methodology has been outlined in this chapter that systematically addresses the experimental and theoretical insights for the realization of dense metal composite membranes. The laboratory fabricated porous supports were characterized with lower average pore size (50 - 70 nm) and lower effective porosity (1- 5%), so as to provide most challenging scenario for the plating processes towards maximum pore densification. Using the concept of lower gas transport resistance of the metal film with respect to the support, the next section elaborates upon the justification to select the support pore morphology (50 – 70 nm) for targeting dense metal composite membranes.

Five different membrane fabrication cases were focused for this work, which refer to membranes prepared with conventional electroless plating (M_1), sonication induced ELP (M_2), surfactant induced ELP (M_3), NaOH treated support and surfactant induced ELP (M_4) and NaOH treated support and sonication induced ELP (M_5) study. For the membranes M_1,

M_2, M_3, M_4 and M_5, achieved with conventional electroless plating (CEP), surfactant induced electroless plating (SIEP) and sonication induced electroless plating (SOEP), the bath temperature was maintained at 353K and the plating characteristics were investigated at a loading ratio of 203 $\frac{cm^2}{L}$.

Prior to plating, membranes M_4 and M_5 were pretreated. The pretreatment involved treatment using NaOH solution (pH 12) in a sonicator bath (Elmasonic, S30 H) under degas mode of continuous operation for six hours at the plating temperature. This modified the support morphology and the pore diameters increased from 50 – 70 nm to 90 – 120 nm respectively. However when sodium hydroxide treatment was carried without sonication and degas mode in a water bath maintained at 80^oC, the improvement in support morphology was not sufficient enough to avoid negative flux trends as discussed in subsequent sections. For all cases, membrane supports with similar average flux values were chosen to maintain coherence amongst various performance characteristics. All experimental investigations were carried for at least two samples to obtain average values and associated standard deviation.

3.2 Morphological fitness of the ceramic support

Using nickel as the electroless plated metal, the objective of this section was to provide insights in plating rate enhancement methods for contributing towards research in dense nickel composite membranes. This was also due to the fact that flux data for dense nickel membranes was not available in the literature. An important functional prerequisite for metal composite membrane was that the metal (Ni) film flux (H_2) shall always be lower than the porous support flux. Since nickel flux increased with temperature, maximum nickel flux was achieved at the highest possible operation temperature and minimal metal thickness. For the present case, these values were assumed to be 550 ^oC and 1 μm respectively. The model

based maximum hydrogen flux achievable through the dense Ni film was evaluated using the expression:

$$J_{H2}^{\mathrm{mod}} = \frac{Perm_{lit}}{\delta_{ass}} \times \delta_{lit} \times A_m \times (P_{ret}^{n'} - P_{per}^{n'}) \tag{3.1}$$

Where $Perm_{lit}$ and δ_{lit} correspond to the theoretical dense Ni film permeability and thickness in the composite membrane. The dense nickel film permeability was estimated using the expression (Altunoglu and Abdulkadir, 1994):

$$Perm_{lit} = 3.35 \times 10^{-7} \exp\left(\frac{-54.25 \times 10^3}{RT}\right) \tag{3.2}$$

Assuming a combination of Knudsen and viscous diffusion, for a given membrane morphological parametric combination of d_p and $\left(\frac{\varepsilon}{q^2}\right)$, the average hydrogen flux through the porous support was evaluated using the expression:

$$J_{H_2}^{\mathrm{sup}} = \left(\frac{2.133}{2}\frac{d_p v}{l}\left(\frac{\varepsilon}{q^2}\right) + \frac{1.6}{4}\frac{d_p^{\,2}}{l\eta}\left(\frac{\varepsilon}{q^2}\right)\overline{P}\right)\frac{\Delta P}{P_2} \tag{3.3}$$

Assuming that the metal ceramic composite membrane was feasible only when the metal film flux was at least 10 % lower than that of the support hydrogen flux, an inequality constraint needs to be satisfied and which was expressed as:

$$\frac{\left(J_{H2}^{\mathrm{sup}} - J_{H2}^{\mathrm{mod}}\right)}{J_{H2}^{\mathrm{sup}}} \times 100 \geq 10 \cdots\cdots \forall \Delta P \tag{3.4}$$

To validate the above system of equations in a systematic format, a simple procedure was followed to evaluate the feasibility of the support morphology:

(i) Using Eq. (1), determine $J_{H_2}^{\mathrm{mod}}$ vs. ΔP data for assumed membrane parameters from the literature.

(ii) Using Nitrogen gas as the transport gas, conduct single gas permeation experiments and obtain $J^{sup}_{N_2}$ (experiment) vs. ΔP. Using the experimental data and eq. (3), determine membrane morphological parameters experimentally (d_p^{sup} and $\left(\frac{\varepsilon}{q^2}\right)$)

(iii) For a specified value of d_p^{sup} or $\left(\frac{\varepsilon}{q^2}\right)$, determine the minimum value of $\left(\frac{\varepsilon}{q^2}\right)^{min}$ or d_p^{min} to satisfy the following optimization problem defined in terms of dense Ni film and support hydrogen flux:

$$
\begin{aligned}
&Min = \sum_{i=1}^{\Delta P\max} E_i \\
&E_i = \frac{\left(J_{Ni_{H_2}} - J_{\sup_{H_2}}\right)}{J_{Ni_{H_2}}} \times 100 \\
&J_{H2}^{\mathrm{mod}} = \frac{Perm_{lit}}{\delta_{ass}} \times \delta_{lit} \times A_m \times (P_{ret}^{n'} - P_{per}^{n'}) \\
&J_{H_2}^{sup} = \left(\frac{2.133}{2} \frac{d_p v}{l} \left(\frac{\varepsilon}{q^2}\right) + \frac{1.6}{4} \frac{d_p^{\,2}}{l\eta} \left(\frac{\varepsilon}{q^2}\right) \overline{P} \right) \frac{\Delta P}{P_2} \\
&E_i \geq 10 \ \ \forall\, i \\
&0 \leq \left(\frac{\varepsilon}{q^2}\right)_{\sup}^{th} \leq 1 \ \text{(OR)} \ d_p^{\,min} \geq 0
\end{aligned}
\tag{3.5}
$$

(iv) The support morphological parameters were regarded to be feasible for plating after either one of the following two constraints were satisfied:

$$
\begin{aligned}
&d_p^{sup} \geq d_p^{min} \\
&\quad \text{OR} \\
&\left(\frac{\varepsilon}{q^2}\right)^{sup} \geq \left(\frac{\varepsilon}{q^2}\right)^{min}
\end{aligned}
\tag{3.6}
$$

Based on our research a case study was presented below to illustrate the above procedure. For an assumed Ni film thickness of $5\,\mu m$, and an evaluated dense Ni film permeability of

$1.207\times10^{-10}\ \frac{mol.m}{m^2.s.Pa^{0.5}}$ (Altunoglu and Abdulkadir, 1994), the theoretical Ni dense film hydrogen flow rate varied from $4.81\times10^{-4}-2.02\times10^{-2}\ \frac{lit}{\min}$ for a trans-membrane pressure difference of 0.1-10 atm. The room temperature N_2 permeation data for the support varied from $4.81\times10^{-4}-2.02\times10^{-2}\ \frac{lit}{\min}$ for a trans-membrane pressure difference variation from 0.1 – 10 atm. Calculations using the N_2 gas permeation data at room temperature indicated that the membrane morphological parametric values were $d_p^{\sup}=57\,\text{nm}$ and $\left(\frac{\varepsilon}{q^2}\right)^{\sup}=0.012$. Assuming $d_p^{\exp}$ as $d_p^{\mod}$, the solution of the optimization model (Eq. (4)) inferred that $\left(\frac{\varepsilon}{q^2}\right)^{\min}=0.003063$, which was lower than the value obtained from experimental data i.e., $\left(\frac{\varepsilon}{q^2}\right)^{\sup}$ = 0.012. Thus, the support morphology can be considered to be feasible for proceeding towards electroless plating related research.

3.3 Feasibility tradeoffs

In the previous section, it has been confirmed that the support morphology ($d_p^{\sup}=57$ nm and $\left(\frac{\varepsilon}{q^2}\right)^{\sup}$ = 0.012) is feasible to serve as a membrane for a dense Ni film thickness of 5 μm. In this section tradeoffs associated to variations in dense metal film thickness have been explored.

Fig. 3.1 presents the nitrogen flux profiles for various combinations of average membrane pore size and effective porosity for various cases. As shown, for a nickel dense film thickness

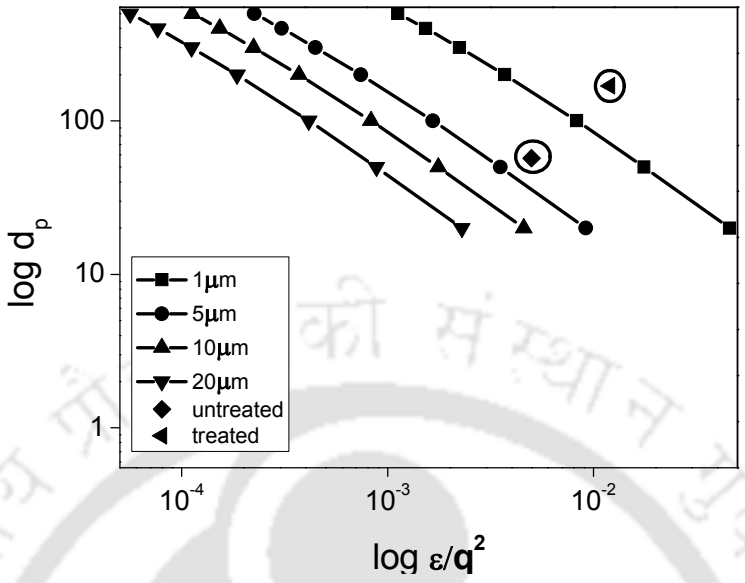

Fig. 3.1: Tradeoff plot for ceramic support compatibility.

of 1 μm, the feasible combinations of porosity $\left(\left(\frac{\varepsilon}{q^2}\right)^{\min}\right)$ varied from $4.5\times10^{-2} - 1.1\times10^{-3}$ for pore diameter (d_p) variation from 20 – 500 nm respectively. However, when the nickel film thickness was enhanced five fold (to 5 μm), $\left(\frac{\varepsilon}{q^2}\right)^{\min}$ varied from $9.1\times10^{-3} - 2.2\times10^{-4}$ for d_p variation from 20 – 500 nm. For a film thickness of 10 μm, $\left(\frac{\varepsilon}{q^2}\right)^{\min}$ varied from $4.5\times10^{-3} - 1.1\times10^{-4}$ for d_p variation from 20 – 500 nm and for a film thickness of 20 μm, $\left(\frac{\varepsilon}{q^2}\right)^{\min}$ varied from $2.2\times10^{-3} - 5.6\times10^{-5}$ for d_p variation from 20 – 500 nm respectively.

As shown in the figure, the obtained membrane morphological parameters ($d_p^{\sup} = 57$ nm and $\left(\frac{\varepsilon}{q^2}\right)^{\sup}$ = 0.012) indicated that the raw support was feasible for a desired minimal dense nickel film thickness of 1 μm and the treated support was feasible for a desired minimal

dense nickel film thickness of 5 μm . These theoretical deductions indicated that irrespective of the fabrication method, the supports were feasible for very low values of dense metal film thickness on the supports (1-5 µm). These thickness values are very difficult to achieve using conventional and rate enhanced metal ELP processes for specified morphologies.

3.4 Surface characterization

3.4.1 LPSA analysis

The major raw materials i.e., kaolin, quartz, feldspar, sodium carbonate and pyrophylite used to fabricate ceramic membrane were characterized using laser particle size analyzer. Fig. 3.2 presents the particle size distribution of the raw material. It was evaluated that the average particle size of kaolin, quartz, feldspar, sodium carbonate and pyrophylite were 5.50 µm, 7.72 µm, 3.46 µm, 7.59 µm and 20.36 µm respectively.

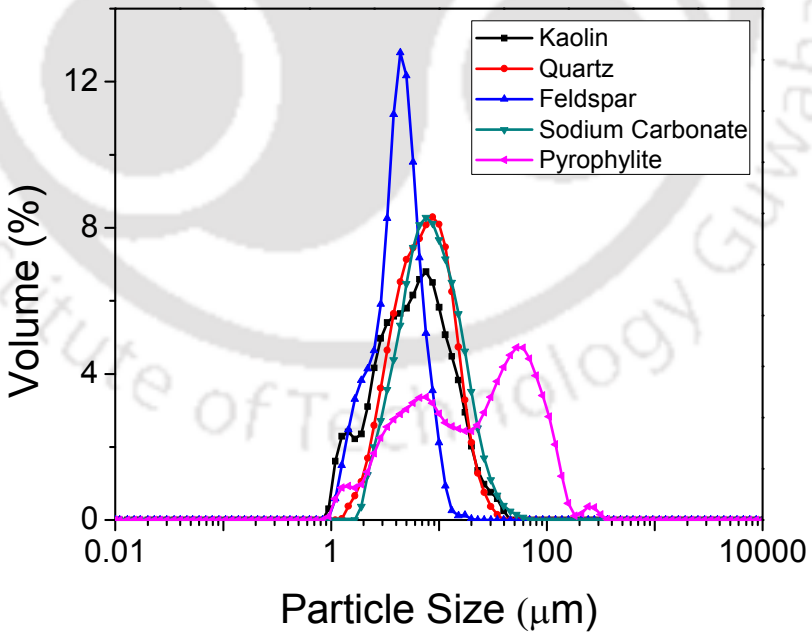

Fig. 3.2: Particle size distribution of inorganic membrane precursors.

3.4.2 BET analysis

The BET surface area and pore size of the support material was determined by N_2 adsorption desorption isotherm at 77K by using a surface area analyzer. Prior to measurement, the samples were degassed at 200 ^oC in vacuum for 60 minutes. The adsorption/desorption isotherms of the support material is shown in Fig. 3.3(a). The isotherms are of type III and H_3 hysteresis loop can be observed. This indicates slit-shaped pores according to IUPAC (Sing et al., 1985). Based on BET, the pore size distribution as a function of volume percentage of pores of the support is shown in Fig. 3.3(b). The average pore size as evaluated from Barrett-Joyner-Halenda (BJH) pore volume distribution was found to be 35 nm which was in agreement to that evaluated from nitrogen permeation (50-70 nm).The BET surface area of support was 2.712 m^2/g and total pore volume was 0.0156 ml/g with no micropore volume.

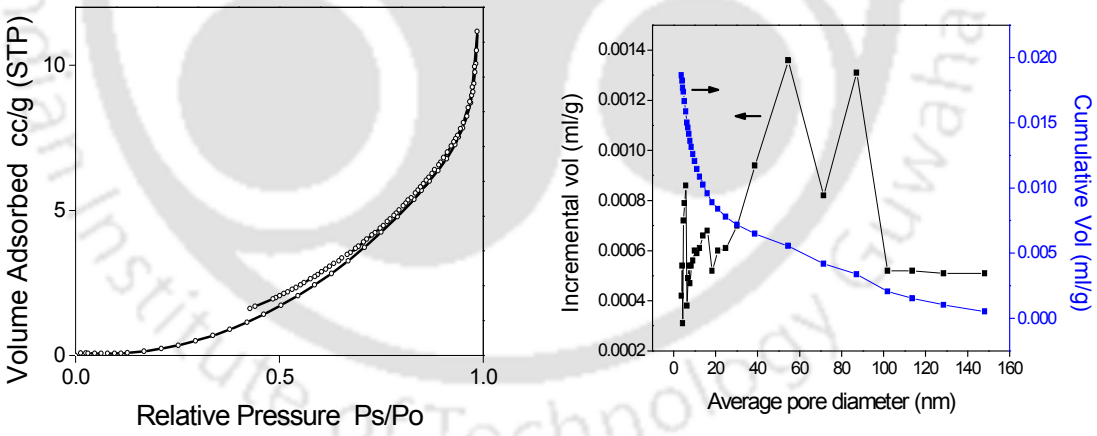

(a) (b)

Fig. 3.3: (a) Nitrogen adsorption/desorption isotherm and (b) Pore size distribution of the ceramic support.

3.4.3 FTIR analysis

The fourier transform infrared spectra recorded from wave number 4000 to 500 cm^{-1} using IR Affinity–1 spectrometer is shown in Fig. 3.4. Characteristic peaks of kaolin were observed at 3668 cm^{-1} corresponding to the OH- stretching vibration for the raw material. After sintering of the raw material mixture at 900 °C for 4 h, the OH^- vibration peaks at 3668 cm^{-1} decreased suggesting that the calcination of kaolin to calcined kaolin was not complete (Granizo et al., 2007). Bands at 2920 cm^{-1} were assigned to C-H bonds which were visible only after sintering and peak at 1658 cm^{-1} was attibuted to C=C bonds. Further H_2O stretching was seen at 1658 cm^{-1} for the raw material which disappeared after sintering. Bands at 1041 cm^{-1} and 983 cm^{-1} were assigned to Si-O bonds. Absorption at 486 cm^{-1} was assigned to Si-O-Al (Jaarsveld et al., 2002).

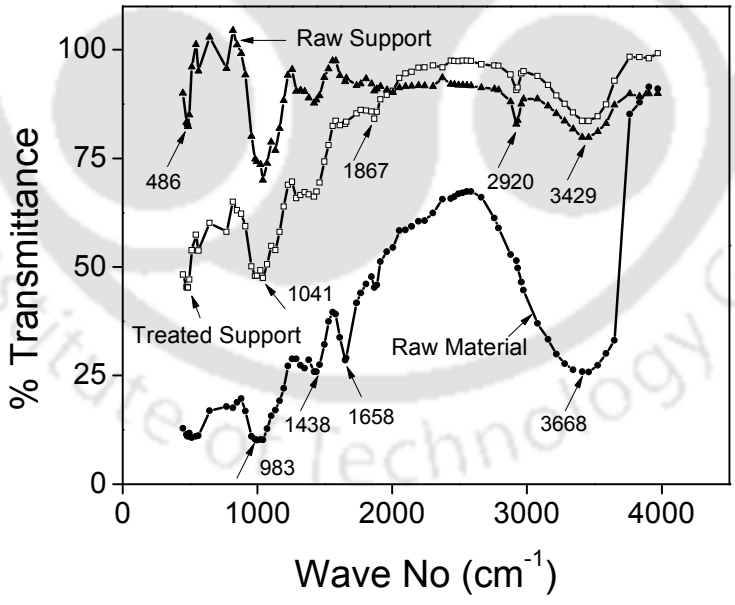

Fig. 3.4: FTIR spectra of inorganic precursors, raw support and treated support.

3.4.4 XRD analysis

The X-ray diffractograms were recorded by a Bucker X-ray D8 advance diffractrometer with a Cu-Kα radiation (λ=1.54056) at 45 KV and 40 mA respectively with scan rate of $0.5\,\mathrm{sec.step}^{-1}$ and increment of 0.05. The X-ray diffractograms were collected in the range of $5-75^{o}$. Phase analyses of the diffraction profiles were done using ICDD-JCPDS database and the crystallite size of the samples were calculated using Scherer's formula: $d=\frac{0.9\lambda}{\beta\cos\theta}$ where d signifies the crystallite size, λ refers to the wavelength of radiation (λ= 1.54056), β refers to the full width of half-maximum intensity of corrected peak and θ the peak position.

Fig. 3.5(a) presents the XRD patterns of raw material mixture, sintered raw support and sintered treated support. The phases for kaolin, quartz and sodium carbonate appeared in the raw material mixture. It was observed that the peak intensity of the main intense peak of quartz (2θ = 26.75^{o}) significantly increased with sintering, thereby indicating that the crystalinity of the quartz increased as compared to raw material, which was further more significant after NaOH treatment. The XRD pattern clearly indicated that NaOH treatment played a vital role in increasing the crystalinity of quartz and thereby enhanced the porosity of the membrane. Further, upon sintering, it was observed that due to the transformation of kaolinite to metakaolinite the peak corresponding to kaolin disappeared (Vasanth et al., 2011) and that corresponding to sodium carbonate disappeared due to thermal decomposition. The new phase that appeared in the XRD pattern on sintering was nephiline (Na_2O, Al_2O_3, $2SiO_2$) which was produced by the reaction of sodium oxide (Na_2O) and metakaolinite at a temperature of 800^{o}C (Wang et al., 1994).

Fig. 3.5(b) presents the XRD pattern of Ni plated membrane and clearly indicates nickel peaks. The metallic nickel peaks appeared at diffraction angle 2θ = 44.6^{o} and 52 ^{o} due to the

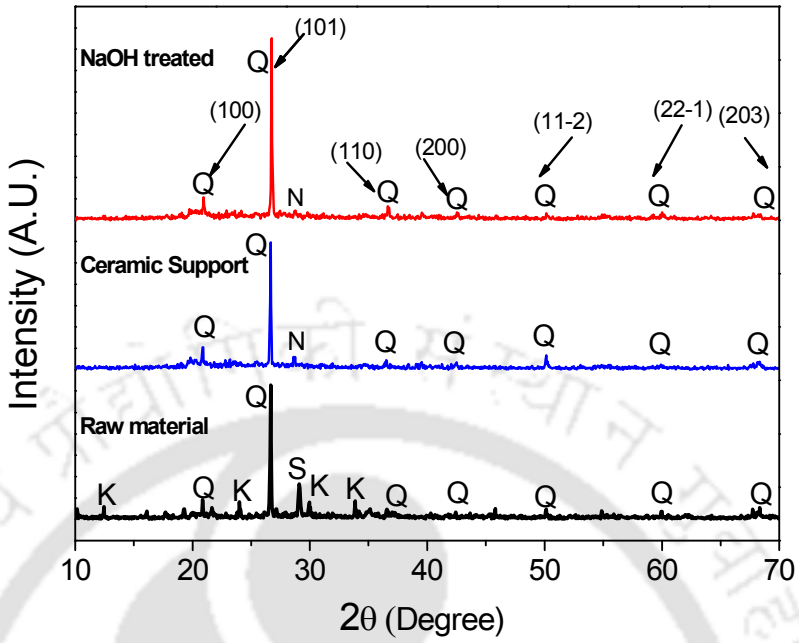

(a)

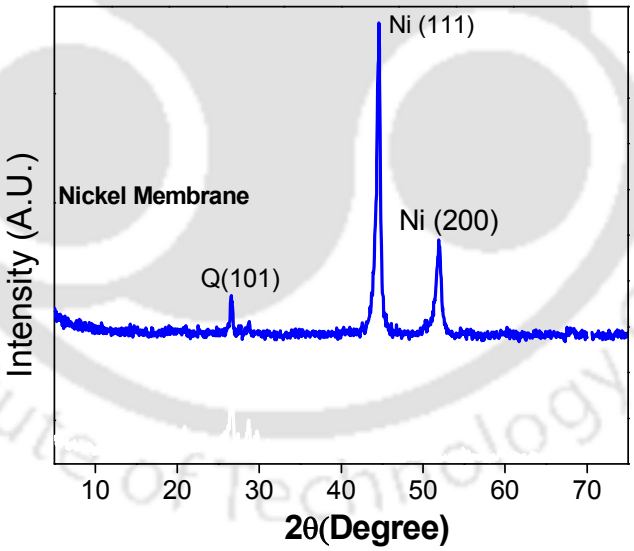

(b)

Fig. 3.5: XRD patterns of (a) inorganic precursor mixture, raw support and treated support (b) Ni-ceramic membrane.

diffraction of (111) and (200) plane [Pdf No 00-001-1260] along with the quartz peaks. It was observed that the peak intensity of quartz significantly decreased after nickel deposition due to plating of nickel on quartz particle thereby reducing the crystalinity of the quartz. The crystal size of the support was calculated based on the maximum intense peak of the pattern ($2\theta = 26.75^{o}$) and was observed to be 30 nm.

3.4.5 FESEM analysis

The surface characterization was also carried out by FESEM. Fig. 3.6 presents the surface FESEM micrographs of the ceramic treated support and SIEP nickel layer deposited with an initial nickel sulfate concentration (C_i) of $0.08\left(\frac{mol}{L}\right)$. It can be observed that well-developed nickel layers were existent for the membrane. Based on the analysis of the FESEM image using ImageJ software, it was observed that the pores were distributed over wider pore size values. The average pore size of the treated support with ImageJ software was found to be 140 nm which was in agreement to that evaluated from nitrogen permeation experiments (90 - 120 nm).

3.5 Synchronity for nickel plating

3.5.1 Average flux profiles

Fig. 3.7 represents the variation in N_2 flux with variation in plating time. The average flux reduced from $5.6\times10^{-2}-5.5\times10^{-3}\left(\frac{mol}{m^2 s}\right)$ in 64 h for M_1 (CEP), $4.1\times10^{-2}-2.1\times10^{-2}\left(\frac{mol}{m^2 s}\right)$ in 24 h for M_2 (SOEP), $3.0\times10^{-2}-1.5\times10^{-3}\left(\frac{mol}{m^2 s}\right)$ in 24 h for M_3 (SIEP), $1.8\times10^{-1}-2.4\times10^{-4}\left(\frac{mol}{m^2 s}\right)$ in 32 h for M_4 (SIEP) and $2.2\times10^{-1}-3.6\times10^{-2}\left(\frac{mol}{m^2 s}\right)$ in 24 h for

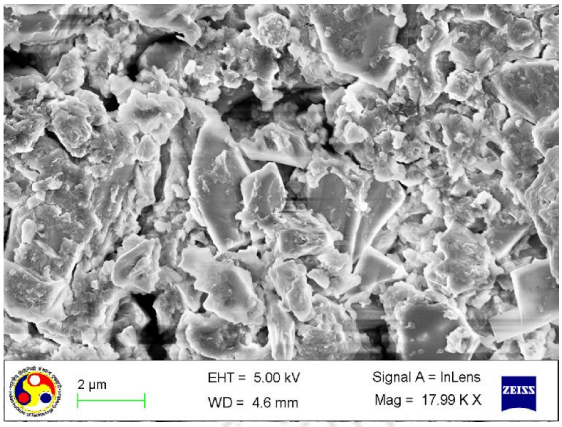

(a)

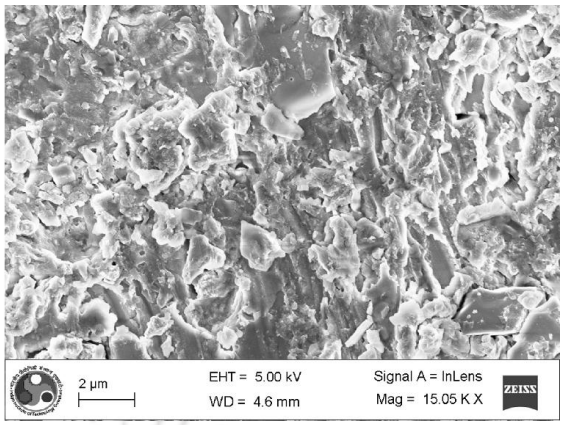

(b)

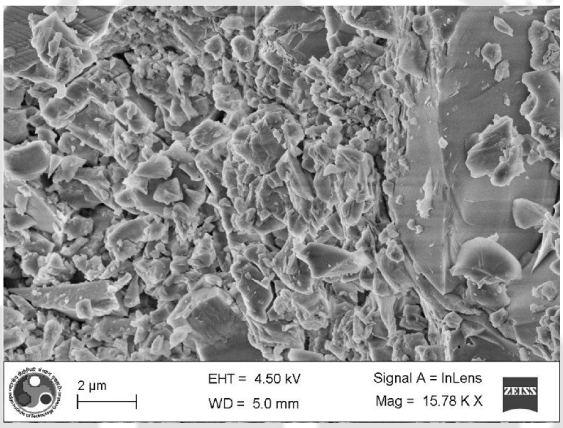

(c)

Fig. 3.6: Surface FESEM micrographs of (a) NaOH treated ceramic support (b) Nickel membrane fabricated with SIEP process (M_4) (c) Nickel membrane fabricated with SOEP process (M_5).

M_5 (SOEP) respectively. It had been evaluated that for membranes M_1 (CEP), M_2 (SOEP) and M_3 (SIEP), the initial plating steps enhanced the average membrane flux. This indicated that for these membranes, morphological modifications (opening of voids/pores) were dominant as compared to metal deposition inside the porous structure. Eventually with increment in plating hours it was observed that morphological modifications became minimal

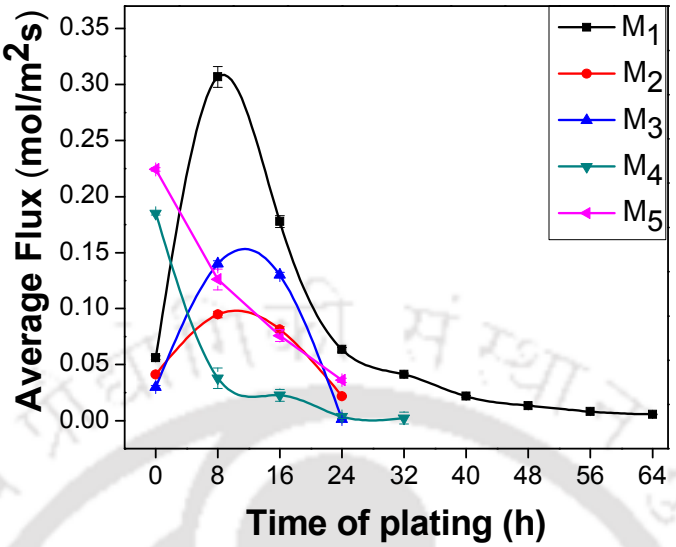

Fig. 3.7: Variation of average flux with time of plating for M_1-M_5 membranes.

and pore densification gradually improved. Further, for the pretreated membrane M_4 (SIEP), it was observed that after 24 h of plating the ratio of initial flux to the final flux was around 48.8 which were quite higher than the value obtained for M_5 membrane (6.2). This confirmed that SIEP reduced the flux six times faster than the SOEP process for the pretreated membranes. For the membrane M_1 fabricated with CEP, the flux reduced 10 times only after 64 h of plating and was therefore not competitive. Therefore, the coupling of rate enhancement techniques is justified for Ni ELP process. Further plating was terminated when (a) saturation was observed in the flux trends and (b) fluxes were very low compared to that of the support and (c) metal layering was dominating in comparison with pore densification.

The preliminary time dependent enhancement in average membrane flux followed with its reduction for membranes M_1, M_2 and M_3 clearly depicted that the low cost ceramic supports were not compatible for Ni ELP processes. Therefore, the supports required further treatment to make them compatible. They did not have good corrosion resistance to withstand the

strong basic environment that existed in Ni ELP baths for prolonged plating times. Therefore, there was a significant enhancement in N_2 flux values. Other than this, it is also apparent that Ni ELP was very difficult for membranes with lower pore size and lower porosity. Hence, it is very important that the physical bonding of Ni to ceramic structure is a strong function of its morphological properties such as pore size and porosity. Therefore, the NaOH pretreatment was regarded to be a viable option to make the supports feasible for low cost metal ceramic composite membrane fabrication.

3.5.2 PPD profiles

Fig. 3.8 presents the time dependency of percent pore densification for various cases. *PPD* values varied from 0 – 90% in 64 h for M_1 (CEP) , 0 – 46.7 % in 24h for M_2 (SOEP) , 0 – 95 % in 24 h for M_3 (SIEP), 0 – 98.7 % in 32 h for M_4 (SIEP) and 0 – 83.9 % in 24 h for M_5 (SOEP). Further the *PPD* values for M_1 after 24 h was observed to be negative (-12.82%) indicating clearly that the membrane healing process was too slow with CEP. This was also

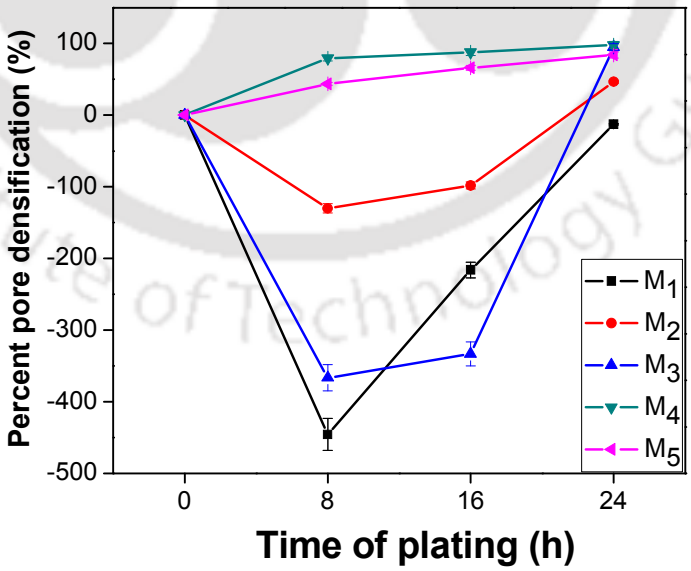

Fig. 3.8: Variation of PPD with time of plating for M_1-M_5 membranes.

an indication to the fact that the rate of pore opening was faster than the rate of pore densification. However, this was not the case for membranes M_2 and M_3 where SOEP and SIEP processes not only repaired the damage morphologies but also densified the membranes. From process perspective, it was inferred that surfactant was the only choice that could give a PPD of 90+% in 24 h even for a support that underwent surface and pore modifications (e.g. M_3). Further, it was also analyzed that for membrane M_4, the PPD was 98% after 24h and further 8h of plating increased the PPD to only 98.7%. This was an clear indication to the fact that PPD profiles reached saturation and process modifications would be further required to achieve 100 % PPD. Even for the untreated supports for the same time of plating (24h), SIEP (M_3) reduced the PPD twice as faster as compared to SOEP (M_2). Thus it can be inferred that surfactant played an important role in reducing the average flux through the membrane and served better than sonication in achieving pore densification.

3.5.3 Average plating rate profiles

Fig. 3.9 presents the variation in average plating rate with plating time for various cases. It was analyzed that the plating rates varied from $0.43 - 2.07 \times 10^{-5}$ $\left(\frac{mol}{m^2.s}\right)$ in 64 h for M_1 (CEP) , $3.14 - 3.60 \times 10^{-5}$ $\left(\frac{mol}{m^2.s}\right)$ in 24 h for M_2 (SOEP) , $1.98 - 2.12 \times 10^{-5}$ $\left(\frac{mol}{m^2.s}\right)$ in 24h for M_3 (SIEP), $2.25 - 2.6 \times 10^{-5}$ $\left(\frac{mol}{m^2.s}\right)$ in 32 h for M_4 (SIEP) and $5.23 - 4.31 \times 10^{-5}$ $\left(\frac{mol}{m^2.s}\right)$ in 24 h for M_5 (SOEP). For various cases, the ratios of plating rates with respect to the CEP process (base case), are presented in Table 3.1. From the data, it was analyzed that for both the cases of treated (M_5) and untreated supports (M_2), SOEP membranes gave higher plating rate when compared to both CEP and SIEP. Thus the data trends were comparable to Wu et al. (2009) who inferred that introduction of ultrasonic waves during electroless nickel

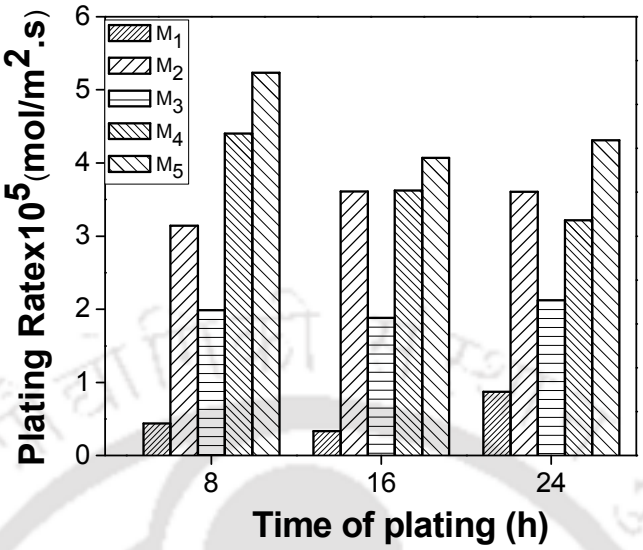

Fig. 3.9: Variation of average plating rate with time of plating for M_1-M_5 membranes.

deposition would enhance the plating rate. Further Lu et al. (2010) hypothesized that agitation generated from the ultrasonic waves resulted in high quality of metal deposition. Ceramic supports provided lower plating rates as compared to stainless steel supports. As compared to Bulasara et al. (2011d) who reported a CEP rate of 1.51×10^{-6} - 9.79×10^{-6} $\left(\frac{mol}{L.s}\right)$ for an average pore size of 275 nm, porosity of 0.44 and varying stirrer speed, our work indicated a lower volumetric plating rate of 6.65×10^{-9} $\left(\frac{mol}{L.s}\right)$ [2.19×10^{-5} $\left(\frac{mol}{m^2.s}\right)$].Therefore, it was inferred that plating rate was strongly influenced with average pore size and porosity and hence plating rate enhancement techniques became predominantly significant to influence the quality of plating characteristic for the supports considered for this work.

Experimentally, it was reported that the plating rate and the quality of plating was optimal for

Table 3.1: Ratios of average Ni plating rate of various ELP baths with respect to CEP bath.

Type of plating	Ratio of plating rates w.r.t to CEP*		
	8h	**16h**	**24h**
SOEP (M_2)	9.97	6.18	3.82
SIEP(M_3)	6.31	3.22	2.25
SIEP(M_4)	13.98	6.21	3.41
SOEP(M_5)	16.62	6.97	4.58

*Starting for CEP baths taken as 40 h.

supports with in the pore size of 250 – 300 nm and porosity of 35 – 50 % (Kitiwan and Atong, 2010). On the other hand, a support with higher pore size and porosity required thicker dense metal films to achieve dense composite membranes (Mardilovich et al., 2002) with good adhesion strength.

Therefore, the metal densification perspective shall not only be regarded from the perspective of only achieving thin dense metal film thickness, as the mechanical strength of the film was also of paramount importance. Therefore, further research was required to identify optimal membrane pore size and porosity values that enabled achieving stable dense metal films on the surface. Nonetheless, the role of plating rate enhancement techniques to alter the strength related properties could not be ignored in this context. The evaluated trends of metal film densification indicated that for support surfaces with poor morphological properties, SIEP was the best choice to achieve dense membranes and further research needs to address other issues related to SIEP.

3.5.4 Theoretical metal film thickness profiles

Fig. 3.10 illustrates the variation in theoretical Ni film thickness with plating time. For all membranes, the metal film thickness values evaluation was erroneous due to lack of measurement of porosity and weight loss during insitu pretreatment. It was analyzed that for 8-24 h of nickel plating, the metal film thickness increased from 0.82 - 4.96 μm for M_1 (CEP), 5.96 - 20.53 μm for M_2 (SOEP), 3.77 – 12.10 μm for M_3 (SIEP), 8.36 – 18.31 μm for M_4 (SIEP) and 9.93- 24.57 μm for M_5 (SOEP). Further, it was evaluated that the nickel film plating rate was $1.04\ \frac{\mu m}{h}$ for the SIEP baths which was 10 times higher than the value obtained for CEP baths ($0.1\ \frac{\mu m}{h}$). Subsequently, it was observed that the nickel film plating rate was $1.24\ \frac{\mu m}{h}$ for the sonication assisted baths. Literature indicated that the

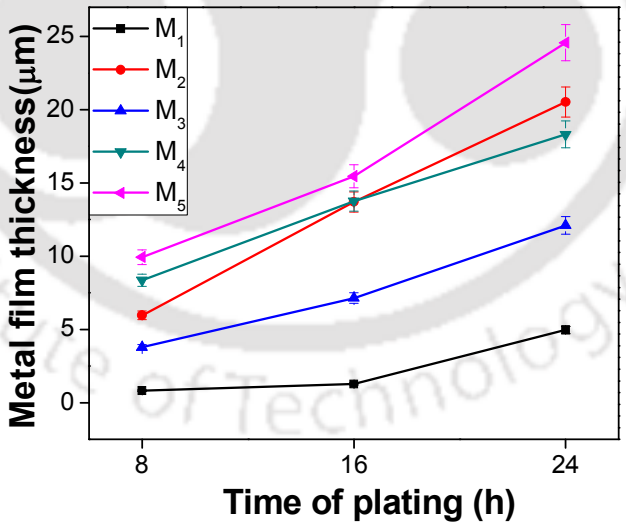

Fig. 3.10: Variation of theoretical Ni film thickness with time of plating for M_1-M_5 membranes.

corresponding plating rates for a macroporous support were 1.9, 1.75 and $3.13\frac{\mu m}{h}$ for CEP, SIEP and SOEP respectively (Bulasara et al., 2012; Bulasara et al., 2011c). Once again it was observed that the significant reduction in plating rate was due to poor morphology of the support which served as a bias to choose the most competent plating rate enhancement towards maximum pore densification purpose. Thus sonication resulted in tremendous increase in film thickness due to simultaneous increase in both deposition rate and plating efficiency for both treated and untreated supports. These observations were in agreement with Kathirgamanathan (1994) who concluded that sonication enhanced metal deposition and improved adhesion of the metal to the membrane surface. Similar conclusions were inferred by Ilias et al. (2012) who conveyed that surfactant utilization in ELP reduces the plating time required to obtain same thickness obtained with CEP process. Further, Chen et al. (2002) also concluded that the addition of surfactant not only increased the deposition rate but also diminished pitting on the electroless deposits.

3.5.5 Metal conversion and plating efficiency profiles

For a solution concentration of $0.08\left(\frac{mol}{L}\right)$, nickel conversion values varied from 2.8 - 7.7% for the SIEP case. However, for SOEP, slightly higher conversion values of about 5.29 – 10% were achieved. Similarly, the plating efficiencies trends varied from 35 – 76% for SIEP and 72 - 92.8% for SOEP respectively. For the untreated supports, very low plating efficiency values (13 – 46%) were evaluated for the CEP case in comparison with the SIEP case (29 – 60%). The possible reason for significantly lower values for conversion and plating efficiency for CEP indicates significant metal deposition on the beaker surface or in the plating solution. Overall, the evaluated conversion profiles referred to lower conversions

which was probably due to lower surface area of the membrane and hence lesser opportunities for noble metal activation during seeding.

Bulasara et al. (2012) concluded that conversion profiles for sonication assisted baths (33.5 – 80%) were better than the base case (17.5 – 54 %) as well as stirring (24–58.5 %) for a loading ratio of 393 $\frac{cm^2}{L}$. Their work further conveyed that sonication assisted baths provide better conversion profiles than surfactant assisted baths even for very small pore size supports. This work was also in agreement to the work of Bulasara et al. (2012) which confirmed that higher plating efficiencies exist for sonication assisted baths because of the fact that ultrasonic waves enhance the rate of electroless plating process.

3.5.6 Efficacy of rate enhancement techniques

Fig. 3.11 presents the time dependent variation of (100 - PPD) and $\frac{PPD}{\delta}$ values for nickel composite membrane fabricated by various rate enhancement techniques. The graph corresponds to conceptual extensions of the measured data to visualize the extent of pore densification (x-axis) with respect to the amount of metal required to densify the pores (y-axis). Conceptually, an ideal electroless plating process supplemented with optimal rate enhancement technique should achieve maximum $\frac{PPD}{\delta}$ and minimal (100 - PPD) values and therefore should refer to the values closely located to upper portions of the y-axis. From the figure, it was observed that PPD values varied from 26-90 % and from 2.2 - 2.86 in 32 – 64 h of rigorous plating experimentation for M_1. Further, PPD and $\frac{PPD}{\delta}$ values varied from 34.9 - 83.9 % and 3.5 - 4.7 for M_5 after 24 h of sequential plating. However, for the same time of plating, PPD and $\frac{PPD}{\delta}$ values varied from 24 – 98 % and 11.2 – 5.35 were for the surfactant

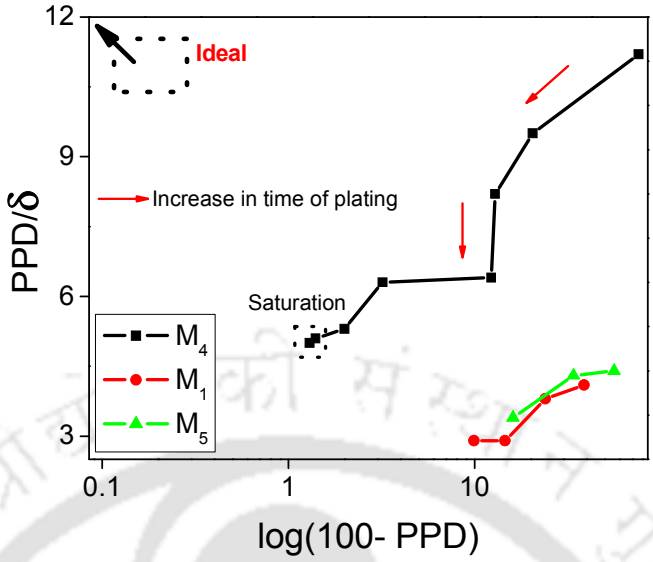

Fig. 3.11: Tradeoffs for $\frac{PPD}{\delta}$ Vs (100- PPD).

assisted baths (M_4). Therefore, from membrane pore densification perspective, surfactant induced electroless plating (SIEP) yielded the best possible conditions of nickel metal deposition on the membrane surface and corresponded to a combinatorial performance characteristics of 98.7% PPD and 4.98 $\frac{PPD}{\delta}$ for a nickel composite membrane with a film thickness (δ) of 19.82 μm after 32h of sequential Ni ELP. Further, it was observed that there exists a saturation point for membrane M_4, as there was no significant improvement in the PPD value (from 98 to 98.7%) from 24 to 32 h of sequential deposition. The saturation phase in the plating period was represented by a sharp reduction in the length of the consecutive points. However, the case did not correspond to 100% saturation, which should have been indicated by a vertical straight line in the graph. Since PPD could not be altered much with the prevalent conditions. This is an interesting issue for further research into the role of solution concentrations (metal or reducing agent concentration or both) and their mode of contacting. These variations in the PPD saturation phase and process parameters are

hypothesized to ensure 100% pore densification.

If we consider the case which has comparatively higher values of PPD and lower time of plating, the only feasible option corresponds to surfactant induced electroless plating (M_4). A PPD value of about 98% along with the experimental inference of porous membranes presumably indicated that the utilization of supports with lower surface pore sizes could yield a dense nickel–ceramic composite membrane in about 24 – 32 h of sequential electroless plating steps at lower metal concentration $\left(0.08\,\frac{mol}{L}\right)$. Further it can be stated that although sonication improved the plating rate and film thickness, it did not provide significant pore size reduction as compared to surfactant induced electroless plating.

The efficient design of electroless plating process needs to maximize percent pore densification (PPD) and minimize the metal film thickness (δ). This work also recognized the immediate need to identify suitable rate enhanced electroless plating processes that could provide good combinations of PPD and film thickness (δ). The approach presented in this work could be used as a new methodology for the assessment of nickel electroless plating baths with variant morphological parameters and conditions of operations.

This work gave many important conclusions. Firstly, surfactant had been identified to be effective to enhance the PPD values significantly close to 100 %. It was in agreement with the trends presented by Islam et al. (2012) who inferred that dense and thinner films could be produced with shorter deposition time using SIEP process. A possible reason for not achieving 100 % PPD was that beyond a particular point the solution concentration imposes limitation on the quality of plating.

3.6 Summary

This chapter presented an integrated experimental and theoretical approach for the development of compatible functional supports towards dense metal ceramic composite membrane fabrication. The challenging scenario of this study was to work with laboratory fabricated supports that are characterized with lower combinations of average pore size and effective porosity. For such supports, etching in alkaline medium served to be favorable in terms of compatibility of the support and corrosion resistance. NaOH treatment prior to plating enabled enlargement of the membrane pores to its target diameter such that the early plating steps does not serve as a treatment steps for the supports. Further, XRD patterns clearly indicated that NaOH treatment increased the crystalinity of the raw materials thereby enhancing the pore size and porosity of the membrane. Moreover, the morphological fitness of the ceramic support clearly indicated that the supports were feasible for very low values of dense metal film thickness irrespective of the fabrication technique. The fabricated nickel composite membranes were anticipated to serve as functional supports for dense palladium membranes. A tentative combination of optimal support morphological properties and optimal electroless plating process as highlighted in this article would be useful to serve as a guideline for the realization of low cost multi - metal composite membranes. Further this work involved a preliminary study of various plating rate enhancement techniques that could be supplemented to electroless plating process for the fabrication of dense metal composite membranes. Most importantly, this work enabled to realize that sonication did not contribute to 100 % pore densification for the chosen support, even though they contributed to enhance efficient nickel deposition rate substantially. In this work, average time dependent performance of electroless plating baths for nickel–ceramic composite membrane fabrication was reported which would promote further insights in the metal deposition characteristics such as variation in metal film thickness, PPD and average pore size with time of deposition.

Thereby, this work featured the minimal number of plating steps required to achieve desired membrane characteristics. Interesting feature of such research was to examine the compatibility of nickel films. The conceptual insights gathered in this work required further refinement and fine tuning towards assessing the role of better quality porous supports in combinatorial performance characteristics of electroless plating baths.

The experimental investigation confirmed that nickel deposition on non-conducting surfaces was extremely slow and efforts are required to enhance the plating rate as well as quality of deposition of metal on non-conducting surfaces. The stagnation of time dependent PPD profiles needed more experimental investigation and careful contacting of reducing agent with metal precursors to substantially enhance PPD and could not be ruled out. This was especially evident from time dependent nickel PPD profiles in the later stages of plating. Optimization of conditions that drive away the achievement of saturation in product quality would require simple or sophisticated process modification. For example, a time dependent variable frequency sonicator may provide better PPD profiles or good quality of plating. Further SIEP was exceptionally good to achieve highest values of $\frac{PPD}{\delta}$ for both treated and untreated supports. Thus, it could be inferred that SIEP possessed maximum potential towards metal ceramic composite membranes and would be investigated substantially to improve the quality of plating.

Precisely, this work emphasized upon the criticality of rate enhancement techniques to accommodate morphological parametric sensitivities to achieve dense metal ceramic composites. This work exclusively focused upon the quality of deposition (PPD profiles) using supports with lower pore sizes. It confirmed that SIEP was the most promising process in terms of economics, simplicity, ease of operation and quality of deposition as the technique

enabled the realization of maximum value of $\frac{PPD}{\delta}$. Further research was required with respect to metal concentration since the plating rate increased with metal solution concentration and decreased with loading ratio. Higher conversions without jeopardizing the PPD variation with SIEP needs to be studied and will be taken up in subsequent chapters. Further it is well known that reducing agents such as hydrazine are heat sensitive and disintegrate within a short span of time, when they are brought in contact with the hot plating solution (Cheng and Yeung, 2001). Therefore, there is a need to study controlled contacting pattern of reducing agent and its effect from the perspective of PPD. This will be as well considered in the next chapter.

Effect of Reducing Agent Contacting Pattern on the Performance Characteristics of Surfactant Induced Nickel Electroless Plating Process

In this chapter, the results are presented in four sections. Section 4.2 summarizes the surface and physical characterization techniques. Section 4.3 summarizes the plating characteristics of two distinct contacting modes (bulk and drop wise contacting pattern) of the reducing agent for nickel SIEP baths. Section 4.4 elaborates on the effect of reducing agent concentration (50, 100, and 200% excess) for electroless plating bath with a nickel concentration of 0.08mol/L. Finally, section 4.5 elaborates on the compatibility of variation in nickel concentration (0.08 - 0.24 mol/L) with respect to variation in reducing agent concentration (50, 100, 200% excess).

4.1 Introduction

Based on results summarized in the previous chapter, it was analyzed that SIEP baths were optimal as compared to CEP and SOEP baths in the context of providing better combinatorial plating characteristics. However, the process has a major drawback of higher plating time for the fabrication of metal ceramic composite membrane.

The reduction of Ni^{2+} by reducing agent hydrazine hydrate in solution comprises of the equations 2.1-2.3 as mentioned in section 2.4. In the above reactions, reaction (2.1) occurs on the activated support surface and is desired. However, reactions (2.2) and (2.3) correspond to decomposition and disproportionation reactions respectively. These occur primarily in the plating solution and are undesired reactions. These reactions follow from the heat sensitivity and instability of hydrazine at the conditions of the metal electroless plating.

Therefore, bulk addition of hydrazine is bound to provide lower selectivity towards reaction (2.1) when compared to reactions (2.2) and (2.3) and hence controlled addition of hydrazine to the metal electroless plating baths is anticipated to enhance the selectivity towards reaction (2.1). Thus, with efficient contacting pattern for the reducing agent, the time period for one plating step can be reduced to 30 min along with the usage of supports with little higher pore size (150-250nm) and porosity(10 - 15%) to eliminate the support incompatibility and NaOH treatment time which was not the case for results presented in chapter 3.

The efficacy of reducing agent contacting pattern has been investigated for SIEP-DWR-BS and SIEP-BR-BS baths. Details with respect to these baths have been presented in section 2.4.2 and 2.4.5 of the thesis. For the present study, the membrane support possessed a pore size and effective porosity of about 150 – 250 nm and 10 - 15% respectively. The supports were fabricated at a fabrication pressure of 4.9 MPa using the compositions presented in Table 2.1 of the thesis. Similar supports have been used for fabricating Ni and Pd membrane presented in chapters 5-7. Thus, results obtained for the modifications with respect to contacting pattern and optimal reducing agent and metal concentration have been presented in this chapter. Further the time of plating for the cases reported in this chapter has been reduced from 1h to ½ h for one depositional step. Thus, further optimization of SIEP process for Ni membrane fabrication has been targeted in this chapter.

4.2 Structural characterization

4.2.1 LPSA, FTIR and BET analysis

The particle size distribution curve of the raw materials evaluated from LPSA indicated that the particle size varied from 0.955 to 34.674 µm, 1.259 to 39.811 µm, 0.822 to 15.31 µm,

1.905 to 52.81 µm and 0.955 to 316.28 µm for kaolin, quartz, feldspar, sodium carbonate and pyrophylite respectively. Further, Fig. 4.1 (a) depicts the FTIR spectra for the raw material and ceramic support. Characteristic peaks of kaolin were observed for the raw material and sintered raw material mixture. Further, the other corresponding peaks were assigned to C-H, C=C, Si-O-Al & Si-O bonds. Detailed discussion with respect to the peaks is similar to that presented previously in section in the chapter 3.4.3 of the thesis.

Nitrogen adsorption - desorption experiment at 77K performed by using a surface area analyzer for the support material confirmed the presence of meso and macro pores with no micropores. Type III isotherm with H_3 hysteresis loop was observed (Fig. 4.1(b)). This indicates slit-shaped pores according to IUPAC (Sing et al., 1985). The inset graph in

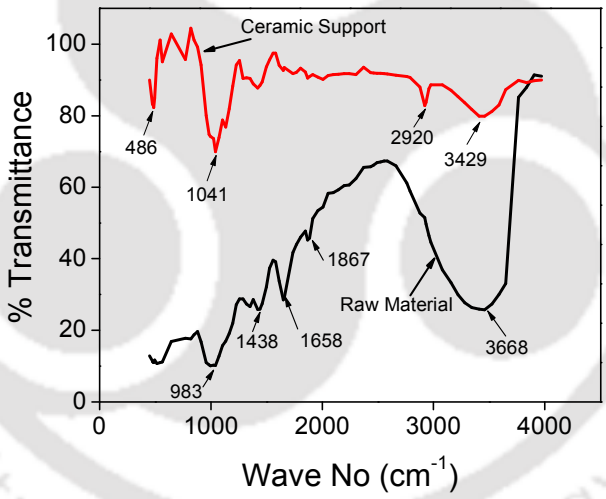

Fig. 4.1(a): FTIR spectra of inorganic precursors and ceramic support in the pore size range of 150 -250 nm.

Fig. 4.1(b) shows the desorption Barrett-Joyner-Halenda (BJH) pore size distribution of the support material. The BET surface area of support was 4.130 m^2/g and total pore volume was 0.0325 ml/g with no micro pore volume.

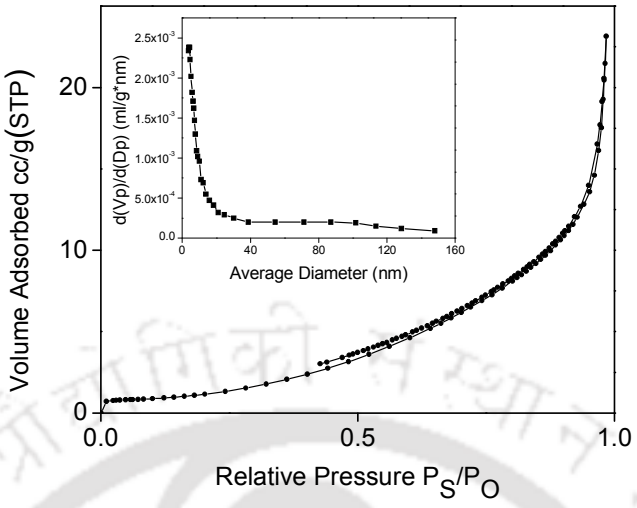

Fig 4.1(b): Nitrogen adsorption - desorption isotherm of the ceramic support. Inset: Pore size distribution from BJH analysis.

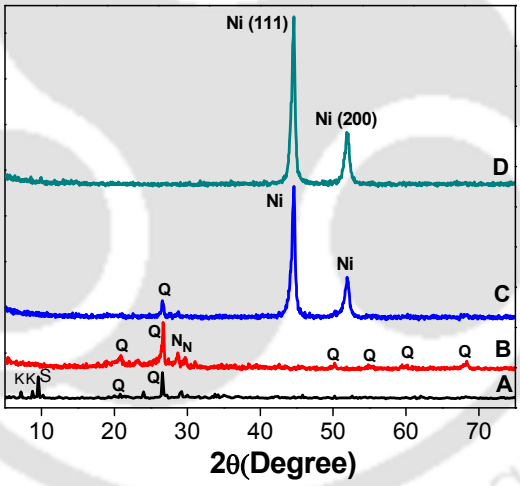

Fig 4.2: XRD patterns for (i) A - Raw material (ii) B - Sintered support (iii) C – Ni ELP with bulk addition of reducing agent (SM_1) (iv) D - Ni ELP with drop - wise addition of reducing agent (SM_2) (K -Kaolin, S- Sodium Carbonate, Q - Quartz, N - Nephiline, Ni – Nickel).

4.2.2 XRD analysis

Fig. 4.2 presents the XRD patterns of raw material mixture, sintered ceramic support, and the nickel membrane obtained with 100% excess reducing agent for bulk and drop wise addition modes. ICDD-JCPDS database was used for the phase analysis of the diffraction profile. As outlined in chapter 3, the XRD patterns for raw material mixture and sintered ceramic support (profiles A and B in Fig. 4.2) indicate: (a) the presence of phases for kaolin, quartz and sodium carbonate in the raw material mixture (b) the disappearance of the peaks corresponding to kaolin after sintering and (c) the appearance of nephiline phase after sintering.

Corresponding to the bulk and drop wise addition of reducing agent during Ni ELP, the Ni metal peaks (profiles C and D in Fig. 4.2) appeared at diffraction angle $2\theta = 44.5^{o}$ and 51.8^{o} due to the diffraction of (111) and (200) plane [Pdf No 00-004-0850]. For Ni ELP with bulk wise addition of reducing agent, it can be observed that the peak intensity of quartz significantly decreased after nickel deposition due to nickel plating on quartz surface to reduce quartz crystallinity. However, the quartz peak did not dis appear suggesting poor densification and non-uniform plating. But, this was not the case for nickel ELP with drop wise addition of reducing agent. Diffraction profiles for drop wise addition of reducing agent (profile D) suggested significant increase in nickel crystalinity in comparison with that in profile C. No quartz peaks were detected. Thus, from the XRD analysis it can be concluded that drop wise addition of reducing agent served better to promote uniformity of metal deposition on the support surface.

4.2.3 FESEM analysis

The surface FESEM micrographs of the ceramic support and the nickel layer deposited with

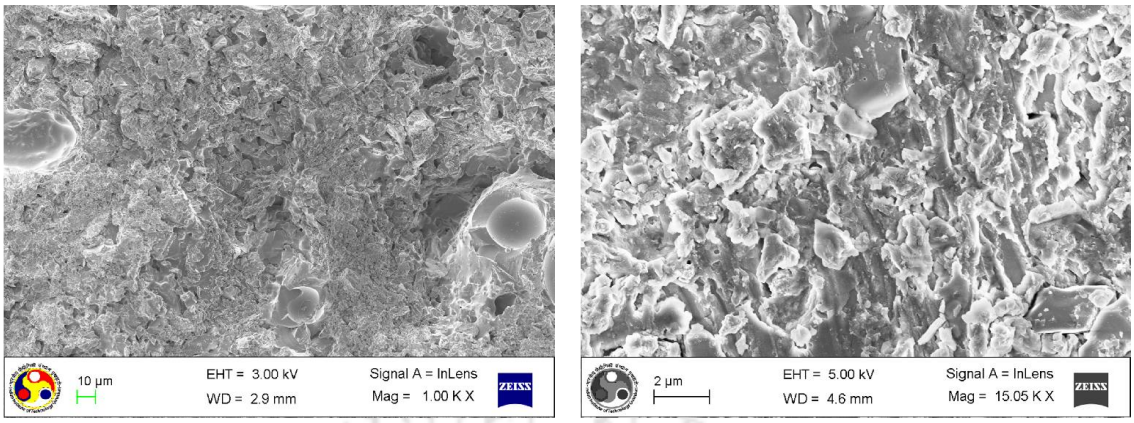

(a) (b)

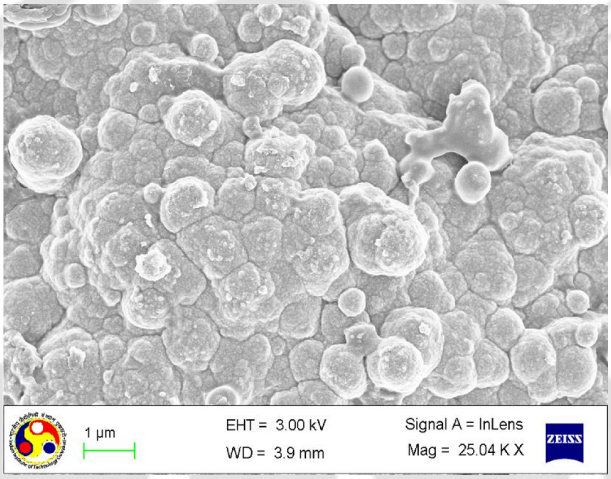

(c)

Fig. 4.3: Surface FESEM micrographs of (a) ceramic support (b) SM_1 membrane prepared with bulk addition (c) SM_2 membrane with drop wise addition of 100% excess reducing agent.

an initial nickel sulfate concentration (C_i) of $0.08\left(\frac{mol}{L}\right)$ are shown in Fig 4.3. It can be observed that well-developed nickel layers exist for the membrane. Based on the ImageJ analysis of the FESEM image for the ceramic support, it was analyzed that the pores were distributed over wider pore size values and the average pore size of the support was about 300 nm which was close to that evaluated from nitrogen permeation experiments (150-250

nm). The FESEM images were in good agreement with XRD patterns which confirmed that the dropwise addition of reducing agent gave better surface finish in terms of desired attributes such as faster pore densification and lesser pinholes.

4.3 Efficacy of reducing agent contacting pattern

Fig. 4.4 illustrates the variation in the time dependent plating inefficiency and average plating rate for both cases namely bulk and drop wise contacting pattern of the reducing agent during nickel electroless plating. The results presented in the figure correspond to the case of 0.08mol/L nickel solution concentration, 100% excess reducing agent and 1.2g/L of CTAB surfactant solution concentration. For a variation in total plating time of 4-12 h, it can be observed that the plating inefficiencies varied from 64 – 72% for the bulk case (SM_1). These values reduced significantly to 46 – 52 % (SM_2) for the drop wise addition case.

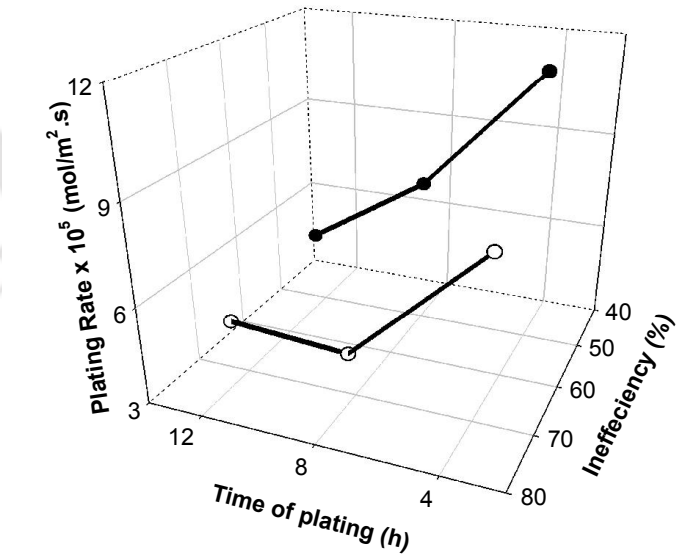

Fig. 4.4: Variation of average plating rate and inefficiency with plating time for (a) bulk (SM_1) and (b) drop wise (SM_2) addition of the reducing agent.

Corresponding variation in average plating rate was from 7.48 - 5.03× 10^{-5} $\left(\frac{mol}{m^2.s}\right)$ for SM_1 (bulk case) and 11.16 – 5.52 × 10^{-5} $\left(\frac{mol}{m^2.s}\right)$ for SM_2 (drop wise). Thus, it is evident that the drop wise addition of the reducing agent enhances plating rate by about 1.5 times in comparison with the bulk addition case. For the plating time period in the range of 4 – 12 h, it was evaluated that the PPD for the SM_1 membrane (bulk addition case) varied from 41 – 84.5%, which enhanced to 57.4 – 89.3 % for the SM_2 membrane (drop wise addition case). Once again, this profile confirmed that the drop wise contacting pattern of the reducing agent provided higher pore densification during Ni ELP.

The drop wise addition of the reducing agent enables the timely replenishment of the electron source in the SIEP bath and is more effective to aid the removal of nitrogen and ammonia bubbles on the support, thereby providing higher PPD rates. For the bulk addition case of the reducing agent, controlling the evolution rate of the nitrogen and ammonia gas bubbles with minimal metal nucleation in the solution is highly difficult and this is evident from plating inefficiency and PPD profiles observed for the SM_2 case. Further, it was also observed for the bulk addition case that no significant amount of metal was deposited on the support surface during the 1st hour of plating, which indicates that the SIEP process is highly ineffective despite using a surfactant to promote the plating characteristics. In conclusion, the dropwise addition of the reducing agent favored higher metal plating rate, PPD and lower inefficiency which are all the desired attributes of a highly efficient metal plating process.

The next section elaborates upon the effect of reducing agent excess concentration for the drop wise contacting pattern case.

4.4 Optimality of reducing agent concentration

In the previous section, drop wise contacting pattern has been identified to provide optimal performance. In this section, the reducing agent concentration has been explored for its optimality. Fig. 4.5 illustrates the time dependent variation of nickel electroless plating characteristics namely plating inefficiency, plating rate, PPD and theoretical metal film thickness respectively for various cases of reducing agent concentration (50, 100 and 200% excess). For all these cases, the reducing agent contacting pattern corresponds to drop wise addition. As shown, for a variation in plating time from 4-12h, and for the 50 % excess case (SM_3), these parameters varied as 64 – 79.2 % (plating inefficiency), 7.65 – 3.7 × 10^{-5} $\left(\frac{mol}{m^2 s}\right)$ (plating rate), 49.7- 77% (PPD) and 7.2-10.5 µm (metal film thickness) respectively. Enhancing the reducing agent concentration to 100 % excess (SM_2) corresponds to the variation in these parameters as 46.8-52.2% (plating inefficiency), 11.16 – 5.52 × 10^{-5} $\left(\frac{mol}{m^2 s}\right)$ (plating rate), 57.4 – 89.3% (PPD) and 10.6 – 15.7 µm (film thickness). A further enhancement in the reducing agent concentration to 200 % excess (SM_4) corresponds to the variation in these parameters as 23.7- 43.6% (plating inefficiency), 11.52 – 7.07 × 10^{-5} $\left(\frac{mol}{m^2 s}\right)$ (plating rate), 64.7 – 94.9 % (PPD) and 12 - 20.2 µm (film thickness).

Therefore, it is apparent that at a lower nickel solution concentration of 0.08 mol/L, the enhancement in % excess of reducing agent is favorable to provide good combinations of plating characteristics (higher combinations of plating rate, PPD and lower theoretical metal film thickness and lower plating inefficiency).

For the case of 50% excess reducing agent, the nickel plating rate was low and this is probably due to strong surfactant adsorption to the support surface. Also, surfactant

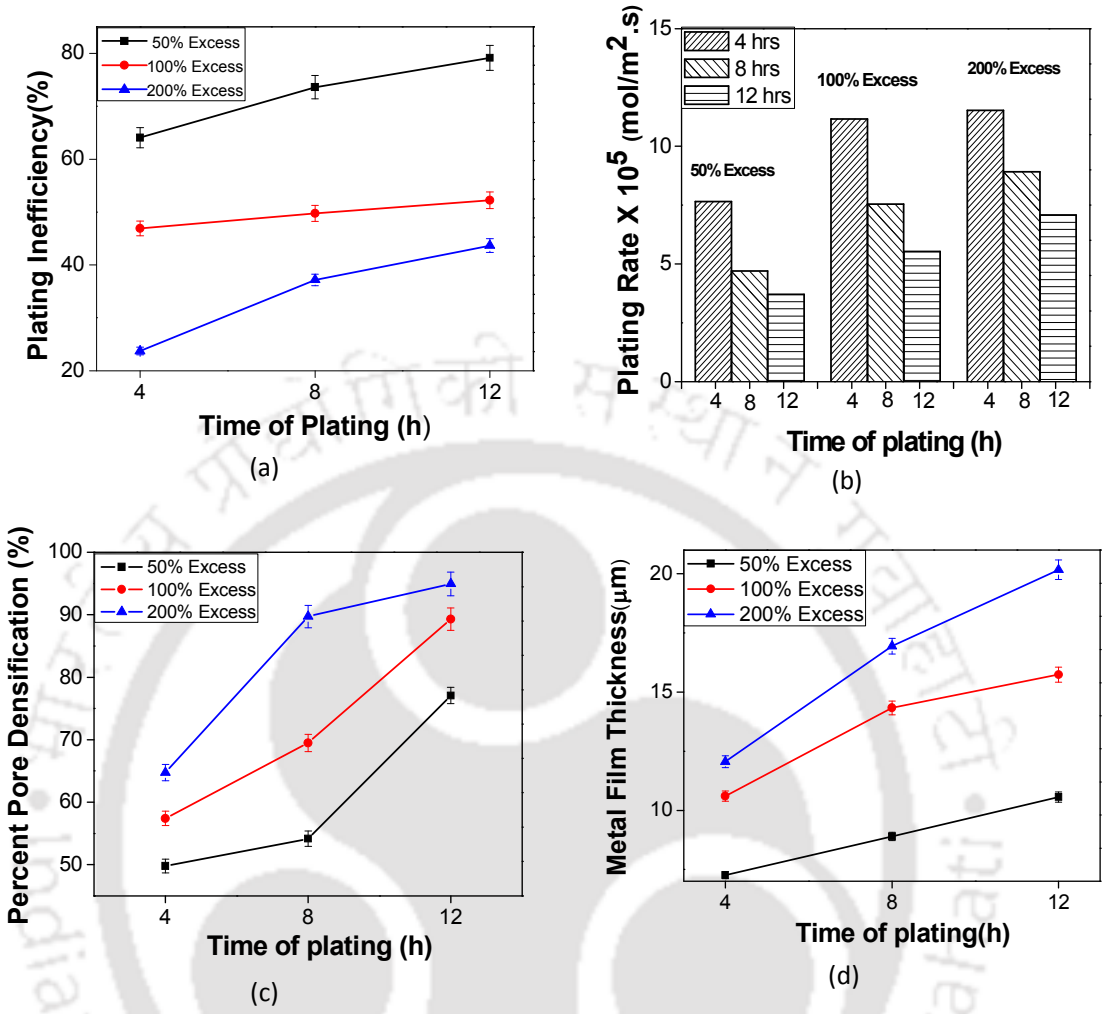

Fig. 4.5: Variation of (a) plating inefficiency (b) metal plating rate (c) PPD (d) theoretical metal film thickness with plating time for membranes SM_2, SM_3 and SM_4 (50 - 200 % excess reducing agent).

adsorption on the support surface is very likely to affect the morphological parameters of the nickel film including film stability. The stronger bonding of the surfactant could weaken the physical bonding of the metal and thus could promote metal delamination (Nwosu et al., 2012), unwanted metal nucleation in the solution and higher plating inefficiencies. On the other hand, for the case of higher concentration of reducing agent, nickel plating rates are significant and hence the gas bubbles leaving the support surface at a faster rate may

influence the surfactant-support equilibrium. In such a scenario, the surfactant adsorption on the surface may not be able to control the metal deposition on the surface, thus indicating minimal pitting effect, less surfactant adsorption, less metal nucleation in the solution and hence higher plating efficiencies.

The enhancement in plating efficiency with higher concentrations of reducing agent is indicative towards the complexity involved in the surface phenomena during SIEP. Typically in a conventional nickel electroless plating bath, higher concentrations of the reducing agent are not favorable to enhance the plating characteristics which is exactly opposite to the trends obtained in this work. Thus, the generalized rules of thumb that are often presented for regular electroless plating baths are not applicable for the SIEP baths. The reduction of plating inefficiency at lower reducing agent concentrations is possibly due to the instability of the metal film deposited on the membrane surface which may provide more metal nucleation sites in the plating solution. Thereby, these observations that have been verified at least twice indicate that the reducing agent concentration also needs to be studied with respect to the film stability in due course of nickel electroless plating.

With respect to the time dependency of several plating characteristic parameters, it can be observed for all cases in the figure that all the variables namely plating inefficiency, PPD and thickness increased with increasing plating time. Further, it can be also evaluated that the non-linearity in the variable variation is significant at highest concentration of the reducing agent (200 % excess). Also, it can be observed that the film thickness was strongly affected with the variation in the concentration of reducing agent. An enhancement in the reducing agent concentration from 100 to 200 % excess enabled the enhancement in the film thickness by 22 times with only 5 % enhancement in the PPD after 12 h of plating. Therefore, it is apparent that 100% excess reducing agent concentration is the optimal choice due to the fact

that the PPD variation is not significant for the case of 200 % excess plating solution concentration. It is anticipated that for the case of 100 % excess reducing agent concentration, a further increment of plating time to 16 h gave a higher PPD (> 94.9%) and lower metal film thickness (< 20.2 μm). The reduction in the PPD at higher reducing agent concentrations (about 200 % excess) is indicative to the fact that higher reducing agent concentrations do not favor pore densification and contribute to layering of films which is a highly undesired feature in the fabrication of dense metal ceramic composite membranes.

Comparing plating performance characteristics with the literature data, it can be observed that Bulasara et al. (2011b) reported a plating rate of $7.6 \times 10^{-6} \left(\frac{mol}{L.s} \right)$ and a PPD of 91.1% for a high surfactant concentration (1.5 g/L) and a higher pore size of the support (275 nm). The optimal case in this work corresponds to a plating rate of $5.7 \times 10^{-7} \left(\frac{mol}{L.s} \right)$ [$11.16 \times 10^{-5} \left(\frac{mol}{m^2 s} \right)$] and a PPD of 89.3% which is slightly lower than that reported by the authors, for the utilization of a support with a lower average pore size (200 nm) and lower surfactant concentrations (1.2 g/L) but with a controlled contacting pattern of the reducing agent. However, it shall be noted that the PPD calculation procedure reported in this work is different and better than that reported by the authors, given the fact that the authors have evaluated PPD in terms of average pore size which is not the same as PPD evaluated with average flux. In summary, it is apparent that the drop wise contacting pattern is highly favorable towards furthering process modifications to the SIEP process.

4.5 Optimality of nickel solution concentration

In this section, the optimality of Ni solution concentration has been elaborated within the range of 0.08-0.24 mol/L.

4.5.1 Plating inefficiency tradeoffs

Table 4.1 summarizes the combinatorial plating characteristics corresponding to various cases of nickel solution concentrations (0.08, 0.16 and 0.24 mol/L) and excess reducing agent concentrations (50, 100 and 200 %). For all cases, the plating time was varied from 4-12 h. As presented, the plating inefficiencies for 0.08 mol/L nickel solution concentration varied from 64 – 79.2 % for SM_3 (50% excess), 46.9 - 52.2 % for SM_2 (100% excess), and from 17 – 43.6 % for SM_4 (200% excess). Similarly, for 0.16 mol/L nickel solution concentration, plating inefficiencies varied from 48.1 – 54.6% for SM_5 (50% excess) and from 37.3 – 11.1% for SM_6 (100% excess). For 0.24 mol/L nickel solution concentration case, the variable varied from 68.5 – 82.8% for SM_7 (50% excess) and 55.7 -52.5% for SM_8 (100% excess) respectively for 4-12 h of nickel plating. This indicates that there exists an optimal metal solution concentration and excess reducing agent concentration at which minimal plating inefficiency can be obtained. In general, all experimental data can be analyzed for five cases namely:

(a) Lower combinations of metal (0.08 mol/L) and reducing agent concentrations (50% excess).

(b) Moderately high metal concentration (0.16mol/L) and lower reducing agent concentration (50% excess).

(c) Moderately higher combinations of metal (0.16mol/L) and reducing agent concentration (100% excess).

(d) Higher metal concentration (0.24mol/L) and moderate reducing agent concentration (100% excess).

(e) Moderate and high metal solution concentration (0.16 & 0.24 mol/L) and higher reducing agent concentration (200% excess).

The chemistry involving the interaction between surfactant, metal and reducing agent appears to be highly complex. For instance, when the nickel solution concentration is enhanced from 0.08 to 0.24mol/L, it was evaluated that plating inefficiency reduced from 49.7% (SM_2) to 33.4% (SM_6) which further increased to 54.2% (SM_8) after 8 hours of plating. Typically higher metal concentration enables higher combinations of plating rate, pitting, metal nucleation in solution and hence higher plating inefficiencies. Also, the variation in the reducing agent concentration varies the net amount of free electrons available for the reduction of metal ion in both the solution (unwanted) and on surface (desired).

The hypothesis for the case of lower nickel solution concentration (0.08 mol/L) has already been addressed in our previous subsection. Further, for second case (0.16mol/L, 50% excess) the plating inefficiency trends were in agreement with the trends observed for lower metal concentration. The only variation for this case was in the reduction of plating inefficiencies from 79.2% to 54.6%. This could be explained with the reason that at moderately higher

Table 4.1: Combinatorial plating characteristics for SIEP Ni baths for various cases of metal solution concentration and reducing agent.

Reducing Agent	50% Excess			100% Excess			200% Excess		
Time of Plating	4 h	8 h	12 h	4 h	8 h	12 h	4 h	8 h	12 h
Metal Concentration	Plating Inefficiency (%)								
0.08	64	73.6	79.2	46.9	49.7	52.2	17	37.2	43.6
0.16	48.1	51.5	54.6	37.3	33.4	11.1	-	-	-
0.24	68.5	78.6	82.8	55.7	54.2	52.5	-	-	-
	Plating Rate $\times 10^5$ (mol/m^2.s)								
0.08	7.6	4.7	3.7	11.2	7.5	5.5	11.5	8.9	7.1
0.16	10.9	9.4	8.1	13.2	10	7.9	-	-	-
0.24	22	13.3	10.6	25.4	21.9	20.3	-	-	-
	Percent Pore Densification (%)								
0.08	49.8	54.2	77.1	57.4	69.5	89.3	64.7	89.7	95.0
0.16	57.8	78.8	89.7	76	88	94.4	-	-	-
0.24	67.1	84.2	92.7	84.7	90	97.1	-	-	-
	Metal Film Thickness (µm)								
0.08	7.3	8.9	10.6	10.6	14.3	15.7	10.9	16.9	20.2
0.16	9.24	18.8	25.2	12.5	19	29.3	-	-	-
0.24	20.9	25.2	30.2	24.3	41.5	57.8	-	-	-

metal concentration, the metal plating rate will be higher and surfactant adsorption to the support surface will not be able to control the surface bonding of the nickel metal, thereby reducing metal nucleation in the solution and enhancing the plating efficiency.

Conceptually it can be hypothesized that for a given metal and reducing agent concentration the plating inefficiency increases with time of plating. However, for the third case (0.16mol/L, 100% excess), it was analyzed that with time, the plating inefficiencies decreased from 37.3% (4 h) to 11.1% (12 h). This is possibly due to compatibility of concentrations (metal, surfactant and reducing agent) during prolong Ni ELP wherein the conditions bonding between the metal and the support surface minimizes pitting and plating inefficiency favored good.

Also, for the case of higher metal concentration (0.24 mol/L) and moderate reducing agent (100 % excess), it was evaluated that the plating inefficiencies decreased from 55.7% (4 h) to 52.5 % (12 h) and the values were quite higher as compared to the previous case. This can be explained with the view that at higher metal concentration, the conversion of nickel ion to nickel metal is very fast due to the availability of large number of free electrons from the reducing agent (Nwosu et al., 2012). Thus, faster metal deposition on the surface favors higher rates of metal delamination that enhances metal nucleation in the solution. This has also been confirmed by physical observation of the plating solution after plating process. Lastly, for 0.16 mol/L and 0.24 mol/L metal concentration, 200 % excess reducing agent was not reported because of the fact that physically nickel precipitates were observed at the bottom of the beaker and nickel plating also occurred on the beaker corners. At high concentrations of metal and reducing agents, surfactant concentration is likely to play a dominant role in the bath due to evolution of large amounts of gas bubbles. Under such circumstances, either the surfactant has to bind more gas bubbles to itself and leave the

support surface with a higher force to cause metal pitting or the surfactant concentration would be insufficient to carry all the evolved gas bubbles. Thus the un-evolved gas bubbles would either adhere to the surface thus hindering metal deposition or remove metal from the support surface due to shear effects induced by the released gas bubbles thereby enhancing metal nucleation in the solution.

The plating inefficiencies reduced with moderately high metal solution concentrations (0.16 mol/L) but not for higher metal concentrations (0.24 mol/L). This indicates the fact that the film stability and inefficient plating are a strong function of metal solution and reducing agent concentrations. Considering plating inefficiency as the sole tradeoff, the optimal case corresponds to 0.16 mol/L with 100 % excess reducing agent that provided an inefficiency of 11.1 % after 12 h of nickel plating.

4.5.2 Tradeoffs associated to membrane morphological parameters

Other than the complexity in the plating inefficiency, profiles for all other variables namely plating rate, PPD and metal film thickness indicate their enhancement with increasing metal solution and reducing agent concentrations. As presented in Table 4.1, the plating rates for 0.16 mol/L metal solution concentration varied from 10.9 – 8.1 × 10^{-5} $\left(\frac{mol}{m^2 s}\right)$ for SM_5 (50% excess) and from 13.2 – 7.9 × 10^{-5} $\left(\frac{mol}{m^2 s}\right)$ for SM_6 (100% excess). Similarly, for a higher metal solution concentration of 0.24 mol/L, the plating rate varied from 22– 10.6 × 10^{-5} $\left(\frac{mol}{m^2 s}\right)$ for SM_7 (50% excess) and from 25.4 – 20.3 × 10^{-5} $\left(\frac{mol}{m^2 s}\right)$ for SM_8 (100% excess) respectively.

The efficient design of electroless plating process needs to visualize the maximum extent of pore densification with respect to minimum amount of metal required to densify the pores i.e.

to achieve maximum $\frac{PPD}{\delta}$ value. It was evaluated that for 12 h of sequential nickel ELP, for membrane SM_2 (100% excess reducing agent and 0.08 mol/L metal solution concentration) the PPD was 89.3% with a metal film thickness of 15.7μm, whereas for SM_6 (100% excess reducing agent and 0.16 mol/L metal solution concentration) the PPD was 94.4% with a metal film thickness of 29.3 μm. Thus $\frac{PPD}{\delta}$ for SM_2 was evaluated to be 5.7 whereas for SM_6 it was 3.2 respectively. Thus for SM_6, it was evaluated that for a little increment of PPD (4%), the metal film thickness increased 100% and therefore these conditions are not favorable from the process-product perspective. The insignificant enhancement in PPD with a significant enhancement in metal film thickness suggests the undesired feature of layering during membrane fabrication for the cases of moderate and higher metal concentrations. In summary, from the perspective of minimal thickness for the desired PPD it would be inferred that the optimal process parameters refer to lower nickel solution concentration (0.08mol/L), moderate reducing agent concentrations (100% excess) along with suggested contacting pattern of the reducing agent in the SIEP process.

4.6 Summary

The existing gap in the literature with respect to the role of reducing agent in affecting both nickel electroless process and membrane characteristics has been successfully addressed in this work. Several insights have been obtained by carrying out this work. Firstly, compared to bulk addition strategy of the reducing agent, the drop wise contacting pattern of the reducing agent is worth investigating to obtain membranes with good morphological characteristics (uniformity of deposition, low thickness, high PPD and lower time of plating). Secondly, this work focused towards the optimality of reducing agent concentration (50%, 100% & 200% excess) and concluded that 100% excess concentration of reducing agent

would suffice better towards deliberating desired process parameters. Finally, this work provided good amount of physical insights towards analyzing the complex plating chemistry of metal concentration ranging from 0.08 mol/L to 0.24 mol/L and reducing agent concentration from 50% excess to 200% excess. Thus this work provided new observations in the field of metal electroless plating for membrane fabrication with the fact that moderately high concentration of metal (0.16 mol/L) and reducing agent (100 % excess) along with drop wise addition strategy provided lowest plating inefficiency. This indicates that there exists a complex chemistry in the interaction between metal, surfactant, reducing agent and the ceramic support. Efforts to reduce the theoretical metal film thickness without compromising upon pore densification and plating rates were successful for a lower metal solution concentration (0.08mol/L).

Thus the optimal combinations of SIEP process parameters were identified as 0.08mol/L of nickel metal solution concentration with 100% excess reducing agent. These conditions provided a plating rate of $5.5 \times 10^{-5} \left(\frac{mol}{m^2 s} \right)$, PPD of 89.3% and a metal film thickness of 15.7μm respectively after 12h of sequential plating in an SIEP process. These observations further need to be investigated for the case of palladium-ceramic composite membrane fabrication in order to relate the physical insights gained in this work towards the large scale application perspective. Further, additional work needs to be addressed with regards to nearly 100% densification in order to confirm upon the feasibility of nickel-ceramic membranes as supports for dense palladium membranes. All in all, experimental findings in this chapter provided significant amount of data in furthering the process engineering aspects related to the metal ceramic composite membrane fabrication using surfactant induced metal electroless plating (SIEP).

Efficacy of Reducing Agent and Surfactant Contacting Pattern on the Performance Characteristics of Nickel ELP Baths Coupled with and Without Ultrasound

This chapter addresses furthering the role of sonication for the optimal fabrication of nickel ceramic composite membranes using electroless plating. Section 5.2 summarizes surface characterization of the metal membrane. Section 5.3 elaborates upon the combinatorial plating characteristics of SIEP baths (without sonication) and section 5.4 focuses towards the coupled effect of sonication and surfactant (SSOEP) in providing the desired combinatorial plating characteristics. Thus deliberating upon process modifications for SIEP and combined surfactant and sonication induced electroless plating (SSOEP), this chapter highlights the relevance of a novel method of contacting of the reducing agent and surfactant to the conventional electroless nickel plating baths.

5.1 Introduction

In chapter 3, a comparative assessment of surfactant and sonication induced electroless plating baths concluded that surfactant induced electroless plating (SIEP) baths provide better surface engineering and combinatorial performance characteristics whereas sonication induced electroless plating (SOEP) baths were favorable in terms of enhancing plating rates. Despite improving the plating rates, the SOEP baths failed to achieve higher pore densification and have phenomenally contributed to the layering effect without improving upon the surface pore coverage and pore densification. Since SIEP process also has fundamental limitations in terms of limited enhancement in the plating rate, a further enhancement in the plating rate without jeopardizing upon the pore densification was desired.

To achieve the same, it was hypothesized that a combination of sonication and surfactant would suffice the purpose of targeting the fabrication of dense metal composite membranes. Further, few researchers (Haas and Gedanken, 2006; Mizukoshi et al., 2001; Yang et al., 2013) have investigated ELP coupled with sonication and surfactant variants for the development of products other than metal ceramic membranes. But till date, the literature is scarce on the coupled effect of two most scalable rate enhancement techniques namely surfactant and sonication for the fabrication of metal ceramic composite membrane using ELP technique.

On the other hand, SIEP and SSOEP baths can be operated in several ways. As a first alternative, all the constituents can be mixed initially and plating could be initiated. Otherwise, the reducing agent can be added in a phase wise or continuous mode to the mixture of surfactant and metal solution in an ELP bath. As a third alternate, both reducing agent and surfactant can be added in a phase wise or continuous mode to the ELP baths. While these options may appear naïve for the general application of ELP, they may be of paramount relevance for dense metal composite membranes. Till date there is no literature that elaborates upon the role of contacting pattern of the surfactant in electroless plating bath for dense composite membrane fabrication. All relevant literatures (Elansezhian et al., 2008; Elansezhian et al., 2009; Islam et al., 2012) addressed bulk addition of surfactant for metal deposition using electroless plating. The bulk addition of surfactant encourages adsorption of surfactant on the membrane surface which promotes uneven charge distributions on the surface (Chen et al., 2002).This encourages greater metal nucleation in the solution. Variation in the surfactant contacting pattern is hypothesized to promote better depositional characteristics and membrane pore densification due to lesser adsorption of surfactants on the support surface. Thus to increase the efficacy of the electroless plating process, there is a need to focus upon the contacting pattern of the dispersing agent (surfactant).

Thus with efficient contacting pattern for the reducing agent, the time period for one plating step could be reduced by 50% (30 min) which was not the case for experiments referred in chapter 3. In addition, the controlled addition of surfactant could reduce stronger adsorption of surfactant on the support surface, which can in turn alter the metal adhesion properties and removal rate of generated gas bubbles. The desired effect of minimal metal solution nucleation and maximum metal film adhesion strength is an interesting issue in the context of surfactant contacting pattern. Thus, the efficacy of reducing agent and surfactant contacting pattern has been investigated for SIEP-DWR-BS (SM_2), SIEP-DWR-DWS (SM_9), SSOEP-DWR-BS (SSM_1) and SSOEP-DWR-DWS (SSM_2) baths. Details with respect to these baths have been presented in sections 2.4.5 and 2.4.6 of the thesis.

This chapter addresses various types of SIEP and SSOEP processes considering options such as bulk addition of surfactant (BS), continuous (drop wise) addition of surfactant (DWS) and continuous (drop wise) addition of reducing agent (DWR).Two major objectives were targeted. The first objective corresponds to the comparative assessment of SIEP and SSOEP processes supplemented with the dropwise addition of the reducing agent. Secondly, it is envisaged to evaluate upon the competence of the dropwise addition of the dispersing agent (surfactant) for SIEP and SSOEP baths. The ultimate goal of the experimental investigations is to identify the best process combinations with which maximum combinations of percent pore densification (PPD), plating rate ($\overline{r_i}$), plating efficiency (η) and minimum metal film thickness (δ) can be achieved. The next section summarizes surface characterization of raw materials and achieved membranes.

5.2 Surface characterization

5.2.1 LPSA, FTIR and BET analysis

The particle size distribution curve of the raw materials evaluated from LPSA indicated that the particle size varied from 0.955 to 34.674 μm, 1.259 to 39.811 μm, 0.822 to 15.31 μm, 1.905 to 52.81 μm and 0.955 to 316.28 μm for kaolin, quartz, feldspar, sodium carbonate and pyrophylite respectively. Further FTIR analysis indicated the existence of the characteristic peaks of kaolin for the raw material and sintered raw material mixture. The corresponding peaks were assigned to C-H, C=C, Si-O-Al & Si-O bonds. Discussion with respect to these is similar to that presented previously in section in the chapter 4.2.1 of the thesis. Further, the BET surface area of support was 4.130 m^2/g and total pore volume was 0.0325 ml/g with no micro pore volume as discussed in section 4.2.1 of the thesis.

5.2.2 XRD analysis

Fig. 5.1 presents the XRD patterns of nickel membrane fabricated with various processes. ICDD-JCPDS database was used for the phase analysis of the diffraction profiles. The XRD patterns of the ceramic support are similar to that outlined in our previous chapter work. The metallic nickel peaks for electroless nickel plating for all baths appeared at diffraction angle of $2\theta = 44.5^o$ and 51.8^o due to the diffraction of (111) and (200) plane [Pdf No 00-004-0850]. It can be also observed that the quartz peak exists for SIEP-DWR-BS (SM_2) and SSOEP-DWR-DWS (SSM_2) baths at a diffraction angle of $2\theta = 26.6^o$ [Pdf No 00-083-2465] suggesting non uniform deposition. However, for the case of SIEP-DWR-DWS (SM_9) and SSOEP-DWR-BS (SSM_1) baths, no such quartz peaks were observed suggesting uniform plating, higher metal film thickness and better PPD.

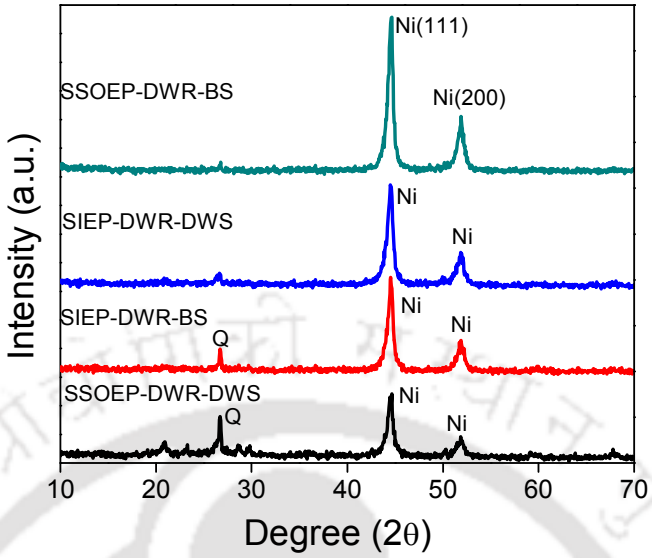

Fig. 5.1: XRD patterns of nickel membrane fabricated with SSOEP-DWR-BS, SSOEP-DWR-DWS, SIEP-DWR-BS and SIEP-DWR-DWS baths (SSM_1, SSM_2, SM_2 and SM_9).

5.2.3 FESEM analysis

The surface FESEM micrographs of the nickel films deposited with various baths are shown in Fig. 5.2. It can be observed that the FESEM micrographs are in good agreement with the XRD profiles (Fig. 5.1) thereby illustrating that non-uniform nickel deposition with low PPD occurred for SIEP-DWR-BS (SM_2) (Fig 5.2(a)) and SSOEP-DWR-DWS (SSM_2) baths (Fig 5.2(c)). However, this is not the case for SIEP-DWR-DWS (SM_9) baths (Fig 5.2(b)) where uniform nickel deposition occurred with metal aggregates that do not have uniformity in their size. Lastly for SSOEP-DWR-BS (SSM_1) baths (Fig 5.2(d)), it has been observed that well developed similar shaped metal aggregates have been observed. This effect confirms that the agitation caused by ultrasonic waves during sonication has been effective towards uniform metal deposition. The same has also been confirmed by the XRD spectral profiles presented for SSOEP-DWR-BS baths in Fig. 5.1, where a strong peak for nickel indicates highest crystallinity. Further Fig. 5.2(e) depicts

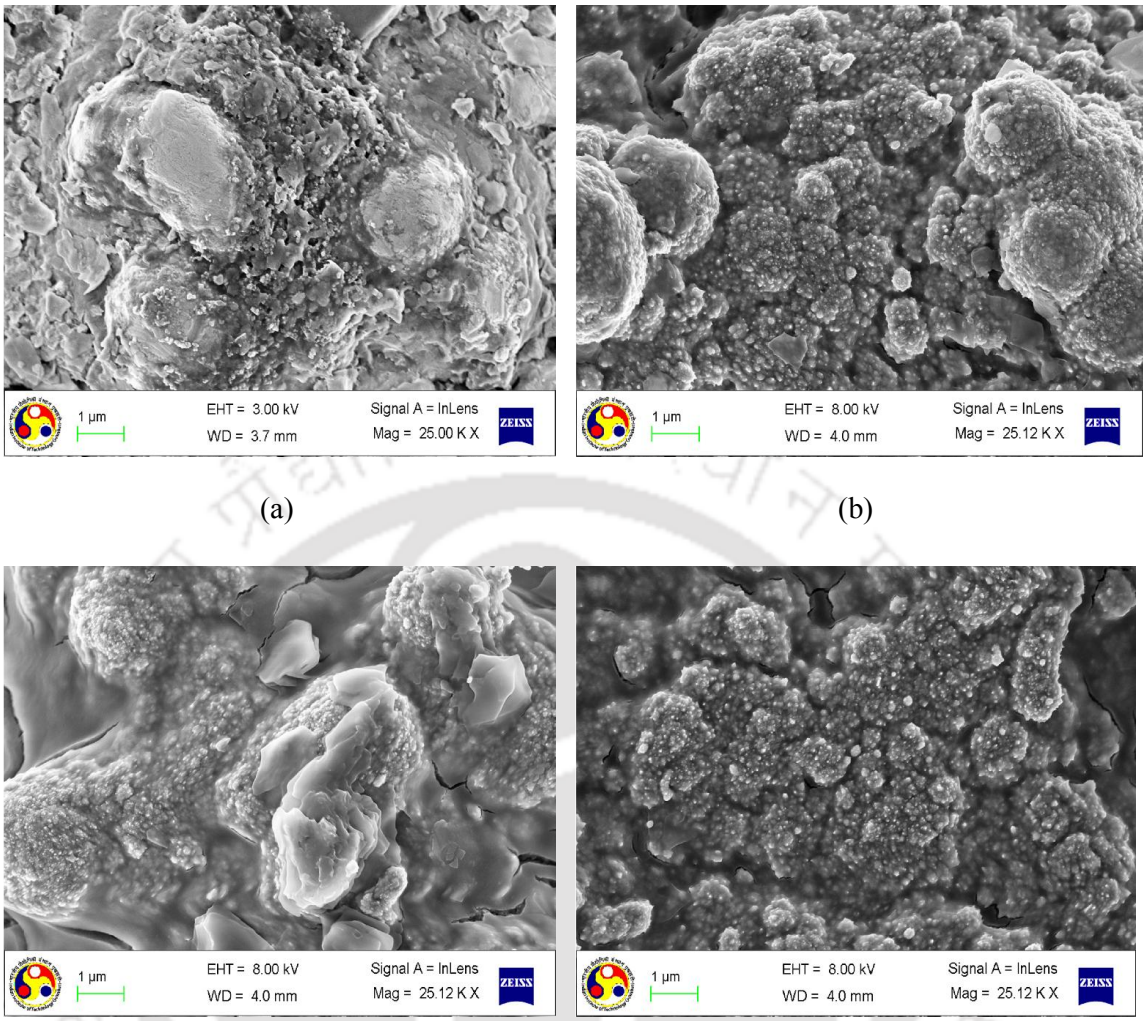

Fig. 5.2 (a-d): Surface FESEM micrographs of membranes fabricated with (a) SIEP-DWR-BS (b) SIEP-DWR-DWS(c) SSOEP- DWR-DWS (d) SSOEP-DWR-BS baths (SM_2, SM_9, SSM_2 and SSM_1).

the grain size distribution of SIEP-DWR-DWS (SM_9) and SSOEP-DWR-BS (SSM_1) baths using ImageJ software. It was observed that the average agglomerate grain size was 198 and 135nm respectively for SIEP-DWR-DWS (SM_9) and SSOEP-DWR-BS (SSM_1) baths. This indicates that sonication was successful in providing more uniform deposition. The achievement of smaller grain sizes using SSOEP-DWR-BS baths is an interesting feature that has not been reported till date.

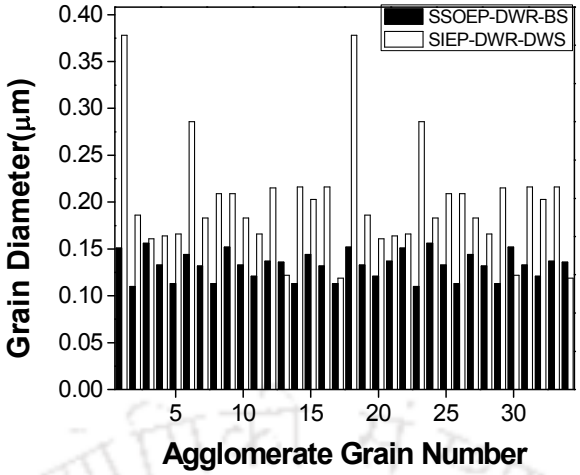

(e)

Fig. 5.2 (e): ImageJ based grain size distribution for SSOEP-DWR-BS (SSM_1) and SIEP-DWR-DWS (SM_9) baths.

5.3 Plating characteristics of SIEP-DWR baths

5.3.1 PPD profiles

Fig. 5.3 presents the variation of PPD with plating time for SIEP-DWR-BS (SM_2) and SIEP-DWR-DWS (SM_9) baths. It can be observed that the PPD profiles varied from 30.5 -71.4 % and from 50.4– 76.5% for a variation in plating time from 2-8 h for membranes SM_2 and SM_9 respectively. For similar metal concentration (0.08mol/L) and plating time (8h) values, it was

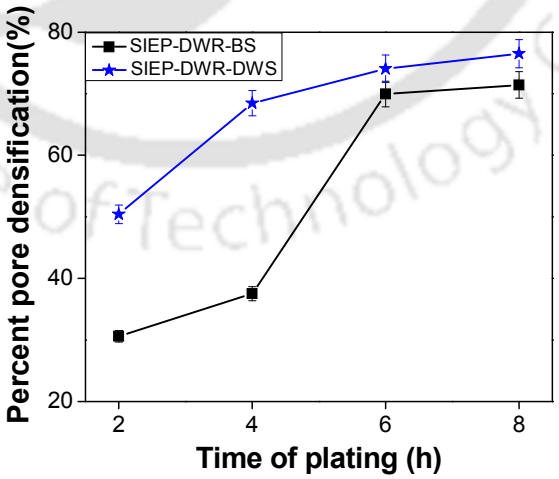

Fig. 5.3: Variation of PPD with plating time for SIEP-DWR-BS (SM_2) and SIEP-DWR-DWS (SM_9) baths.

observed that modifying the contacting strategy of surfactant from bulk to dropwise increased the PPD by 7%. Hypothetically, dropwise addition of reducing agent to an ELP plating bath facilitates the availability of electron source throughout the time of deposition and thus enhances PPD. On the other hand, the main objective of adding a surfactant i.e. for the removal of unwanted gas bubbles has been supported by dropwise contacting pattern surfactant. For any plating time, if the surfactant concentration is too high it can get adsorbed on the surface and hinders metal deposition. This was the possible reason for very low PPD values of SIEP-DWR-BS (SM_2) baths after 2 h of sequential deposition. However this was not the case for SIEP-DWR-DWS (SM_9) baths where the controlled addition of surfactant in the plating bath restricted the surfactant adsorption and hence did not hinder the metal electroless plating. Another probable reason of lower PPD values for membrane SM_2 could also be that bulk surfactant addition without any agitation did not reduce the strong adsorption of surfactant on the support surface. Thus, agitation during bulk surfactant addition could minimize surfactant adsorption on the support surface and thereby enhance pore densification. Circulating ELP baths with SIEP are thus promising options for future research work.

5.3.2 Theoretical metal film thickness profiles

Fig. 5.4 illustrates the time dependent variation of theoretical metal film thickness for SIEP-DWR-BS (SM_2) and SIEP-DWR-DWS (SM_9) baths. As shown, the nickel film thickness varied from 3.9 -9.8 and 6.3 -9.4 μm for a variation in plating time from 2-8 h for membranes SM_2 and SM_9 respectively. For SIEP-DWR-BS (SM_2) baths, in the initial stages (2h) of plating, the metal film thickness was very low due to poor pore densification, and increased significantly after 8 h of sequential deposition. It was also analyzed that after 8 h of total

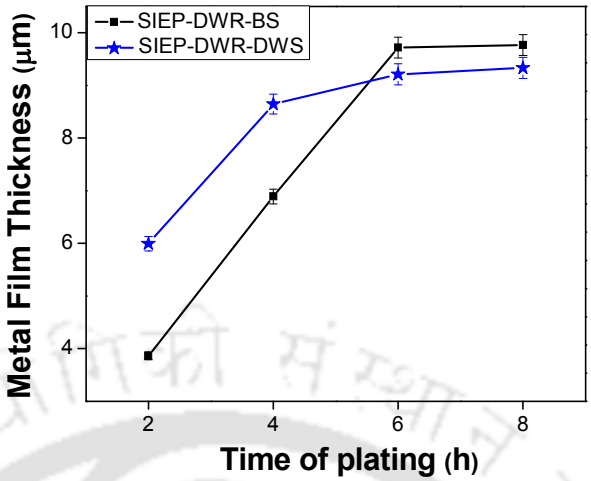

Fig. 5.4: Variation of theoretical Ni film thickness with plating time for SIEP-DWR-BS (SM_2) and SIEP-DWR-DWS (SM_9) baths.

plating time, low PPD exists for SIEP-DWR-BS (SM_2) bath in comparison to the SIEP-DWR-DWS (SM_9) bath. This could be attributed to the undesired phenomena of layering without significant densification. But for SIEP-DWR-DWS (SM_9) baths, higher PPD with lower metal film thickness was achieved. Thus dropwise contacting pattern of surfactant maximized pore densification and minimized metal layering.

In the previous chapter, for bulk addition of both surfactant and reducing agent i.e. SIEP-BR-BS (M_4) baths, a PPD of 87.7% and a metal film thickness of 13.8 μm on a support pore size of 90-120 nm could be obtained after 16 sequential depositions of 1h each. Compared to this case, the SIEP-DWR-DWS (SM_9) baths reported in this chapter provided a PPD of 76.5% and metal film thickness of 9.4 μm on the support (pore size of 150 -250 nm) after 16 sequential depositions in 8 h total plating time. The PPD/δ value for the case presented in the previous chapter was 6.3, which enhanced to 8.1 in this case. Also there has been 50% reduction in total plating time for the case presented in this chapter. In summary, higher pore

size and SIEP process optimality with DWS feature are important inferences during the comparative assessment.

5.3.3 Average plating rate profiles

Fig. 5.5 illustrates the variation of nickel average plating rate with plating time. It can be observed that the plating rates decreased with an increase in plating time. For a variation in plating time from 2-8 h, the average plating rates varied from 8.1- 5.1 × 10^{-5} and from 13.2 – 4.9 × 10^{-5} $\left(\frac{mol}{m^2.s}\right)$ for membranes SM_2 and SM_9 respectively. It was evaluated that for SIEP-DWR-BS (SM_2) baths, the metal average plating rate was lower in the initial hours of plating. This is probably due to the fact that bulk surfactant addition favors its strong adsorption on the support surface and thereby hinders metal deposition. However, with increasing plating time, as more and more reducing agent was added into the bath, the surfactant molecules contributed significantly for the removal of gas bubbles from the surface. At longer plating time, the average plating rates for both baths matched with one another, thus indicating that both SIEP-DWR-DWS (SM_9) and SIEP-DWR-BS (SM_2) baths have similar role of adsorbed

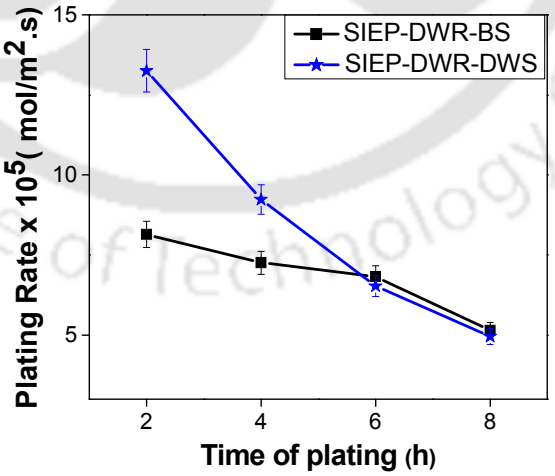

Fig. 5.5: Variation of average Ni plating rate with plating time for SIEP-DWR-BS (SM_2) and SIEP-DWR-DWS (SM_9) baths.

surfactant on support surface to influence metal deposition.In chapter 4, for bulk addition of both surfactant (BS) and reducing agent (BR) i.e. SIEP-BR-BS (M_4) baths, the average plating rate varied from 2.3 – 3.6 × 10^{-5} $\left(\frac{mol}{m^2.s}\right)$ for 4 – 16 h (4 -16 plating steps) on a support pore size of 90-120 nm. As compared to it, the case in this chapter corresponds to an average plating rate variation from 13.2 – 4.9 × 10^{-5} $\left(\frac{mol}{m^2.s}\right)$ for 2 - 8 h (4 -16 plating steps) of nickel deposition on a support pore size of 150-250 nm for SIEP-DWR-DWS (SM_9) baths. This indicates that about 40% enhancement in plating rates and 50% reduction in plating time can be achieved by modifying the process from SIEP-BR-BS (M_4) to SIEP-DWR-DWS (SM_9) baths and enhancement in support pore size.

These analyses are also in agreement with the trends presented by Kitwan et al. (2010). The authors reported that the plating rate and the quality of plating were optimal for supports with in the pore size of 250 – 300 nm and porosity of 35 – 50 %. The case in this chapter referred to the performance characteristics of a low cost ceramic membrane that was characterized with even lower combinations of pore size (150 - 250 nm) and effective porosity (10-15%).

5.3.4 Plating inefficiency profiles

Fig. 5.6 demonstrates the variation of plating inefficiency with plating time. For a variation in plating time from 2-8 h, it can be observed that the plating inefficiency varied from 40.3 – 64.5% and from 30.6 – 40.5 % for SIEP-DWR-BS (SM_2) and SIEP-DWR-DWS (SM_9) baths respectively. For membrane SM_9, the plating inefficiencies reduced by 35% as compared to membrane SM_2. The reason for higher plating inefficiency for SIEP-DWR-BS baths would be due to higher surfactant adsorption on the support which favored higher metal nucleation in the solution. For both cases, the plating inefficiency increased with plating time. This could be explained with the fact that a controlled addition of combined reducing agent (DWR) and surfactant (DWS) could provide a strong metal-support bonding. This resulted

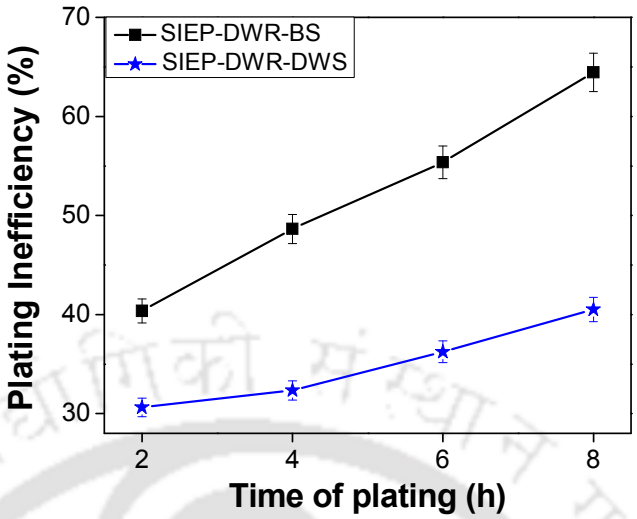

Fig. 5.6: Variation of plating inefficiency with plating time for SIEP-DWR-BS (SM_2) and SIEP-DWR-DWS (SM_9) baths.

in the reduction of metal nucleation in the solution and eventually lower plating inefficiency. But with increasing plating time, as more and more active sites are occupied, the metal has to bond with another metal particle. The metal - metal bond adhesion is not as strong as compared to metal – support adhesion which resulted in higher metal nucleation in the solution and eventually higher plating inefficiency at prolonged plating time.

5.4 Plating characteristics for SSOEP-DWR baths

5.4.1 PPD profiles

Fig. 5.7 presents the time dependent variation of PPD for SSOEP baths. For a variation in plating time from 2-8 h, it can be observed that the PPD profiles varied from 54.6 -73.4 % and from 33 – 66.9 % for SSOEP-DWR-BS (SSM_1) and SSOEP-DWR-DWS (SSM_2) baths respectively. Thus, membrane SSM_1 provided faster pore densification as compared to

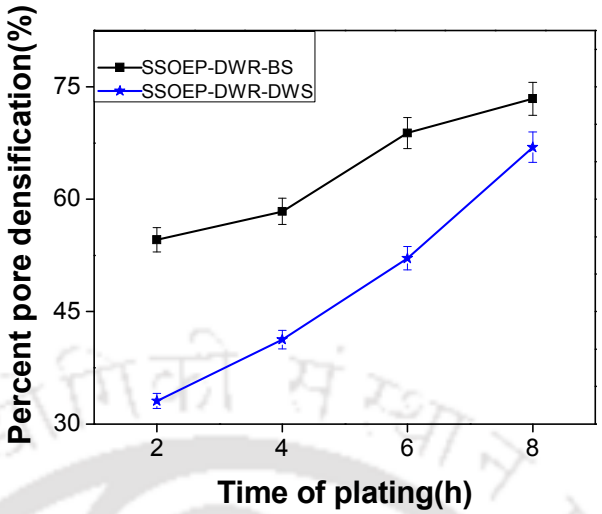

Fig. 5.7: Variation of PPD with plating time for SSOEP-DWR-BS (SSM_1) and SSOEP-DWR-DWS (SSM_2) baths.

membrane SSM_2. For SSOEP-DWR-BS (SSM_1) baths, the surfactant adsorption on the surface is minimized by cavitation effect (caused by ultrasonic waves) which also favored the minimization of pitting and metal nucleation in the solution and hence faster densification. However, for SSOEP-DWR-DWS (SSM_2) baths, the combination of agitation caused by ultrasonic waves and dropwise addition of surfactant failed to provide higher densification as compared to the case with SSOEP-DWR-BS (SSM_1) baths. This is due to the fact that cavitation effect favored faster removal of gas bubbles adhering to the support surface which causes greater metal nucleation in the solution and reduce the PPD. Thus it is interesting to note that there exists a sensitive dependence of PPD on the contacting pattern of the surfactant and cavitation effect. A comparison of PPD profiles for SIEP-DWR-DWS (SM_9) baths (Fig. 5.5) and SSOEP baths (Fig. 5.9) confirm that the SIEP baths perform better than SSOEP baths in terms of pore densification.

5.4.2 Theoretical metal film thickness profiles

Fig. 5.8 illustrates the profiles for time dependent variation of theoretical metal film thickness with plating time. It can be observed that the nickel film thickness varied from 5.2 – 8.4 µm and from 10.6 -13.3 µm for a plating time variation from 2-8 h for SSOEP-DWR-BS (SSM_1) and SSOEP-DWR-DWS (SSM_2) baths respectively. It was analyzed that for membrane SSM_1, the variation in metal film thickness was uniform with plating time which indicates higher stability and better adhesion of the metal film. The desired feature of efficient electroless plating is higher pore densification with lower metal film thickness. These features were better achieved for SSOEP-DWR-BS (SSM_1) baths. For SSOEP-DWR-DWS (SSM_2) baths the metal film thickness doubled along with 9% reduction in pore densification as compared to SSOEP-DWR-BS (SSM_1) baths. The probable reasons for the same have been explained in section 5.2.2.

Till date, to the best of our knowledge, no literatures are available for SSOEP baths from the perspective of achieving faster PPD and quality metal deposition. Therefore, SOEP (BR) has

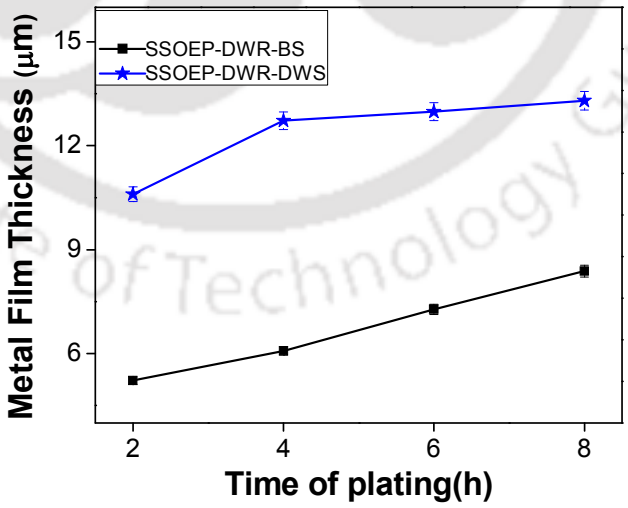

Fig. 5.8: Variation of theoretical Ni film thickness with plating time for SSOEP-DWR-BS (SSM_1) and SSOEP-DWR-DWS (SSM_2) baths.

been considered for comparison. In chapter 3 (sections 3.5.2 and 3.5.4),with bulk addition of reducing agent for SOEP-BR (M_5) baths, a PPD of 72.8% with a metal film thickness of 15.5 μm on a support pore size of 90-120 nm was obtained after 16 sequential depositions of 1h time duration for each plating step. As compared to it, for the case corresponding to SSOEP-DWR-BS (SSM_1) baths, a PPD of 73.4% and a metal film thickness of 8.8 μm were achieved on a support pore size of 150 -250 nm after 8 h of total plating time. The PPD/δ for the case in chapter 3 (i.e. SOEP-BR (M_5) baths) was 4.7 whereas in the present case (i.e SSOEP-DWR-BS (SSM_1) baths) it is 8.3. Further, a reduction in total plating by 50% is promising. A comparison of metal thickness growth profiles for SIEP-DWR-DWS (SM_9) baths (Fig. 5.4) and SSOEP baths (Fig. 5.8) confirms that lower film thicknesses were achieved for SSOEP-DWR-BS (SSM_1) baths. The possible reason to achieve lower film thickness profiles for this case is due to the optimality of coupled cavitation and dispersion effect which were induced by sonication and surfactant respectively.

5.4.3. Average plating rate profiles

Fig. 5.9 illustrates the variation of metal average plating rate with plating time. It can be observed that the plating rates decreased with an increase in plating time. The average plating rates varied from 11- 4.4 × 10^{-5} and from 22.3 – 7 × 10^{-5} $\left(\frac{mol}{m^2.s}\right)$ for SSOEP-DWR-BS (SSM_1) and SSOEP-DWR-DWS (SSM_2) baths respectively. It can be observed that there was a significant difference in plating rate trends for both cases. Higher plating rates exist for membrane SSM_2 which implies to the prominent effect of cavitation phenomena that favored the formation and collapse of the bubbles without subsequent enhancement in pore densification. However, due to significantly higher PPD (73.4%) and lower film thickness (8.4 μm) for SSOEP-DWR-BS (SSM_1) baths as compared to SSOEP-DWR-DWS (SSM_2)

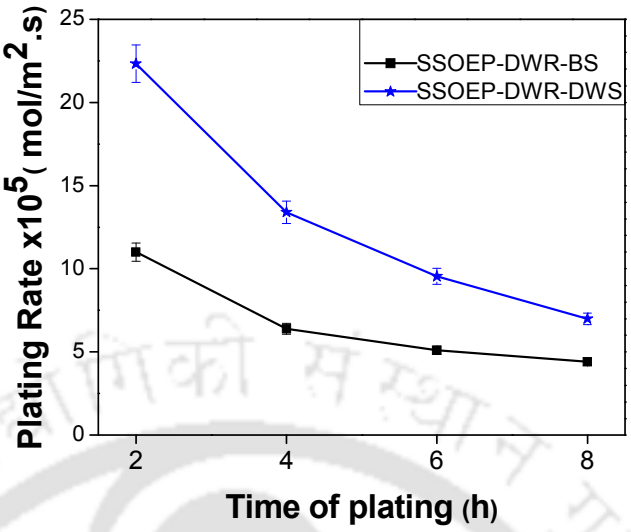

Fig. 5.9: Variation of average plating rate with plating time for SSOEP-DWR-BS (SSM_1) and SSOEP-DWR-DWS (SSM_2) baths.

baths (PPD of 66.9% and film thickness of 13.3 μm), the SSOEP-DWR-BS (SSM_1) baths can be inferred to provide higher $\frac{PPD}{\delta}$ which is highly desired. Compared to SIEP-DWR-DWS (SM_9) plating baths (Fig. 5.5), comparatively higher plating rates were obtained for both SSOEP-DWR-DWS (SSM_2) and SSOEP-DWR-BS (SSM_1) plating baths (Fig. 5.9). This observation is in accordance with the crystal (Fig. 5.1) and particle size growth (Fig. 5.2) trends. Hence, it is apparent that cavitation effect improved plating rates.

In chapter 3, with bulk addition of both surfactant and reducing agent i.e. SOEP-BR (M_5) baths, the plating rate varied from 5.2- 4.3 × 10^{-5} $\left(\frac{mol}{m^2.s}\right)$ for 8 – 24 h (1h duration for each plating step) on a support possessing an average pore size of 90-120 nm. As compared to it, the case in this chapter referred to a plating rate of 11- 4.4 × 10^{-5} $\left(\frac{mol}{m^2.s}\right)$ for 2 - 8 h (½ h duration for one plating step) on a support with an average pore size of 150 -250 nm adopting SSOEP-DWR-BS (SSM_1) baths. Therefore, at higher support pore size and relevant

modifications (SSOEP-DWR-BS (SSM_1) baths), the plating rates enhanced many times by altering the process from SOEP-BR (M_5) to SSOEP-DWR-BS (SSM_1) baths.

5.4.4 Plating inefficiency profiles

Fig. 5.10 demonstrates the variation of plating inefficiency with plating time. It can be observed that the plating inefficiency varied from 32.8 – 10.2 % and from 37– 61.6 % for SSOEP-DWR-BS (SSM_1) and SSOEP-DWR-DWS (SSM_2) baths respectively. It was analyzed that for SSOEP-DWR-DWS (SSM_2) baths the inefficiency profiles were similar to the trends discussed in section 5.3.4. However, contradictory trend was observed for SSOEP-DWR-BS (SSM_1) baths. This might be due to significant surfactant adsorption on the surface at prolonger plating time periods, which enhanced metal adhesion to the support surface and minimized pitting and metal nucleation in the solution. It is further interesting to note that stronger nickel film adhesion to the support surface could be explored further to deposit a different metal (Pt or Pd) and hence provide promising opportunities to explore further in future research.

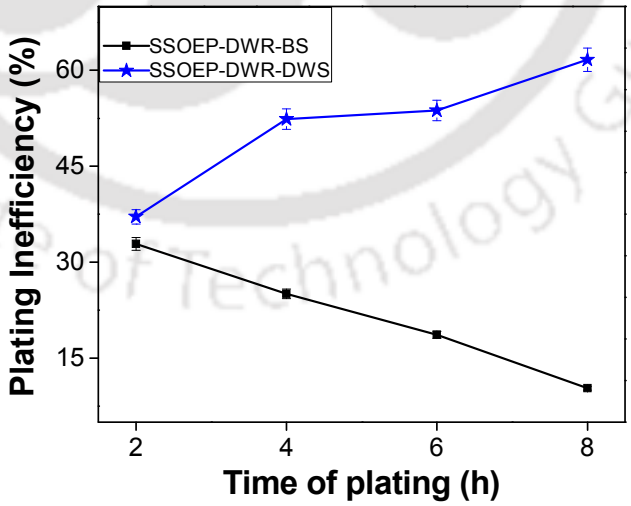

Fig. 5.10: Variation of plating inefficiency with plating time for SSOEP-DWR-BS (SSM_1) and SSOEP-DWR-DWS (SSM_2) baths.

5.5 Tradeoffs

5.5.1 PPD/δ profiles

Fig. 5.11 illustrates the variation of $\frac{PPD}{\delta}$ with plating time for various combinations of SIEP and SSOEP baths. It can be observed that $\frac{PPD}{\delta}$ varied from 7.9 -7.3, 8 - 8.1, 3.1 - 5 and 10.5 – 8.8 for a plating time variation from 2 – 8 h for membranes SM_2, SM_9, SSM_9 and SSM_1 respectively. In general, an efficient electroless plating process must provide faster pore densification with minimal metal film thickness i.e. higher $\frac{PPD}{\delta}$ values. From $\frac{PPD}{\delta}$ perspective, the most promising option is SSOEP-DWR-BS (SSM_1) baths and the most unfavorable process is SSOEP-DWR-DWS (SSM_9) baths. An undesired feature of reduction in $\frac{PPD}{\delta}$ as observed for SIEP-DWR-BS (SM_2) baths could be due to the fact that PPD and δ

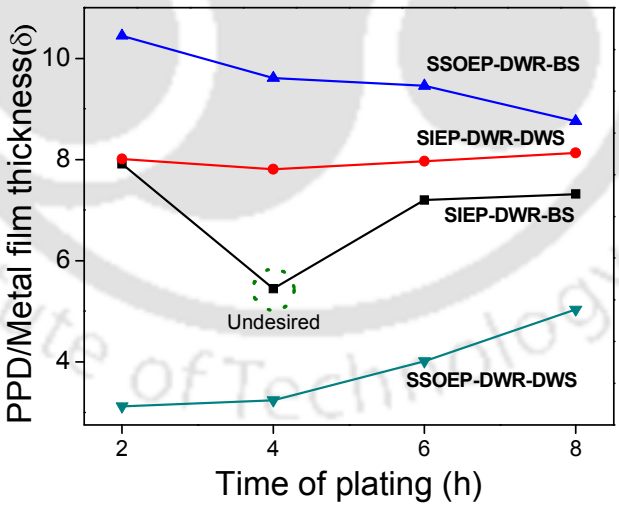

Fig. 5.11: Variation of PPD/δ with plating time for SIEP-DWR-BS (SM_2), SIEP-DWR-DWS (SM_9), SSOEP-DWR-BS (SSM_1) and SSOEP-DWR-DWS (SSM_2) baths.

did not enhance simultaneously. For such a scenario, metal layering was significant in comparison with the PPD which might be due to the strong surfactant adsorption on the surface due to its bulk addition.

5.5.2 PPD/Plating rate profiles

Fig. 5.12 is a conceptual extension of the experimental findings to observe clear distinction between metal layering and pore densification in terms of PPD vs. $\frac{\text{PPD}}{\bar{r}_i}$. Hypothetically, $\frac{\text{PPD}}{\bar{r}_i}$ is a measure to quantify the dominance of pore densification or layering. Higher value of $\frac{\text{PPD}}{\bar{r}_i}$ for similar time of plating signifies that the plating favors better PPD and a lower $\frac{\text{PPD}}{\bar{r}_i}$ refers to significant layering. It can be observed that SSOEP-DWR-DWS baths

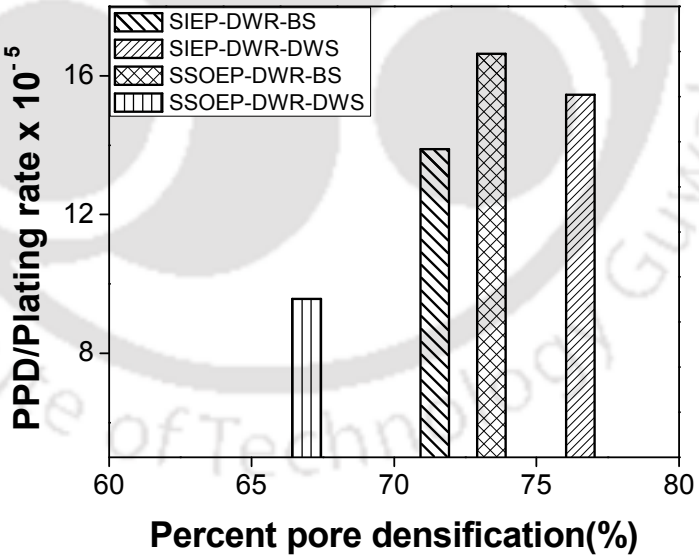

Fig. 5.12: Variation of PPD/plating rate with plating time for SIEP-DWR-BS (SM_2), SIEP-DWR-DWS (SM_9), SSOEP-DWR-BS (SSM_1) and SSOEP-DWR-DWS (SSM_2) baths.

provided lower $\frac{PPD}{\bar{r}_i}$ thereby indicating that sonication for this case provided metal layering which is in agreement with the literatures (Lu, 2010; Touyeras et al., 2005). For a process to be suitable for commercialization, it is very important that the plating is favorable towards pore densification but not metal layering. Thus SSOEP-DWR-BS (SSM_1) baths are the best amongst the four modified electroless techniques in terms of PPD but not layering. Thus depending on objectives and priorities the processes could be deployed.

In summary, the process modification approach presented in this work can be used as a new methodology for the assessment of nickel electroless plating baths with desired morphological parameters. The experimental research findings in this work extend the conclusions presented by Kathirgamanathan (1994) for SOEP baths and Islam et al. (2012) for SIEP baths. While Kathirgamanathan (1994) inferred that SOEP baths enable enhancing the metal film thickness on the membrane surface, the SSOEP baths with suggested variation (dropwise addition of reducing agent) reduce the metal film thickness along with the enhancement in PPD. On the other hand, while Islam et al. (2012) inferred that the utilization of surfactant enhances plating rate and therefore reduce required total plating time for desired thickness. Overall this chapter confirmed that the dropwise addition of the reducing agent and surfactant in the SIEP simultaneously enhanced plating rate and reduced metal film thickness, which is the most relevant characteristic for metal composite membrane fabrication.

5.6 Summary

The chemistry involving the interaction between surfactant, metal and reducing is highly complex. This work gives good number of insights with respect to possible modification to metal ELP for metal composite membrane fabrication. Inferences drawn from this work are presented as follows: (a) SIEP-DWR-DWS (SM_9) baths performed better than SIEP-DWR-BS (SM_2) baths which indicates that stronger adsorption of surfactant molecules in the latter

case hindered pore densification (b) SSOEP-DWR-BS (SSM_1) baths performed better than SSOEP-DWR-DWS (SSM_2) baths which indicates that cavitation is useful only when surfactant addition has been facilitated in bulk mode, which is a very important inference.

In summary, the optimal order of various baths from the perspective of various desired process characteristics is presented as follows:

a) Maximization of PPD: SIEP-DWR-DWS > SSOEP-DWR-BS > SIEP-DWR-BS > SSOEP-DWR-DWS.

b) Maximization of $\frac{PPD}{\delta}$: SSOEP-DWR-BS > SIEP-DWR-DWS > SIEP-DWR-BS > SSOEP-DWR-DWS

c) Maximization of $\frac{\text{PPD}}{\bar{r}_i}$: SSOEP-DWR-BS > SIEP-DWR-DWS > SIEP-DWR-BS > SSOEP-DWR-DWS

d) Maximization of η: SSOEP-DWR-BS > SIEP-DWR-DWS > SSOEP-DWR-DWS > SIEP-DWR-BS.

Typically, during dense metal composite membrane fabrication, case (a) or case (b) are preferred and therefore, the suggested modifications to SIEP and SSOEP baths presume paramount relevance and need to be more thoroughly investigated from the perspective of process scale up and large scale fabrication.Thus the most viable options for metal electroless plating process for maximizing $\frac{PPD}{\delta}$, $\frac{\text{PPD}}{\bar{r}_i}$ and η are SSOEP-DWR-BS (SSM_1), and for maximizing PPD are SIEP-DWR-DWS (SM_9) baths respectively. This indicates that the cavitation effect induced by a sonicator bath is comparatively effective to achieve thin dense metal films on ceramic supports which are not the case for SIEP baths. This being the most important inference of this chapter thereby requires furthering studies towards the scale up and cost effective sonication assisted fabrication of dense metal composites membranes.

Efficacy of Surfactant Concentration on the Performance Characteristics of Nickel ELP Baths Coupled with Ultrasound

This chapter addresses the combinatorial plating characteristics for the fabrication of nickel ceramic composite membranes elaborating upon the role of surfactant type, and its concentration in SSOEP baths. CTAB (cationic) and SDS (anionic) surfactants were investigated for their optimality. Section 6.2 summarizes relevant surface characterization results. Section 6.3 elaborately presents the effect of solution concentration of surfactants (1-6 CMC) on combinatorial plating characteristics and associated tradeoffs. Finally, summary is presented in section 6.4.

6.1 Introduction

In recent years, researchers have explored the role of either surfactant (Elansezhian et al., 2008; Elansezhian et al., 2009; Nwosu et al., 2012) or sonication (Touyeras et al., 2005; Wu et al., 2009) separately from several chemical engineering perspectives. However, only very few researchers have studied a combination of ultrasound with surfactant in various fields of chemical engineering which do not target the fabrication of metal ceramic composite membranes. Therefore, there is a need to generate data that elaborates upon the role and influence of surfactant (concentration, type) in achieving dense metal composite membranes.

Also literature conveys that researchers have studied SDS (anionic) surfactant because of its low cost(Nwosu et al., 2011; Zielinska et al., 2012). However, combinatorial plating characteristics (PPD, plating efficiency, metal film thickness) have not been the target of their work. Further, amongst cationic surfactants, DTAB has been studied in a number of

literatures (Ilias and Islam, 2012; Islam et al., 2012) but a systematic study targeting the optimal combination of plating time, metal layer thickness and pore densification was not studied by the authors. Amongst various cationic surfactants, CTAB is more promising to explore than DTAB due to its lower cost (40 times lower than the average cost of DTAB) and lower HLB value (Chen et al., 2002; Nwosu et al., 2012). Also, authors (Bulasara et al. 2011b) used CTAB and studied the effect of surfactant concentration on the performance characteristics of the electroless plating baths using sodium hypophosphite as the reducing agent. However, literature is not available for the utilization of hydrazine as reducing agent during surfactant induced electroless plating for the fabrication of nickel ceramic composite membranes. Thus the major objective of this work is to explore upon the role of surfactant type and sonication on the efficient fabrication of metal composite membranes adopting hydrazine as the reducing agent.

This chapter addresses the combinatorial plating characteristics for SSOEP plating baths to fabricate nickel ceramic composite membranes. Cationic surfactant CTAB and anionic surfactant SDS have been deployed to elaborate upon the role of the surfactant type during coupled sonication and surfactant assisted nickel electroless plating. Laboratory fabricated circular ceramic substrates (with an average pore size of 150 – 250 nm, diameter of 36 mm and a thickness of 3.5 mm) were used as supports in this work. Variations in solution concentrations (1 – 6 CMC) for both surfactants have been primarily targeted to maximize percent pore densification per unit metal film thickness deposited on the membrane. Thereby, comparative experimental investigations attempts to identify optimal combinations of surfactant type and its concentration during ultrasound assisted nickel electroless plating for metal ceramic composite membrane fabrication. The combinatorial plating characteristics were evaluated in terms of average trans-membrane flux $\overline{J}$, plating inefficiency, theoretical metal film thickness (δ) and percent pore densification $PPD(\%)$.

6.2 Surface characterization

For the raw materials, particle size distribution profiles evaluated from LPSA and FTIR spectral analysis were similar to those elaborated in sections 3.4.1 and 4.2.1 of the thesis. The N_2 adsorption-desorption study conducted using a surface area analyzer for the ceramic substrate had been presented in section 4.2.1 of the thesis. Fig. 6.1 presents the XRD patterns of nickel membrane SSM_1 and SSM_8 fabricated with both cationic and anionic surfactant for SSOEP-DWR-BS baths. ICDD-JCPDS database was used for the phase analysis of the diffraction profiles. The XRD patterns of the ceramic support are similar to those presented in section 3.4.4 of the thesis. The metallic nickel peaks for the fabricated membranes appeared at diffraction angles of $2\theta = 44.5^{o}$ and 51.8^{o} due to the diffraction of (111) and (200) plane [Pdf No 00-004-0850]. It was observed that the quartz peak exists for anionic surfactant after 8 h of plating which confirmed non-uniform deposition. But for SSOEP-DWR-BS baths with cationic surfactant (SSM_1) no such quartz peaks were visible.

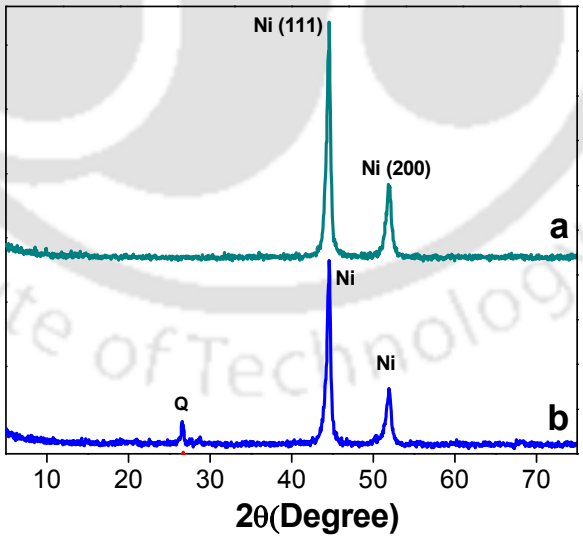

Fig. 6.1: XRD patterns of Ni membrane fabricated with SSOEP-DWR-BS baths with for (a) CTAB (cationic) (SSM_1) and (b) SDS (anionic) (SSM_8) surfactant.

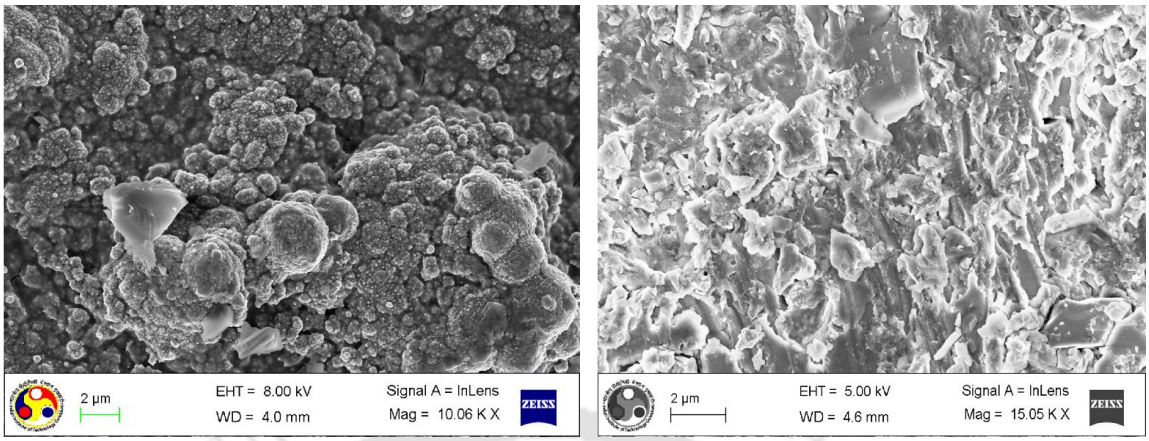

(a) (b)

Fig. 6.2: Surface FESEM micrographs of membranes fabricated with (a) CTAB (cationic) (SSM_1) and (b) SDS (anionic) (SSM_8) surfactant using SSOEP-DWR-BS baths.

Fig. 6.2 presents the FESEM micrographs for cationic and anionic surfactant respectively. It was observed that for CTAB, well developed metal aggregates exist which affirmed that the agitation caused by ultrasonic waves during sonication was effective towards uniform metal deposition. This was not the case for the membrane fabricated with SDS surfactant as no such metal aggregates were observed in the micrographs

6.3 Performance characteristics of SSOEP-DWR-BS baths

6.3.1 Plating inefficiency profiles

Fig. 6.3 presents the time dependent variation of plating inefficiency for both CTAB (SSM_3, SSM_4, SSM_1 and SSM_5) and SDS (SSM_6, SSM_7, SSM_8 and SSM_9) surfactant respectively. It was evaluated that the plating inefficiencies varied from 62.4 – 59.9, 40.6 – 23.3, 32.8 - 10.2, 57.4 – 40.1% for membranes SSM_3, SSM_4, SSM_1 , SSM_5 and from 72-31.4, 62.5-31.4, 63.5-49.7, 61-26.3% for membranes SSM_6, SSM_7, SSM_8 and SSM_9 with a surfactant concentration of 1, 2, 4 and 6 CMC respectively and a variation in plating time from 2-8 h respectively.

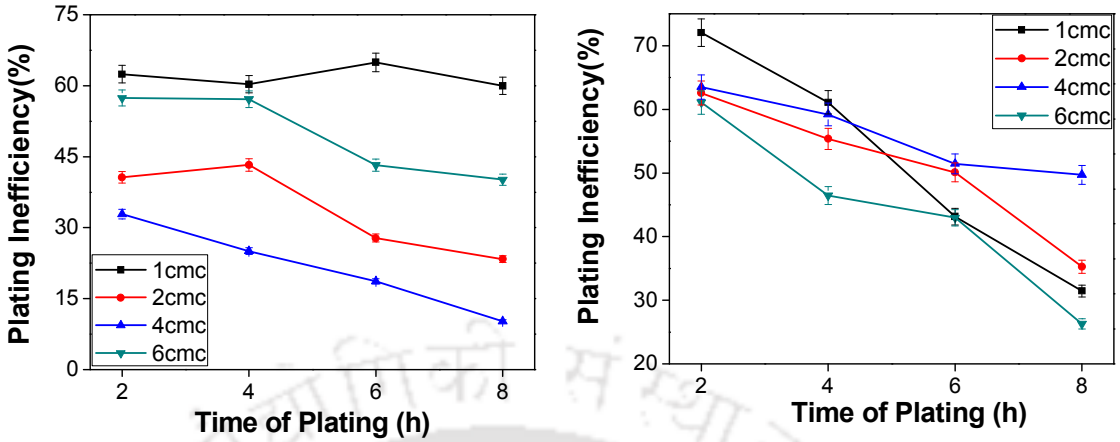

(a) **(b)**

Fig. 6.3: Variation of plating inefficiency with plating time for Ni membranes prepared with (a) cationic (CTAB) and (b) anionic (SDS) surfactant using SSOEP-DWR-BS baths.

It can be observed that for all surfactant concentrations, the plating inefficiencies were lower for CTAB as compared to SDS surfactant. This could probably be due to the significant role of cationic surfactant to take part in the reaction and thereby minimize pitting, lower metal nucleation in the solution and eventually lower plating inefficiencies. Further for cationic surfactant amongst all concentrations it was observed that at 4 CMC (SSM_1) the plating inefficiencies were lowest which further increased for a solution concentration of 6 CMC (SSM_5). This is in agreement to the work of Chen et al. (2002) who inferred that an optimal surfactant concentration exists beyond which the plating characteristics tend to degrade due to the uneven charge distributions on the membrane surface at higher surfactant solution concentration. This in turn enhances pitting, metal nucleation in solution and reduces plating efficiency.

6.3.2 PPD profiles

Fig. 6.4 presents the time dependent variation of PPD for CTAB (SSM_3, SSM_4, SSM_1 and SSM_5) and SDS (SSM_6, SSM_7, SSM_8 and SSM_9) surfactant respectively. It can be observed that PPD varied from 28.5 – 47.6, 39 – 60.2, 54.5 – 73.4 and 31.1 – 64.4 % for membranes SSM_3, SSM_4, SSM_1 , SSM_5 and from 8.7- 28.7, 12-33.5, 17.3-43.8 and 19.2-45 % respectively for membranes SSM_6, SSM_7, SSM_8 and SSM_9 with a surfactant concentration of 1, 2, 4 and 6 CMC and a variation in plating time from 2-8 h. It can be also observed that the pore densification process was low when anionic surfactant was used in the plating bath. This is in agreement to the work of Su et al. (1985) who reported that there was a drop in its CMC when SDS interacted with divalent copper ions.

Further Nwosu et al. (2012) also stated that a reduction in the concentration at which a surfactant achieves its CMC is an undesired feature. It resembles a lower effectiveness of the surfactant. Thus lower pore densification for anionic surfactant represents either lower effectiveness of the surfactant or a probable need for a higher concentration of it. But that

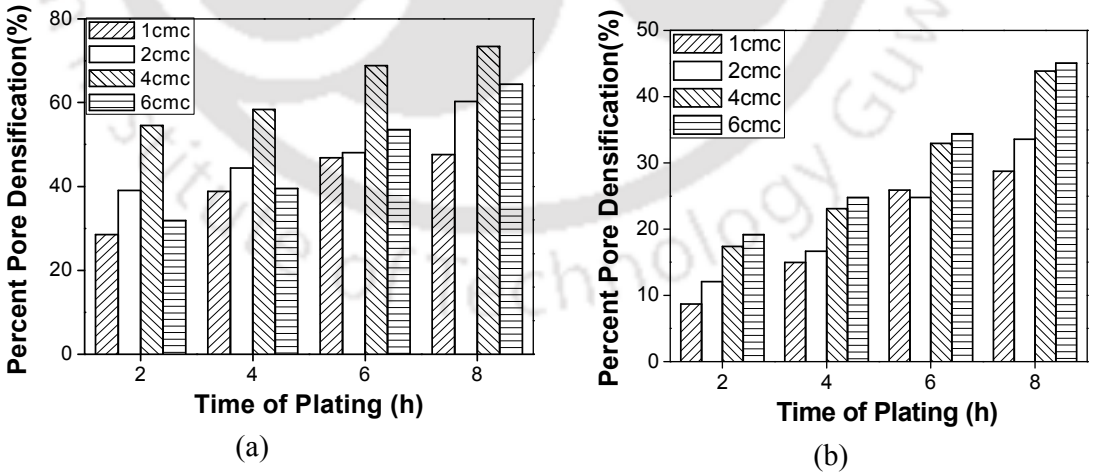

Fig. 6.4: Variation of PPD with plating time for Ni membranes prepared with (a) cationic (CTAB) and (b) anionic (SDS) surfactant using SSOEP-DWR-BS baths.

was not the case with cationic surfactant where the pore densification rate was comparatively fast. Amongst all cases for CTAB, it was observed that 4 CMC was the optimal surfactant concentration that provided the highest PPD (73.4%) for a plating time of 8 h. The reduction in the PPD at higher surfactant concentration (6 CMC) for cationic surfactant is indicative to the fact that higher surfactant concentrations do not favor pore densification and contribute to layering of films which is a highly undesired feature in the fabrication of dense metal composite membranes. Probable reason for the same has been presented in section 6.3.1.

6.3.3 Theoretical metal film thickness Profiles

Fig. 6.5 presents the time dependent variation of theoretical metal film thickness (δ) for CTAB and SDS surfactant respectively. It can be observed that for membranes SSM_3, SSM_4, SSM_1, SSM_5 and for membranes SSM_6, SSM_7, SSM_8 and SSM_9 the metal film thickness varied from 4.4 – 7.6, 5.3 – 7.8, 5.2- 8.4, 3.9 – 10.9 µm and 2.2-5.4, 2.4-7.7, 3.3-8.7 and 3.5-8.7 µm for a surfactant concentration of 1, 2, 4 and 6 CMC and a variation in plating time from 2-8 h respectively. It was observed that metal film thickness increases with increasing surfactant concentration. For CTAB, it can be analyzed that for an increase in CMC from 4-6, the increase in metal film thickness was 31% for a corresponding PPD reduction by 12 %. The reduction in the PPD with enhancement in metal film thickness is due to the phenomenon of layering as discussed in in section 6.3.1.

6.3.4 PPD/Metal film thickness tradeoffs

Fig. 6.6 illustrates the variation of $\frac{PPD}{\delta}$ with plating time for both cationic and anionic surfactant at higher surfactant concentration (4-6 CMC) (SSM_1, SSM_5, SSM_8 and SSM_9) It can be observed that $\frac{PPD}{\delta}$ varied from 10.4-8.7 (SSM_1) and 8.2 – 5.9 (SSM_5) for CTAB and

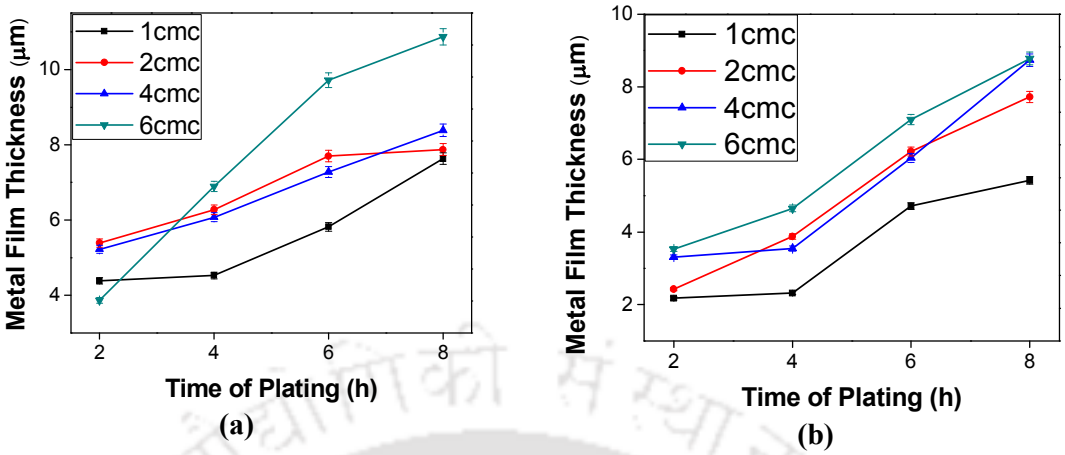

Fig. 6.5: Variation of theoretical metal film thickness (δ) with plating time for Ni membranes prepared with (a) cationic (CTAB) and (b) anionic (SDS) surfactant using SSOEP-DWR-BS baths.

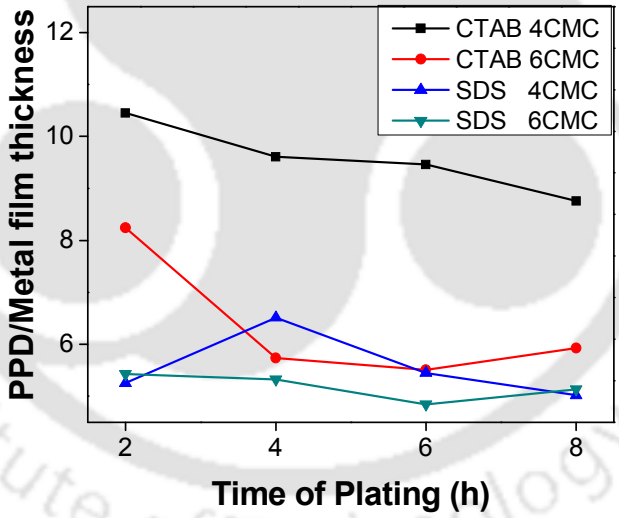

Fig. 6.6: Variation of PPD/δ with plating time for various cases.

from 5.2 - 5 (SSM_8) and 5.4– 5.1 (SSM_9) for SDS with a surfactant solution concentration of 4-6 CMC. Hypothetically, an efficient electroless plating process shall provide maximum pore densification and minimal metal film thickness i.e. higher $\frac{PPD}{\delta}$ values. From $\frac{PPD}{\delta}$ perspective, the most promising option is CTAB with a concentration of 4 CMC (SSM_1) and

the most unfavorable option is SDS with a concentration of 6 CMC (SSM_9). For anionic surfactant a drop in $\frac{PPD}{\delta}$ clearly states that, metal layering or layered structure was significant for this case. This is probably due to the strong surfactant adsorption on the surface due to its bulk addition.

6.3.5 Comparison with literature data

Till date, to the best of our knowledge, no literatures are available for SSOEP baths from the perspective of achieving faster PPD and quality metal deposition. The case presented in chapter 3, corresponds to bulk addition of reducing agent and CTAB (4 CMC). For that case it was observed that SOEP-BR (M_5) and SIEP-BR (M_4) baths gave a PPD of 72.8 % and 87.7 % with a metal film thickness of 15.5μm and 13.8μm on a substrate pore size of 90-120 nm after 16 sequential depositions of 1h time duration for each plating step. As compared to it, in this work for SSOEP-DWR-BS (SSM_1) baths with CTAB (4 CMC) a PPD of 73.4% and a metal film thickness of 8.8 μm were achieved on a substrate pore size of 150 -250 nm after 8 h of total plating time. The PPD/δ in chapter 3, for SOEP-BR (M_5) and SIEP-BR (M_4) baths was 4.7 and 6.3 respectively whereas in the present case (i.e SSOEP-DWR-BS (SSM_1) baths) it is 8.7. Further, a reduction in total plating by 50% is promising. Thus, coupled sonication and surfactant technique seems to be the optimal process for the effective fabrication of metal ceramic composites with maximum pore densification and minimal metal film thickness.

6.4 Summary

Several insights could be gained from this work with respect to surfactant type and concentration along with possible modification to metal ELP for metal composite membrane fabrication. Specific inferences drawn include: (a) The efficacy of CTAB in comparison with SDS to achieve desired combinatorial plating characteristics (b) The optimal concentration of

CTAB as evaluated from rigorous experimentation was found to be 4 CMC (SSM_1) where maximum $\frac{PPD}{\delta}$ has been obtained. A higher CMC reduced plating process characteristics drastically (c) Anionic surfactants were not all suitable from the perspective of faster pore densification, lower metal film thickness and higher plating efficiency (d) Optimal combinatorial plating characteristics correspond to pore densification (73.4%), metal film thickness (8.4μm) and plating efficiency (89.9%) using SSOEP-DWR-BS (SSM_1) baths.

In summary the most feasible options for fabricating metal electroless plating process with higher $\frac{PPD}{\delta}$ is SSOEP-DWR-BS (SSM_1) baths with a cationic surfactant namely CTAB at 4CMC solution concentration. Further, this work indicated that the ultrasonic cavitation effect induced by sonication was useful to achieve thin dense metal films on ceramic supports.

Performance Characteristics of Palladium Electroless Plating Baths Coupled with and Without Rate Enhancement Techniques

In this chapter the results are presented in five sections. Section 7.2 summarizes on physical and surface characterization techniques. Section 7.3 presents details with respect to the optimal process for the fabrication of dense palladium ceramic composite membranes. Section 7.4 elaborates on the effect of palladium concentration from the perspective of better process characteristics. Section 7.5 addresses upon the retail cost perspectives of the fabricated membrane and those reported in the literature. Finally, section 7.6 briefly summarizes the optimal process and membrane characteristics for the fabrication of dense Ni and Pd ceramic membranes.

7.1 Introduction

In the past decade, significant research efforts have been made in the development of palladium composite membranes for gas separation on stainless steel supports (Islam et al., 2012). However, there exists a significant effort in the research related to fabrication of these membranes on ceramic supports. Further, due to high cost of Pd, there is a need to focus upon reducing the Pd solution concentration to achieve the dense membranes. This chapter explicitly focuses on the fabrication of palladium ceramic composite membrane from the insights gained in the previous chapters.

The market for palladium composite membranes towards commercial hydrogen separation is significantly restricted due to their higher fabrication costs, which is in turn a function of the higher Pd metal cost. Thus, achieving dense Pd composites without jeopardizing upon their

fabrication process characteristics at a lower material and fabrication cost is a challenging task and has been the major goal of Pd membrane research targeted in this work.

The high cost of material and fabrication are important issues for commercialization and drive research and innovation for dense Pd membrane fabrication in the following perspectives: (a) Identification and deployment of a cost effective fabrication technique that has the versatility of process scale up, by employing a low cost support (support) material and (b) Optimizing the identified fabrication technique for efficient dense Pd membrane fabrication to achieve minimal Pd utilization and maximum process efficiency. The insights obtained from the previous chapters for nickel plating baths with reference to the controlled addition of the reducing agent and surfactant were used for the fabrication of dense palladium ceramic composite membranes. The reducing agent strategy for various plating baths referred to drop wise addition of hydrazine hydrate. Further, as discussed in section 5.3 of the thesis, SIEP-DWR-DWS (SM_9) baths served better than SIEP-DWR-BS (SM_2) baths due to controlled addition of surfactant. This is due to the tendency of surfactant to get adsorbed on the support surface. Thus, SIEP baths in this chapter refers to SIEP-DWR-DWS (PM_3) baths whereas CEP, SOEP and SSOEP baths refer to CEP-DWR (PM_1), SOEP-DWR (PM_2) and SSOEP-DWR-BS (PM_4) baths respectively. Further details with respect to composition of the Pd plating bath has been presented in section 2.5 of the thesis.

In this chapter, section 7.2 elaborates upon the membrane characterization details such as FESEM and XRD analysis. Section 7.3 presents the combinatorial plating characteristics for various plating baths namely CEP (PM_1), SOEP (PM_2), SIEP (PM_3) and SSOEP (PM_4) respectively. Further, section 7.4 details with respect to the effect of palladium solution concentration (in the range of 0.005-0.015 mol/L) in influencing combinatorial plating characteristics. Tradeoffs associated with various fabrication processes and palladium

solution concentration have been presented in section 7.5. Further section 7.6 addresses the retail cost of the fabricated dense ceramic composite membrane along with cost comparison of similar dense palladium membranes reported in the literature. Finally, section 7.7 summarizes optimal nickel and palladium ELP process and membrane characteristics for comparison purposes.

7.2 Membrane characterization

7.2.1 LPSA, FTIR & BET analysis

Laser particle size analysis of the raw materials confirmed the presence of particle size in the range of 3.4- 20.3µm respectively. Further, Fourier transform infrared spectra recorded from wavenumber 4000 to 500 cm^{-1} confirmed the presence of characteristics peaks of kaolin for the raw material. Details with respect to other characteristic peaks have been presented section 4.2.1 of the thesis. Nitrogen adsorption - desorption experiment at 77K performed by using a surface area analyzer for the support material confirmed the presence of meso and macropores with no micropores. Type III isotherm with H_3 hysteresis loop was observed.

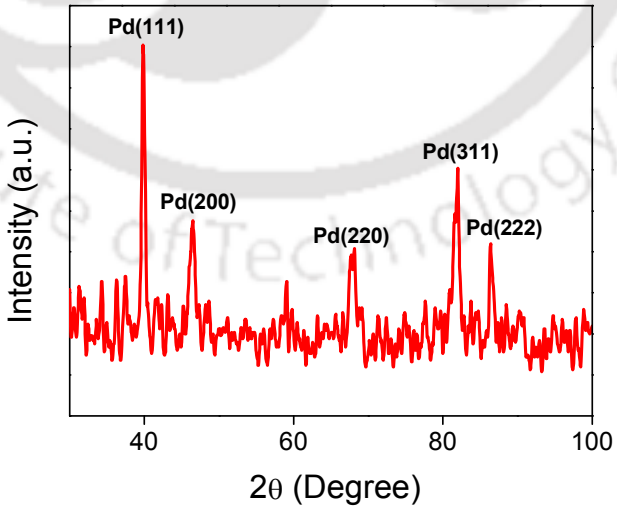

Fig. 7.1: XRD pattern of Pd-ceramic composite membrane (PM_4) fabricated using SSOEP baths.

Further details with respect to BET surface area and total pore volume are similar to that discussed in section 4.2.1 of the thesis.

7.2.2 XRD analysis

Fig. 7.1 illustrates the XRD profiles of dense Pd ceramic membrane fabricated by coupled sonication and surfactant induced electroless plating (PM_4). ICDD-JCPDS database was used for the phase analysis of the diffraction profiles. The metallic Pd peaks appeared at diffraction angle 2θ= 40.1°, 46.6°, 68.1° , 82.1° and 86.6° due to the diffraction of (111), (200), (220), (311) and (222) plane respectively [Pdf No 00-005-0681] which confirms the existence of polycrystalline Pd structure throughout the surface.

7.2.3 FESEM analysis

Fig. 7.2 illustrates the FESEM cross sectional micrograph of Pd-ceramic composite membrane fabricated with SSOEP baths. It can be analyzed that the palladium dense metal film thickness varied in the range of 10-12µm respectively.

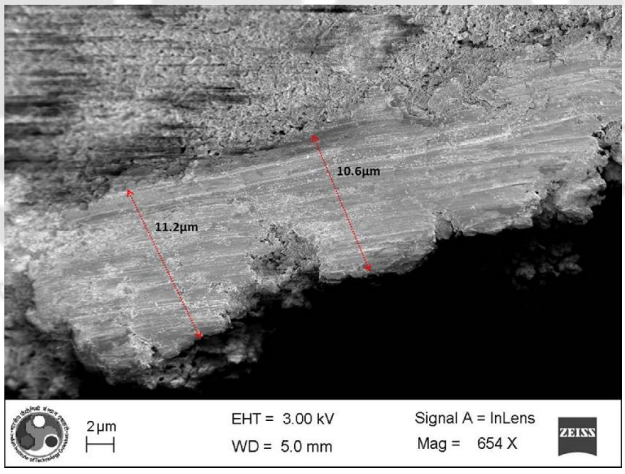

Fig. 7.2: FESEM cross-sectional micrograph of Pd-ceramic composite membrane (PM_4) fabricated with SSOEP baths.

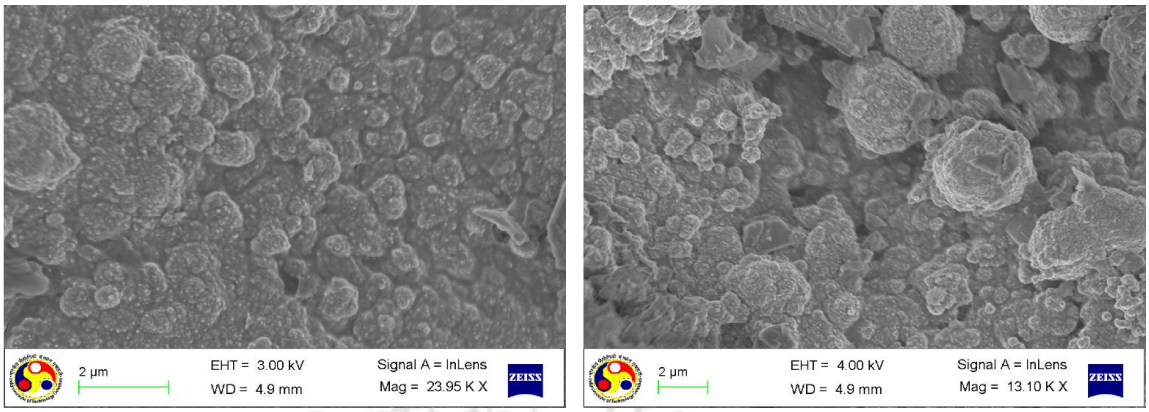

(a) **(b)**

Fig.7.3. (a-b): FESEM micrograph of Pd-ceramic composite membrane fabricated using (a) SSOEP (PM_4) and (b) SIEP (PM_3) baths.

Fig. 7.3(a-b) illustrates the FESEM micrograph of Pd-ceramic composite membrane PM_3 and PM_4 fabricated with SIEP and SSOEP baths. It can be analyzed that uniform metal particle dispersion occurred for SSOEP-DWR-BS (PM_4) baths as compared to SIEP-DWR-DWS (PM_3) baths. The probable reason for the same refers to agitation caused by ultrasonic waves in a sonicator baths which led to uniform dispersion throughout the support surface. But for SIEP baths as observed in Fig. 7.3(b) metal aggregates of non-uniform sizes were observed.

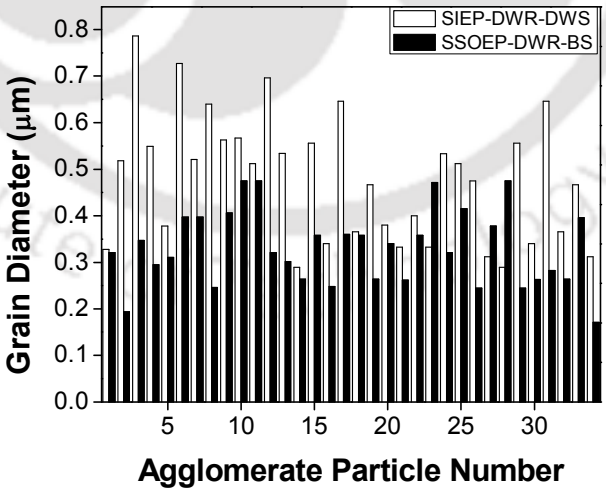

Fig.7.3 (c): ImageJ based Pd grain size distribution for SSOEP-DWR-BS (SSM_1) and SIEP-DWR-DWS (SM_9) baths.

These clearly indicate the lack of agitation for such baths. Further, Fig. 7.3 (c) depicts the grain size distribution of SIEP-DWR-DWS (PM_3) and SSOEP-DWR-BS (PM_4) baths using ImageJ software. It was analyzed that the average agglomerate grain size was 470 and 330nm respectively for SIEP-DWR-DWS (PM_3) and SSOEP-DWR-BS (PM_4) baths. This indicates that sonication was successful in reducing grain sizes which thereby facilitated uniform deposition.

7.3 Process optimization

7.3.1 PPD profiles

Fig. 7.4 illustrates the effect of various processes namely CEP (PM_1), SOEP (PM_2), SIEP (PM_3) and SSOEP (PM_4) baths on the time dependent variation of percent pore densification (PPD) for a palladium solution concentration of 0.01mol/L. PPD is an important parameter for the evaluation of ELP baths. It is defined as a measure of the fractional surface pore

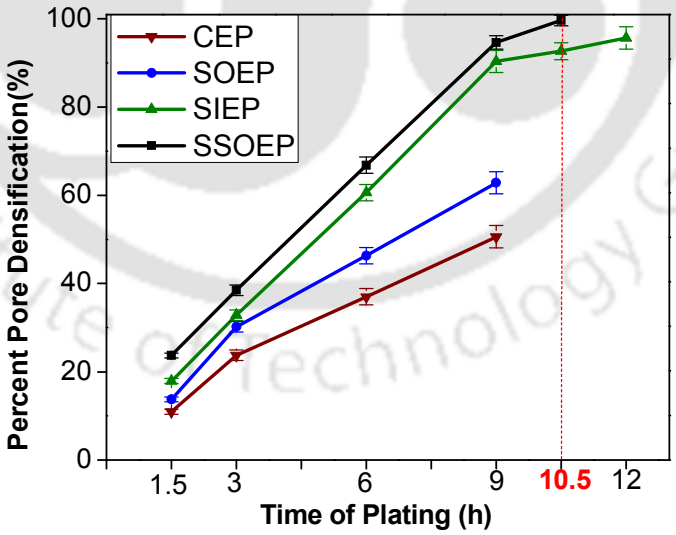

Fig. 7.4: Variation of PPD with plating time for Pd membranes fabricated with CEP, SIEP, SOEP and SSOEP baths (PM_1, PM_2, PM_3 and PM_4).

coverage which progressively increases with plating time. Referring to Fig. 7.4, it has been evaluated that the maximum PPD values obtained are 50.6 (9 h), 62.9 (9 h), 95.7 (12 h) and 99.7 (10.5 h) % for membranes PM_1, PM_2, PM_3 and PM_4 respectively. The possible reason of lower PPD profile for CEP (PM_1) baths is attributed to the slow autocatalytic reaction during ELP. For SOEP (PM_2) baths, moderate PPD profile is attributed to significant layering rather than densification. The SIEP (PM_3) bath PPD profile has been analyzed to be higher but little lower than SSOEP (PM_4) baths due to surfactant adsorption on the surface. SIEP when coupled with sonication i.e. SSOEP (PM_4) process significantly reduces poor plating rate, layering and pore densification rate thereby enabling the achievement of a dense Pd ceramic membrane in a shorter span of total plating time.

7.3.2 Average plating rate profiles

Fig. 7.5 presents the time dependent variation of noble metal average plating rate for ELP processes coupled with and without rate enhancement techniques. The plating rates varied from 1.37- 0.65 × 10^{-4} (1.5 – 9 h), 1.68 - 0.84 × 10^{-4} (1.5 – 9 h), 1.11 – 0.78 × 10^{-4}(1.5 – 12 h)

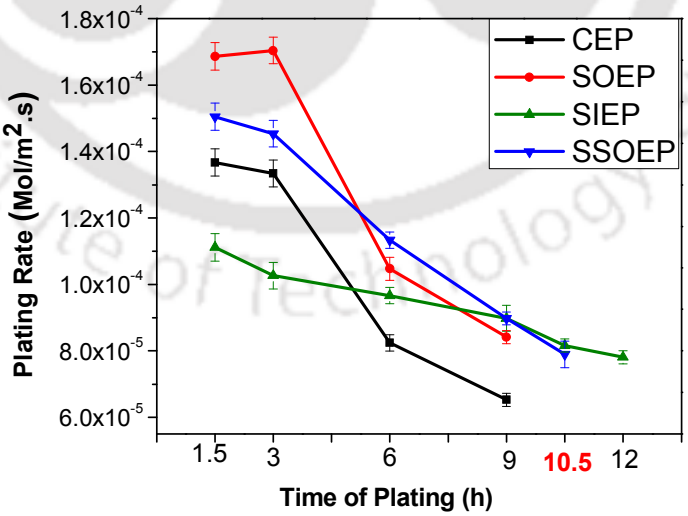

Fig. 7.5: Variation of average Pd plating rate with plating time for CEP, SIEP, SOEP and SSOEP baths (PM_1, PM_2, PM_3 and PM_4).

and 1.50 - 0.79 × 10-4 (1.5 - 10.5 h) mol/m2.s for membranes PM_1, PM_2, PM_3 and PM_4 respectively. As presented in the figure, during the initial plating time, SOEP (PM_2) bath offers the highest metal plating rate but not highest PPD profiles. Similarly, the plating rates were higher for CEP (PM_1) baths initially but as plating progressed, the plating rates reduced significantly along with no significant enhancement in pore densification. An essential feature of an efficient Pd ELP process is to ensure higher combinations of plating rate and PPD throughout the total plating time. For SIEP (PM_3) baths, the plating rates were low initially suggesting lesser support-metal compatibility, but once the support was compatible with Pd metal, the plating rates enhanced with significant enhancement in pore densification. However, this was not the case for SSOEP (PM_4) baths where the support-metal compatibility was observed during the entire plating time which enhanced to optimal combinations of PPD and plating rates at larger total plating time values. Thus, it could be inferred that SSOEP (PM_4) baths are the most favorable option for the fabrication of dense metal ceramic composite membranes.

7.3.3 Efficiency profiles

Fig. 7.6(a) and (b) depicts the effect of plating time on plating and transport efficiency for various ELP processes. It has been evaluated that the plating efficiency varied from 63-26.9 %, 85.1-30.8 %, 88 – 48.2 %, and 95.9-60.6% and the transport efficiency varied from 37.5-17.9 %, 46.3-23.1 %, 30.5-21.4 %, and 41.3-21.7 % for membranes PM_1, PM_2, PM_3 and PM_4 respectively. Plating efficiency is defined as the selective transport of converted noble metal to the membrane surface whereas transport efficiency is defined as a product of bath conversion and plating efficiency. As illustrated in Fig. 7.6(b), SOEP (PM_2) baths achieved highest transport efficiency. Higher transport efficiency could be achieved from two cases:

In the first case, the plating efficiency could be high and bath conversions could be moderate. On the other hand, for bath conversions could be high and plating efficiency could be low.

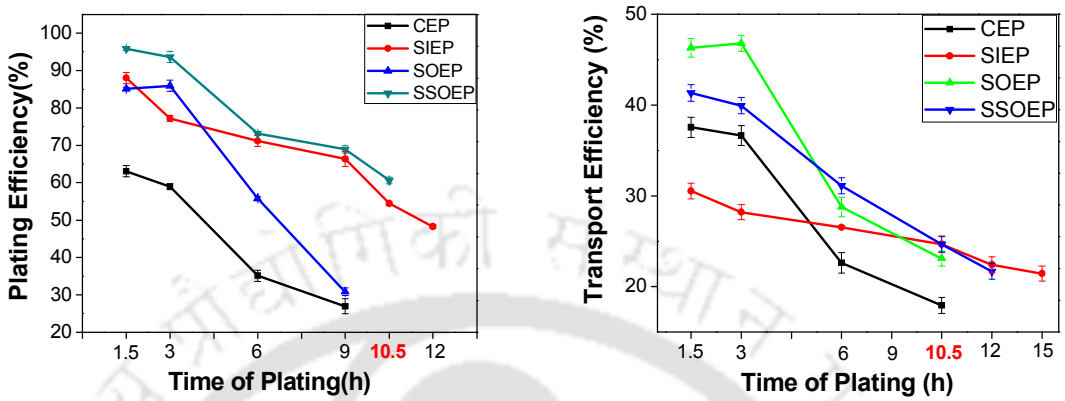

(a) (b)

Fig. 7.6: Time dependent variation of (a) Pd plating efficiency and (b) transport efficiency for CEP, SIEP, SOEP and SSOEP baths (PM_1, PM_2, PM_3 and PM_4).

Among these, the first case is desired and the second case is undesired. Highest transport efficiency for SOEP (PM_2) baths with lower PPD, plating rate and plating efficiency clearly demonstrate higher bath conversion. The optimal process that provides higher combination of plating rate, PPD and plating efficiency refers to SSOEP (PM_4) which provided slightly lower transport efficiency. However, the net metal converted during the SSOEP (PM_4) process has been successfully transported to the membrane surface and hence highly efficient plating could be achieved.

7.3.4 Comparison with literature

Lack of performance characteristics during composite membrane fabrication research is indicative to the fact that combinatorial plating characteristics have not been thoroughly studied. The literature with reference to CEP, SIEP and SOEP baths are very limited. There are no literatures on SSOEP baths regarding palladium plating on ceramic supports. It is

solely the invention reported in this work. The available literature either covers qualitative plating parameters or a costlier support (Islam et al., 2012), but there still lacks quantitative as well as combinatorial plating characteristics study for dense-Pd-ceramic composite membrane fabrication. The present work addresses a detailed description of various plating baths and indicates how SSOEP (PM_4) baths are favorable in delivering better combinations of process and plating characteristics in comparison with CEP (PM_1), SOEP (PM_2) and SIEP (PM_3) baths. One recent literature from our research group (Pujari et al., 2014) elaborates on combinatorial plating characteristics of palladium on PSS supports. The authors reported a dense Pd membrane for SSOEP baths with a plating rate of 4.38×10^{-5} mol/m^2.s, plating efficiencies of greater than 90% and transport efficiency of about 30−35 % for a palladium solution concentration of 0.005 mol/L and a surfactant concentration of 2 CMC. The results obtained in this work are similar or little higher for 100% excess palladium solution concentration (0.01 mol/L) (PM_4) but for a low cost clay (kaolin) based ceramic support.

7.4 Effect of Pd solution concentration on the combinatorial Pd plating characteristics for SSOEP plating baths

In the previous section, the efficacy of SSOEP Pd baths has been confirmed. This section addresses the optimality of Pd solution concentration.

7.4.1 PPD Profiles

Fig. 7.7 illustrates the time dependent variation of percent pore densification for variant Pd solution concentration. It has been evaluated that the time dependent PPD values varied from 19.5-96.3 % (1.5-15 h), 23.6-99.7 % (1.5-10.5 h) and 17.4-47.9 % (1.5-6 h) for a Pd solution concentration of 0.005 (PM_5), 0.01(PM_4) and 0.015 (PM_6) mol/L respectively. In general, as concentration increases, the PPD values should increase. However, such a case does not exist always. The possible reason for reduction of PPD for a higher Pd solution

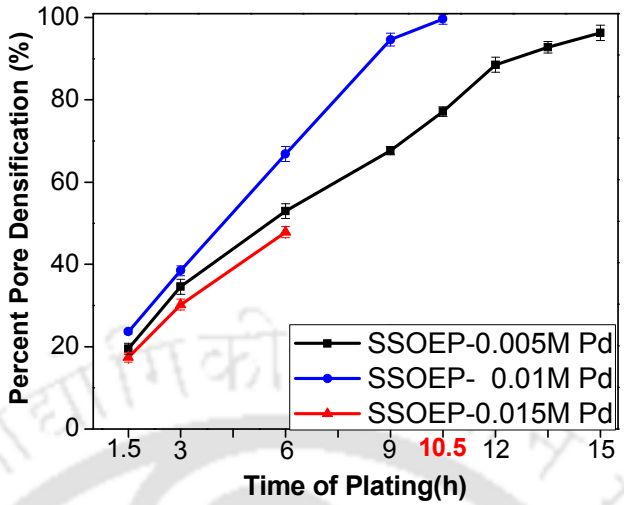

Fig. 7.7: Time dependent variation of PPD with variation in Pd solution concentration (0.005-0.015 mol/L) for SSOEP baths (PM_4, PM_5 and PM_6).

concentration could be probably due to either insitu de-lamination of palladium film from the membrane surface or bulk precipitation (Nwosu et al., 2012). Analyzing bath samples physically, the bulk precipitation of metal has been ruled out and insitu delamination is the most probable reason for the evaluated reduction in PPD. Therefore, there exists an optimal Pd solution concentration at which the desired process features could be achieved. From the evaluated PPD profiles, moderate Pd solution concentration of 0.01mol/L (PM_4) has been inferred to be optimal in achieving higher PPD for the specified total plating time.

7.4.2 Average plating rate profiles

Fig. 7.8 presents the time dependent average Pd plating rate profiles for various Pd solution concentrations. It has been evaluated that the plating rates varied from $1.19 - 0.66 \times 10^{-4}$(1.5-15 h), $1.50 - 0.79 \times 10^{-4}$ (1.5-10.5 h) and $1.60 - 0.81 \times 10^{-4}$ (1.5-6 h) mol/m^2.s respectively for a Pd solution concentration of 0.005 (PM_5), 0.01 (PM_4) and 0.015 (PM_6) mol/L. It can be observed that for a higher metal concentration of 0.015 (PM_6) mol/L, the plating rate were

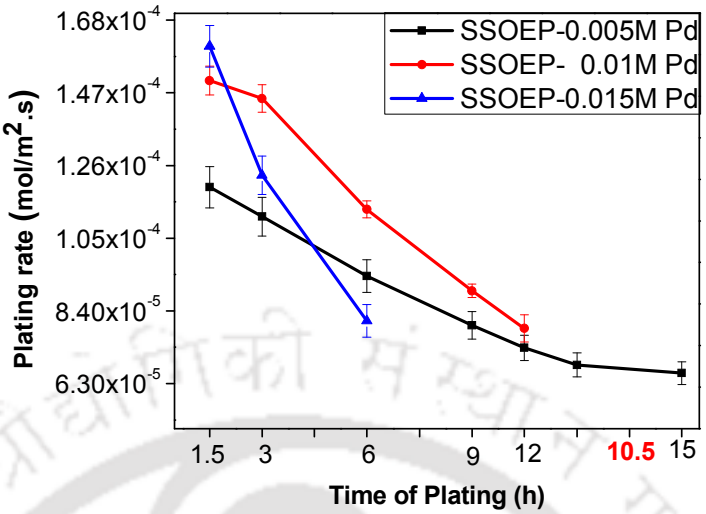

Fig. 7.8: Variation of average Pd plating rate with plating time for various cases of Pd solution concentration (0.005-0.015 mol/L) using SSOEP baths (PM_4, PM_5 and PM_6).

higher initially which reduced significantly at higher plating times. Such significant reduction in plating rate is an unfavorable feature of the SSOEP baths. According to rule of thumb, higher metal solution concentration corresponds to higher metal plating rate. But that might not always be the case. For a moderate Pd solution concentration of 0.01 (PM_4) mol/L, apart from the initial hour of plating, it was evaluated that the plating rates were higher during the entire plating period.

Hypothetically, higher concentration enhances plating rate. However, adhesion of the newly formed Pd film is dependent upon solid - liquid interface properties. While higher solution concentrations could enable higher metal deposition rates, they can significantly enhance metal delamination due to the shear stress induced by the faster evolution of gas bubbles (Chen et al., 2002). In this regard, it should be noted that the usage of surfactant can only reduce but not eliminate shear stresses. Therefore, an optimal Pd solution concentration exists that provides highest combinations of plating rates and PPD.

7.4.3 Efficiencies profiles

Fig. 7.9 (a) and (b) illustrates the effect of Pd solution concentration on the time dependent variation of plating and transport efficiency for membranes PM_4, PM_5 and PM_6. It can be observed that the plating efficiency varied from 81.6 -61 % (1.5-15 h), 95.9 - 60.6 % (1.5-10.5 h), 95.6-57.8 % (1.5-6 h) and the transport efficiency varied from 32.9 -18.1 % (1.5-15 h), 41.3-21.7 %(1.5-10.5 h), and 44-22.3% (1.5-6 h) respectively for a Pd solution concentration of 0.005(PM_5), 0.01(PM_4) and 0.015 (PM_6) mol/L. As discussed in section 7.2.3, higher plating efficiency coupled with moderate transport efficiency defines optimal concentration. As illustrated in Fig. 7.9, for the SSOEP baths, higher Pd solution concentration (0.015mol/L) (PM_6) enabled the achievement of highest combinations of plating and transport efficiency during initial plating time. However, as time progressed a sharp decline in both the parameters illustrates incompatibility of the chosen higher metal concentration to achieve the desired process parameters in terms of PPD and plating rates. Thus, 0.01mol/L (PM_4) Pd solution concentration can be concluded to provide optimal

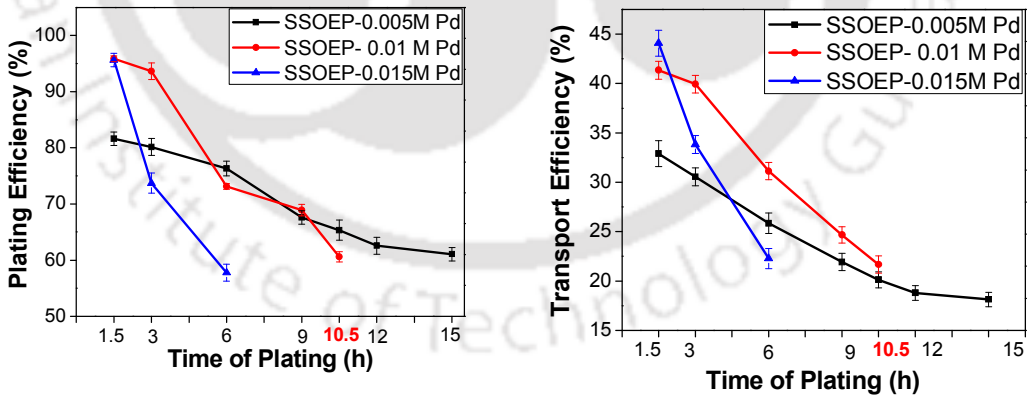

(a) **(b)**

Fig. 7.9: Time dependent variation of (a) Pd plating efficiency and (b) transport efficiency for various cases of Pd solution concentration (0.005-0.015 mol/L) using SSOEP baths (PM_4, PM_5 and PM_6).

combinations of process and membrane characteristics.

7.4.4 Comparison with literature

In a U.S. patent by Collins and Way (1997), the authors fabricated dense Pd tubular ceramic composite membranes by CEP process using a Pd solution concentration of 0.03 mol/L to achieve 10 – 20 μm metal film thickness. In another U.S. patent by Rhoda (1966), the author fabricated dense Pd ceramic composite membranes by CEP process using a Pd solution concentration of 0.028 – 0.056 mol/L with asymmetric addition of dimethylhydrazine (concentration of 0.05 – 0.45 g/L) reducing agent.

Further Ilias et al. (1997) disclosed details with respect to CEP to achieve dense Pd ceramic membranes. For an alumina support (pore size of 150 nm), the authors used a Pd solution concentration of 0.03 mol/L to achieve a dense metal film thickness of 12 μm. In a similar context Zhang et al. (2007) reported CEP supplemented with SDS anionic surfactant to be effective to achieve Pd composite membranes. On a α- alumina support of 270-280 nm average pore size , the authors used a Pd solution concentration of 0.189 mol/L to achieve a dense Pd metal film thickness of 2 μm after a total plating time of 8 – 12 h.

Thus, this work clearly indicated that by modifying the plating process from CEP to SSOEP, significantly lower palladium solution concentration is sufficient for the fabrication of dense palladium ceramic composite membranes.

Lack of performance characteristics during composite membrane fabrication research is indicative to the fact that combinatorial plating characteristics has not been studied in details and this work elaborates on the same. One recent literature from our research group by Pujari et al. (2014) elaborates on combinatorial plating characteristics of palladium on PSS supports. Their work reported a dense Pd membrane for SSOEP baths with a plating rate of

4.38×10^{-5}mol/m^2.s for a palladium solution concentration of 0.005 mol/L and a surfactant concentration of 2 CMC. The plating rate in the present work is 7.9×10^{-5}mol/m^2.s for a palladium solution concentration of 0.01 mol/L (PM_4) and a surfactant concentration of 2 CMC. In the present work, a similar surfactant and palladium solution concentration provided an average plating rate of 6.6×10^{-5}mol/m^2.s but with a PPD of 96.3%.

Thus, it could be inferred that ceramic supports also provide similar or higher plating rates than PSS supports for similar Pd precursor concentration. However, higher plating time is required. In other words, if similar plating time is to be used for both the supports, the solution concentration of palladium needs to be doubled for ceramic supports as compared to PSS supports.

Further, Pujari et al. (2014) achieved plating efficiencies greater than 90% and transport efficiency of about 30−35% in their work whereas this work provided a plating efficiency of 95.9% and transport efficiency of about 41.3-21.7% for 100% excess metal concentration (0.01mol/L) on an inexpensive clay based porous ceramic support.

7.5 Tradeoffs

7.5.1 Process tradeoffs

Fig. 7.10 demonstrates the tradeoffs associated with PPD vs. PPD/Plating rate for various processes namely CEP (PM_1), SOEP (PM_2), SIEP (PM_3) and SSOEP (PM_4) respectively. This graph is a conceptual extension of the experimental findings to observe clear distinction between metal layering and pore densification in terms of PPD vs. PPD/Plating rate. Hypothetically, PPD/Plating rate is a measure to quantify the dominance of pore densification or layering. Higher value of PPD/Plating rate for similar time of plating signifies that the plating favors better PPD and lower metal layering. As observed, for SSOEP (PM_4) bath (9

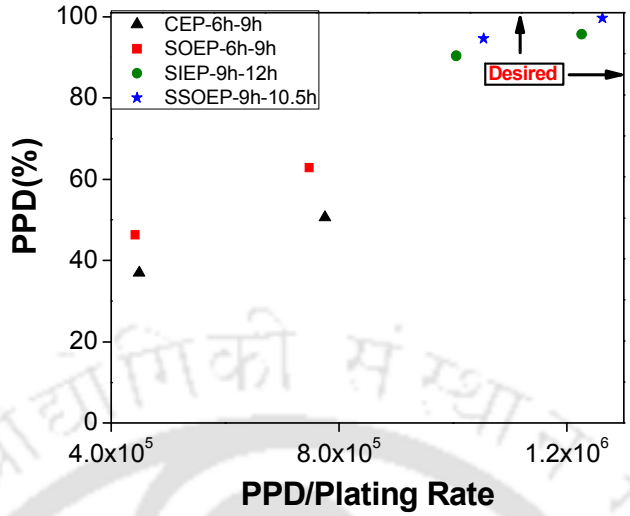

Fig. 7.10: PPD/Plating rate Vs. PPD tradeoff plot for CEP, SOEP, SIEP and SSOEP processes (PM_1, PM_2, PM_3 and PM_4).

and 10.5h), higher PPD/Plating rate has been achieved in comparison with CEP (PM_1), SOEP (PM_2) and SIEP (PM_3) baths. From the perspective of industrialization and scalability, it is very important that the plating is favorable towards pore densification and not metal layering. Thus SSOEP (PM_4) baths were the best amongst the investigated processes (CEP (PM_1), SOEP (PM_2), SIEP (PM_3) and SSOEP (PM_4)) in terms of higher PPD and lower metal layering.

In summary, for a total plating time of 9h, the SSOEP (PM_4) process is:

a) 46.5% and 27.3% effective for PPD and plating rate/transport efficiency respectively in comparison with conventional Pd electroless plating (CEP (PM_1))

b) 33.6%and 6.4% effective for PPD and plating rate/transport efficiency respectively in comparison with sonication induced Pd electroless plating (SOEP (PM_2)).

c) 4.5% and 0% effective for PPD and plating rate/transport efficiency respectively in comparison with surfactant induced Pd electroless plating (SIEP (PM_3)).

In terms of the final total plating time, the SSOEP (PM_4) process is:

a) 49.2% and 17.3% effective for PPD and plating rate/transport efficiency respectively in comparison with conventional Pd electroless plating (CEP (PM_1))

b) 36.9%and -6.5% effective for PPD and plating rate/transport efficiency respectively in comparison with sonication induced Pd electroless plating (SOEP (PM_2)).

c) 4% and 1.1% effective for PPD and plating rate/transport efficiency respectively in comparison with surfactant induced Pd electroless plating (SIEP (PM_3)).

7.5.2 Tradeoffs for metal solution concentration in SSOEP plating baths

Fig. 7.11 illustrates the tradeoffs associated with PPD/Plating rate Vs. PPD for SSOEP baths with variant Pd solution concentrations (0.005 – 0.015mol/L). It has been evaluated that for a particular plating time (say 6h),both PPD and PPD/Plating rate values were higher for a Pd solution concentration of 0.01mol/L (PM_4).Thus, 0.01mol/L Pd solution concentration is the optimal concentration for the mentioned bath composition (Table 2.4) on porous ceramic supports. Thus, the process disclosed in this work indicates the potential of the SSOEP process to effectively achieve dense Pd ceramic composite membranes.

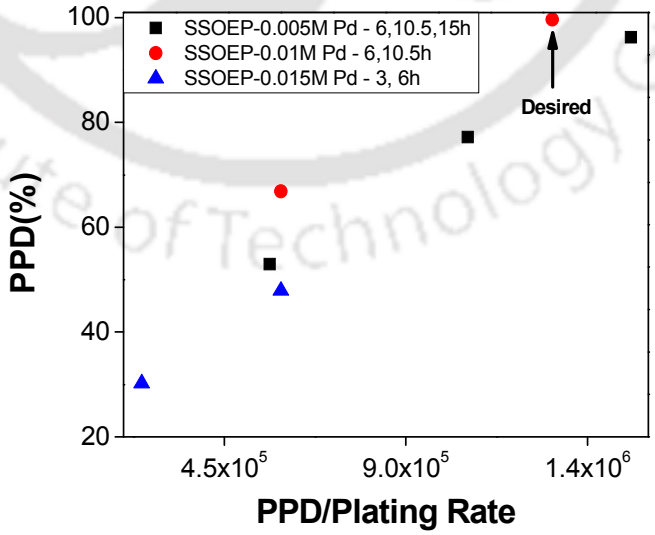

Fig. 7.11: PPD Vs. PPD/Plating rate tradeoff plot for various Pd solution concentrations (PM_4, PM_5 and PM_6).

7.6 Cost analysis and optimality

Parameters considered for the retail cost analysis of various dense membranes on various supports is presented in Table 7.1. The cost calculations are conceptual in nature and do have an error of estimate of about 30 – 40%. Therefore, the obtained retail costs should not be considered as absolute standard for rigorous cost analysis. The costs are only indicative with respect to the comparison of various competent Pd fabrication processes. Various assumptions for the cost analysis has been presented as follows:

a) Ilias et al. (1997) and Islam et al. (2010) used 50mL of Pd ELP bath solution for each plating step (i.e. similar to the loading ratio of 203 cm^2/L taken in our work).

Table 7.1: Parameters for the estimation of retail cost for various dense Pd composite membranes.

Parameters	Cost	Units/Quantity
Support Type		
PSS	2800	₹ (3.6 cm dia)
α- alumina	50	₹ (3.9 cm dia)
Clay	5	₹ (3.6 cm dia)
Palladium Precursors		
Palladium chloride	3719	₹/g
Tetra-amine palladium nitrate	1337.8	₹/g
Surfactant Type		
DTAB	178	₹/g
SDS	65	₹/g
CTAB	3.22	₹/g
Other Plating Precursors		
Hydrazine Hydrate	2364	₹/L
Liquor Ammonia	196.8	₹/L
Sodium Hypophosphite	30.9	₹/g
Na_2EDTA	2.6	₹/g
Miscellaneous		
Manpower	250	₹/h
Electricals	8.78	₹/KW

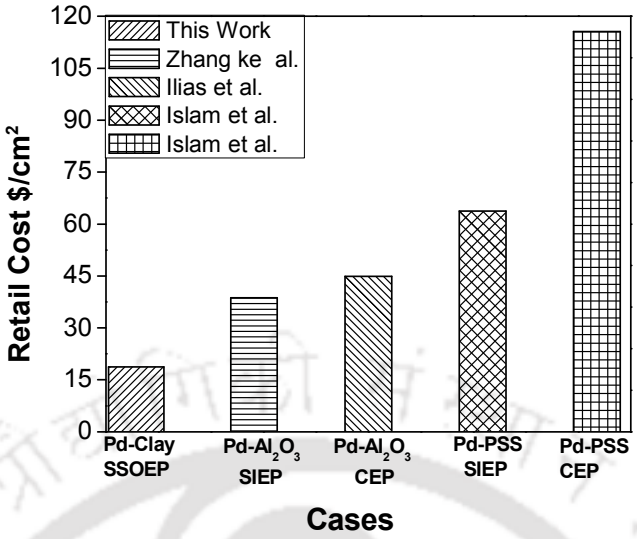

Fig. 7.12: Retail cost of dense Pd membranes fabrication with CEP, SIEP and SSOEP (PM_4) processes.

b) Ilias et al. (1997) fabricated a dense Pd ceramic composite membrane in a total plating time of 15h.

Fig. 7.12 presents the retail fabrication cost of dense Pd membrane using various approaches namely SSOEP (DW) on ceramic (Clay based) (PM_4); SIEP (Bulk) on PSS; SIEP (Bulk) on alumina; CEP (Bulk) on alumina and CEP (bulk) on PSS supports. As shown in Fig. 7.12, the cost of fabricated dense Pd membrane is 18.75 \$/cm^2, which is significantly lower than the cost of the membrane fabricated with conditions mentioned by Islam and Ilias (2010)(63.7 \$/cm^2), Zhang et al. (2007) (38.7 \$/cm^2), Ilias et al. (1997) (44.9 \$/cm^2) and Islam and Ilias (2010) (115.6 \$/cm^2). The retail cost of the membrane using parameters reported in this work is 51.6% cost effective as compared to SIEP process and 58.2% cost effective as compared to CEP process on a ceramic support (Ilias et al., 1997; Zhang et al., 2007).Further it is 70.6% and 83.8% cost effective as compared to SIEP and CEP process on PSS supports(Islam and Ilias, 2010). Therefore, it is apparent that the mentioned SSOEP (DW) process reduces the fabrication cost by about 51-83%.

The cost of the SSOEP (DW) process is low due to the following facts. Firstly, using sonication induced ELP, the time of plating could be reduced to 10.5h in comparison to 12h reported by Zhang et al. (2007). Secondly, the utilized surfactant (CTAB) is highly inexpensive (retail cost of CTAB is 0.077 $/g, whereas cost of DTAB is 3.62 $/g and cost of SDS is 1.04$/g in India). In addition, the CMC concentration of DTAB (4.93 g/L) is significantly higher than the CMC concentration of CTAB (0.33 g/L). Thirdly, this process utilizes a lower palladium solution concentration of 1.76 g/L in comparison to values reported in the literature where higher total Pd consumption was reported (5.4 g/L (Ilias et al., 1997) and 33.6 g/L (Zhang et al., 2007) of $PdCl_2$). Fourthly, the ceramic support used is low cost as compared to alumina and PSS supports. Fifthly, the membrane area considered in this work (10.17 cm^2) is significantly higher than the values reported in the literature (3.14 cm^2(Zhang et al., 2007) and 5.06 cm^2(Islam and Ilias, 2010)). Considering all these aspects, the retail dense Pd membrane cost is significantly low and even lower than the Pd – PSS membranes fabricated with the patented SIEP process (Ilias and Islam, 2012).

Further Fig. 7.13 presents a detailed cost analysis of five different palladium dense composite membranes fabricated by various groups on different supports in the form of a pie chart. It is divided into a number of subsections for costs associated to the following heads:

a) Palladium precursor ($PdCl_2$/ $Pd(NO_3)_2.NH_3$)
b) Chemicals (stabilizer, buffering agent, reducing agent etc.)
c) Support (PSS/Clay/Alumina)
d) Manpower (including electricals)
e) Surfactants(CTAB/SDS/DTAB)

It was evaluated that for fabrication of dense Pd membrane on clay based support using SSOEP Pd baths (Fig. 7.13(a)), noble metal cost contributed 77% and manpower contributed

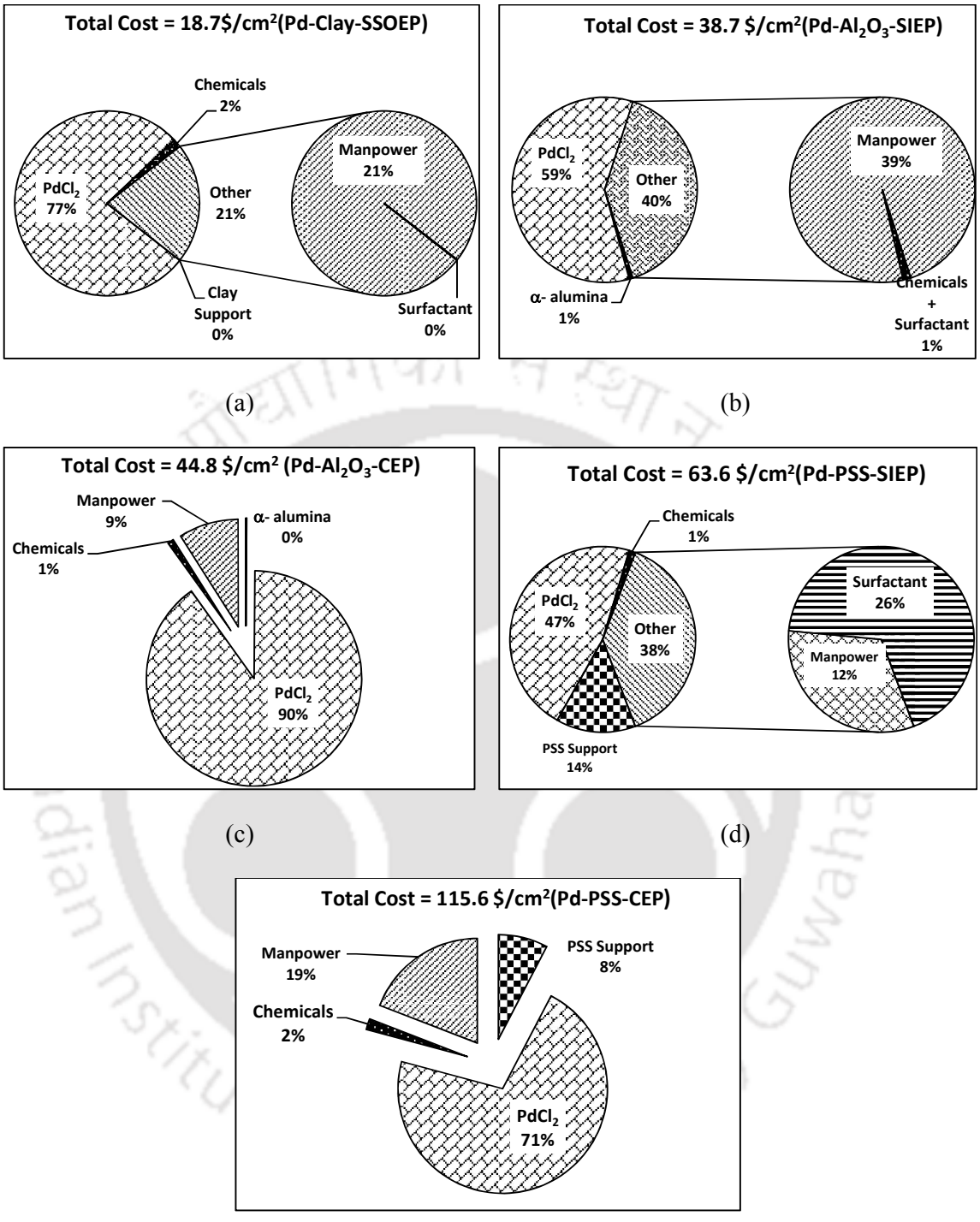

Fig 7.13: Cost contributions of various heads to the retail cost of dense Pd composite membranes.

21%, with other cost being neglible. Further, for the case of fabrication of dense Pd membrane on an Al_2O_3 based support using SIEP baths ((Fig. 7.13(b)), noble metal contributed 59%. Further, 39% and 1% cost contributions were from manpower and chemicals including surfactant. For the same support using CEP process, (Fig. 7.13(c)) higher cost contributions were due to the noble metal itself (90%). Similarly, for fabrication of dense Pd membrane on PSS support using SIEP baths ((Fig. 7.13(d)), noble metal contribution was 47% and higher cost of the surfactant (26%) and support (14%) exist. Thus, further optimization of electroless plating processes enabled a significant cost in total noble metal utilization, chemicals and support cost. On the other hand, for the fabrication of Pd composite membrane with the same support and CEP process (Fig. 7.13(e)), noble metal cost is significantly high (71%) apart from notable contribution of the support cost (8%). In summary the identified SSOEP process in conjunction with inexpensive clay based support are successful ventures of the process-product optimality that has been stressed as the central research theme of the research carried out in this work. Further, it is of immense importance that: (a) The cost contribution of various heads for each process is exclusive and cannot be referred for comparison with the heads of other processes and (b) The pie charts provide useful insights with respect to the dominance or irrelevance of a particular head to the overall cost of fabrication. For example for the CEP significant cost contribution was from the chemicals and especially palladium. Similar insights can be drawn for other processes.

7.7 Comparative assessment of combinatorial plating characteristics for Ni and Pd composite membranes

The target for such an exercise was to encourage rigorous experimentation with Ni ELP which eventually enables for the identification of optimal processes. Using these processes, the optimality for Pd ELP baths can be mapped. It is strongly envisaged that such a research

methodology will be important to overcome many scientific and technological hurdles that exist between the present state of metal membrane fabrication and those required for a competitive sustainability and commercialization. The comparative study addressed in this section would also serve as useful guidelines for researchers working in the field of multichannel ceramic conduits, catalyst etc. This will be very helpful on the ground that one does not have to perform a number of experiments on palladium membranes. This will not only save a lot of money, manpower and time but also provide insights on the theoretical relations between Ni and Pd plating data and subsequent development of a mapping model. Based on extensive lab scale experimentation, the best performance characteristics of palladium plating baths are compared with that of nickel plating baths for its fabrication on similar ceramic support. Based on inferences drawn from chapters 3-7, it is evident that the optimal processes refer to:

(1) SSOEP-DWR-BS baths

(2) SIEP-DWR-DWS baths

Rigorous Pd experiments need not be planned and Ni ELP can be carried out even before Pd plating experiments could be conducted. Such an approach will save significant amount of time. However, Ni ELP is not the same as Pd ELP as it can be seen that Ni ELP parameters are significantly different from the Pd ELP and therefore, they cannot be compared straight away. However, a functional mapping of both these cases is possible to indicate that a PPD of Ni of about 90% could mean a PPD of 99.9% of Pd. Such approaches will therefore reduce time of investigations and most importantly costs, as the cost of Ni precursors are significantly lower in comparison with that of the Pd. Thus for the optimal processes a comparative sketch of metal ceramic composite fabrication using nickel and palladium are outlined in Tables 7.2 and 7.3 respectively. Such a comparison will enable lot of insights for

Table 7.2: A comparative summary of various parameters associated to optimal Ni (SSM_1) and Pd (PM_4) membrane fabrication for SSOEP-DWR-BS baths.

Parameters	Nickel	Palladium
Metal Concentration (mol/L)	0.08	0.01
Reducing Agent concentration (% Excess)	100	40
CTAB concentration (CMC)	4	2
Total plating time (h)	2 - 8	1.5 - 10.5
Time /Plating step (min)	30	20 - 25
Percent pore densification (%)	54.6 - 73.4	23.6 – 99.7
Plating efficiency (%)	67.1 - 89.8	95.9 - 60.6
Plating rate (mol/m^2.s)	$1.1 – 0.44 \times 10^{-4}$	$1.5 - 0.79 \times 10^{-4}$
PPD/δ	10.5 - 8.8	3.3 – 3.8
PPD/Plating Rate	$4.9 – 16.6 \times 10^{5}$	$1.6 – 12.6 \times 10^{5}$

Table 7.3: A comparative summary of various parameters associated to optimal Ni (SM_9) and Pd (PM_3) membrane fabrication for SIEP-DWR-DWS baths.

Parameters	Nickel	Palladium
Metal Concentration (mol/L)	0.08	0.01
Reducing Agent concentration (% Excess)	100	40
CTAB concentration (CMC)	4	2
Total plating time (h)	2 - 8	1.5 - 12
Time /Plating step (min)	30	20 - 25
Percent pore densification (%)	50.4 - 76.5	17.9 – 95.7
Plating efficiency (%)	69.3 - 58	88 - 48.3
Plating rate (mol/m^2.s)	$1.3 – 0.49 \times 10^{-4}$	$1.1 - 0.78 \times 10^{-4}$
PPD/δ	8 – 8.1	3.4 – 3.2
PPD/Plating Rate	$3.8 – 15.4 \times 10^{5}$	$1.6 – 12.2 \times 10^{5}$

of average pore size 150-250 nm the data trends for nickel and palladium are elaborated in the next sub - section.

7.7.1 Optimal Ni and Pd membrane fabrication process conditions for SSOEP-DWR-BS baths

It can be observed that a very high concentration of nickel (0.08mol/L) (SSM_1) corresponds to a very low concentration of palladium (0.01mol/L) (PM_4). A PPD of 73% for Ni could indicate a dense palladium membrane for the said concentration. It appears that similar plating rate and PPD/plating rate are the important parameters for comparing nickel and palladium baths.

7.7.2 Optimal Ni and Pd membrane fabrication process conditions for SIEP-DWR-DWS baths

The conclusions drawn from Table 7.3 are as follows: Plating rate and PPD/plating rate are important parameters for comparison. Difficult parameters for comparison refer to PPD/δ. In case such a comparative study needs to be performed, one should first target similar plating rates for both Ni and Pd ELP baths and eventually target nearly similar values for PPD/plating rate.This will be very useful to reduce number of experiments required for palladium membranes. Thus, the suggested methodology saves money and time along with providing relevant insights for data mapping and generic model development.

7.8 Summary

This chapter addresses the process perspective of electroless plating technique to fabricate dense palladium-ceramic composite membranes and the effect of various processes coupled with and without ultrasound on the performance characteristics of palladium hydrazine baths**.**

The main objective of this work is to investigate upon the benefits of ultrasound and surfactant to conventional electroless plating for achieving better combinatorial characteristics which seems to be a missing issue in many relevant studies. This work also critically targets the cost analysis of the fabricated dense palladium ceramic composite membranes with a detailed study of the cost of other similar membranes fabricated in the literature.

The optimal combinatorial Pd plating characteristics for SSOEP (PM_4) baths corresponds to a combination of plating efficiencies varying between 95.9 – 60.6%; moderate transport efficiency ranging in between 41.3 - 21.7 %; plating rates ranging in between 1.50 – 0.79 × 10^{-4} mol/m^2.s; minimal palladium solution concentration of 0.01 mol/L, lower surfactant concentration of 2 CMC, optimal plating time of 10.5 h and pore densification of 99.7 %.

Further the fabricated membrane is highly cost effective even on a retail basis i.e. 51.6% cost effective in comparison with dense Pd-alumina composite membrane fabricated with SIEP process; 58.2% cost effective in comparison with dense Pd-alumina membrane fabricated with CEP; 83.8% cost effective in comparison with dense Pd-stainless membrane fabricated with CEP and 70.6% cost effective in comparison with dense Pd-stainless steel composite membrane fabricated with SIEP process. Further, the insights obtained from the comparative study of nickel and palladium plating bath characteristics could critically target generic mapping and modeling for the prediction of other parameters for both palladium and nickel hydrazine baths.

Regardless of its application, the cost effective fabrication of palladium dense composite membrane using coupled sonication and surfactant with ELP would serve as a paramount invention which the membrane research community could further explore to make the "hydrogen economy" as a reality.

Conclusions and Future Work

This chapter summarizes the conclusions drawn from the results presented in chapters 3 – 7 of the thesis. Following this, possible scope towards future research has been presented.

8.1 Conclusions

The aim of the thesis was to investigate upon the fabrication of metal ceramic composite membranes by optimizing both process and plating parameters. Palladium and nickel ceramic composite membranes were fabricated and characterized using BET, FESEM, FTIR, LPSA, XRD, weight gain method and nitrogen permeation techniques. The most important findings in this work can be summarized as follows:

1. **Potential Rate enhancement techniques:** Two potential and scalable rate enhancement techniques namely surfactant and sonication have been identified for efficient nickel and palladium electroless plating on porous ceramic supports.
2. **Optimality of SSOEP baths:** For all cases, coupled surfactant and sonication based ELP (SSOEP) baths performed better than sonication baths (SOEP).
3. **Reducing agent contacting pattern:** The drop wise reducing agent (DWR) served better than bulk addition (BR) of the reducing agent in fostering better combinations of performance characteristics for both Ni and Pd ELP baths.
4. **Surfactant contacting pattern:** The drop wise addition of surfactant (DWS) served better than bulk addition of surfactant (BS) for SIEP baths. For SSOEP baths, the bulk addition of surfactant (BS) served better than drop wise surfactant addition (DWS) strategy.

5. **Optimal Ni bath formulation:** Optimal nickel solution, reducing agent, cationic surfactant concentration were evaluated to be 0.08mol/L, 100% excess and 4CMC respectively to achieve optimal combinations of membrane and process parameters. These correspond to an average plating rate of 13.2 – 4.9 × 10^{-5}mol/m^2.s, PPD of 76.5% and a metal film thickness of 9.4 μm respectively after 8h of sequential plating in an SIEP-DWR-DWS process. For the SSOEP-DWR-BS process an average plating rate of 11 - 4.4× 10^{-5}mol/m^2.s, PPD of 73.4% and a metal film thickness of 8.4μm was obtained after 8h of sequential plating.
6. **Optimal Pd bath formulation:** Optimal palladium solution, reducing agent, cationic surfactant concentration were evaluated to be 0.01mol/L, 40% excess and 2 CMC respectively towards deliberating desired process parameters in less than 11hrs. For the Pd ceramic composite membrane, the optimal bath composition provides higher plating efficiencies (95.8 %), higher transport efficiency (41.3%), higher plating rates (1.5 × 10^{-4} mol/m^2.s), minimal palladium solution concentration (0.01 mol/L), lower surfactant concentration (2 CMC), minimal total plating time (10.5h) and maximum pore densification (99.7 %) for SSOEP (PM_4) baths. The optimal SIEP-DWR-DWS Pd ELP (PM_3) baths provided optimal combinatorial characteristics of PPD (95.7%), plating rate (1.11 – 0.78 × 10^{-4} mol/m^2.s), plating efficiency (88 – 48.2%) and transport efficiency (30.5 - 21.4%) after 12h of total plating time.
7. **Low fabrication cost:** The identified Pd SSOEP (PM_4) baths have been evaluated to offer lower retail cost to fabricate dense Pd ceramic membranes (18.75 \$/cm^2).

In summary, the Ph.D. thesis enabled to provide significant insights with respect to the concentrations and contacting pattern of metal precursors, reducing agent, surfactant and sonication (if any) for the efficient and cost effective fabrication of dense nickel ceramic composite and dense palladium ceramic composite membranes. All experimental

investigations and results are anticipated to be relevant for process engineering studies associated to dense metal composite membrane fabrication. The identified optimal combinations for both SIEP and SSOEP baths are of significance to further catalyze insights with respect to the engineering and fabrication characteristics of metal ELP baths from the perspective of process scale up and large scale fabrication.

8.2 Future Work

1. **Further optimality of SSOEP plating baths for dense Pd-ceramic composite membrane fabrication:** Experimental investigations need to affirm whether further optimal combinations of Pd solution, surfactant, reducing agent contacting pattern, sono-process parameters exist and whether such optimal combinations yield dense Pd ceramic composite membranes with significant reduction in critical Pd film thickness.
2. **Further insights into solution thermodynamics:** These aspects are of paramount relevance for dense metal ceramic composite membranes after saturation in the time dependent profiles has been evaluated. Parameters that strongly influence the dynamics of the equilibrium conditions need to be more thoroughly investigated from experimental as well as theoretical frameworks.
3. **Optimality of SSOEP-DWR-BS baths for tubular dense Pd ceramic composite membranes:** The objective of such investigations is to confirm whether the identified set of parameters for circular disks are applicable or not for mono-channel tubular membranes.
4. **Optimality of agitated SIEP-DWR-DWS baths for dense tubular Pd ceramic composite membranes:** Till date, no such work has been conducted and future research in this direction will be extremely beneficial to provide further insights into scale up related issues for large scale metal ceramic membrane fabrication.

5. **Optimality of SSOEP (DW) baths for multichannel ceramic conduits:** To study the performance characteristics of sonication and surfactant coupled metal ELP baths (SSOEP) on multichannel ceramic conduits.
6. **Pd-alumina membrane fabrication using SSOEP (DW) baths:** To study the metal plating and performance characteristics on alumina supports particularly Pd-alumina for SSOEP-DWR-BS baths. Further, such studies can be also targeted to evaluate upon the role of support morphology on the efficacy of SSOEP-DWR-BS baths for dense Pd-alumina composite membrane fabrication.
7. **Porous Cr_2O_3-ceramic composite membranes using ELP technique:** To envisage upon an efficient SSOEP-DWR-BS bath composition for the achievement of porous Cr_2O_3-ceramic composite membranes which can serve as functional supports for dense Pd-Cr_2O_3-ceramic composite membranes fabrication.
8. **Reuse of spent Pd ELP bath solutions for membrane fabrication:** Till date, there has not been any data in this regard. Such data will be of relevance towards waste minimization and fabrication cost reduction.
9. **Sensitivity of Pd deposition with respect to reducing agent strength:** To evaluate upon the sensitivity of Pd ELP baths with respect to the strength of hydrazine reducing agent. This has been observed during experimentation to be an important variable. It was evaluated that the freshly prepared dilute hydrazine reducing agent solutions had a significantly higher potential than those prepared and stored in laboratory experimental conditions.
10. **SSOEP (DW) and SIEP processes for noble metal supported catalyst fabrication:** The reuse and applicability of waste noble metal solutions to achieve functional products such as noble metal supported catalysts is a novel area of research and can

be targeted using the rate and depositional characteristics presented for Pd-ceramic composite membrane fabrication.

11. **Kinetic study of Ni^{+2} reduction:** Further investigations associated to the kinetic study of Ni^{+2} reduction in ELP baths would be useful to elaborate upon the quantitative aspects associated to the metal deposition process for Ni-ceramic composite membrane fabrication.
12. **Evaluation of mechanical strength of the metal film:** The mechanical strength of the metal film was not evaluated in this work and can be addressed as a future work. Such investigations need to evaluate the ability of the metal film to withstand high pressures and high temperatures. Thereby, the life cycle assessment of ELP technique for metal ceramic composite membranes can be carried out. As far as support is concerned, the mechanical strength of the support is similar to that provided in the literature (Vasanth et al.).

This work addressed a conceptual framework for the evaluation of most likely combinations of optimal parameters. Further optimization of large number of operating parameters is a complex exercise and needs to be addressed using more rigorous statistical design of experiments. In summary, the carried out research has catalyzed to venture out mature research horizons for dense metal ceramic composite membrane fabrication using electroless plating technique. The suggested and identified process modifications are simplistic to implement and are easy for process scale up. All these features encourage further academic research in this novel and unique area of research.

References

Altinisik, O., Dogan, M., Dogu, G., 2005. Preparation and characterization of palladium-plated, porous glass for hydrogen enrichment. Catalysis Today 105, 641-646.

Altunoglu, Abdulkadir, 1994. Hydrogen permeation through nickel and nickel alloys: surface reactions and trapping, The Open University, PhD Thesis.

Ayturk, M.E., Ma, Y.H., 2009. Electroless Pd and Ag deposition kinetics of the composite Pd and Pd/Ag membranes synthesized from agitated plating baths. Journal of Membrane Science 330, 233-245.

Brien, J.O., Hughes, R., Hisek, J., 2001. Pd/Ag membranes on porous alumina substrates by unbalanced magnetron sputtering. Surface Coating Technology 253, 142–144.

Bryden, K.J., Ying, J.Y., 1998. Pulsed electrodeposition synthesis and hydrogen absorption properties of nanostructured palladium-iron alloy films, Journal of the Electrochemical Society 145, 3339-3346.

Bulasara, V.K., Abhimanyu, M.S., Pranav, T., Uppaluri, R., Purkait, M.K., 2012. Performance characteristics of hydrothermal and sonication assisted electroless plating baths for nickel–ceramic composite membrane fabrication. Desalination 284, 77–85.

Bulasara, V.K., Thakuria, H., Uppaluri, R., Purkait, M.K., 2011a. Combinatorial performance characteristics of agitated nickel hypophosphite electroless plating baths. Journal of Materials and Processing Technology 211, 1488-1499.

Bulasara, V.K., Babu, C.S., Uppaluri, R., 2011c. Effect of surfactants on performance of electroless plating baths for nickel – ceramic composite membrane fabrication. Surface Engineering 4, 51-55.

Bulasara, V.K., Chandrashekar, O., Uppaluri, R., 2011b. Effect of surface roughness and mass transfer enhancement on the performance characteristics of nickel-hypophosphite electroless plating baths for metal–ceramic composite membrane fabrication. Chemical Engineering Research and Design 89, 2485-2494.

Bulasara, V.K., Thakuria, H., Uppaluri, R., Purkait, M.K., 2011d. Nickel–ceramic composite membranes: Optimization of hydrazine based electroless plating process parameters. Desalination 275, 243-251.

Bunshah, R.F., 1994. Handbook of Deposition Technologies for Films and Coatings. Noyes Publications, New Jersey.

Changrong, X., Xiaoxia, G., Fanqing, L., Dingkun, P., Guangyao, M., 2001. Preparation of asymmetric Ni/ceramic composite membrane by electroless plating. Colloids and Surfaces A: Physicochemical and Engineering Aspects 179, 229- 235.

Chen, B.H., Hong, L., Ma, Y.H., Ko, T.M., 2002. Effects of surfactants in an electroless nickel – plating bath on the properties of Ni –P alloy Deposits. Industrial & Engineering Chemistry Research 41, 2668-2678.

Cheng, Y.S., Yeung, K.L., 2001. Effects of electroless plating chemistry on the synthesis of palladium membranes. Journal of Membrane Science 182, 195-203.

Collins, J.P., Way, J.D., 1993. Preparation and Characterization of a Composite Palladium-Ceramic Membrane. Industrial & Engineering Chemistry Research 32, 3006-3013.

Collins, J.P., Way, J.D., 1993. Hydrogen-selective membrane, Patent No. US 5652020 A.

Elansezhian, R., Ramamoorthy, B., Nair, P.K., 2008. Effect of surfactants on the mechanical properties of electroless (Ni–P) coating. Surface & Coatings Technology 203, 709-712.

Elansezhian, R., Ramamoorthy, B., Nair, P.K., 2009. The influence of SDS and CTAB surfactants on the surface morphology and surface topography of electroless Ni–P deposits. Journal of Materials and Processing Technology 209, 233-240.

Ernst, B., Haag, S., Burgard, M., 2007. Permselectivity of a nickel/ceramic composite membrane at elevated temperatures: A new prospect in hydrogen separation? Journal of Membrane Science 288, 208-217.

Gielens, F.C., Tong, V., Van Rijn, C.J.M., Vorstman, M.A.G., Keurentjes, J.T.F., 2002. High flux palladium–silver alloy membranes fabricated by micro system technology. Desalination 147, 417.

Granizo, M.L., Blanco-Varela, M.T., Martinez-Ramirez, S., 2007. Alkali activation of metakaolins: parameters affecting mechanical, structural and microstructural properties. Journal of Materials Science 42, 2934–2943.

Haag, S., Burgard, M., Ernst, B., 2006. Pure nickel coating on a mesoporous alumina membrane: Preparation by electroless plating and characterization. Surface & Coatings Technology 201, 2166–2173.

Haas, I., Gedanken, A., 2006. Sonoelectrochemistry of Cu^{2+} in the Presence of Cetyltrimethylammonium Bromide: Obtaining CuBr Instead of Copper. Chemistry of materials 18, 1184–1189.

Hu, X., Chen, W., Huang, Y., 2010. Fabrication of Pd/ceramic membranes for hydrogen separation based on low-cost macroporous ceramics with pencil coating. International Journal of Hydrogen energy 35, 7803-7808.

Ilias, S., Islam, M.A., 2012. Methods of preparing thin films by elctroless plating, Patent No. US 8,298,620 B2.

Ilias, S., Su, N., Udo-Aka, U.I., King, F.G. 1997. Application of Electroless Deposited Thin-Film Palladium Composite Membrane in Hydrogen, Separation science and technology, 32 , 487-504.

Islam, M.A., Ilias, S., 2010. Characterization of Pd-Composite Membrane Fabricated by Surfactant Induced Electroless Plating (SIEP): Effect of Grain Size on Hydrogen Permeability, Separation Science and Technology, 45, 1886-1893.

Islam, M.A., Rahman, M.M., Ilias, S., 2012. Characterization of Pd-Cu membranes fabricated bysurfactant induced electroless plating (SIEP) for hydrogen Separation. International Journal of Hydrogen Energy 37, 3477-3490.

Jaarsveld, J.G.S.V., Deventer, J.S.J.V., Lukey, G.C., 2002. The effect of composition and temperature on the properties of fly-ash and kaolinite-based geopolymers. Chemical Engineering Journal 89, 63-73.

Jayraman, V.,Lin, Y.S., 1995. Synthesis and hydrogen permeation properties of ultrathin palladium–silver alloy membranes. Journal of Membrane Science 104, 251.

Jha, S., Rubow, K.L., 1999. Nickel Microfiltration media for gas and liquid filtration. Advances in Filtration and Separation Technology 13, 512–520.

Jiang, J.L., Lu, H.Q., Zhang, L.X., Xu, N.P., 2007. Preparation of monodisperse Ni/PS spheres and hollow nickel spheres by ultrasonic electroless plating. Surface & Coatings Technology 201, 7174–7179.

Kathirgamanathan, P., 1994. Ultrasound-Assisted Electroless Deposition of Copper onto and into Microporous Membranes for Electromagnetic Shielding. Polymer 35, 430-432.

Kishore, N., Sachan, S., Rai, K.N., Kumar, A., 2003. Synthesis and characterization of a nanofiltration carbon membrane derived from phenol - formaldehyde resin. Carbon 41, 2961-2972.

Kitiwan, M., Atong, D.,2010. Effects of Porous Alumina Support and Plating Time on Electroless Plating of Palladium Membrane. Journal of Materials Science & Technology, 26 1148-1152.

Li, A., Liang, W., Hughes, R.,1999. Fabrication of defect-free Pd/alpha-Al_2O_3 composite membranes for hydrogen separation. Thin Solid Films 350, 106-112.

Li, Z., Han, C., 2006. Reduction of Ni^{2+} by hydrazine in solution for the preparation of nickel nano-particles. Journal of Materials Science 41, 3473–3480.

Lin, W.H., Liu, Y.C., Chang, H.F., 2010. Autothermal reforming of ethanol in a Pd-Ag/Ni composite membrane reactor. International Journal of Hydrogen Energy 35, 12961- 12969.

Lu, Y.X., 2010. Improvement of copper plating adhesion on silane modified PET film by ultrasonic-assisted electroless deposition. Applied Surface Science 256, 3554–3558.

Ma, Y.H., Mardilovich, I.P., Mardilovich, P.P., 2001. Effects of porosity and pore size distribution of the porous stainless steel on the thickness and hydrogen flux of palladium membranes. Journal of American Chemical Society 46, 154-156.

Mabande, G.T.P., Pradhan, G., Schwieger,W., Hanebuth, M., Dittmeyer, R., Selvam, T., Zampieri, A., Baser, H., Herrmann, R., 2004. A study of silicalite-1 and Al-ZSM-5 membrane synthesis on stainless steel supports. Microporous and Mesoporous Materials 75, 209-220.

Mafi, I.R., Dehghanian, C., 2011. Comparison of the coating properties and corrosion rates in electroless Ni–P/PTFE composites prepared by different types of surfactants. Applied Surface Science 257 8653– 8658.

Mardilovich, I.P., Engwall, E., Ma, Y.H., 2002. Dependence of hydrogen flux on the pore size and plating surface topology of asymmetric Pd-porous stainless steel membranes, Desalination 144, 85-89.

Merdivan, M., Aygun, R. S., Kulcu, N., 1997. Flame AAS Determination of Platinum, Palladium, and Rhodium in Catalysts. Atomic spectroscopy 18, 122-126.

Mizukoshi, Y., Takagi, E., Okuno, H., Oshima, R., Maeda, Y., Nagata, Y., 2001. Preparation of platinum nanoparticles by sonochemical reduction of the Pt(IV) ions: role of surfactants. Ultrasonic Sonochemistry 8, 1-6.

Nandi, B. K., Uppaluri, R., Purkait, M. K., 2009. Treatment of Oily Waste Water Using Low-Cost Ceramic Membrane: Flux Decline Mechanism and Economic Feasibility, Separation Science and Technology 44:12, 2840-2869.

Nam, S.E., Lee, K.H., 2000. A study on the palladium/nickel composite membrane by vacuum electrodeposition. Journal of Membrane Science 170, 91-99.

Nwosu, N., Davidson, A., Hindle, C., Barker, M.,2012. On the Influence of Surfactant Incorporation during Electroless Nickel Plating. Industrial & Engineering Chemistry Research 51, 5635 -5644.

Nwosu, N.O., Davidson, A.M., Hindle, C.S., 2011. Effect of Sodium Dodecyl Sulphate on the Composition of Electroless Nickel—Yttria Stabilized Zirconia Coatings. Advances in Chemical Engineering and Science 1, 118-124

Potdar, A., Shukla, A., Kumar, A., 2002. Effect of gas phase modification of analcime zeolite composite membrane on separation of surfactant by ultrafiltration. Journal of Membrane Science 210, 209–225.

Rhoda, R.N., 1966. Palladium deposition, Patent No. US 3274022 A.

Ryi, S.K., Park, J.S., Kim, S.H., Cho, S.H., Kim, D.W.,Um, K.Y., 2006a. Characterization of Pd–Cu–Ni ternary alloy membrane prepared by magnetron sputtering and Cu-reflow on porous nickel support for hydrogen separation. Separation and Purification Technology 50, 82-91.

Ryi, S.K., Park, J.S., Kim, S.H., Cho, S.H., Park, J.S., Kim, D.W., 2006b. Development of a new porous metal support of metallic dense membrane for hydrogen separation. Journal of Membrane Science 279, 439–445.

Ryi, S.K., Park, J.S., Park, S.J., Lee, D.G., Cho, S.H., 2007. Fabrication of nickel filter made by uniaxial pressing process for gas purification: Fabrication pressure effect. Journal of Membrane Science 299, 174-180.

Sari, R.,Yaakob, Z., Ismail, M., 2013. Palladium – alumina composite membrane for hydrogen separator fabricated by combined sol – gel, and electroless plating technique. Ceramics International 39, 3211-3219.

Seshimo, M., Ozawa, M., Sone, M., Sakurai, M., Kameyama, H., 2008. Fabrication of a novel Pd/g-alumina graded membrane by electroless plating on nanoporous alumina. Journal of Membrane Science 324, 181-187.

Silva, L.L.O., Vasconcelos, D.C.L., Nunes, E.H.M., Caldeira, L., Costa, V.C., Musse, A.P., Hatimondi, S.A., Nascimento, J.F., Grava, W., Vasconcelos, W.L., 2012. Processing, structural characterization and performance of alumina supports used in ceramic membranes. Ceramics International 38, 1943–1949.

Sing, K.S.W., Everett, D.H., Haul, R.A.W., Moscou, L., Pierotti, R.A., Rouquerol, J., Siemieniewska, T., 1985. Reporting Physisorption Data for Gas Solid Systems with Special Reference to the Determination of Surface-Area and Porosity. Pure and Applied Chemistry 57, 603 – 619.

Soloviev, M., Gedanken, A.,2011. Coating a stainless steel plate with silver nanoparticles by the sonochemical method. Ultrasonic Sonochemistry 18, 356–362.

Su, S., Chen, Y.L., Mou, C.Y.,1985. Micelle-counterion interaction, I. Critical micelle concentrations of SDS under the influence of copper counterion. Journal of Chinese Chemical Society 32, 5-10.

Tong, J., Shirai, R., Kashima, Y., Matsumara, Y.,2005. Preparation of a pinhole-free Pd–Ag membrane on a porous metal support for pure hydrogen separation. Journal of Membrane Science 260, 84-87.

Touyeras, F., Hihn, J.Y., Bourgoin, X., Jacques, B., Hallez, L., Branger, V.,2005. Effects of ultrasonic irradiation on the properties of coatings obtained by electroless plating and electro plating. Ultrasonic Sonochemistry 12, 13-19.

Vasanth, D., Pugazhenthi, G., Uppaluri, R., 2011. Fabrication and properties of low cost ceramic microfiltration membranes for separation of oil and bacteria from its solution. Journal of Membrane Science 379, 154-163.

Vichaphund, S., Atong, D.,2010. Fabrication of Ni-alumina Composite Membrane via Powder and Bulk Impregnation Method for Hydrogen Separation. Journal of Materials Science & Technology 26, 589-596.

Wang, M.C., Wu, N.C., Hon, M.H.,1994. Preparation of Nepheline Glass-Ceramics and Their Application as Dental Porcelain. Materials Chemistry and Physics 37, 370-375.

Ward, T.L., Dao, T.,1999. Model of hydrogen permeation behavior in palladium membranes. Journal of Membrane Science 153, 211- 231.

Wu, Z.J., Ge, S.H., Zhang, M.H., Li, W., Tao, K.Y., 2009. Synthesis of nickel nanoparticles supported on metal oxides using electroless plating: Controlling the dispersion and size of nickel nanoparticles, Journal of Colloid and Interface Science 330, 359–366.

Xue, D., Deng, J., 2001. Amorphous Ni–B alloy/ceramic composite membrane prepared by an improved electroless plating technique. Materials Letters 47, 271–275.

Yang, K., Yi , Z.L., Jing, Q.F., Yue, R.L., Jiang, W., Lin, D.H., 2013. Sonication-assisted dispersion of carbon nanotubes in aqueous solutions of the anionic surfactant SDBS: The role of sonication energy Chinese Science Bulletin 58, 2090-2094.

Yeung, K.L., Christiansen, S.C., Varma, A., 1999. Palladium composite membranes by electroless plating technique - Relationships between plating kinetics, film microstructure and membrane performance. Journal of Membrane Science 159, 107–122.

Zhang, K., Huiyan, G., Zebao, R., Yuesheng, L., Yongdan, L. (2007). Preparation of Thin Palladium Composite Membranes and Application to Hydrogen/Nitrogen Separation.Chinese Journal of Chemical Engineering, 15, 643—647.

Zhang, X.L., Xiong, G.X., Yang, W.S., 2008. A modified electroless plating technique for thin dense palladium composite membranes with enhanced stability. Journal of Membrane Science 314, 226-237.

Zhao, H.B., Xiong, G.X., Baron, G.V., 2000. Preparation and characterization of palladium-based composite membranes by electroless plating and magnetron sputtering. Catalysis Today 56.

Zheng, W., Wu, L., 2000. Preparation and pore size shrinkage of palladium–ceramic composite membrane by electroless plating under hydrothermal conditions. Materials Science and Engineering: A 283, 122–125

Zielinska, K., Stankiewicz, A., Szczygiel, I., 2012. Electroless deposition of Ni-P-nano-ZrO_2 composite coatings in the presence of various types of surfactants. Journal of Colloid and Interface Science 377, 362-367.

Web Links:

WL1: Mott Corporation, USA, Gas Shield® PENTA® Filters, Available at: http://www.mottcorp.com/products/biotechnology-semiconductor/penta.cfm (October 2012).

WL2: Mykron, China, Mykrolis™ Nickel Membrane Filters, Available at: http://www.mykrons.com/ProductThree.asp?id=72 (October 2012).

WL3: Entegris, USA, Surface Mount Metal Gas Filter, Available at: http://www.entegris.com/ProductLine_catGasFilter_divFiltration_lineGF_Surface_Mount_Metal_Gas_Filter.aspx (October 2012).

WL4: Johnson Matthey Gas Purification Technology, USA, The PureGuard™ Palladium Hydrogen Gas Purifiers, Available at: http://pureguard.net/cm/About_Us/About_JM_Gas_Purification_Technology.html (May 2013).

WL5: ECN, Netherlands, Energy efficient hydrogen separator, Available at: http://www.ecn.nl/news/newsletter-en/2010/september-2010/energy-efficient hydrogen-separator/ (May 2013).

WL6:http://www.leaninstructionalconsulting.com/LeanID%20Nickel%20Titration%20Lesson%20Intro.pdf (April 2014)

Appendix A: Determination of average pore size and effective porosity of the ceramic support

Based on the gas permeation data, average pore radius (d_p) and $\left(\frac{\varepsilon}{q^2}\right)$ effective porosity can be estimated according to the following expression (Vichaphund and Atong, 2010):

$$K_i^{cal} = \left(\frac{2.133}{2}\frac{d_p v}{l}\left(\frac{\varepsilon}{q^2}\right) + \frac{1.6}{4}\frac{d_p^{\,2}}{l\eta}\left(\frac{\varepsilon}{q^2}\right)\overline{P}\right) \qquad \text{(A1)}$$

where, $\overline{P}$ is the average pressure on the membrane, v (m/s) is the molecular mean velocity of the gas, cal refers to calculated, i is an integer greater than zero, l (m) is the pore length, q is the tortuosity, η (Pa.s) is the viscosity of gas, and K (m/s) is the effective permeability factor evaluated as:

$$K_i^{cal} = \frac{J_i\,\Delta P}{P_2} \qquad \text{(A2)}$$

where J is the nitrogen flux, P_2 (Pa) is the membrane pressure at permeate side (1 atm) and ΔP (Pa) is the trans-membrane pressure drop.

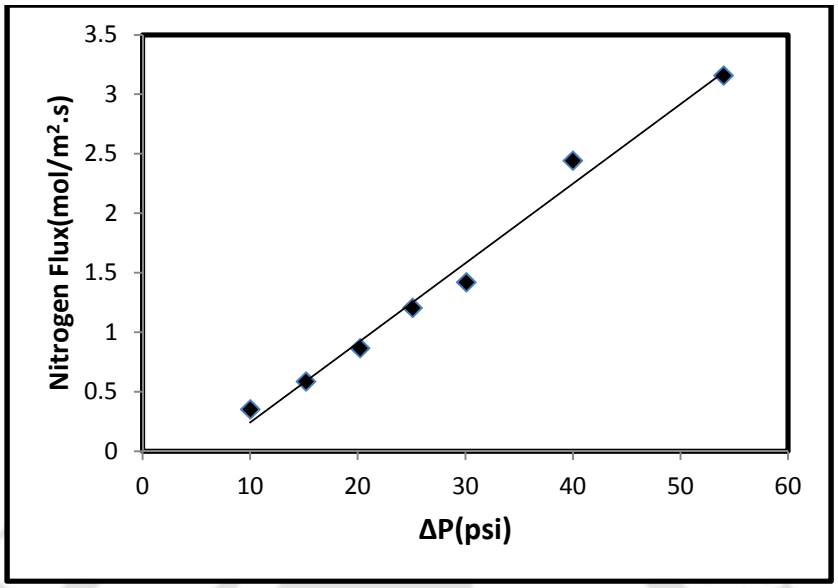

Fig. A1: Nitrogen flux data for the ceramic membrane support

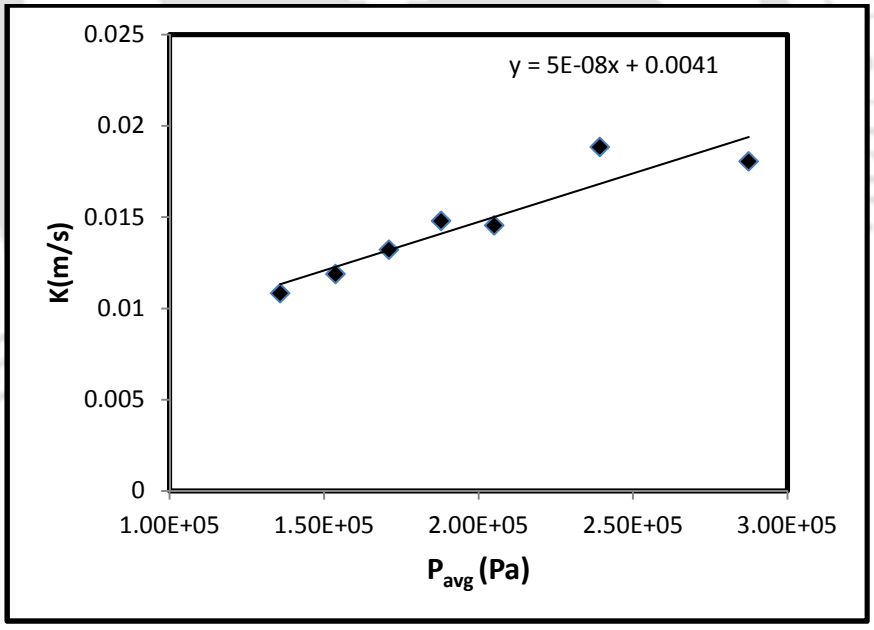

Fig. A2: Plot of effective permeability factor versus average pressure.

Equation (A1) is in the form of a straight line:

$$K = A\overline{P} + B \qquad \text{(A3)}$$

for which 'A' and 'B' are the slope and the intercept respectively. Using J_i, ΔP, P_2 values, K can be evaluated for distinct values of ΔP. Fig. A1 presents the obtained J vs ΔP can be drawn (as shown in Fig. A2), using which the intercept 'A' and slope 'B' can be calculated. Using the 'A' and 'B' values, the average pore radius can be evaluated using the expression (Vichaphund and Atong, 2010):

$$r_g = 1.333\frac{A}{B}v\eta \qquad \text{(A4)}$$

With the known value of r_g the pore radius, the effective porosity $\left(\frac{\varepsilon}{q^2}\right)$ can be calculated using the expression:

$$\frac{\varepsilon}{q^2} = \frac{B}{2.133}\frac{l}{r_g v} \qquad \text{(A5)}$$

For the considered ceramic support, the slope and intercept values have been obtained as 5×10^{-8} and 0.0041 respectively (Fig. A2). Using equation A4 and A5, the average pore diameter (r_g) and effective porosity $\left(\frac{\varepsilon}{q^2}\right)$ have been evaluated as 247.5 nm and 0.153 respectively.

Appendix B: Determination of Ni solution concentration

The procedure to determine nickel solution concentration before and after plating process is summarized in this appendix. Complexometric titration was used to analyze the concentration of Ni^{2+} in the plating bath before and after plating. The titration was conducted with ethylenediaminetetraacetic acid (EDTA) using xylenol orange (1% in KNO_3) indicator at a temperature of 80°C. Buffering agents (NaOH + CH_3COOH (glacial), 5:8 mole ratio) were also added to the mixture during titration carried out under continuous agitation [WL6].

The sequence of steps involved in the titration process was as follows.

(i) 5 ml of bath sample was taken into a 250 ml beaker.

(ii) The sample was diluted (10 times) with de-ionized water.

(iii) Buffer solution was added until the solution becomes colorless (≈10 ml).

(iv) The solution was heated (≈80°C) on a hot plate under continuous stirring.

(v) Xylenol orange indicator (1% in KNO_3) was added (solution becomes red).

(vi) Standardized (0.1 N) EDTA solution was added drop by drop (using burette) until the equivalence point was reached (color changes to yellow).

The above procedure (steps i–vi) was repeated 3–4 times for accuracy. From the volume (V_2) of standard (N_2) EDTA solution run down during the titration, the concentration (N_1) of Ni^{+2} in the plating bath can be evaluated using the following expression

$$N_1 \times V_1 = N_2 \times V_2$$

Where, (V_1) is the volume of bath sample taken for analysis (5 ml). Subsequently, dilution factor was considered to estimate the actual plating solution concentration.

Appendix C: Sample calculations for the evaluation of combinatorial plating characteristics for Ni membrane

The sample calculations for evaluation of various parameters involved in the electroless fabrication of Ni- ceramic membrane are presented as follows:

1. Metal Conversion (x (%))

After four sequential deposition $V_i = 4\times50\times.001$L, $C_i = 0.08$ mol/L , $V_iC_i = 0.2 \times0.08$ mol

$= 0.016$ mol

Titration : $N_1 = \frac{N_2 \times V_2}{V_1} = \frac{0.1\times3.4}{5} = 0.068N$

Volume of solution accumated after 4 sequential deposition $V_f =$ 190ml

$C_f = 0.068$ mol/L, $V_fC_f = .013$mol

Conversion : $x = \frac{V_iC_i - V_fC_f}{V_iC_i}\times100$

x= 19.25%

2. P**lating efficiency (**η(%))

$\eta = \frac{w_2 - w_1}{w_0\, x}\times100$

$w_0x = (V_iC_i - V_fC_f)M_{Ni} = 0.18g$

$w_2 - w_1 = 0.096$ g

$\eta = 53.1\%$

3. Average Plating rate $\left(\bar{r}_i \left(\frac{mol}{m^2.s}\right)\right)$

$$\overline{r_i} = \frac{w_2 - w_1}{M_{Ni} \times A_m \times t_i}$$

$$\overline{r_i} = \frac{0.096}{58.69 \times 0.0010174 \times 2 \times 3600} = 2.23 \times 10^{-4} \frac{mol}{m^2.s}$$

4. Percent Pore Densification (PPD (%))

$$PPD = \frac{\overline{J_0} - \overline{J_i}}{\overline{J_0}} \times 100 = \frac{2.72 - 1.22}{2.72} \times 100 = 55.1\%$$

$\overline{J_0}$ and $\overline{J_i}$ were determined for the ceramic support using room temperature permeation experiments. Thereby by J vs. ΔP data was subjected to numerical integration analysis using trapezoidal rule. Using these procedure $\overline{J_0} = 2.72\left(\frac{mol}{m^2.s}\right)$ and $\overline{J_i} = 1.22\left(\frac{mol}{m^2.s}\right)$ were obtained.

5. Theoretical metal film thickness (δ(µm))

$$\delta = \frac{w_2 - w_1}{\rho_{Ni}\ A_m} = \frac{0.096}{8.9 \times 0.0010174} = 10.6 \mu m$$

Appendix D: Preparation of AAS calibration curve to determine Pd solution concentration

Appendix D briefly presents the procedure adopted to prepare calibration curve for the evaluation of Pd solution concentration after ELP. Atomic absorption spectroscopy (Make: M/S Varian BV, Model: Spectra AA 220FS) in the flame mode with a Pd lamp of wavelength 247.6 Å (Merdivan, 1997) was used to determine the calibration curve. Using the calibration curve, the unknown concentration of Pd in the ELP solution can be determined.

The composition used for the preparation of standard solution includes preparation of $PdCl_2$ solution as mentioned in chapter 2. The concentration of 0.01mol/L $PdCl_2$ corresponds to 112.2 ppm. Using that concentration various standards in the range of (5-50 ppm) are prepared.

The steps involved in the preparation of calibration curve are sequentially presented as follows:

1. Preparation of standard palladium solution using electroless plating solution consisting of $PdCl_2$, EDTA, NH_3 and Millipore water in the desired range of 5 – 50 ppm. Standard solution for ELP solutions with surfactant (CTAB) has been as well prepared.
2. The instrument was calibrated using several solutions of specified concentrations.
3. The absorbance of each known standard solution was measured and then a calibration curve with concentrations of the standard element on the abscissa and the absorbance on the ordinate was plotted.

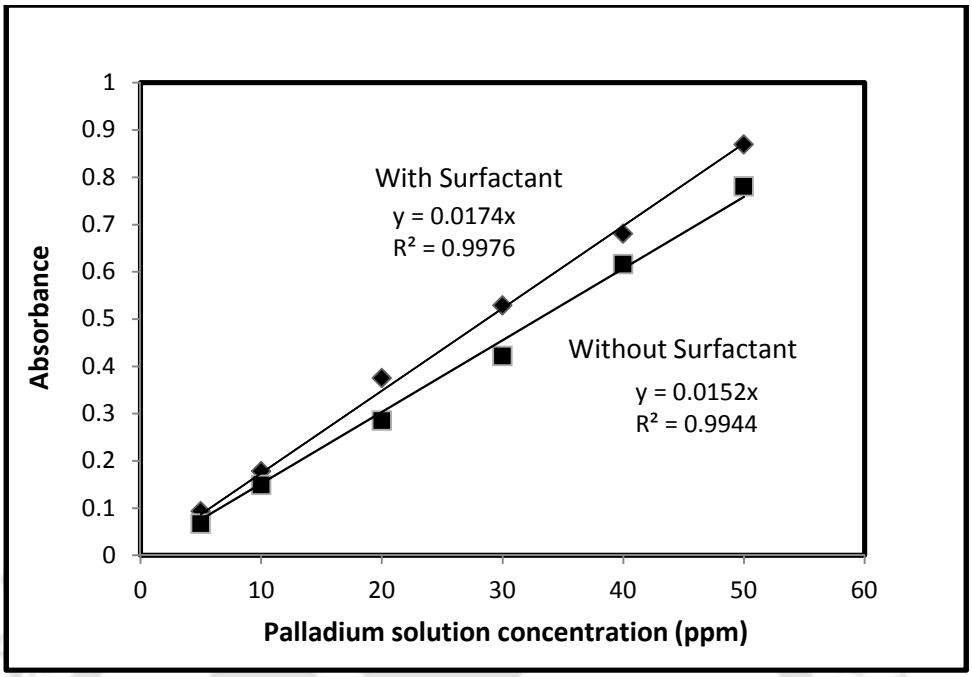

Fig. C1: Standard curve for Palladium electroless plating bath with and without surfactant

Fig. C1 presents the standard calibration curve obtained from the AAS for ELP solutions with and without CTAB surfactant. It can be observed that there exists a linear fitness of the absorbance with respect to the variation in the Pd solution concentration. Using the calibration curves, the unknown Pd solution was determined by estimating its absorbance.

Appendix E: Sample calculations for the evaluation of combinatorial plating characteristics for Pd membrane

The sample calculations for evaluation of various parameters involved in the electroless fabrication of Pd- ceramic membrane are presented as follows:

1. Metal Conversion (x (%))

After four sequential deposition $V_i = 4\times50\times.001$ L, $C_i = 0.01$ mol/L, $V_iC_i = 0.2 \times0.01 = 0.002$ mol

From AAS the absorbance of the feed solution was observed to be 0.898 which corresponds to a final concentration of 0.0043 mol/L

Volume of solution at the end of four sequential deposition $V_f = 236\times0.001$L, $V_f C_f = 0.00114$ mol

Conversion : $x = \frac{V_iC_i - V_fC_f}{V_iC_i}\times100$

x= 43.13%

2. Plating efficiency ($\eta(\%)$)

$$\eta = \frac{w_2 - w_1}{w_0\, x}\times100$$

$$w_0 x = (V_iC_i - V_fC_f)M_{Pd} = 0.09g$$

$w_2 - w_1 = 0.088$ g

$\eta = 95.8\%$

3. Average Plating rate $\left(\bar{r}_i \left(\frac{mol}{m^2.s}\right)\right)$

$$\bar{r}_i = \frac{w_2 - w_1}{M_{Pd} \times A_m \times t_i}$$

$$\bar{r}_i = \frac{0.088}{106.4 \times 0.0010174 \times 1.5 \times 3600} = 1.5053 \times 10^{-4} \frac{mol}{m^2.s}$$

4. Percent Pore Densification (PPD (%))

$$PPD = \frac{\overline{J_0} - \overline{J_i}}{\overline{J_0}} \times 100 = \frac{1.02 - 0.125}{1.02} \times 100 = 87.7\%$$

$\overline{J_0}$ and $\overline{J_i}$ were determined for the ceramic support using room temperature permeation experiments. Thereby by J vs. ΔP data was subjected to numerical integration analysis using trapezoidal rule. Using these procedure $\overline{J_0} = 1.02\left(\frac{mol}{m^2.s}\right)$ and $\overline{J_i} = 0.125\left(\frac{mol}{m^2.s}\right)$ were obtained.

5. Theoretical metal film thickness (δ (µm))

$$\delta = \frac{w_2 - w_1}{\rho_{Pd}\ A_m} = \frac{0.088}{12.02 \times 0.0010174} = 7.1 \mu m$$

International Journals

1. **Amrita Agarwal,** Murali Pujari, Ramgopal Uppaluri and Anil Verma, Efficacy of reducing agent & surfactant contacting pattern on the performance characteristics of nickel electroless plating baths, Ultrasonic Sonochemistry, Elsevier, 21 (2014) 1382–1391.
2. **Amrita Agarwal**, Murali Pujari, Ramgopal Uppaluri and Anil Verma, Optimal Electroless Plating Rate Enhancement Techniques for the Fabrication of Low Cost Dense Nickel/Ceramic Composite Membranes. Ceramics International, Elsevier, 40, (2014) 691–697.
3. **Amrita Agarwal**, Murali Pujari, Ramgopal Uppaluri and Anil Verma, Preparation, optimization and characterization of low cost ceramics for the fabrication of dense nickel composite membranes, Ceramics International, Elsevier, 39 (2013) 7709-7716.
4. **Amrita Agarwal**, Murali Pujari, Ramgopal Uppaluri and Anil Verma, A novel method of reducing agent contacting pattern for metal ceramic composite membrane fabrication, Applied Surface Science, Elsevier, 320 (2014) 52-59.
5. **Amrita Agarwal**, Murali Pujari, Ramgopal Uppaluri and Anil Verma, Rate Enhanced Electroless Fabrication of Nickel Ceramic Composite Membranes, Surface Engineering, Maney, DOI: http://dx.doi.org/10.1179/1743294414Y.0000000368.
6. **Amrita Agarwal**, Murali Pujari, Ramgopal Uppaluri and Anil Verma, Efficacy of Palladium Solution Concentration on Electroless Fabrication of Dense Metal Ceramic

Composite Membranes Coupled with Surfactant and Sonication, Materials and Manufacturing Processes, Taylor & Francis, DOI:10.1080/10426914.2014.973596.

Indian Patent

1. **Amrita Agarwal**, Murali Pujari, Ramgopal Uppaluri, Anil Verma, Composition and Method for Dense Palladium Ceramic Composite Membrane Fabrication, Indian Patent filed (05-06-2014), Application No. 612/KOL/2014.

Manuscripts Communicated

1. **Amrita Agarwal**, Murali Pujari, Ramgopal Uppaluri and Anil Verma, Effect of rate enhancement techniques for the fabrication of dense palladium composite membranes, Ultrasonic Sonochemistry (Under review).

Available online at www.sciencedirect.com

SciVerse ScienceDirect

Ceramics International 39 (2013) 7709–7716

CERAMICS INTERNATIONAL

www.elsevier.com/locate/ceramint

Preparation, optimization and characterization of low cost ceramics for the fabrication of dense nickel composite membranes

Amrita Agarwal, Murali Pujari, R. Uppaluri*, A. Verma

Department of Chemical Engineering, Indian Institute of Technology Guwahati, Guwahati-781039 Assam, India

Received 11 February 2013; accepted 10 March 2013
Available online 16 March 2013

Abstract

This article addressed a broad research methodology for the development of low cost ceramics to serve as functional supports for dense metal composite membranes. The experimental challenge of this study is to work with laboratory fabricated supports characterized with lower combinations of average pore size (50–70 nm) and lower effective porosity (0.012) and hence lower surface area for activation and plating reaction. Apart from fabrication parameters, the research emphasis has been towards ensuring morphological fitness of the ceramic support, good corrosion resistance and continuous enhancement in pore densification during prolonged nickel electroless plating of about 24 h. Surface and physical characterization using LPSA, BET, FTIR, XRD, FESEM and nitrogen permeation techniques yielded valuable insights. It has been observed that the sonication of the raw membrane support in alkaline conditions enormously contributed towards good corrosion resistance during nickel ELP. The morphological fitness of the ceramic support has been targeted by assuming a combination of Knudsen and Viscous diffusion through the membrane support and activated diffusion through the dense nickel film. Thereby the morphological fitness is ensured by evaluating whether or not nickel film nitrogen flux values are lower than the support fluxes.

Keywords: Electroless plating; Surfactant; Average flux; Nickel membrane

1. Introduction

Amongst organic and inorganic/metal membranes, the latter are highly promising towards various industrial schemes that involve higher processing temperatures and corrosive environments. Inorganic/metal membranes have been further classified into porous and dense composite membranes. Typically, alumina, carbon or stainless steel are commonly used materials for metal composite membranes [1–4]. Amongst these, sintered stainless steel membranes have received attention due to possessing higher durability as a filter medium for superior separations and consistent performance under extreme process conditions and high operating temperatures. However, large scale applications of stainless steel membranes are highly expensive when compared to ceramic membranes and fabrication research is also equally focused towards utilizing ceramic membrane supports [5].

Presently, metal ceramic composite membranes have been suggested for several applications including TiO_2 recovery from waste water streams [6], production of ultrapure gases for special applications [7], bacteriostatic treatment [8], asymmetric supports for dense palladium (Pd) composite membranes [9] and hydrogen separation [10]. Presently companies such as Mykron, Entegris and Mott Corporation fabricate ceramic composite membranes for several commercial applications. Typically, amongst ceramics, alpha-alumina supports are used for Pd membrane fabrication. However, alpha-alumina being expensive, its large scale application for Pd composite membranes is also bound to contribute higher costs for the composite membrane and hence there is a need for research into low cost ceramic supports for dense Pd membrane fabrication.

The consistent performance of ceramic membranes to serve as functional supports for dense Pd membranes needs to ensure their compatibility from several perspectives. First, membranes with lower pore size, good porosity and narrow pore size distribution are required so as to reduce the critical thickness of Pd required for the realization of dense membrane. Second, the membrane shall possess excellent corrosion resistance to withstand conditions during alkaline nickel electroless plating as well as industrial processing schemes. Third, the support shall enable continuous enhancement in pore densification during sequential metal deposition using electroless plating. Fourth, the

*Corresponding author. Tel.: +91 3612582260; fax: +91 3612582291.
E-mail address: ramgopalu@iitg.ernet.in (R. Uppaluri).

0272-8842/$ - see front matter © 2013 Elsevier Ltd and Techna Group S.r.l. All rights reserved.
http://dx.doi.org/10.1016/j.ceramint.2013.03.024

nickel film shall provide lower gas flux when compared to the support flux and therefore the support morphological parameters need to be fine-tuned during fabrication research. A critical review of literatures available for dense Pd membranes research indicates the lack of integrated methodologies and approaches towards research in the functional supports [1,9]. The cost of a composite membrane is a function of both metal film and the support and hence, cost reductions in support fabrication along with metal film deposition would be highly useful to drive economic competitiveness of the metal ceramic composite membranes.

Combinatorial performance characteristics of metal ceramic membranes were addressed by our research group [11,12]. However these studies were not directed towards support morphological issues for dense membrane fabrication. In addition time dependency of process and membrane parameters was also not reported. Based on our past experience with electroless plating (ELP) and its mass transfer coupled variance this work anticipates to obtain useful insights towards dense metal membrane fabrication with supports characterized with lower pore size and lower porosity.

Considering nickel as the target plating metal, a conceptual research methodology has been outlined that systematically addresses the experimental and theoretical insights for the realization of dense metal composite membranes. The laboratory fabricated porous supports were characterized with lower average pore size (50–70 nm) and lower effective porosity (0.012), so as to provide most challenging scenario for the plating processes towards maximum pore densification. Using the concept of lower gas transport resistance of the metal film with respect to the support, the next section elaborates upon the justification to select the support pore morphology (50–70 nm) for targeting dense metal composite membranes.

2. Morphological fitness of the ceramic support

Using nickel as the electroless plated metal, the ultimate objective of the research was to provide insights in plating rate enhancement methods for contributing towards research in dense nickel composite membranes. This was also due to the fact that flux data for dense nickel membranes was not available in the literature. An important functional prerequisite for metal composite membrane was that the metal (Ni) film flux (H_2) shall always be lower than the porous support flux. Since nickel flux increased with temperature, maximum nickel flux was achieved at the highest possible operation temperature and minimal metal thickness. For the present case, these values were assumed to be 550 °C and 1 μm, respectively. The model based maximum hydrogen flux achievable through the dense Ni film was evaluated using the expression:

$$J_{H_2}^{\mathrm{mod}} = \frac{Perm_{\mathrm{lit}}}{\delta_{ass}} \times \delta_{\mathrm{lit}} \times A_m \times (P_{\mathrm{ret}}^{n'} - P_{\mathrm{per}}^{n'}) \tag{1}$$

where $Perm_{\mathrm{lit}}$ and δ_{lit} correspond to the theoretical dense Ni film permeability and thickness in the composite membrane. The dense nickel film permeability was estimated using the expression [13]:

$$Perm_{\mathrm{lit}} = 3.35 \times 10^{-7} \exp\left(\frac{-54.25 \times 10^3}{RT}\right) \tag{2}$$

Assuming a combination of Knudsen and viscous diffusion, for a given membrane morphological parametric combination of d_p and (ε/q^2), the average hydrogen flux through the porous support was evaluated using the expression:

$$J_{H_2}^{\mathrm{sup}} = \left(\frac{2.133}{2}\frac{d_p v}{l}\left(\frac{\varepsilon}{q^2}\right) + \frac{1.6}{4}\frac{d_p^2}{pl\eta}\left(\frac{\varepsilon}{q^2}\right)\overline{P}\right)\frac{\Delta P}{P_2} \tag{3}$$

Assuming that the metal ceramic composite membrane was feasible only when the metal film flux was at least 10% lower than that of the support hydrogen flux, an inequality constraint needs to be satisfied, which was expressed as:

$$\frac{(J_{H_2}^{\mathrm{sup}} - J_{H_2}^{\mathrm{mod}})}{J_{H_2}^{\mathrm{sup}}} \times 100 \geq 10 \cdots \forall \Delta P \tag{4}$$

To validate the above system of equations in a systematic format, a simple procedure was followed to evaluate the feasibility of the support morphology:

(i) Using Eq. (1), determine $J_{H_2}^{\mathrm{mod}}$ vs. ΔP data for assumed membrane parameters from the literature.

(ii) Using Nitrogen gas as the transport gas, conduct single gas permeation experiments and obtain $J_{N_2}^{\mathrm{sup}}$ (experiment) vs. ΔP. Using the experimental data and Eq. (3), determine membrane morphological parameters experimentally (d_p^{sup} and (ε/q^2))

(iii) For a specified value of d_p^{sup} or (ε/q^2), determine the minimum value of (ε/q^2) min or d_p^{min} to satisfy the following optimization problem defined in terms of dense Ni film and support hydrogen flux:

$$\begin{aligned}
&\mathrm{Min} = \sum_{i=1}^{\Delta P\max} \\
&E_i = \frac{(J_{\mathrm{Ni}_{H_2}} - J_{\mathrm{sup}_{H_2}})}{J_{\mathrm{Ni}_{H_2}}} \times 100 \\
&J_{H_2}^{\mathrm{mod}} = \frac{Perm_{\mathrm{lit}}}{\delta_{ass}} \times \delta_{lit} \times A_m \times (P_{\mathrm{ret}}^{n'} - P_{\mathrm{per}}^{n'}) \\
&J_{H_2}^{\mathrm{sup}} = \left(\frac{2.133}{2}\frac{d_p v}{l}\left(\frac{\varepsilon}{q^2}\right) + \frac{1.6}{4}\frac{d_p^2}{l\eta}\left(\frac{\varepsilon}{q^2}\right)\overline{P}\right)\frac{\Delta P}{P_2} \\
&E_i \geq 10 \ \forall \ i \\
&0 \leq \left(\frac{\varepsilon}{q^2}\right)_{\mathrm{sup}}^{th} \leq 1 \ (OR) \ d_p^{\mathrm{min}} \geq 0
\end{aligned} \tag{5}$$

(iv) The support morphological parameters were regarded to be feasible for plating after either one of the following two constraints were satisfied:

$$d_p^{\mathrm{sup}} \geq d_p^{\mathrm{min}} \ \mathrm{OR} \ \left(\frac{\varepsilon}{q^2}\right)^{\mathrm{sup}} \geq \left(\frac{\varepsilon}{q^2}\right)^{\mathrm{min}} \tag{6}$$

Based on our research a case study was presented below to illustrate the above procedure. For an assumed Ni film thickness

of 5 μm, and an evaluated dense Ni film permeability of 1.207×10^{-10} (mol/m/m^2/s/Pa$^{0.5}$) [13], the theoretical Ni dense film hydrogen flow rate varied from 4.81×10^{-4}–2.02×10^{-2} (lit/min) for a trans-membrane pressure difference of 0.1–10 atm. The room temperature N_2 permeation data for the support varied from 4.81×10^{-4}–2.02×10^{-2} (lit/min) for a trans-membrane pressure difference variation from 0.1 to 10 atm. Calculations using the N_2 gas permeation data at room temperature indicated that the membrane morphological parametric values were $d_p^{sup} = 57$ nm and $(\varepsilon/q^2)^{sup} = 0.012$. Assuming d_p^{exp} as d_p^{mod}, the solution of the optimization model (Eq. (4)) inferred that (ε/q^2) min = 0.003063, which was lower than the value obtained from experimental data i.e., $(\varepsilon/q^2)^{sup} = 0.012$. Thus, the support morphology was concluded to be feasible for proceeding towards electroless plating research. Additional trade-offs associated to dense film thickness variations are presented in the results and discussion section of this article. The next section elaborates upon the experimental investigations towards support fabrication and ELP for dense membrane fabrication.

3. Experimental

3.1. Low cost ceramic membranes

Laboratory made disk shaped ceramic substrates with a diameter of 36 mm and thickness of 3.5 mm were prepared for all experiments. The supports were fabricated at a pressure of 4.9 MPa using a hydraulic press (Make—Velan Engineering) by the dry compaction method. The support possessed a pore size d_p^{sup} and effective porosity (ε/q^2) of about 50–70 nm and 0.012 nm, respectively.

Seven inorganic raw materials viz. kaolin, feldspar, quartz, sodium carbonate, pyrophyllite, boric acid and sodium metasilicate were used in the fabrication of ceramic membrane supports. Kaolin was obtained from CDH Ltd., India, feldspar and pyrophyllite from National Chemicals, India, quartz from Research-lab Fine Chem Industries, India, sodium metasilicate from SD Fine-chem Ltd., India and the other inorganic precursors (sodium carbonate and boric acid) were obtained from Merck Ltd., India. Composition of various raw materials along with their average particle size (as shown in Fig. 1) were mentioned in Table 1. The fabrication methodology consists of the following hierarchical steps: mixing of raw materials to make a paste; casting of the paste into circular moulds; drying of the raw discs; sintering; polishing of the membranes and ultrasonically cleaning. All membranes were prepared by sintering at 900 °C with a controlled heating/cooling rate (1.5 °C/min).

3.2. Surface and flux characterization

Raw material, support and membrane characterizations were carried out by laser particle size analyzer (LPSA), Brunauer Emmett Teller (BET) surface area analyzer, fourier transform infrared spectroscopy (FTIR), X-ray diffraction (XRD) and field emission scanning electron microscopy (FESEM).The mean pore size of the bulk membrane was estimated from

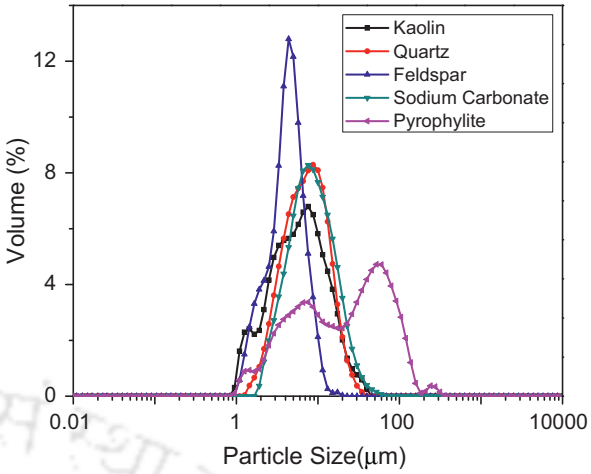

Fig. 1. Particle size distribution for different raw materials.

Table 1
Composition of raw materials for the fabrication of ceramic membrane supports.

Material	Composition on dry basis (wt %)	Average particle size (μm)
Kaolin	40	5.50
Feldspar	15	3.46
Quartz	15	7.72
Na_2CO_3	10	7.59
Pyrophyllite	10	20.36
Boric acid	5	–
Sodium metasilicate	5	–

nitrogen permeation experiments. Membrane porosity was determined by weight gain method. The flux of the composite membranes was anticipated from nitrogen permeation data and the experimental setup was similar to the one as discussed by Bulasara et al. [12]. For all permeation experiments, high purity N_2 (99.99% obtained from Assam Air Products Ltd., Guwahati) was used for an effective permeation area of1.0173×10^{-3} m^2.

3.3. Electroless plating

Electroless plating technique was taken up for nickel deposition with the typical compositions summarized in Table 2. Prior to plating, seeding was carried on which involved the conventional procedure of activation and sensitization of the support with palladium seeds. Eight sequential 1 h nickel deposition steps with a nickel concentration of 0.08 (mol/L) were taken up to yield the nickel ceramic composite membranes. A 50% excess hydrazine hydrate was used as a reducing agent. The plating was carried on a water bath maintained at 80 °C and the plating characteristics were investigated at a loading ratio of 203 (cm^2/L). Four different cases as listed in Table 3 were focused for this work which involved membranes prepared with sonication assisted ELP (M_1), surfactant assisted ELP (M_2), NaOH treated support and

Table 2
Typical composition of conventional and surfactant induced nickel electroless plating baths.

S. no.	Component	Formula	Role	Amount
1.	Nickel sulfate	$NiSO_4 \cdot 7H_2O$	Source of nickel	0.08 mol/L
2.	Hydrazine Hydrate	$H_2NNH_2 \cdot H_2O$	Reducing agent	50% excess
3.	Trisodium citrate	$Na_3C_6H_5O_7 \cdot 2H_2O$	Stabilizer	0.2 mol/L
4.	Sodium Hydroxide	NaOH	pH	10–12
5	Cetyltrimethylammonium bromide	$(C_{16}H_{33})N(CH_3)_3Br$	Dispersion	1.2 g/L

surfactant assisted ELP (M_3) and NaOH treated support and sonication assisted ELP (M_4) study.

Prior to plating, membranes M_3 and M_4 were treated. The treatment involved etching of the membrane in NaOH solution of pH 12 in a sonicator bath (Elmasonic, S30 H) under degas mode of continuous operation for 6 h at 80 °C (plating temperature). This modified the support morphology and enhanced support corrosion resistance. Subsequently, the support pore size (based on nitrogen gas permeation) enhanced from 50–70 nm to 90–120 nm, respectively. However when sodium hydroxide treatment was carried without sonication and degas mode in a water bath maintained at 80 °C, the improvement in support morphology was not sufficient enough to avoid negative flux trends. For all cases, membrane supports with similar average flux values were chosen to maintain coherence amongst various performance characteristics.

3.4. Evaluation of plating characteristics

The performance assessment of various plating baths for fabricating dense nickel membranes was characterized by the determination of parameters namely average trans-membrane flux $\overline{J}$ and percent pore densification *PPD*(%).

The nitrogen flux through the membrane (J) at varying pressure was evaluated from the volumetric flow rate data

$$J = \frac{Q}{A_m}$$

where Q represents the volumetric flow rate in LPM, A_m the permeable area of the membrane in m^2 and J the flux through the membrane in (mol/m^2/s)

$$\overline{J} = \frac{\int_{P_1}^{P_2} J dP}{P_2 - P_1}$$

where $\overline{J}$ represents the average flux through the membrane, $\int_{P_1}^{P_2} J dP$ corresponds to the area under the curve of a plot between the membrane flux (mol/m^2/s) and pressure (psi).The term $P_2 - P_1$ corresponds to the trans-membrane pressure drop. Pore densification during the plating process was defined as the fractional volume of the pores covered by the deposited metal and it was expressed as a time dependent expression

$$PPD_i = \frac{\overline{J}_0 - \overline{J}_i}{\overline{J}_0} \times 100$$

where $\overline{J}_0$ represents the average flux through the support and $\overline{J}_i$ represents the average flux through the membrane after ith hour of nickel plating. *PPD* calculations were carried using the average flux data because they provide appropriate time dependency as compared to the *PPD* calculated using the pore diameter procedure in the literature [12].

Table 3
Summary of various cases investigated for the development of low cost ceramic membranes.

Case	Type of support	Type of ELP
M_1	Raw	Sonication
M_2	Raw	Surfactant
M_3	Treated	Surfactant
M_4	Treated	Sonication

4. Results and discussions

4.1. Surface characterization

The major raw materials i.e., kaolin, quartz, feldspar, sodium carbonate and pyrophylite used for the membrane fabrication process were characterized using laser particle size analyzer (Make: Malvern; Model: Mastersizer 2000, UK). Fig. 1 presents the particle size distribution of the raw materials which were the building stones for the ceramic support. It was observed that average particle size of kaolin, quartz, feldspar, sodium carbonate and pyrophylite were 5.50 μm, 7.72 μm, 3.46 μm, 7.59 μm and 20.36 μm, respectively.

The BET surface area and pore size of the support material was determined by N_2 adsorption desorption isotherm at 77 K by using a surface area analyzer (Beckman-Coulter; Model: SA3100). Prior to measurement, the samples were degassed at 200 °C in vacuum for 60 min. The adsorption/desorption isotherms of the support material was shown in Fig. 2(a). The isotherms were of type III and H_3 hysteresis loop was observed that gave rise to slit-shaped pores according to IUPAC [14]. Based on BET, the pore size distribution as a function of volume percentage of pores of the support was shown in Fig. 2(b). The average pore size as evaluated from Barrett–Joyner–Halenda (BJH) pore volume distribution was found to be 35 nm which was close to that evaluated from nitrogen permeation (50–70 nm). The BET surface area of support was 2.712 m^2/g and total pore volume was 0.0156 mL/g with no micropore volume.

The fourier transform infrared spectra recorded from wave number 4000 to 500 cm^{-1} using IR Affinity—1 spectrometer as shown in Fig. 3. Characteristic peaks of kaolin were

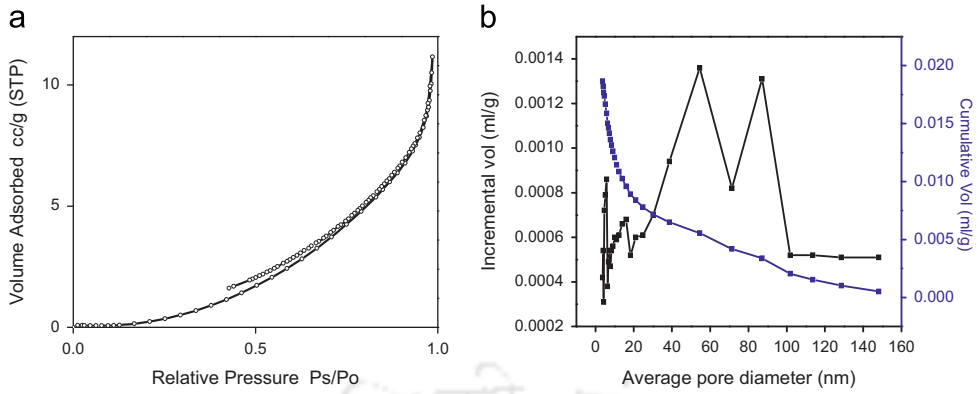

Fig. 2. (a) Nitrogen adsorption/desorption isotherms of the ceramic support material (b) Pore size distribution of the ceramic support by BET method.

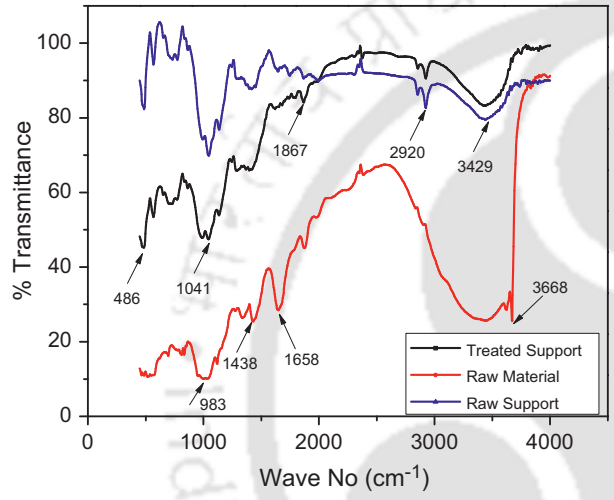

Fig. 3. FTIR Spectral analysis of various ceramic supports and raw material.

observed at 3668 cm^{-1} corresponding to the OH^- stretching vibration for the raw material. After sintering of the raw material mixture at 900 °C for 4 h, the OH^- vibration peaks at 3668 cm^{-1} decreased suggesting that the calcination of kaolin to calcined kaolin was not complete [15]. Bands at 2920 cm^{-1} were assigned to C–H bonds which were visible only after sintering and peak at 1658 cm^{-1} was attributed to C=C bonds. Further H_2O stretching was seen at 1658 cm^{-1} for the raw material which disappeared after sintering. Bands at 1041 cm^{-1} and 983 cm^{-1} were assigned to Si–O bonds. Absorption at 486 cm^{-1} was assigned to Si–O–Al [16].

The X-ray diffractograms were recorded by a Bucker X-ray D8 advance diffractometer with a Cu-K_α radiation (λ=1.54056) at 45 kV and 40 mA, respectively with scan rate of 0.5 $s \times step^{-1}$ with an increment of 0.05. The X-ray diffractograms were collected in the range of 5–75°. Phase analyses of the diffraction profiles were done using ICDD-JCPDS database and the crystallite size of the samples were calculated using Scherer's formula: $d = 0.9\lambda/\beta\cos\theta$ where d signifies the crystallite size, λ refers to the wavelength of radiation (λ=1.54056), β refers to the full width of half-maximum intensity of corrected peak and θ the peak position.

Fig. 4(a) presents the XRD patterns of raw material mixture, sintered raw support, sintered treated support and the nickel membrane. The phases for kaolin, quartz and calcium carbonate appeared in the raw material mixture. It was observed that the peak intensity of the main intense peak of quartz (2θ=26.75°) significantly increased with sintering, thereby indicating that the crystalinity of the quartz increased as compared to raw material, which was further more significant after NaOH treatment. The XRD pattern clearly indicated that NaOH treatment played a vital role in increasing the crystalinity of quartz and thereby enhancing the porosity of the membrane. Further on sintering it was observed that due to the transformation of kaolinite to metakaolinite the peak corresponding to kaolin disappeared [8].

Similarly the peak corresponding to calcium carbonate also disappeared on sintering due to thermal decomposition. The new phases that appeared in the XRD pattern were anorthite ($CaO \cdot Al_2O_3 \cdot 2SiO_2$) and mullite ($3Al_2O_3 \cdot 2SiO_2$).

Fig. 4(b) replicates the XRD pattern of Ni plating to clearly visualize the nickel peaks. The metallic nickel peaks appeared at diffraction angle 2θ=44.6° and 52° due to the diffraction of (1 1 1) and (2 0 0) plane [Pdf No 00-001-1260] along with the quartz peaks. It was observed that the peak intensity of quartz significantly decreased after nickel deposition due to plating of nickel on quartz particle thereby reducing the crystalinity of the quartz. The crystal size of the support was calculated based on the maximum intense peak of the pattern (2θ=26.75°) and was observed to be 30 nm.

The surface characterization was also carried out by FESEM (Make: Zeiss). Fig. 5 presents the surface FESEM micrographs of the ceramic treated support and SIEP nickel layer deposited with an initial nickel sulfate concentration (C_i) of 0.08 (mol/L). It can be observed that well-developed nickel layers were existent for the membrane. Based on the analysis of the FESEM image using ImageJ software, it was observed that the pores were distributed over wider pore size values and the average pore size of the treated support as evaluated from the ImageJ software was found to be 140 nm which was close to that evaluated from nitrogen permeation (90–120 nm), respectively.

4.2. Feasibility of the ceramic support

Fig. 6 presents the nitrogen flux profiles for various combinations of average membrane pore size and effective

porosity for various cases. As shown, for a nickel dense film thickness of 1 μm, the feasible combinations of porosity ((ε/q^2) min) varied from 4.5×10^{-2} to 1.1×10^{-3} for pore diameter (d_p) variation from 20 nm to 500 nm, respectively. However, when the nickel film thickness was enhanced 5-fold (to 5 μm), (ε/q^2) min varied from 9.1×10^{-3} to 2.2×10^{-4} for d_p variation from 20 nm to 500 nm, for a film thickness of 10 μm, (ε/q^2) min varied from 4.5×0^{-3} to 1.1×10^{-4} for d_p variation from 20 nm to 500 nm and for a film thickness of 20 μm, (ε/q^2) min varied from 2.2×10^{-3} to 5.6×10^{-5} for d_p variation from 20 nm to 500 nm, respectively. The obtained membrane morphological parameters indicated that the raw support was feasible for a desired minimal dense nickel film thickness of 1 μm and the treated support was feasible for a desired minimal dense nickel film thickness of 5 μm. These theoretical deductions indicated that irrespective of the fabrication method, the supports were feasible for very low values of dense metal film thickness on the supports which was very difficult to achieve using conventional and novel metal deposition methods on porous ceramic supports with achieved morphologies.

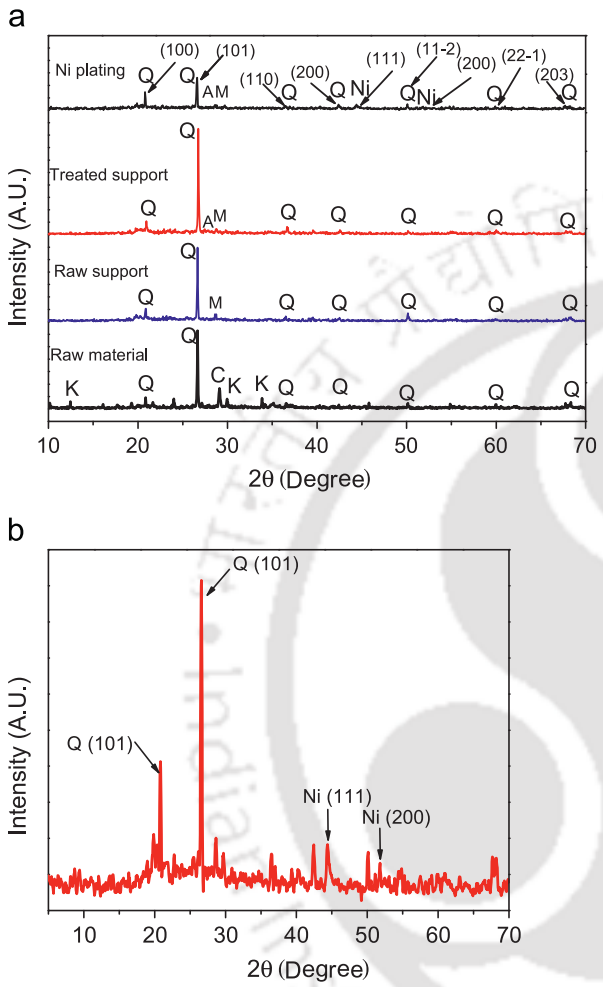

Fig. 4. (a) XRD patterns of raw material mixture, sintered raw support, sintered treated (NaOH) support and the nickel membrane (b) XRD pattern of Nickel membrane.

4.3. Synchronity for nickel plating (average flux and percent pore densification)

Fig. 7(a) represents the average flux data trends with respect to the time of plating. The average flux through the membrane reduced from 4.1×10^{-2} to 2.1×10^{-2} (mol/m^2/s) in 24 h for M_1 (SOEP), 3.0×10^{-2}–1.5×10^{-3} (mol/m^2/s) in 24 h for M_2 (SIEP), 1.8×10^{-1}–3.7×10^{-3} (mol/m^2/s) in 24 h for M_3 (SIEP) and 2.2×10^{-1}–3.6×10^{-2} (mol/m^2/s) in 24 h for M_4 (SOEP), respectively. It was observed that for membranes M_1 and M_2 the initial plating steps increased the average flux through the membrane. This indicated that for these membranes, morphological modifications (opening of voids/pores) were dominant as compared to metal deposition inside the porous structure. Eventually with increment in plating hours it was observed that morphological modifications became minimal and pore densification gradually improved. Further for the treated membrane M_3 (SIEP) it was observed that after 24 h of plating the ratio of initial flux to the final flux was around 48.8 which was quite higher than the value obtained for M_4 membrane (6.2).

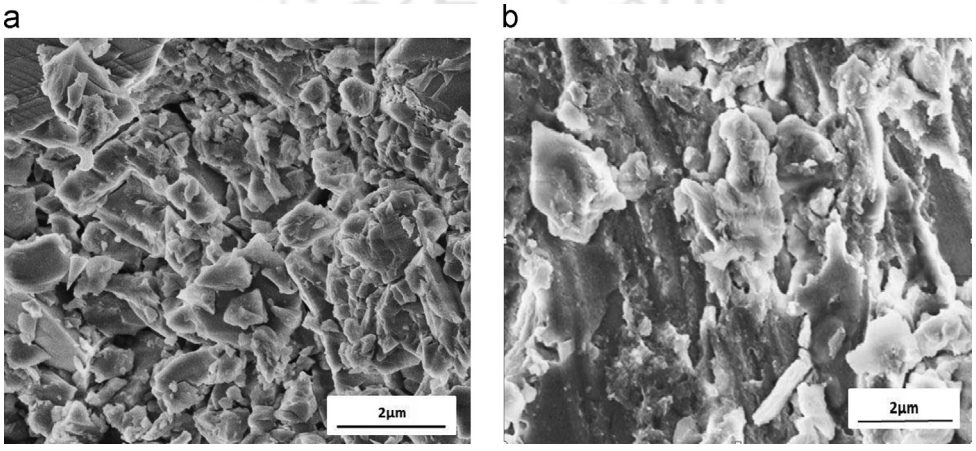

Fig. 5. Surface FESEM micrographs of (a) treated support (b) SIEP membrane (M_3).

The time dependent enhancement and reduction in average membrane flux for membranes M_1 and M_2 clearly depicted that the low cost ceramic supports were not compatible enough to handle the plating process and therefore, the supports required further treatment so that the supports could withstand the corrosive environment that prevailed during the long term exposure of electroless plating in a highly alkaline environment. Various possible reasons for opening of pores correspond to surface and pore modifications of the substrate at the plating conditions. Therefore, the NaOH pretreatment was regarded to be a viable option to make the supports feasible for low cost dense metal ceramic composite membrane research.

Fig. 7(b) presents the time dependency with respect to percent pore densification trends. *PPD* values varied from 0% to 46.7% in 24 h for M_1 (SOEP), 0% to 95% in 24 h for M_2 (SIEP), 0% to 98% in 24 h for M_3 (SIEP) and 0% to 83.9% in 24 h for M_4 (SOEP). Further the *PPD* values for M_1 and M_2 were initially observed to be negative indicating to the fact that the rate of pore opening was faster than the rate of pore densification thereby confirming that membrane healing process was too slow for the raw supports. However, plating in the later hours indicated that positive profiles were observed for M_1 and M_2 which clearly indicated that SOEP and SIEP processes not only repaired the damage morphologies but also densified the membranes. But this was not the case with NaOH treated supports where systematic reduction in flux was observed with plating time. However, excessive deposition of nickel in the ceramic matrix is not desired for the functional supports, as this could lead to higher thermal stresses that could be induced with temperature cycling phenomena for the Pd composite membranes.

Even for the raw supports, for the same time of plating (24 h), SIEP (M_2) reduced the *PPD* twice as compared to SOEP (M_1). Thus it can also be concluded that surfactant played an important role in reducing the average flux through the membrane and served better than sonication in achieving densification both for the raw and the treated supports. Therefore, more detailed research in process engineering of materials manufacturing processes involving surfactants is as well needed.

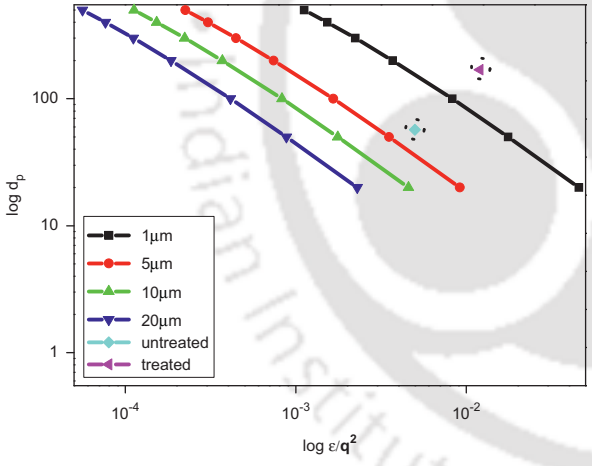

Fig. 6. Log d_p vs. log (ε/q^2).

5. Conclusions

This work presented an integrated experimental and theoretical approach for the development of compatible functional supports towards dense metal ceramic composite membrane fabrication. The challenging scenario of this study was to work with laboratory fabricated supports characterized with lower combinations of average pore size and lower effective porosity. For such supports etching in alkaline medium served to be favourable in terms of compatibility of the support and corrosion resistance. NaOH treatment prior to plating enabled enlargement of the membrane pores to its target diameter such that the early plating steps does not serve as a treatment steps for the supports. Further XRD patterns clearly indicated that NaOH treatment increased the crystalinity of the raw materials thereby enhancing the pore size and porosity of the membrane. Moreover the morphological fitness of the ceramic support clearly indicated that the supports were feasible for very low values of dense metal film thickness irrespective of the fabrication technique. The fabricated nickel composite membranes were anticipated to serve as functional supports for dense palladium membranes. A tentative combination of optimal support morphological properties and optimal electroless plating process as highlighted in this article would be

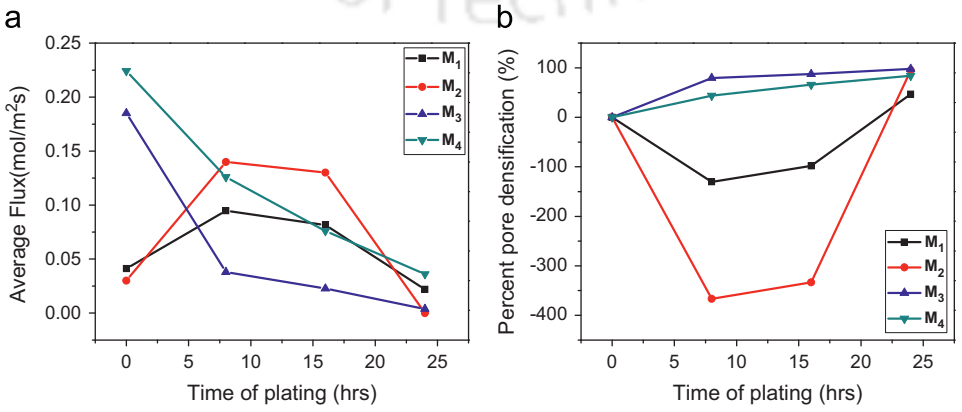

Fig. 7. Performance of nickel plated membranes in terms of time dependent (a) average flux and (b) PPD.

useful to serve as a guideline for the realization of low cost multi-metal composite membranes.

Nomenclature

$Perm_{lit}$	Maximum hydrogen permeability of the nickel film reported in the literature (mol/m^2/s/Pa$^{0.5}$)
δ_{lit}	Critical dense nickel film thickness in the literature (μm)
δ_{ass}	10 μm (μm)
n'	Exponent (=0.5 according to Stewart's law)
A_m	Permeable area of the membrane (m^2)
Q	Volumetric flow rate (m^3/s)
P_2	Membrane pressure at permeate side (Pa)
ΔP	Trans-membrane pressure drop (Pa)
d_p	Average pore size (μm)
(ϵ/q^2)	Effective porosity
$\overline{P}$	Average pressure on the membrane (Pa)
v	Molecular mean velocity of the gas (m/s)
l	Pore length (m)
q	Tortuosity
η	Viscosity of gas (Pa s)
K	Effective permeability factor (m/s)
J	Flux through the membrane (mol/m^2/s)
$\overline{J}$	Average flux through the membrane (mol/m^2/s)
i	Hour of nickel plating (as exponent)
$\overline{J}_0$	Average flux through the support (mol/m^2/s)
$\overline{J}_i$	Average flux through the membrane after ith hour of nickel plating (mol/m^2/s)
PPD	Percent pore densification (%)
ELP	Electroless plating
SIEP	Surfactant induced electroless plating
SOEP	Sonication induced electroless plating

Acknowledgements

This work is partially supported by a grant from the DST (Department of Science and Technology) New Delhi. Any opinions, findings and conclusions expressed in this paper are those of the authors and do not necessarily reflect the views of DST, New Delhi. Special thanks to Dibjyoti Saloi who worked as project assistant and helped us for this work.

References

[1] M. Kitiwan, D. Atong, Effects of porous alumina support and plating time on electroless plating of palladium membrane, Journal of Materials Science & Technology 26 (2010) 1148–1152.
[2] L.L.O. Silva, D.C.L. Vasconcelos, E.H.M. Nunes, L. Caldeira, V. C. Costa, A.P. Musse, S.A. Hatimondi, J.F. Nascimento, W. Grava, W. L. Vasconcelos, Processing, structural characterization and performance of alumina supports used in ceramic membranes, Ceramics International 38 (2012) 1943–1949.
[3] N. Kishore, S. Sachan, K.N. Rai, A. Kumar, Synthesis and characterization of a nanofiltration carbon membrane derived from phenol-formaldehyde resin, Carbon 41 (2003) 2961–2972.
[4] G.T.P. Mabande, G. Pradhan, C. Schwieger, M. Hanebuth, R. Dittmeyer, T. Selvam, A. Zampieri, H. Baser, R. Herrmann, A study of silicalite-1 and Al-ZSM-5 membrane synthesis on stainless steel supports, Microporous and Mesoporous Materials 75 (2004) 209.
[5] A. Potdar, A. Shukla, A. Kumar, Effect of gas phase modification of analcime zeolite composite membrane on separation of surfactant by ultrafiltration, Journal of Membrane Science 210 (2002) 209–225.
[6] S. Jha, K.L. Rubow, Nickel microfiltration media for gas and liquid filtration, Advances in Filtration and Separation Technology 13 (1999) 512–520.
[7] S.K. Ryi, J.S. Park, S.J. Park, D.G. Lee, S.H. Kim, Fabrication of nickel filter made by uniaxial pressing process for gas purification: fabrication pressure effect, Journal of Membrane Science 299 (2007) 174–180.
[8] D. Vasanth, G. Pugazenthi, R. Uppaluri, Fabrication and properties of low cost ceramic microfiltration membranes for separation of oil and bacteria from its solution, Journal of Membrane Science 379 (2011) 154–163.
[9] Wen-Hsiung Lin, Ying-Chi Liu, Hsin-Fu Chang, Autothermal reforming of ethanol in a Pd–Ag/Ni composite membrane reactor, International Journal of Hydrogen Energy 35 (2010) 12961–12962.
[10] B. Ernst, S. Haag, M. Burgard, Permselectivity of a nickel/ceramic composite membrane at elevated temperatures: a new prospect in hydrogen separation?, Journal of Membrane Science 288 (2007) 208–217
[11] V.K. Bulasara., M.S. Abhimanyu, T. Pranav, R. Uppaluri, M.K. Purkait, Performance characteristics of hydrothermal and sonication assisted electroless plating baths for nickel–ceramic composite membrane fabrication, Desalination 284 (2012) 77–85.
[12] V.K. Bulasara, R. Uppaluri, H. Thakuria, M.K. Purkait, Nickel–ceramic composite membranes: optimization of hydrazine based electroless plating process parameters, Desalination 275 (2011) 243–251.
[13] Altunoglu, Abdulkadir, Hydrogen Permeation Through Nickel and Nickel Alloys: Surface Reactions and Trapping, Ph.D. Thesis, The Open University, (1994).
[14] K.S.W. Sing, D.H. Everett, R.A.W. Haul, L. Moscou, R.A. Pierotti, J. Rouquerol, T. Siemieniewska, Reporting physisorption data for gas/solid systems with special reference to the determination of surface area and porosity, Pure and Applied Chemistry 57 (1985) 603–619.
[15] M.L. Granizo, M.T.B. Varela, S. Martinez-Ramirez, Alkali activation of metakaolins: parameters affecting mechanical, structural and microstructural properties, Journal of Materials Science 42 (2007) 2934–2945.
[16] J.G.S. van Jaarsveld, J.S.J. van Deventer, G.C. Lukey, The effect of composition and temperature on the properties of fly-ash and kaolinite-based geopolymers, Chemical Engineering Journal 89 (2002) 63–73.

Available online at www.sciencedirect.com

ScienceDirect

Ceramics International 40 (2014) 691–697

CERAMICS INTERNATIONAL

www.elsevier.com/locate/ceramint

Optimal electroless plating rate enhancement techniques for the fabrication of low cost dense nickel/ceramic composite membranes

Amrita Agarwal, Murali Pujari, R. Uppaluri*, A. Verma

Department of Chemical Engineering, Indian Institute of Technology Guwahati, Guwahati 781039, Assam, India

Received 17 May 2013; received in revised form 14 June 2013; accepted 14 June 2013
Available online 24 June 2013

Abstract

Addressing combinatorial plating characteristics for dense metal ceramic composite membranes, this article attempts to identify the most suitable electroless plating rate enhancement technique. The support morphology considered for this work corresponds to low combinations of pore size and porosity. Cases considered for comparative assessment include conventional electroless plating (CEP), surfactant induced electroless plating (SIEP) and sonication induced electroless plating (SOEP). BET, FTIR, XRD, FESEM and nitrogen permeation techniques were employed for surface and physical characterization. It was observed that with SIEP the average metal film thickness was about 18.3 μm and with SOEP it was 24.6 μm. Correspondingly it was also observed that for SIEP baths the ratio of percent pore densification (PPD) to metal film thickness (δ) i.e. PPD/δ varied from 11.2 to 5.35 and for SOEP baths PPD/δ varied from 3.5 to 4.7 for 8–24 h of sequential plating. Thereby, it was inferred that SIEP possessed maximum potential towards dense metal ceramic composite membrane fabrication for the realization of maximum PPD with minimal metal film thickness.

Keywords: E. Membrane; Ceramic; Surfactant; Densification

1. Introduction

Metal composite membranes have numerous applications such as TiO_2 recovery from waste water streams [1], asymmetric supports for dense palladium composite membranes [2], production of ultrapure gases for special applications [3] and hydrogen separation [4]. Presently companies involved in fabricating composite membranes for various industrial applications include Mykron, Entegris and Mott Corporation.

Amongst several fabrication processes, electroless plating (ELP) offers a good number of advantages such as uniformity in deposition irrespective of shape and size, simple experimental setup, scalability, minimal usage of electrical power, applicability for deposition on internal surfaces, edges, irregular and complex shapes, etc.

The autocatalytic metal electroless plating process is an extremely slow process and therefore plating rate enhancement techniques were explored to enhance the plating rate. However, the quality of plating remained a central issue for which plating rate enhancement techniques and their associated parameters need to be optimized. Several plating rate enhancement techniques include agitation (in the form of either membrane stirring [5] or gas sparging [6]), vacuum [7], hydrothermal [8], sonication [8] and surfactant assisted electroless plating baths [9]. However, amongst these techniques, from the perspectives of combinatorial plating characteristics and ease of operation, sonication and surfactant remained attractive, as industrial scale sonication baths are available and surfactant assisted electroless plating could be scaled up easily. Even amongst these two, surfactant induced electroless plating has significant number of features. The usage of surfactant is advantageous in two ways—firstly surfactant reduces the surface tension of the gas bubble and therefore enables the generation of smaller bubbles on the surface thereby minimizing the pitting effect. Secondly since gas bubbles are removed at a faster pace, the redox reaction shifts to the forward direction and therefore metal plating is enhanced [9]. Further

*Corresponding author. Tel.: +91 361 2582260; fax: +91 361 2582291.
E-mail address: ramgopalu@iitg.ernet.in (R. Uppaluri).

0272-8842/$ - see front matter © 2013 Elsevier Ltd and Techna Group S.r.l. All rights reserved.
http://dx.doi.org/10.1016/j.ceramint.2013.06.056

Nomenclature

A_m	permeable area of the membrane, m^2
w_0	dry weight of the membrane before plating, g
w_i	dry weight of the membrane after *i*th hour of plating, g
w	total amount of nickel originally available in the plating bath, g
n	number of plating cycles
V_0	volume of plating solution in each plating cycle, L
M_{Ni}	molecular weight of nickel metal, g/mol
ρ_{Ni}	density of nickel metal, g/cm^3
J	flux through the membrane, mol/m^2 s
$\overline{J}$	average flux through the membrane, mol/m^2 s
i	hour of nickel plating (as exponent)
$\overline{r}_i$	plating rate, mol/L s
t_i	time of plating for the *i*th hour, h
PPD	percent pore densification, %
CEP	conventional electroless plating
ELP	electroless plating
SIEP	surfactant induced electroless plating
SOEP	sonication induced electroless plating

ultrasonic waves in sonication induced electroless plating account for increased mass transport, interfacial cleaning and thermal effects [10].

To date, electroless plating research for metal composite membranes was primarily targeted from a product quality oriented perspective, but not from process engineering perspectives. Combinatorial plating characteristics involving the simultaneous assessment of plating process parameters (such as plating rate) and product parameters (such as average pore size, average pore densification and metal film thickness) are important areas of research that could drive the efficacy of both manufacturing processes and materials. From such a perspective for dense metal composite membranes, the literature is scarce. Further, time dependency of the plating and process characteristics and rate enhancement techniques (sonication and surfactant) for metal composite membranes were not addressed. Also in the literature, while SIEP has been studied significantly for stainless steel supports, alumina supports [11] and palladium deposition, SIEP studies toward nickel composite membranes have not been addressed for ceramic supports. Such studies are also required from a processing perspective as well, given the fact that stainless steel membranes are significantly more expensive than ceramic membranes and thus the utilization of ceramic membrane could pave the way for faster research commercialization and scaleup.

Process engineering studies toward materials fabrication need to first address compatibility of support materials towards the desired application. Deliberating towards the synchronity of process–material compatibility, our previous work addressed the preparation, characterization and optimization of a low cost ceramic support for the preparation of nickel ceramic composite membranes [12]. This work is a natural extension of such work and aims towards a critical examination of electroless plating process characteristics for the optimized support.

2. Experimental

Laboratory made ceramic substrates with a diameter of 36 mm and thickness of 3.5 mm fabricated at a pressure of 4.9 MPa were used as supports for the electroless plating experiments. The pore size d_p^{sup} and effective porosity (ε/q^2) of the substrates were about 50–70 nm and 10–15% respectively. The ceramic substrates were fabricated by the dry compaction method and sintered at 900 °C and the inorganic raw materials used for fabrication of ceramic substrate were as mentioned in Table 1.

Surface and physical characterizations were performed using a number of techniques. The BET surface area and pore size of the support material were determined by N_2 adsorption desorption isotherm at 77 K by using a surface area analyzer (Beckman-Coulter; Model: SA3100). Fourier transform infrared spectroscopy (FTIR) analysis was done to record the characteristic peaks of various raw materials. X-Ray diffraction (XRD) analysis of the inorganic ceramic substrate and metal membrane was conducted to evaluate the extent of phase transformations. Field emission scanning electron microscopic (FESEM) study (Make: Oxford; Model: LEO 1430VP, UK) was carried out to analyze the presence of possible defects and estimate the membrane pore size. The estimation of average membrane pore size from FESEM micrographs was carried out using ImageJ software. The effective porosity of the membrane was evaluated by weight gain method with water as the wetting liquid. Nitrogen permeation experiments were conducted to quantify membrane morphological parameters such as flux of the composite membranes and average pore size (d_p) that contribute to the transport and the experimental procedure was similar to the one as discussed in our previous work [12].

2.1. Electroless plating

Typical composition for nickel electroless plating technique is summarized in Table 2. Prior to plating, the substrates were seeded with the conventional procedure of activation and sensitization with palladium seeds. Eight sequential 1 h nickel deposition steps with a nickel concentration of 0.08 mol/L, loading ratio

Table 1
Composition of raw materials of ceramic membrane supports.

Material	Composition on dry basis (wt%)
Kaolin	40
Feldspar	15
Quartz	15
Na_2CO_3	10
Pyrophyllite	10
Boric acid	5
Sodium metasilicate	5

of 203 cm^2/L, 50% excess hydrazine hydrate (reducing agent) and plating bath temperature of 80 °C were used to yield the nickel composite membranes.

Five different membranes as mentioned in Tables 3 and 4 were focused for the development of nickel composite membranes. Prior to plating, raw membranes M_4 and M_5 were treated. The treatment involved immersion of the support in an alkaline (NaOH) solution which modified the support morphology and the pore diameters increased from 50–70 nm to 90–120 nm as discussed in detail in our previous work [12].

2.2. Evaluation of plating characteristics

The process and plating parameters for evaluating the performance of various electroless plating baths for fabricating dense nickel membranes are average trans-membrane flux $\overline{J}$, average plating rate ($\overline{r}_i$), average thickness of the nickel layer (δ) and percent pore densification PPD (%). Average trans-membrane flux and PPD calculations were similar to our earlier reported work [12].

Table 2
Typical composition of conventional and surfactant induced nickel electroless plating baths.

S. no.	Component	Amount
1	Nickel sulfate	0.08 mol/L
2	Hydrazine hydrate	50% excess
3	Trisodium citrate	0.2 mol/L
4	Sodium hydroxide	10–12
5	Cetyltrimethylammonium bromide	1.2 g/L

Table 3
Summary of various cases investigated for the development of nickel composite membranes.

Case	Type of support	Type of ELP
M_1	Raw	Conventional
M_2	Raw	Sonication
M_3	Raw	Surfactant
M_4	Treated	Surfactant
M_5	Treated	Sonication

Table 4
Ratio of plating rate with respect to the base case (CEP).

Type of plating	Ratio of plating rate		
	8 h	16 h	24 h
SOEP (M_2)	9.97	6.18	3.82
SIEP (M_3)	6.31	3.22	2.25
SIEP (M_4)	13.98	6.21	3.41
SOEP (M_5)	16.62	6.97	4.58

Starting taken as 40 h for CEP (M_1).

The theoretical nickel film thickness (δ) was evaluated using the weight gain method and was expressed as follows:

$$\delta = \frac{w_i - w_0}{\rho_{Ni} A_m} \quad (1)$$

where ρ_{Ni} $\left(g/cm^3\right)$ represents the density of nickel metal and A_m (m^2) the membrane surface area for nitrogen permeation experiments. The plating rate $\overline{r}_i\left(\mathrm{mol}/(\mathrm{L\ s})\right)$ was evaluated as follows:

$$\overline{r}_i = \frac{w_i - w_0}{M_{Ni} n V_0 t_i} \quad (2)$$

where t_i corresponds to the time of plating for the ith hour.

3. Results and discussions

3.1. Surface characterization

The BET surface area of support was 2.712 m^2/g and total pore volume was 0.0156 ml/g with no micropore volume. The average pore size as evaluated from Barrett–Joyner–Halenda (BJH) pore volume distribution was found to be 35 nm similar to our previous addressed work [12]. Similarly the Fourier transform infrared spectra recorded characteristic peaks of kaolin for the raw material and after sintering of the raw material mixture at 900 °C were assigned to C–H bonds, C═C bonds, Si–O–Al and Si–O bonds as discussed earlier in detail [12].

X-Ray diffraction phase analysis was done using the ICDD-JCPDS database. Fig. 1 presents the XRD patterns of raw material mixture, sintered ceramic support, and the nickel membrane. The phases for kaolin, quartz and sodium carbonate appeared in the raw material mixture as reported earlier [12]. Further on sintering it was also observed that the peak corresponding to kaolin disappeared due to the transformation of kaolinite to metakaolinite and that corresponding to sodium

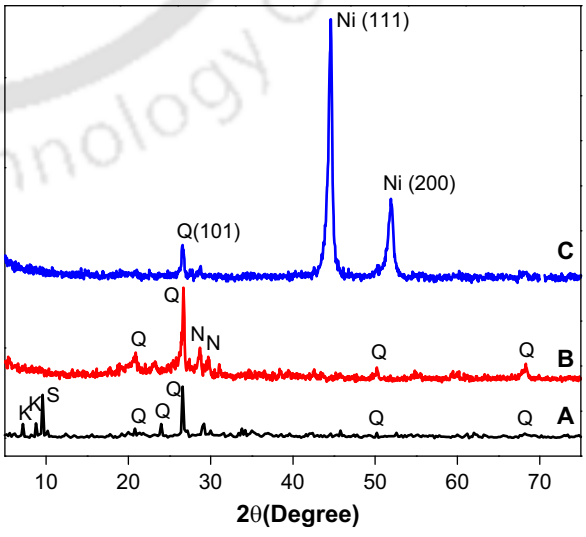

Fig. 1. XRD patterns for (i) A—raw material, (ii) B—sintered support and (iii) C—nickel plated membrane (M_4) where K signifies kaolin, S—sodium carbonate, Q—quartz, N—Nephiline and Ni—nickel.

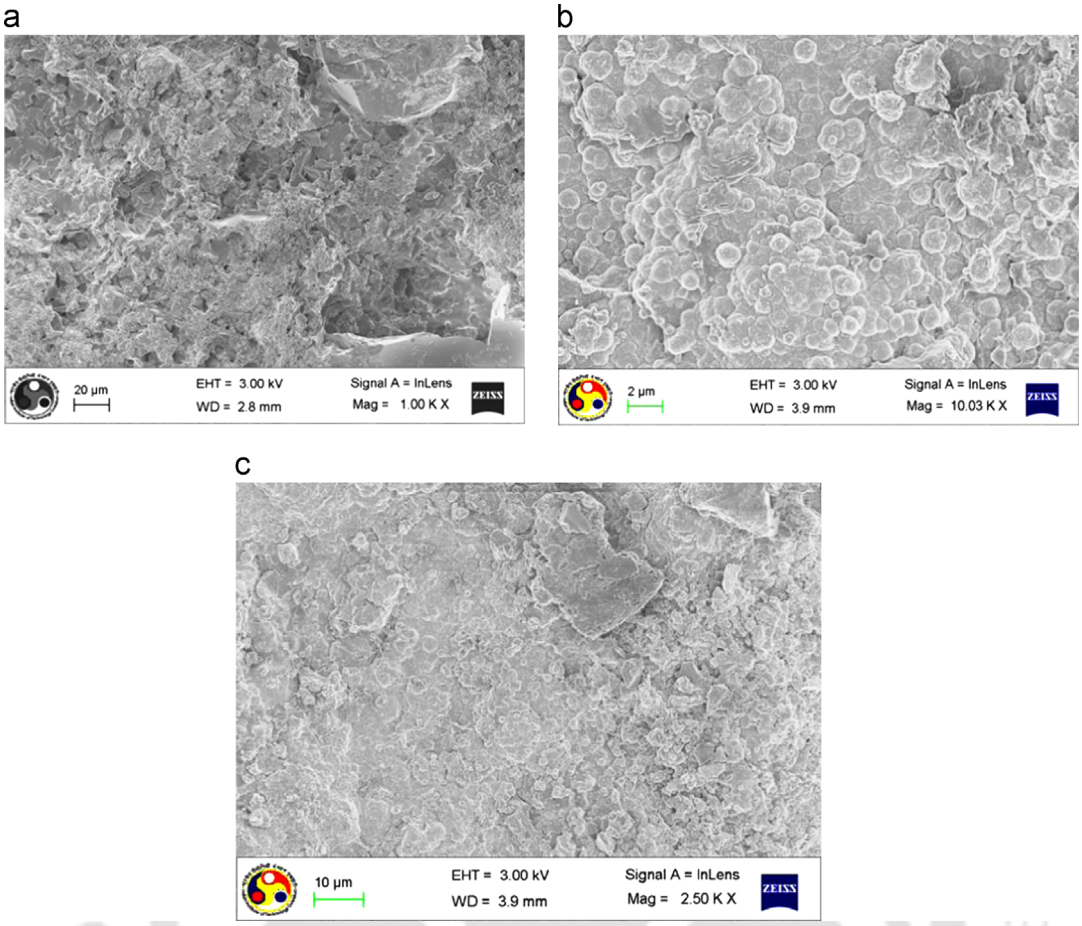

Fig. 2. Surface FESEM micrographs of (a) ceramic treated support, (b) nickel membrane fabricated with SIEP process (M_4) and (c) nickel membrane fabricated with SOEP process (M_5).

carbonate disappeared due to thermal decomposition. The new phase that appeared in the XRD pattern on sintering was Nephiline (Na_2O, Al_2O_3, $2SiO_2$) which was produced by the reaction of sodium oxide (Na_2O) and metakaolinite at temperature around 800 °C [13]. Moreover the diffractogram graphs after sintering (profile B) indicated no change in the quartz peak trends thereby implying that quartz phase was not at all affected by sintering of inorganic materials within the studied temperature range considered in this work. The metallic nickel peaks for electroless plating (profiles C) appeared at diffraction angle $2\theta = 44.5^\circ$ and 51.8° due to the diffraction of (111) and (200) planes [Pdf no. 00-004-0850]. Further, temperature programmed reduction analysis (Model: Chemisorb 2720; Make: Micrometrics) was also conducted for the nickel plated membrane and no reduction peak was observed indicating that only metallic nickel was deposited on the ceramic substrate.

Fig. 2 presents the surface FESEM micrographs of the ceramic substrate and nickel layer deposited with an initial nickel sulfate concentration (C_i) of 0.08 (mol/L) after 12 h of sequential plating with SIEP and SOEP processes. The nickel particles were uniformly dispersed as observed on the surface. Further it was observed that SIEP process showed better surface finish with agglomerates, thereby providing faster densification with lesser pinholes as desired. Average pore size analysis of the ceramic substrate done using ImageJ software gave an average pore size of 150 nm which was close to that evaluated from nitrogen permeation experiments (90–120 nm).

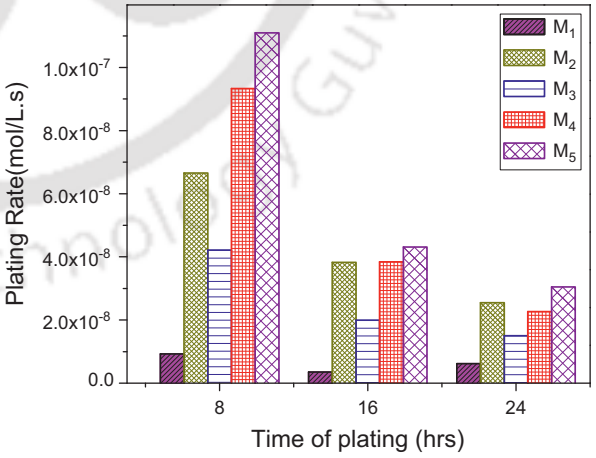

Fig. 3. Variation of plating rate with time of plating.

3.2. Plating rate

Fig. 3 presents the trends for fluctuation in plating rate with respect to time of plating. It was observed that the plating rates for M_1 varied from 6.68×10^{-9} to 6.58×10^{-9} (mol/L s), for M_2 from 6.65×10^{-8} to 2.54×10^{-8} (mol/L s), for M_3 from 4.2×10^{-8} to 1.5×10^{-8} (mol/L s), for M_4 from 9.3×10^{-8} to 2.2×10^{-8} (mol/L s) and for M_5 from 11.1×10^{-8} to 3.58×10^{-8} (mol/L s). Further, Table 3 illustrates the ratio of plating rate with respect to the base case (CEP). From the data it was analyzed that for both the cases of treated (M_5) and raw supports (M_2), SOEP membranes gave higher plating rate when compared to both CEP and SIEP. Such data trends are also in agreement to Wu et al. [14] who inferred that introduction of ultrasonic waves during electroless nickel deposition enhances the plating rate.

As compared to Bulasara et al. [15] who reported a CEP rate of 1.51×10^{-6}–9.79×10^{-6} (mol/L s) for an average pore size of 275 nm, porosity of 0.44 and varying stirrer speed, our work indicated a lower plating rate of 6.68×10^{-9} (mol/L s). Therefore, it was inferred that plating rate was strongly influenced by average pore size and porosity and hence plating rate enhancement techniques became predominantly significant to influence the quality of plating characteristic for the supports considered for this work.

Experimentally it was reported that the plating rate and the quality of plating were optimal for supports within the pore size of 250–300 nm and porosity of 35–50% [16]. This work referred to the performance characteristics of a low cost ceramic membrane that was characterized with even lower combinations of pore size (90–120 nm) and effective porosity (10–15%). From metal film densification perspective, a support with lower pore size and porosity enabled faster densification but did not provide good adhesion of the metal film to the support. On the other hand, a support with higher pore size and porosity required thicker dense metal films to achieve dense composite membranes [17] with good adhesion strength.

Therefore, the metal densification perspective shall not be regarded from the perspective of achieving only thin dense metal film thickness, as the mechanical strength of the film was also of paramount importance. Therefore, further research was required to identify optimal membrane pore size and porosity values that enabled achieving stable dense metal films on the surface. Nonetheless, the role of plating rate enhancement techniques to alter the strength related properties could not be ignored in this context.

3.3. Film thickness

Fig. 4 reports the data trends for increment in metal film thickness with time of plating. It was observed that for 8–24 h of nickel plating, the metal film thickness increased from 0.8 to 5 μm for M_1 (CEP), 6–20.5 μm for M_2 (SOEP), 3.7–12.1 μm for M_3 (SIEP), 8.4–18.3 μm for M_4 (SIEP) and 9.9–24.6 μm for M_5 (SOEP). Further, it was observed that the nickel film plating rate was 1 μm/h for the SIEP baths which was 10 times higher than the value for CEP baths (0.1 μm/h). Subsequently it was observed that the nickel film plating rate was 1.2 μm/h for the sonication assisted baths. Literature indicated that the corresponding plating rates for a macroporous support were 1.9, 1.8 and 3.1 μm/h for CEP, SIEP and SOEP respectively [15]. While the desired objective is to achieve a dense nickel film on the surface of the porous ceramic support, it was observed that the first few plating steps enabled the deposition of nickel film inside the support pores which would facilitate good bonding between the support and the metal film. In addition, further insights to gain information related to the uncertainities associated to theoretical metal film thickness have not been obtained using FESEM cross section images, as Bulasara et al. [18] have indicated that the theoretical thickness values are as good as those measured using the FESEM image analysis.

Thus sonication resulted in tremendous increase in film thickness due to simultaneous increase in both deposition rate and plating efficiency for both the treated and the untreated supports. These observations are in agreement with Kathirgamanathan [19] who concluded that sonication enhanced metal deposition and improved adhesion of the metal to the membrane

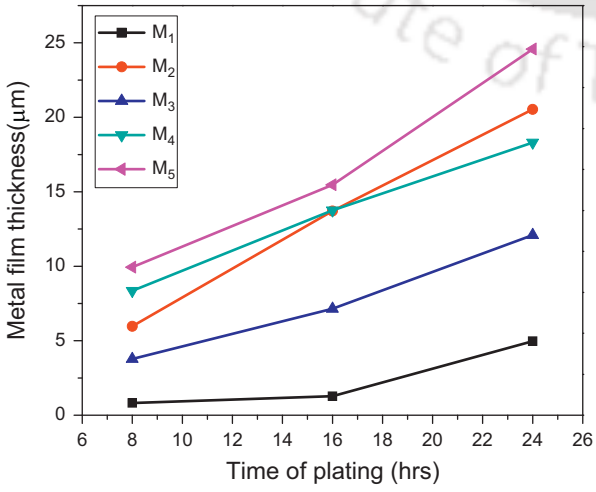

Fig. 4. Variation of film thickness with time of plating.

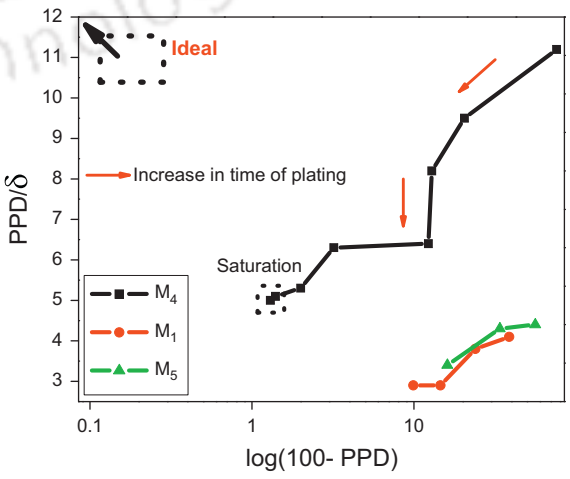

Fig. 5. PPD/δ vs. log(100−PPD) tradeoffs.

surface. Similar conclusions were inferred by Ilias et al. [20] through their statement that the same thickness could be obtained by reducing the plating time if a suitable surfactant was used during electroless plating.

3.4. Efficacy of mass transfer enhancement

Fig. 5 presents the time dependent variation of (100−PPD) and PPD/δ values for nickel composite membrane fabricated by various rate enhancement techniques. The graph corresponds to conceptual extensions of the measured data to visualize the extent of pore densification (x-axis) with respect to the amount of metal required to densify the pores (y-axis). Conceptually, an ideal electroless plating process supplemented with optimal rate enhancement technique should achieve maximum PPD/δ and minimal (100−PPD) values and therefore should refer to the values closely located to the y-axis. From the figure, it is observed that PPD values varied from 26% to 90% and PPD/δ from 2.2 to 2.86 in 32–64 h of rigorous plating experimentation for M_1. Further, PPD values varied from 34.9% to 83.9% and PPD/δ values from 3.5 to 4.7 for M_5 after 24 h of sequential plating. However, for the same time of plating, PPD values varied from 24% to 98% and PPD/δ values from 11.2 to 5.35 were obtained for the surfactant assisted baths (M_4). Therefore from membrane pore densification perspective, surfactant assisted electroless plating yields the best possible conditions of nickel metal deposition on the membrane surface and corresponds to a combinatorial performance characteristics of 98.7% PPD and PPD/δ value of 4.98 for a nickel composite membrane with a film thickness (δ) of 19.8 μm after 32 h of rigorous experimentation.

Further, it was observed that there exists a saturation point for membrane M_4, as there was no significant improvement in the PPD value (from 98% to 98.7%) from 24 to 32 h of sequential deposition. The saturation phase in the plating period was represented by a sharp reduction in the length of the consecutive points. However, the case did not correspond to 100% saturation, which should have been indicated by a vertical straight line in the graph. Since PPD could not be altered much with the prevalent conditions, an interesting issue for further research was to examine the role of solution concentrations (metal or reducing agent concentration or both) as well as the mode of contacting to bypass the saturation phase and continue the plating process to ensure that 100% densification could be achieved.

If we consider the case which has comparatively higher values of PPD and lower time of plating, the only feasible option was for surfactant induced electroless plating as shown in Fig. 5. A PPD value of about 98% along with the experimental inference of porous membranes presumably indicated that the utilization of supports with lower surface pore sizes could yield a dense nickel/ceramic composite membrane in about 24–32 h of sequential electroless plating steps at lower metal concentration (0.08 mol/L). Further, it can be stated that although sonication improved the plating rate and metal film thickness, it did not provide significant reduction in pore size as compared to surfactant induced electroless plating.

The efficient design of electroless plating process needs to maximize percent pore densification (PPD) and minimize the metal film thickness (δ). This work also recognized the immediate need to identify suitable mass transfer enhanced electroless plating processes that could provide good combinations of PPD and film thickness (δ). The approach presented in this work could be used as a new methodology for the assessment of nickel electroless plating baths with variant morphological parameters and conditions of operations.

Thus surfactant techniques were observed to be more effective to enhance the PPD values significantly close to 100% as shown clearly in Fig. 5. This is also in agreement with the work of Islam et al. [21], who inferred that dense and thinner films could be formed with shorter deposition time using SIEP method. A possible reason for not achieving 100% PPD was that beyond a particular point the solution concentration imposes limitations on the quality of plating.

4. Conclusions

This work elaborated upon engineering research approaches and experimental methodologies required for the cost effective fabrication of nickel/ceramic composite membranes for electroless plating processes. It could further be extended towards palladium composite membranes and multi-metal membranes that have functional applications as efficient gas separating devices. Emphasis was primarily towards the efficacy of various rate enhancement techniques that could be supplemented to electroless plating process for the fabrication of dense metal/ceramic composite membranes. Most importantly, this work showed that sonication did not contribute to 100% pore densification for the chosen support, even though sonication contributed to enhanced nickel deposition rate substantially. This work reported time dependent performance of electroless plating baths for nickel/ceramic composite membrane fabrication which promoted further insights in the metal deposition characteristics such as variation in thickness, PPD and average pore size with time of deposition. Thereby, this work featured the minimal number of plating steps required to achieve desired membrane characteristics. Interesting feature of such research was to examine the compatibility of nickel films in terms of adhesion during electroless plating. The conceptual insights gathered in this work required further refinement and fine tuning towards assessing the role of better quality porous supports in combinatorial performance characteristics of electroless plating baths.

The experimental investigation confirmed that nickel deposition on non-conducting surfaces was an extremely slow process and efforts were required to enhance the plating rate as well as the quality of deposition of metal on non-conducting surfaces. The stagnation of time dependent PPD profiles needed further experimental investigation and careful contacting of reducing agent with metal precursors to substantially enhance PPD and could not be ruled out. This was especially evident from time dependent nickel PPD profiles in the later

stages of plating. Optimization of conditions that drive away the achievement of saturation in product quality would require sophisticated process modification. For example a time dependent variable frequency sonicator may provide better PPD profiles or good quality of plating. Further, SIEP was exceptionally good to achieve highest values of PPD/δ for the membranes. Thus, it could be concluded that SIEP possessed maximum potential towards metal ceramic composite membranes and would be investigated substantially to improve the quality of plating.

This work emphasized upon the criticality of mass transfer enhancement to accommodate morphological parametric features to achieve dense metal ceramic composites. It exclusively focused upon the quality of deposition (PPD profiles) using supports with lower pore sizes. It appeared that SIEP was the most promising action in terms of economics, simplicity, ease of operation and quality of deposition as the technique enabled the realization of maximum value of PPD/δ. Further research was anticipated with respect to metal concentration since the plating rate increased with metal solution concentration and decreased with loading ratio. Higher conversions without jeopardizing the PPD variation with SIEP need to be studied and will be taken up as the future work.

Acknowledgments

This work is partially supported by a grant from the DST (Department of Science and Technology), New Delhi. Any opinions, findings and conclusions expressed in this paper are those of the authors and do not necessarily reflect the views of DST, New Delhi. Special thanks to Dwipjyoti Saloi who worked as project assistant and helped us for this work.

References

[1] S. Jha, K.L. Rubow, Nickel microfiltration media for gas and liquid filtration, Advances in Filtration and Separation Technology 13 (1999) 512–520.
[2] W.H. Lin, Y.C. Liu, H.F. Chang, Autothermal reforming of ethanol in a Pd–Ag/Ni composite membrane reactor, International Journal of Hydrogen Energy 35 (2010) 12961–12962.
[3] S.K. Ryi, J.S. Park, S.J. Park, D.G. Lee, S.H. Kim, Fabrication of nickel filter made by uniaxial pressing process for gas purification: fabrication pressure effect, Journal of Membrane Science 299 (2007) 174–180.
[4] B. Ernst, S. Haag, M. Burgard, Permselectivity of a nickel/ceramic composite membrane at elevated temperatures: a new prospect in hydrogen separation?, Journal of Membrane Science 288 (2007) 208–217
[5] M.E. Ayturk, Y.H. Ma, Electroless Pd and Ag deposition kinetics of the composite Pd and Pd/Ag membranes synthesized from agitated plating baths, Journal of Membrane Science 330 (2009) 233–245.
[6] O. Altinisik, M. Dogan, G. Dogu, Preparation and characterization of palladium plated porous glass for hydrogen enrichment, Catalysis Today 105 (2005) 641–646.
[7] S.E. Nam, S.H. Lee, K.H. Lee, Preparation of a palladium alloy composite membrane supported in a porous stainless steel by vacuum electrodeposition, Journal of Membrane Science 153 (1999) 2163–2173.
[8] V.K. Bulasara, M.S. Abhimanyu, T. Pranav, R. Uppaluri, M.K. Purkait, Performance characteristics of hydrothermal and sonication assisted electroless plating baths for nickel–ceramic composite membrane fabrication, Desalination 284 (2012) 77–85.
[9] B.H. Chen, L. Hong, Y. Ma, T.M. Ko, Effects of surfactants in an electroless nickel-plating bath on the properties of Ni–P alloy deposits, Industrial and Engineering Chemistry Research 41 (2002) 2668–2678.
[10] I. Haas, A. Gedanken, Sonoelectrochemistry of Cu^{2+} in the presence of cetyltrimethylammonium bromide: obtaining CuBr instead of copper, Chemistry of Materials 18 (2006) 1184–1189.
[11] L.L.O. Silva, D.C.L. Vasconcelos, E.H.M. Nunes, L. Caldeira, V.C. Costa, A.P. Musse, S.A. Hatimondi, J.F. Nascimento, W. Grava, W.L. Vasconcelos, Processing, structural characterization and performance of alumina supports used in ceramic membranes, Ceramics International 38 (2012) 1943–1949.
[12] A. Agarwal, M. Pujari, R. Uppaluri, A. Verma, Preparation, optimization and characterization of low cost ceramics for the fabrication of dense nickel composite membranes, Ceramics International (2013), http://dx.doi.org/10.1016/j.ceramint.2013.03.024.
[13] M.C. Wang, N.C. Wu, M.H. Hon, Preparation of nepheline glass–ceramics dental porcelain, Materials Chemistry and Physics 37 (1994) 370–375.
[14] Z. Wu, S. Ge, M. Zhang, W. Li, K. Tao, Synthesis of nickel nanoparticles supported on metal oxides using electroless plating: controlling the dispersion and size of nickel nanoparticles, Journal of Colloid and Interface Science 330 (2009) 359–366.
[15] V.K. Bulasara, R. Uppaluri, H. Thakuria, M.K. Purkait, Combinatorial performance characteristics of agitated nickel hypophosphite electroless plating baths, Journal of Materials Processing Technology 211 (2011) 1488–1499.
[16] M. Kitiwan, D. Atong, Effects of porous alumina support and plating time on electroless plating of palladium membrane, Journal of Materials Science and Technology 26 (2010) 1148–1152.
[17] I.P. Mardilovich, E. Engwall, Y.H. Ma, Dependence of hydrogen flux on the pore size and plating surface topology of asymmetric Pd-porous stainless steel membranes, Desalination 144 (2002) 85–89.
[18] V.K. Bulasara, H. Thakuria, R. Uppaluri, M.K. Purkait, Effect of process parameters on electroless plating and nickel–ceramic composite membrane characteristics, Desalination 268 (2011) 195–203.
[19] P. Kathirgamanathan, Ultrasound-assisted electroless deposition of copper onto and into microporous membranes for electromagnetic shielding, Polymer Communications 35 (1994) 430–432.
[20] S. Ilias, M.A. Islam, Fabrication of Pd/Pd-alloy Films by Surfactant Induced Electroless Plating for H_2 Separation from Advanced Coal Gasification Processes, Patent Application #20100068391 (USPTO assignment date: March 18, 2010).
[21] M.S. Islam, M.M. Rahman, S. Ilias, Characterization of Pd–Cu membranes fabricated by surfactant induced electroless plating (SIEP) for hydrogen separation, International Journal of Hydrogen Energy 37 (2012) 3477–3490.

Ultrasonics Sonochemistry 21 (2014) 1382–1391

Contents lists available at ScienceDirect

Ultrasonics Sonochemistry

journal homepage: www.elsevier.com/locate/ultson

Efficacy of reducing agent and surfactant contacting pattern on the performance characteristics of nickel electroless plating baths coupled with and without ultrasound

Amrita Agarwal, Murali Pujari, Ramgopal Uppaluri *, Anil Verma

Department of Chemical Engineering, Indian Institute of Technology Guwahati, Guwahati 781039, Assam, India

ARTICLE INFO

Article history:
Received 23 October 2013
Received in revised form 2 January 2014
Accepted 8 January 2014
Available online 21 January 2014

Keywords:
Sonication
Reducing agent
Densification
Ceramic
Surfactant

ABSTRACT

This article addresses furthering the role of sonication for the optimal fabrication of nickel ceramic composite membranes using electroless plating. Deliberating upon process modifications for surfactant induced electroless plating (SIEP) and combined surfactant and sonication induced electroless plating (SSOEP), this article highlights a novel method of contacting of the reducing agent and surfactant to the conventional electroless nickel plating baths. Rigorous experimental investigations indicated that the combination of ultrasound (in degas mode), surfactant and reducing agent pattern had a profound influence in altering the combinatorial plating characteristics. For comparison purpose, purely surfactant induced nickel ELP baths have also been investigated. These novel insights consolidate newer research horizons for the role of ultrasound to achieve dense metal ceramic composite membranes in a shorter span of total plating time. Surface and physical characterizations were carried out using BET, FTIR, XRD, FESEM and nitrogen permeation experiments. It has been analyzed that the SSOEP baths provided maximum ratio of percent pore densification per unit metal film thickness ($\frac{PPD}{\delta}$) and hold the key for further fine tuning of the associated degrees of freedom. On the other hand SIEP baths provided lower ($\frac{PPD}{\delta}$) ratio but higher PPD. For SSOEP baths with dropwise reducing agent and bulk surfactant, the PPD and metal film thickness values were 73.4% and 8.4 μm which varied to 66.9% and 13.3 μm for dropwise reducing agent and drop surfactant case.

1. Introduction

Electroless nickel deposition occurs due to the accretion of metal particles on a solid substrate. The autocatalytic nickel electroless plating (ELP) process is a relatively slower process, and thus several researchers have conceptualized the need for suitable supplements to enhance the rate of metal deposition on the porous surface without compromising upon the quality of the deposition. Relevant techniques that have been identified include membrane agitation [1], vacuum [2], sonication [3], surfactant [4], hydrothermal [5] and gas sparging [6]. However, from the perspectives of combinatorial plating characteristics, ease of operation and scalability, sonication and surfactant induced ELP are the most promising options that need to be further investigated and examined for their optimality.

During sonication assisted nickel electroless plating, the ultrasonic energy accelerates and improves the chemical reactivity in the solution as well as on the solid–liquid interface. The origin of sonochemical effects is cavitation. Cavitation in a sonicator bath results in mechanical effects by cavity collapse onto the metal/liquid–substrate surface thereby ensuring rapid mass transfer, surface cleaning, particle size reduction, thin film preparation, agglomeration of crystals and metal activation. It facilitates the step wise formation, growth, and subsequent implosive collapse of bubbles in the liquid [7], which thereby influences the metal depositional characteristics. Many researches have inferred that sonication assisted metal deposition enables the synthesis of nano particles and efficient deposition of metals on different substrates [3,7,8]. On the other hand, the addition of a surfactant during ELP influences particle dispersion and metal plating rates and thereby increases the mechanical bonding strength [9].

In the field of metal membrane fabrication, researches have either explored surfactant [4,10–13] or sonication [14,15] rate enhancement techniques separately and their coupled effect during ELP has been investigated for other chemical engineering applications. Recently our research group carried out a comparative assessment of surfactant and sonication induced electroless plating baths [16,17] and inferred that surfactant induced electroless plating (SIEP) baths provide better surface engineering and combinatorial performance characteristics [16] whereas sonication induced electroless plating (SOEP) baths were favorable in terms of enhancing

* Corresponding author. Tel.: + 91 361 2582260; fax: +91 361 2582291.
E-mail address: ramgopalu@iitg.ernet.in (R. Uppaluri).

1350-4177/$ - see front matter © 2014 Elsevier B.V. All rights reserved.
http://dx.doi.org/10.1016/j.ultsonch.2014.01.015

Nomenclature

A_m	permeable area of the membrane, m^2
Q	volumetric flow rate, $\frac{m^3}{s}$
P_2	Membrane pressure at permeate side, pa
ΔP	trans-membrane pressure drop, pa
d_p	average pore size, μm
$\left(\frac{\varepsilon}{q^2}\right)$	effective porosity
J	flux through the membrane, $(\frac{mol}{m^2 s})$
i	hour of nickel plating(as exponent)
$\bar{J}_0$	average flux through the support, $(\frac{mol}{m^2 s})$
$\bar{J}_i$	average flux through the membrane after *i*th hour of nickel plating, $(\frac{mol}{m^2 s})$
C_i	initial concentration of Ni^{+2} in the plating solution, $\frac{mol}{L}$
C_f	average Ni^{+2} solution concentration after plating, $\frac{mol}{L}$
x	conversion
η	plating efficiency, %
w_0	dry weight of the membrane before plating, g
w_i	dry weight of the membrane after *i*th hour of plating, g
w	total amount of nickel originally available in the plating bath, g
n	number of plating cycles
V_0	volume of plating solution in each plating cycle, L
M_{Ni}	molecular weight of nickel metal $\frac{g}{mol}$
ρ_{Ni}	density of nickel metal, $\frac{g}{cm^3}$
$\bar{r}_i$	plating rate, $\frac{mol}{Ls}$
t_i	time of plating for the *i*th hour, hr
PPD	percent pore densification, %
ELP	electroless plating
CEP	conventional electroless plating
SIEP	surfactant induced electroless plating
SOEP	sonication induced electroless plating
CEP–BR	conventional electroless plating – bulk reducing agent
SOEP-BR	sonication induced electroless plating – bulk reducing agent
SIEP-BR-BS	surfactant induced electroless plating – bulk reducing agent-bulk surfactant
SIEP-DWR-BS	surfactant induced electroless plating–dropwise reducing agent-bulk surfactant
SSOEP-DWR-BS	coupled sonication and surfactant induced electroless plating–dropwise reducing agent-bulk surfactant
SIEP-DWR-DWS	surfactant induced electroless plating–dropwise reducing agent-dropwise surfactant
SSOEP-DWR-DWS	coupled sonication and surfactant induced electroless plating–dropwise reducing agent-dropwise surfactant

plating rates. Despite improving the plating rates, the SOEP baths failed to achieve higher pore densification and have phenomenally contributed to the layering effect without improving upon the pore coverage and densification. Since SIEP process also has fundamental limitations in terms of limited enhancement in the plating rate, a further enhancement in the plating rate without jeopardizing upon the pore densification was desired. To achieve the same, it was hypothesized that a combination of sonication and surfactant would suffice the purpose of targeting the fabrication of dense metal composite membranes.

Further, few researchers [3,18,19] have investigated ELP coupled with sonication and surfactant variants for the development of products other than metal ceramic membranes. But till date, the literature is scarce on the coupled effect of two most scalable rate enhancement techniques namely surfactant and sonication for the fabrication of metal ceramic composite fabrication using ELP technique.

On the other hand, surfactant induced electroless plating (SIEP) and combined surfactant and sonication induced electroless plating (SSOEP) baths can be operated in several ways. As a first alternative, all the constituents can be mixed initially and plating could be initiated. Otherwise, the reducing agent can be added in a phase wise or continuous mode to the mixture of surfactant and metal solution in an ELP bath. As a third alternate, both reducing agent and surfactant can be added in a phase wise and continuous mode to the ELP baths. While these options may appear naïve for the general application of ELP, they may be of paramount relevance for dense metal composite membranes. Till date there is no literature that elaborates upon the role of contacting pattern of the surfactant in electroless plating bath for dense composite membrane fabrication. All relevant literatures [10,11,20] addressed bulk addition of surfactant for metal deposition using electroless plating. The bulk addition of surfactant encourages adsorption of surfactant on the membrane surface which promotes uneven charge distributions on the surface [4] .This encourages greater metal nucleation in the solution. Variation in the surfactant contacting pattern is hypothesized to promote better depositional characteristics and hence higher pore densification due to lesser adsorption of surfactants on the substrate surface. Thus to increase the efficacy of the electroless plating process, there is a need to focus upon the contacting pattern of the dispersing agent (surfactant).

Also, a reducing agent such as hydrazine hydrate is highly heat sensitive and maintaining a steady concentration of the same is highly cumbersome [21]. Conceptually, to overcome the same, a highly controlled reducing agent addition strategy has to be adopted in this work. Such an addition of reducing agent to an electroless plating process would be similar to the optimal current density utilization in an electroplating process. The adopted strategy for controlled addition of the reducing agent in this work corresponds to the dropwise addition of the reducing agent during the SIEP/SSOEP process.

This work addresses various types of SIEP and SSOEP processes considering options such as bulk addition of surfactant (BS), continuous (dropwise) addition of surfactant (DWS) and continuous (dropwise) addition of reducing agent (DWR). This work addresses two major objectives. Firstly, it elaborates upon the comparative assessment of SIEP and SSOEP processes supplemented with the dropwise addition of the reducing agent. Secondly, it focusses upon the dropwise addition of the dispersing agent (surfactant) for SIEP and SSOEP baths. The ultimate goal of our experimental investigations is to identify the best process that can provide maximum percent pore densification (PPD), plating rate ($\bar{r}_i$), plating efficiency (η) and minimum metal film thickness (δ).

2. Experimental

Low cost circular disk shaped ceramic supports with an average pore size of 200–250 nm were prepared using the raw materials presented in Table 1. The laboratory fabricated circular ceramic substrates possessed a diameter of 36 mm and a thickness of 3.5 mm. The fabrication methodology consists of the following hierarchical steps: mixing of raw materials; casting of the mixture into circular moulds; drying of the raw discs at 100 °C; sintering at 900 °C with a controlled heating/cooling rate (1.5 °C/min); polishing of the membranes and finally ultrasonically cleaning the

Table 1
Composition of raw materials.

Material	Composition (wt.%)	Purchased from
Kaolin	40	CDH Ltd., India
Feldspar	15	National Chemicals, India
Quartz	15	Research-lab Fine Chem Industries, India
Na_2CO_3	10	Merck Ltd., India
Pyrophyllite	10	National Chemicals, India
Boric Acid	5	Merck Ltd., India
Sodium metasilicate	5	SD Fine-Chem Ltd, India

Table 2
Composition of surfactant induced electroless nickel plating bath.

S. No.	Component	Purpose	Amount (mol/L)
1	Nickel sulfate	Source of nickel	0.08 mol/L
2	Hydrazine Hydrate	Reducing agent	100% excess
3	Trisodium citrate	Stabilizer	0.2 mol/L
4	Sodium Hydroxide	pH	10–12
5	Cetyltrimethylammonium bromide	Dispersion	1.2 g/L
Plating temperature			353–363 K
Loading ratio			203 cm^2/L
Time for 1 plating step			½ h

membrane in a sonicator bath. The substrates were fabricated by the dry compaction method using a hydraulic press (Make – Velan Engineering) at a pressure of 4.9 MPa. The effective porosity ($\frac{\varepsilon}{\tau^2}$) of the supports was found to be about 10–15% as evaluated from nitrogen permeation experiments.

A number of techniques such as fourier transform infrared spectroscopy (FTIR), Brunauer–Emmett–Teller (BET) analysis, X-ray diffraction (XRD) analysis, field emission scanning electron microscopic (FESEM), weight gain method, nitrogen permeation experiments were used for surface and physical characterization. The FTIR analysis was deployed to observe the characteristic peaks associated to various functional groups in raw materials. N_2 adsorption desorption isotherm was used to evaluate the BET surface area and pore size of the substrate material. Further to evaluate the extent of phase transformations after plating, XRD analysis was carried out. FESEM study was conducted to analyze the surface defects and estimate the average membrane pore size. Nitrogen permeation experiments were conducted to evaluate membrane morphological parameters such as the average flux of the membrane and percent pore densification.

2.1. Electroless plating

Prior to electroless nickel plating the substrates were sensitized and activated with palladium. The activation process produced small Pd metal catalytic sites dispersed on the surface that serve as active sites for electroless nickel deposition. The optimized electroless Ni plating bath composition and parameters are summarized in Table 2.

The conventional electroless plating (CEP) bath composition (as shown in Table 2) consisted of nickel sulfate (source of nickel), hydrazine hydrate (electron source), trisodium citrate (stabilizer), and sodium hydroxide (to maintain pH) respectively. Plating characteristics were investigated at a loading ratio of 203($\frac{cm^2}{L}$), plating bath temperature of 80 °C, pH of 10–12 and ½ h of plating time for one deposition. Since the process involves bulk addition of reducing agent, the CEP process has also been referred to as CEP–BR (bulk reducing agent). For SIEP baths, the process variation refers to the alteration in the bath composition to include a cationic surfactant cetyltrimethylammonium bromide (CTAB) at a solution concentration of 1.2 g/L. Further, for SSOEP baths, the CEP bath has been replaced with a sonicator bath along with an addition of the CTAB surfactant. Ultrasonic cleaning bath (Elma S 30 H) that operated at a frequency of 37 kHZ with a power consumption of 280 W was used for SSOEP process studies. The inner dimensions of the rectangular cleaning bath are 240 mm (Length) × 137 mm (Width) × 100 mm (Height). Further, the sonicator was also facilitated with three different modes of operation namely auto, degas and sweep.

Typically, the reduction of Ni^{2+} with hydrazine hydrate reducing agent during ELP involves the following three reactions [22]:

$$2Ni^{2+} + N_2H_4 + 4OH^- = 2Ni \downarrow + N_2 \uparrow + H_2O \quad (1)$$

$$N_2H_4 = N_2 \uparrow + 2H_2 \quad (2)$$

$$3N_2H_4 = N_2 \uparrow + 4NH_3 \uparrow \quad (3)$$

In the above three reactions, while reaction (1) occurs on the activated substrate surface and is desired, reactions (2) and (3) occurs in the plating solution and are undesired, as they deplete reducing agent concentration in the solution. Reactions (2) and (3) are due to inherent heat sensitivity and instability of hydrazine at the plating temperature. Therefore, bulk addition of hydrazine is bound to provide lower plating efficiency due to lower selectivity towards reaction (1). Hence controlled addition of hydrazine to the metal electroless plating baths is anticipated to enhance the selective conversion of hydrazine towards metal plating on the substrate surface. Thus with efficient contacting pattern for the reducing agent, the time period for one plating step could be reduced by 50% (30 min) which was not the case in our earlier work [8]. In addition, the controlled addition of surfactant could reduce stronger adsorption of surfactant on the substrate surface, which can inturn alter the metal adhesion and removal rate of generated gas bubbles (reaction (1)). The desired effect of minimal metal solution nucleation and maximum metal film adhesion strength is an interesting issue in the context of surfactant contacting pattern. Thus, the efficacy of reducing agent and surfactant contacting pattern has been investigated for the following cases:

(a) **SIEP-DWR-BS baths:** The SIEP baths were modified with dropwise addition of reducing agent (DWR) and bulk addition of the cationic surfactant (BS).
(b) **SIEP-DWR-DWS baths**: For these cases, SIEP baths were supplemented with dropwise addition of reducing agent (DWR) and dropwise addition of the cationic surfactant (DWS).

(c) **SSOEP-DWR-BS baths:** In these experiments, plating was carried out in SSOEP baths with dropwise addition of reducing agent (DWR) and bulk addition of the cationic surfactant (BS).

(d) **SSOEP-DWR-DWS**: For these cases, SSOEP baths were supplemented with dropwise addition of reducing agent (DWR) and dropwise addition of the cationic surfactant (DWS).

2.2. Evaluation of plating characteristics

Parameters involved for the evaluation of combinatorial nickel plating characteristics include average trans-membrane flux ($\bar{J}$), plating efficiency (η), average plating rate ($\bar{r}_i$), metal film thickness (δ) and percent pore densification PPD(%).

The nitrogen flux through the membrane (J) at varying pressure was evaluated from the volumetric flow rate data

$$J = \frac{Q}{A_m} \tag{4}$$

where Q represents the volumetric flow rate in LPM, A_m the permeable area of the membrane in m^2 and J the flux through the membrane in $(\frac{mol}{m^2 s})$

The average membrane flux $\bar{J}$ was estimated using the expression

$$\bar{J} = \frac{\int_{P_1}^{P_2} JdP}{P_2 - P_1} \tag{5}$$

where $\int_{P_1}^{P_2} JdP$ corresponds to the area under the curve for a plot between the membrane flux $(\frac{mol}{m^2 s})$ and pressure differential (psi).The term $P_2 - P_1$ corresponds to the maximum and minimum guage pressure during a nitrogen permeation experiment.

Pore densification was defined as the fractional volume of the pores covered by the deposited metal and it was expressed as follows:

$$\text{PPD}_i = \frac{\bar{J}_o - \bar{J}_i}{\bar{J}_o} \times 100 \tag{6}$$

where $\bar{J}_o$ represents the average flux through the support and $\bar{J}_i$ represents the average flux through the membrane after ith hour of nickel plating.

The theoretical nickel film thickness (δ) was evaluated as follows:

$$\delta = \frac{w_2 - w_1}{\rho_{Ni} A_m} \tag{7}$$

where $\rho_{Ni}(\frac{g}{cm^3})$ represents the density of nickel metal and $A_m(m^2)$ the membrane surface area for nitrogen permeation experiments. In addition, further insights to gain information related to the uncertainties associated to theoretical metal film thickness have not been conducted using FESEM cross section images. This is due to the reason that Bulasara et al. [23] have indicated that the theoretical metal film thickness values are as good as those measured using the FESEM image analysis.

The plating rate $\bar{r}_i(\frac{mol}{L\,s})$ was evaluated as follows:

$$\bar{r}_i = \frac{w_2 - w_1}{M_{Ni} \times n \times V_0 \times t_i} \tag{8}$$

where t_i corresponds to the time of plating for the ith hour.

The plating efficiency $\eta(\%)$ was evaluated as follows:

$$\eta = \frac{w_2 - w_1}{w_0 x} \tag{9}$$

where x corresponds to the conversion in the plating bath and can be expressed as:

$$x = \frac{V_i C_i - V_f C_f}{V_i C_i}. \tag{10}$$

The concentration of nickel ions in the plating baths before (C_i) and after electroless deposition (C_f) were estimated from complexometric titration with EDTA using xylenol orange indicator [23]

3. Results and discussion

3.1. Surface characterization

Fig. 1 confirms the existence of characteristic peaks for kaolin in the raw material and peaks corresponding to C–H, C=C, Si–O–Al and Si–O bonds in the ceramic support. Further details with respect to the FTIR analysis has been elaborated in our earlier work [16]. Further Fig. 2(a) confirms the existence of Type III isotherm with H_3 hysteresis loop giving rise to slit-shaped pores exist as per IUPAC [24] using a surface area analyzer(Make: Beckman-Coulter). Fig. 2(b) illustrates the desorption *Barrett–Joyner–Halenda* (BJH) pore size distribution of the ceramic substrate material. The BET surface area of support is 4.130 m^2/g and total pore volume is 0.0325 ml/g with no micro pore volume.

Fig. 3 presents the XRD (Make: Shimadzu Corporation) of nickel membrane fabricated with various processes. ICDD-JCPDS database was used for the phase analysis of the diffraction profiles. The XRD patterns of the ceramic support are similar to that outlined in our previous work [17]. The metallic nickel peaks for electroless nickel plating for all baths appeared at diffraction angle $2\theta = 44.5°$ and $51.8°$ due to the diffraction of (1 1 1) and (2 0 0) plane [Pdf No 00-004-0850]. It is also observed that the quartz peak exists for SIEP-DWR-BS and SSOEP-DWR-DWS baths at a diffraction angle $2\theta = 26.6°$ [Pdf No 00-083-2465] suggesting non uniform deposition. However, for the case of SIEP-DWR-DWS and SSOEP-DWR-BS baths, no such quartz peaks were observed suggesting uniform plating, higher metal film thickness and better PPD.

The surface FESEM (Make: Oxford; Model: LEO 1430VP, UK) micrographs of the nickel films deposited with various baths are shown in Fig. 4. It can be observed that the FESEM micrographs are in good agreement with the XRD profiles (Fig. 3) thereby illustrating that non-uniform nickel deposition with low PPD occurred for SIEP-DWR-BS (Fig. 4(a)) and SSOEP-DWR-DWS baths (Fig. 4(c)). However, this is not the case for SIEP-DWR-DWS baths (Fig. 4(b)) where uniform nickel deposition occurred with metal aggregates that do not have uniformity in their size. Lastly for SSOEP-DWR-BS baths (Fig. 4(d)), it has been observed that well developed similar shaped metal aggregates have been observed. This effect confirms that the agitation caused by ultrasonic waves during sonication has been effective towards uniform metal deposition. The same has also been confirmed by the XRD spectral profiles presented for SSOEP-DWR-BS baths in Fig. 3, where a strong peak for nickel indicates highest crystallinity.

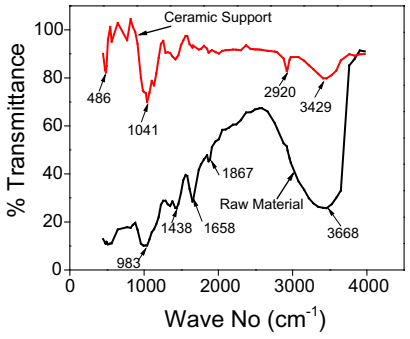

Fig. 1. FTIR spectral analysis of ceramic support and raw material.

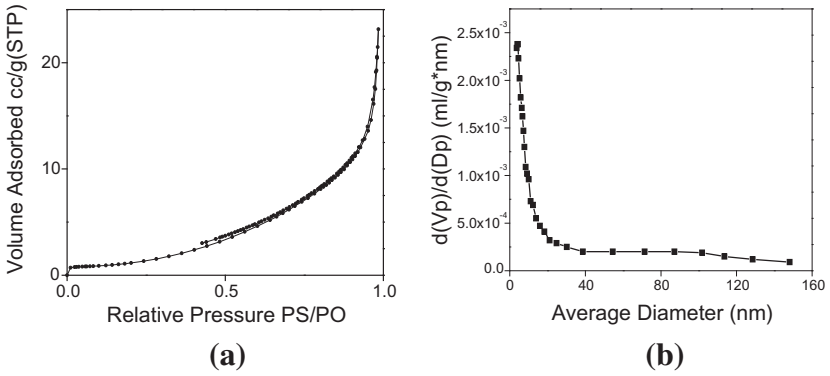

Fig. 2. (a) Nitrogen adsorption/desorption isotherms of the ceramic support material. (b) Desorption *Barrett–Joyner–Halenda* (BJH) pore size distribution of the substrate material.

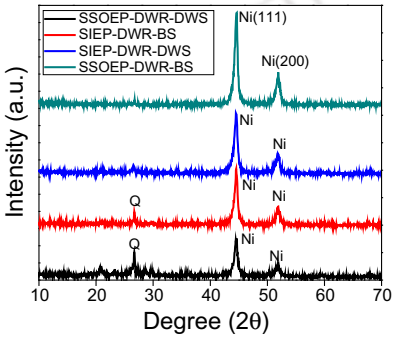

Fig. 3. XRD patterns of nickel membrane fabricated with SSOEP-DWR-BS, SSOEP-DWR-DWS, SIEP-DWR-BS and SIEP-DWR-DWS baths.

3.2. Plating characteristics of SIEP-DWR baths

3.2.1. PPD profiles

Fig. 5 presents the variation of PPD with plating time for SIEP-DWR-BS and SIEP-DWR-DWS baths. It can be observed that the PPD profiles varied from 30.5% to 71.4% and from 50.4% to 76.5% for a variation in plating time from 2 to 8 h for SIEP-DWR-BS and SIEP-DWR-DWS baths respectively. For similar metal concentration (0.08 mol/L) and plating time (8 h) it was observed that modifying the contacting strategy of surfactant from bulk to dropwise increased the PPD by 7%. Hypothetically, dropwise addition of reducing agent to an ELP plating bath facilitates the availability of electron source throughout the time of deposition and thus enhances PPD. Thus the main objective of adding a surfactant i.e. for the removal of unwanted gas bubbles has been supported by dropwise contacting pattern of the reducing agent. For any plating time, if the surfactant concentration is too high it can get adsorbed on the surface and hinders metal deposition. This was the possible reason for very low PPD values of SIEP-DWR-BS baths after 2 h of sequential deposition. However this was not the case for SIEP-DWR-DWS baths where the controlled addition of surfactant in the plating bath restricted the surfactant adsorption and hence did not hinder the metal electroless plating. Another probable reason of lower PPD values with SIEP-DWR-BS baths could also be that lack of agitation did not reduce the strong adsorption of surfactant on the substrate surface during bulk addition. Thus, agitation during bulk surfactant addition could minimize surfactant adsorption on the substrate surface and thereby enhance pore densification.

3.2.2. Metal film thickness profiles

Fig. 6 illustrates the time dependent variation of metal film thickness for SIEP-DWR-BS and SIEP-DWR-DWS baths. As shown, the nickel film thickness varied from 3.9–9.8 to 6.3–9.4 μm for a variation in plating time from 2 to 8 h for SIEP-DWR-BS and SIEP-DWR-DWS baths respectively. For SIEP-DWR-BS baths, in the initial stages (2 h) of plating, the metal film thickness was very low due to poor densification, and increased significantly after 8 h of sequential deposition. It was also analyzed that after 8 h of total plating time, low PPD exists for SIEP-DWR-BS bath in comparison to the SIEP-DWR-DWS bath. This could be attributed to the undesired phenomena of layering without significant densification. But for SIEP-DWR-DWS baths, higher PPD with lower metal film thickness was achieved. Thus dropwise contacting pattern of surfactant maximized densification and minimized layering.

In our earlier reported work [16] with bulk addition of both surfactant and reducing agent i.e. for SIEP-BR-BS baths a PPD of 87.7% and a metal film thickness of 13.8 μm on a substrate pore size of 90–120 nm could be obtained after 16 sequential depositions of 1 h each. As compared to it, in this work for SIEP-DWR-DWS baths could achieve a PPD of 76.5% and a metal film thickness of 9.4 μm were achieved on the substrate (pore size of 200–250 nm) after 16 sequential depositions in 8 h total plating time. The PPD/δ value for our earlier work were 6.3 whereas for our present work it is 8.1. Also there has been 50% reduction in total plating time in the presented work.

3.2.3. Plating rate profiles

Fig. 7 illustrates the variation of metal plating rate with time of plating. It can be observed that the plating rates decreased with an increase in plating time. The plating rates varied from 4.1 to 0.65×10^{-7} and from 6.7 to 0.63×10^{-7} mol/L s for SIEP-DWR-BS and SIEP-DWR-DWS baths respectively. It was observed that for SIEP-DWR-BS baths, the metal plating rate was lower in the initial hours of plating. This is probably due to the fact that bulk surfactant addition favors its strong adsorption on the substrate surface and thereby hinders metal deposition. However, with increasing plating time, as more and more reducing agent was added into the bath, the surfactant molecules contributed significantly for the removal of gas bubbles from the surface. At longer plating time, the plating rates for both baths matched with one another, thus indicating that both SIEP-DWR-DWS and SIEP-DWR-BS baths have similar role of adsorbed surfactant on substrate surface to influence metal deposition.

In our earlier reported work [16], for bulk addition of both surfactant(BS) and reducing agent (BR) i.e. SIEP-BR-BS baths, the plating rate varied from 9.6 to 3.8×10^{-8} mol/L s for 4–16 h of 1 h plating step on a substrate pore size of 90–120 nm. As compared to it, this work reported a plating rate variation from 6.7 to 0.63×10^{-7} mol/L s for 2–8 h of metal deposition on a substrate pore size of 200–250 nm for SIEP-DWR-DWS baths. This indicates

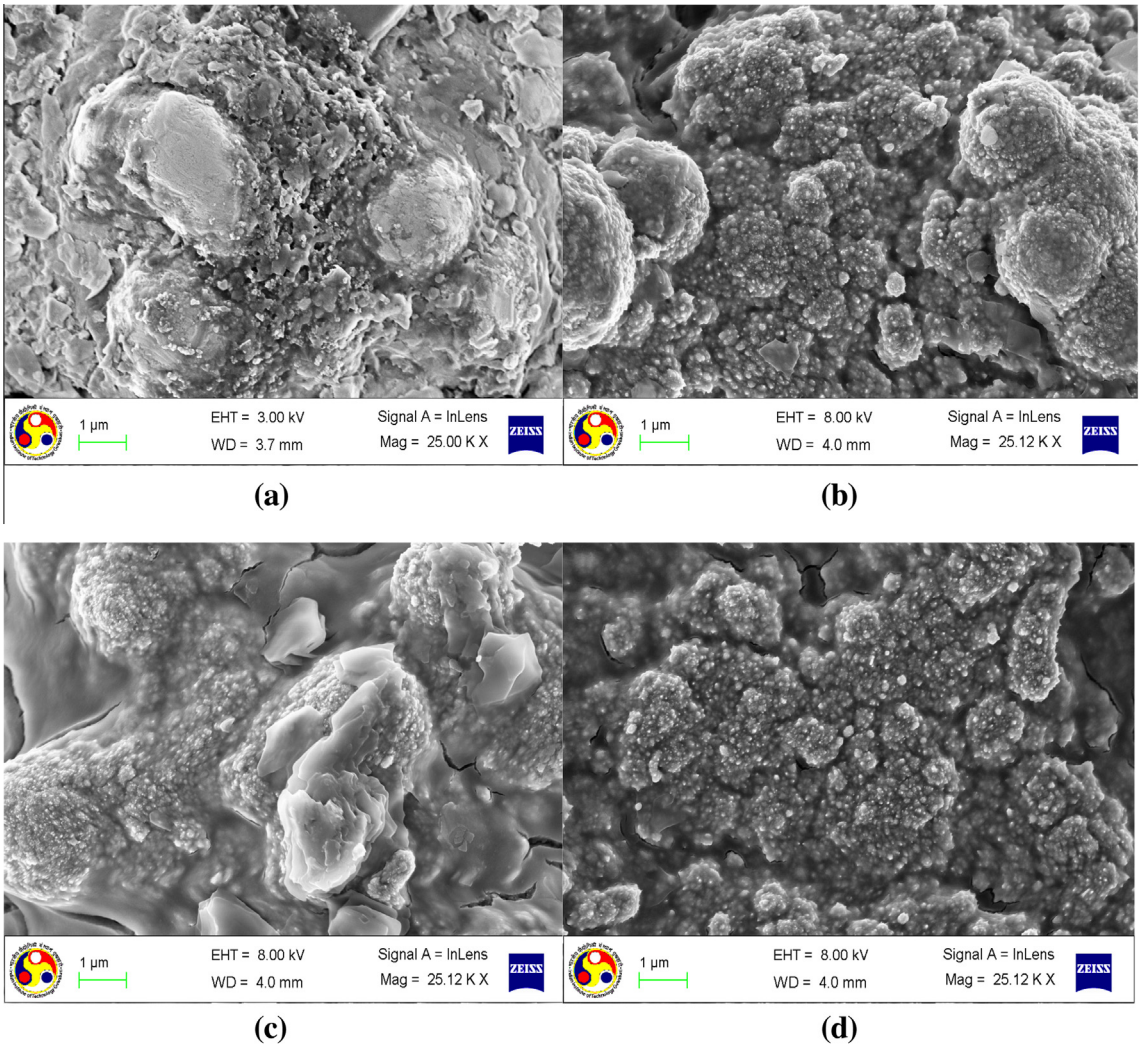

Fig. 4. Surface FESEM micrographs of (a) SIEP-DWR-BS, (b) SIEP-DWR-DWS, (c) SSOEP-DWR-DWS and (d) SSOEP-DWR-BS baths.

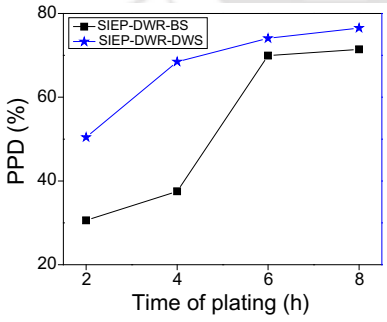

Fig. 5. Variation of PPD with plating time for SIEP baths.

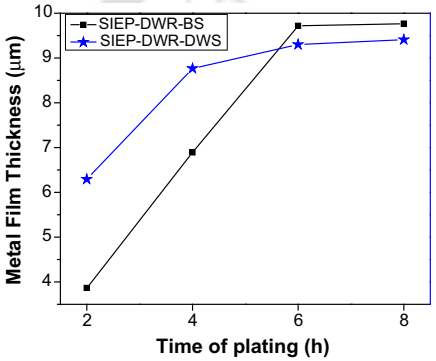

Fig. 6. Variation of metal film thickness with plating time for SIEP baths.

that about 40% enhancement in plating rates and 50% reduction in plating time can be achieved by modifying the process from SIEP-BR-BS to SIEP-DWR-DWS baths.

These observations are also in agreement with the trends presented by Kitwan et al. [25]. The authors reported that the plating rate and the quality of plating were optimal for supports with in the pore size of 250–300 nm and porosity of 35–50%. This work referred to the performance characteristics of a low cost ceramic membrane that was characterized with even lower combinations of pore size (200–270 nm) and effective porosity (10–15%).

3.2.4. Plating inefficiency profiles

Fig. 8 demonstrates the variation of plating inefficiency with plating time. It was observed that the plating inefficiency varied from 40.3% to 64.5% and from 30.6% to 40.5% for SIEP-DWR-BS and SIEP-DWR-DWS baths respectively. For SIEP-DWR-DWS baths, the plating inefficiencies reduced by 35% as compared to SIEP-DWR-BS baths. The reason for higher plating inefficiency for SIEP-DWR-BS baths would refer to higher surfactant adsorption

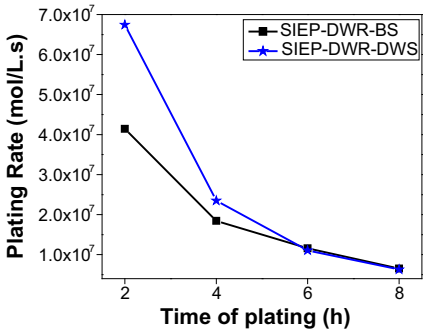

Fig. 7. Variation of metal plating rate with plating time for SIEP baths.

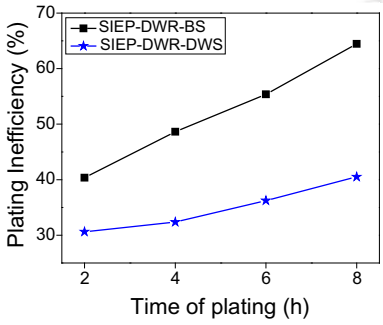

Fig. 8. Variation of plating inefficiency with plating time for SIEP baths.

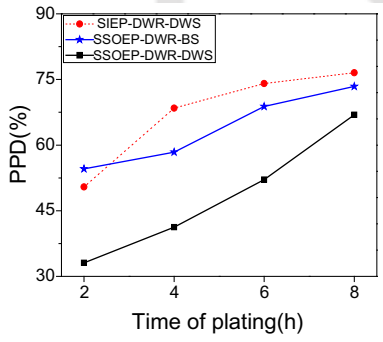

Fig. 9. Variation of PPD with plating time for SSOEP baths.

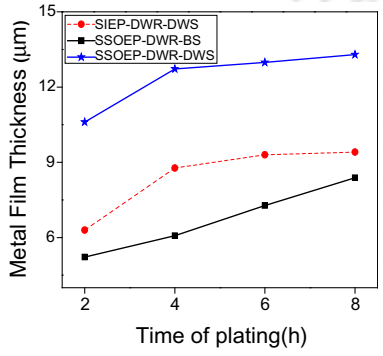

Fig. 10. Variation of metal film thickness with plating time for SSOEP baths.

on the substrate which favored higher metal nucleation in the solution. For both the cases, the plating inefficiency increased with plating time. This could be explained by the fact that a controlled addition of complexing reducing agent (DWR) and surfactant

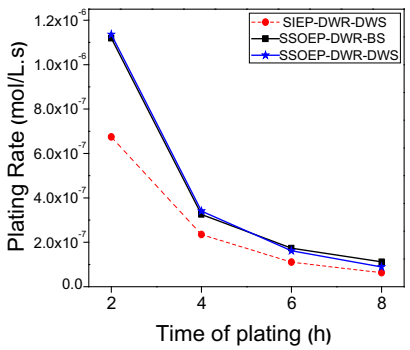

Fig. 11. Variation of plating rate with plating time for SSOEP baths.

(DWS) could provide a strong metal-substrate bonding resulting in the restriction of the metal nucleation in the solution and eventually lower plating inefficiency. But with increasing plating time, as more and more active sites are occupied, the metal has to bond with another metal particle. The metal–metal bond adhesion is not as strong as compared to metal–substrate adhesion which resulted in higher metal nucleation in the solution and eventually higher plating inefficiency at prolonged plating time.

3.3. Plating characteristics for SSOEP-DWR baths

3.3.1. PPD profiles

Fig. 9 presents the time dependent variation of PPD for SSOEP baths. It can be observed that the PPD profiles varied from 54.6% to 73.4% and from 33% to 66.9% for a variation in plating time from 2 to 8 h for SSOEP-DWR-BS and SSOEP-DWR-DWS baths respectively. Thus, SSOEP-DWR-BS baths provided faster pore densification as compared to SSOEP-DWR-DWS baths. For SSOEP-DWR-BS baths, the surfactant adsorption on the surface is minimized by cavitation effect (caused by ultrasonic waves) which favored the minimization of pitting and metal nucleation in the solution and hence faster densification. However, for SSOEP-DWR-DWS baths, the combination of agitation caused by ultrasonic waves and dropwise addition of surfactant failed to provide higher densification as compared to the case with SSOEP-DWR-BS baths. This is due to the fact that cavitation effect favored faster removal of gas bubbles adhering to the substrate surface which cause greater metal nucleation in the solution and reduce the PPD. Thus it is interesting to note that there exists a sensitive dependence of PPD on the contacting pattern of the surfactant and cavitation effect. A comparison of PPD profiles for SIEP-DWR-DWS baths (Fig. 5) and SSOEP baths (Fig. 9) confirm that the SIEP baths perform better than SSOEP baths in terms of pore densification. These observations are also in agreement with the results obtained from surface characterization studies.

3.3.2. Metal film thickness profiles

Fig. 10 illustrates the profiles for time dependent variation of metal film thickness with plating time. It can be observed that the nickel film thickness varied from 5.2 to 8.4 μm and from 10.6 to 13.3 μm for a plating time variation from 2 to 8 h for SSOEP-DWR-BS and SSOEP-DWR-DWS baths respectively. It was observed that for SSOEP-DWR-BS baths, the variation in metal film thickness was uniform with plating time which indicates higher stability and better adhesion of the metal film. The desired feature of efficient electroless plating is higher densification with lower metal film thickness. These features were better achieved for SSOEP-DWR-BS baths. For SSOEP-DWR-DWS baths the metal film thickness doubled along with 9% reduction in pore densification as compared to

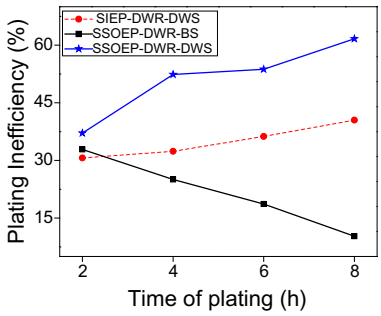

Fig. 12. Variation of plating inefficiency with plating time for SSOEP baths.

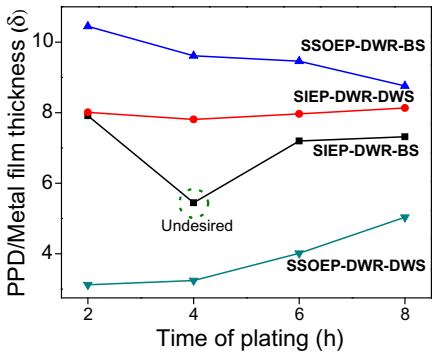

Fig. 13. Variation of PPD/metal film thickness with plating time for SSOEP and SIEP baths.

SSOEP-DWR-BS baths. The probable reasons for the same have been explained in Section 2(b).

Till date, to the best of our knowledge, no literatures are available for SSOEP baths from the perspective of achieving faster PPD and quality metal deposition. In our earlier work [16], with bulk addition of reducing agent for SOEP-BR baths a PPD of 72.8% with a metal film thickness of 15.5 μm on a substrate pore size of 90–120 nm was obtained after 16 sequential depositions of 1 h time duration for each plating step. As compared to it, in this work for SSOEP-DWR-BS baths, PPD of 73.4% and a metal film thickness of 8.8 μm were achieved on a substrate pore size of 200–250 nm after 8 h of total plating time. The PPD/δ for our earlier work (i.e. SOEP-BR baths) [16] was 4.7 whereas in the present case (i.e. SSOEP-DWR-BS baths) it is 8.3.Further a reduction in total plating by 50% is promising. A comparison of metal thickness growth profiles for SIEP-DWR-DWS baths (Fig. 6) and SSOEP baths (Fig. 10) confirms that lower thicknesses were achieved for SSOEP-BS baths. The possible reason to achieve lower thickness profiles for this case is due to the optimality of coupled cavitation and dispersion effect which were induced by sonication and surfactant respectively.

3.3.3. Plating rate profile

Fig. 11 illustrates the variation of metal plating rate with plating time. It can be observed that the plating rates decreased with increase in time of plating. The plating rates varied from 1.1 to 0.11×10^{-6} mol/L s and from 1.1 to 0.09×10^{-6} mol/L s for SSOEP-DWR-BS and SSOEP-DWR-DWS baths respectively. It can be observed that there was an insignificant difference in plating rate trends for both cases. This implies to the fact that no matter what combination of reducing agent and surfactant contacting pattern is used, sonication will finally result in higher plating rates. This is due to cavitation phenomena which results in increased plating rate due to subsequent formation and collapse of the bubles. However, due to significantly higher PPD (73.4%) and lower film thickness (8.4 μm) for SSOEP-DWR-BS baths as compared to SSOEP-DWR-DWS baths (PPD of 66.9% and film thickness of 13.3 μm), the SSOEP-DWR-BS baths can be inferred to provide higher $\frac{PPD}{\delta}$ which is highly desired. Compared to SIEP-DWR-DWS plating baths (Fig. 7), comparatively higher plating rates were obtained for both SSOEP-DWR-DWS and SSOEP-DWR-BS plating baths (Fig. 11). The parametric profile for best process has been indicated with a dotted line in Fig. 11. This observation is in accordance with the crystal (Fig. 3) and particle size growth (Fig. 4) trends. Hence, it is apparent that cavitation effect improved plating rates.

In our earlier work [16] with bulk addition of both surfactant and reducing agent i.e. SOEP-BR baths, the plating rate varied from 1.1 to 0.43×10^{-7} mol/L s for 8–16 h (1 h duration for each plating step) on a substrate possessing an average pore size of 90–120 nm. As compared to it, this work reported a plating rate of 1.1 to 1.0×10^{-6} mol/L s for 2–8 h (½ h duration for one plating step) on a substrate with an average pore size of 200–250 nm adopting SSOEP-DWR-BS baths. Therefore, even when the substrate pore size is doubled, the plating rates enhanced by about 10 times by altering the process from SOEP-BR baths to SSOEP-DWR-BS baths.

3.3.4. Plating inefficiency profiles

Fig. 12 demonstrates the variation of plating inefficiency with plating time. It can be observed that the plating inefficiency varied from 32.8% to 10.2% and from 37% to 61.6% for SSOEP-DWR-BS and SSOEP-DWR-DWS baths respectively. It was observed that for SSOEP-DWR-DWS baths the inefficiency profiles were similar to the trends discussed in Section 1(d). However, contradictory trend was observed for SSOEP-DWR-BS baths. This might be due to significant surfactant adsorption on the surface at prolonger plating time periods, which enhanced metal adhesion to the substrate surface and minimized pitting and metal nucleation in the solution. It is further interesting to note that stronger nickel film adhesion to the substrate surface could be explored further to deposit a different metal (Pt or Pd) and hence provides promising opportunities to explore further.

3.4. Tradeoffs

3.4.1. PPD/Metal film thickness profiles

Fig. 13 illustrates the variation of $\frac{PPD}{\delta}$ with plating time for various combinations of SIEP and SSOEP baths. It can be observed that $\frac{PPD}{\delta}$ varied from 7.9 to 7.3, 8 to 8.1, 3.1 to 5 and 10.5 to 8.8 for a plating time variation from 2 to 8 h for SIEP-DWR-BS, SIEP-DWR-DWS, SSOEP-DWR-DWS and SSOEP-DWR-BS baths respectively. In general, an efficient electroless plating process must provide faster

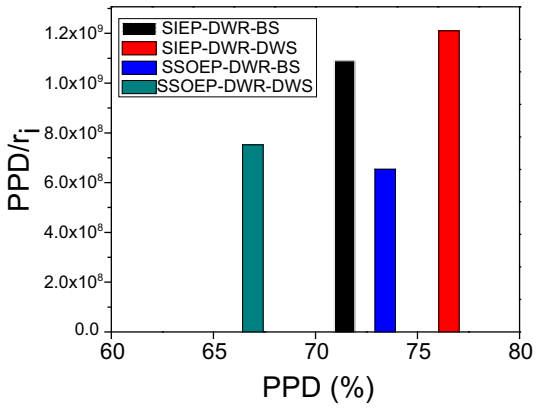

Fig. 14. Variation of PPD/plating rate with plating time for SSOEP and SIEP baths.

pore densification with minimal metal film thickness i.e. higher $\frac{PPD}{\delta}$ values. From $\frac{PPD}{\delta}$ perspective, the most promising option is SSOEP-DWR-BS baths and the most unfavorable process is SSOEP-DWR-DWS baths. An undesired feature of reduction in $\frac{PPD}{\delta}$ as observed for SIEP-DWR-BS baths could be due to the fact that PPD and δ did not enhance simultaneously. In this scenario, metal layering was significant in comparison with the PPD which might be due to the strong surfactant adsorption on the surface due to its bulk addition.

3.4.2. PPD/Plating rate profiles

Fig. 14 is a conceptual extension of the experimental findings to observe clear distinction between metal layering and pore densification in terms of PPD vs. $\frac{PPD}{\bar{r}_i}$. Hypothetically, $\frac{PPD}{\bar{r}_i}$ is a measure to quantify the dominance of pore densification or layering. Higher value of $\frac{PPD}{\bar{r}_i}$ for similar time of plating signifies that the plating favors better PPD and a lower $\frac{PPD}{\bar{r}_i}$ refers to significant layering. As observed, all cases of SSOEP baths provided lower $\frac{PPD}{\bar{r}_i}$ thereby indicating that sonication provided metal layering which is in agreement with the literatures [15,16]. For a process to be suitable for commercialization, it is very important that the plating is favorable towards pore densification but not metal layering. Thus SIEP-DWR-DWS baths were the best amongst the four modified electroless techniques in terms of PPD but not layering. Thus depending on objectives and priorities the processes could be deployed. For cases were layering effect is required (For example interdiffusion barriers), SSOEP could be recommended.

In summary, the process modification approach presented in this work can be used as a new methodology for the assessment of nickel electroless plating baths with desired morphological parameters. The experimental research findings in this work extend the conclusions presented by Kathirgamanathan [14] for SOEP baths and Islam et al. [20] for SIEP baths. While Kathirgamanathan [14] inferred that SOEP baths enable enhancing the metal film thickness on the membrane surface, the SSOEP baths with suggested variation (dropwise addition of reducing agent) reduces the metal film thickness along with the enhancement in PPD. On the other hand, while Islam et al. [20] inferred that the utilization of surfactant enhances plating rate and therefore reduce required total plating time for desired thickness, this work indicated that the dropwise addition of the reducing agent and surfactant in the SIEP simultaneously enhanced plating rate and reduced metal film thickness, which is the most relevant characteristic for metal composite membrane fabrication.

3.4.3. Summary

In conclusion, the optimal order of various baths from the perspective of various desired process characteristics is presented as follows

(a) Maximization of PPD: SIEP-DWR-DWS > SSOEP-DWR-BS > SIEP-DWR-BS > SSOEP-DWR-DWS.
(b) Maximization of $\frac{PPD}{\delta}$: SSOEP-DWR-BS > SIEP-DWR-DWS > SIEP-DWR-BS > SSOEP-DWR-DWS
(c) Maximization of $\frac{PPD}{\bar{r}_i}$: SIEP-DWR-DWS > SIEP-DWR-BS > SSOEP-DWR-DWS > SSOEP-DWR-BS
(d) Maximization of η: SSOEP-DWR-BS > SIEP-DWR-DWS > SSOEP-DWR-DWS > SIEP-DWR-BS.

Typically, during dense metal composite membrane fabrication, case (a) or case (b) are preferred and therefore, the suggested modifications to SIEP and SSOEP baths assume paramount relevance and need to be more thoroughly investigated from the perspective of process scale up and large scale fabrication.

4. Conclusions

The chemistry involving the interaction between surfactant, metal and reducing agent appears to be highly complex. This work gives good number of insights with respect to possible modification to metal ELP for metal composite membrane fabrication. Inferences drawn from this work are presented as follows:

(a) By adopting a controlled mechanism of reducing agent addition, the total plating time was reduced by 50% in comparison to our earlier work [16,17] without compromising upon the quality of plating.
(b) SIEP-DWR-DWS baths performed better than SIEP-DWR-BS baths which indicates that stronger adsorption of surfactant molecules in the latter case hindered pore densification.
(c) SSOEP-DWR-BS baths performed better than SSOEP-DWR-DWS baths which indicates that cavitation is useful only when surfactant addition has been facilitated in bulk mode, which is a very important inference.

Thus the most viable options for metal electroless plating process for maximizing $\frac{PPD}{\delta}$, PPD, and $\frac{PPD}{\bar{r}_i}$ are SSOEP-DWR-BS, SIEP-DWR-DWS, and SIEP-DWR-DWS baths respectively. This indicates that the cavitation effect induced by a sonicator bath is comparatively effective to achieve thin dense metal films on ceramic supports which are not the case for SIEP baths. This being the most important inference of this article thereby requires furthering studies towards the scale up and cost effective sonication assisted fabrication of dense metal composites membranes.

Acknowledgements

This work is partially supported by a grant from the DST (Department of Science and Technology) New Delhi. Any opinions, findings and conclusions expressed in this paper are those of the authors and do not necessarily reflect the views of DST, New Delhi. Special thanks to Central Instruments Facility (CIF) section of IIT Guwahati for analyzing our FESEM samples.

References

[1] M.E. Ayturk, Y.H. Ma, Electroless Pd and Ag deposition kinetics of the composite Pd and Pd/Ag membranes synthesized from agitated plating baths, J. Membr. Sci. 330 (2009) 233–245.
[2] S.E. Nam, K.H. Lee, A study on the palladium/nickel composite membrane by vacuum electrodeposition, J. Membr. Sci. 170 (2000) 91–99.
[3] I. Haas, A. Gedanken, Sonoelectrochemistry of Cu2+ in the presence of cetyltrimethylammonium bromide: obtaining CuBr instead of copper, Chem. Mater. 18 (2006) 1184–1189.
[4] B.H. Chen, L. Hong, Y.H. Ma, T.M. Ko, Effects of surfactants in an electroless nickel – plating bath on the properties of Ni–P alloy deposits, Ind. Eng. Chem. Res. 41 (2002) 2668–2678.
[5] V.K. Bulasara, M.S. Abhimanyu, T. Pranav, R. Uppaluri, M.K. Purkait, Performance characteristics of hydrothermal and sonication assisted electroless plating baths for nickel–ceramic composite membrane fabrication, Desalination 284 (2012) 77–85.
[6] O. Altinisik, M. Dogan, G. Dogu, Preparation and characterization of palladium-plated, porous glass for hydrogen enrichment, Catal. Today 105 (2005) 641–646.
[7] M. Soloviev, A. Gedanken, Coating a stainless steel plate with silver nanoparticles by the sonochemical method, Ultrason. Sonochem. 18 (2011) 356–362.
[8] Z.J. Wu, S.H. Ge, M.H. Zhang, W. Li, K.Y. Tao, Synthesis of nickel nanoparticles supported on metal oxides using electroless plating: controlling the dispersion and size of nickel nanoparticles, J. Colloid Interface Sci. 330 (2009) 359–366.
[9] N.O. Nwosu, A.M. Davidson, C.S. Hindle, Effect of sodium dodecyl sulphate on the composition of electroless nickel–yttria stabilized zirconia coatings, Adv. Chem. Eng. Sci. 1 (2011) 118–124.
[10] R. Elansezhian, B. Ramamoorthy, P.K. Nair, Effect of surfactants on the mechanical properties of electroless (Ni–P) coating, Surf. Coat. Technol. 203 (2008) 709–712.

[11] R. Elansezhian, B. Ramamoorthy, P.K. Nair, The influence of SDS and CTAB surfactants on the surface morphology and surface topography of electroless Ni–P deposits, J. Mater. Process Technol. 209 (2009) (2009) 233–240.
[12] N. Nwosu, A. Davidson, C. Hindle, M. Barker, On the influence of surfactant incorporation during electroless nickel plating, Ind. Eng. Chem. Res. 51 (2012) 5635–5644.
[13] K. Zielinska, A. Stankiewicz, I. Szczygiel, Electroless deposition of Ni-P-nano-ZrO2 composite coatings in the presence of various types of surfactants, J. Colloid Interface Sci. 377 (2012) 362–367.
[14] P. Kathirgamanathan, Ultrasound-assisted electroless deposition of copper onto and into microporous membranes for electromagnetic shielding, Polymer 35 (1994) 430–432.
[15] Y.X. Lu, Improvement of copper plating adhesion on silane modified PET film by ultrasonic-assisted electroless deposition, Appl. Surf. Sci. 256 (2010) 3554–3558.
[16] A. Agarwal, M. Pujari, R. Uppaluri, A. Verma, Preparation, optimization and characterization of low cost ceramics for the fabrication of dense nickel composite membranes, Ceram. Int. 39 (2013) 7709–7716.
[17] A. Agarwal, M. Pujari, R. Uppaluri, A. Verma, Optimal electroless plating rate enhancement techniques for the fabrication of low cost dense nickel/ceramic composite membranes, Ceram. Int. 40 (2014) 691–697.
[18] Y. Mizukoshi, E. Takagi, H. Okuno, R. Oshima, Y. Maeda, Y. Nagata, Preparation of platinum nanoparticles by sonochemical reduction of the Pt(IV) ions: role of surfactants, Ultrason. Sonochem. 8 (2001) 1–6.
[19] K. Yang, Z.L. Yi, Q.F. Jing, R.L. Yue, W. Jiang, D.H. Lin, Sonication-assisted dispersion of carbon nanotubes in aqueous solutions of the anionic surfactant SDBS: the role of sonication energy Chinese sci, Bull. 58 (2013).
[20] M.S. Islam, M.M. Rahman, S. Ilias, Characterization of Pd–Cu membranes fabricated bysurfactant induced electroless plating (SIEP) for hydrogen separation, Int. J. Hydrogen Energy 37 (2012) 3477–3490.
[21] Y.S. Cheng, K.L. Yeung, Effects of electroless plating chemistry on the synthesis of palladium membranes, J. Membr. Sci. 182 (2001) 195–203.
[22] Z. Li, C. Han, Reduction of Ni^{2+} by hydrazine in solution for the preparation of nickel nano-particles, J. Mater. Sci. 41 (2006) 3473–3480.
[23] V.K. Bulasara, H. Thakuria, R. Uppaluri, M.K. Purkait, Effect of process parameters on electroless plating and nickel–ceramic composite membrane characteristics, Desalination 268 (2011) 195–203.
[24] K.S.W. Sing, D.H. Everett, R.A.W. Haul, L. Moscou, R.A. Pierotti, J. Rouquerol, T. Siemieniewska, Reporting physisorption data for gas solid systems with special reference to the determination of surface-area and porosity, Pure Appl. Chem. 57 (1985) 603–619.
[25] M. Kitiwan, D. Atong, Effects of porous alumina support and plating time on electroless plating of palladium membrane, J. Mater. Sci. Technol. 26 (2010) 1148–1152.

Subject: Your Application No.612/KOL/2014
From: "Sharana basava" <sharaniitg@gmail.com>
Date: Thu, June 5, 2014 4:58 pm
To: "Rama Uppaluri" <ramgopalu@iitg.ernet.in>
Priority: Normal
Options: View Full Header | View Printable Version | Download this as a file | Add to Address Book | View Message Details | View as plain text

Dear Dr.Uppaluri,
This is to inform you that your application for grant of Patent has been filed successfully. Application Number: **612/KOL/2014 dated 05.06.2014**.

Please see the attached acknowledgement

Regards
Sharan

Attachments:

untitled-[1.1]	**0.2 k**	[text/plain]	Download | View
612KOL2014 Acknowledgement.pdf	**200 k**	[application/pdf]	Download
printCBR Form-26.pdf	**194 k**	[application/pdf]	Download

TH-1330_10610717

Welcome SHARANABASAVA Sign out

PATENT OFFICE
INTELLECTUAL PROPERTY BUILDING
CP-2, Sector V, Salt Lake City, Kolkata-700091
Tel No. (091)(033) 23671945-46 Fax No. 033 23671988
E-mail: kolkata-patent@nic.in
Web Site: www.ipindia.gov.in

सत्यमेव जयते

INTELLECTUAL PROPERTY INDIA
PATENTS | DESIGNS | TRADE MARKS
GEOGRAPHICAL INDICATIONS

Docket No 7014

Date/Time 05/06/2014 14:49:33

To
SHARANABASAVA

496, Udyog Vihar, Phase-III

User Code: sharan

Sr. No.	Ref. No./Application No.	App. Number	Amount Paid	C.B.R. No.	Fee Payment	Remarks
1	612/KOL/2014	612/KOL/2014	1760	6449	Full	Composition and Method for Dense Palladium Ceramic Composite Membrane Fabrication
2	2209/RQ-KOL/2014	612/KOL/2014	4000	6449	Full	Composition and Method for Dense Palladium Ceramic Composite Membrane Fabrication

Total Amount : ₹ 5760
Amount in Words: Rupees Five Thousand Seven Hundred Sixty Only

Print

Home About Us Contact Us

TH-1330_10610717

Welcome SHARANABASAVA Sign out

PATENT OFFICE
INTELLECTUAL PROPERTY BUILDING
CP-2, Sector V, Salt Lake City, Kolkata-700091
Tel No. (091)(033) 23671945-46 Fax No. 033 23671988
E-mail: kolkata-patent@nic.in
Web Site: www.ipindia.gov.in

सत्यमेव जयते

INTELLECTUAL PROPERTY INDIA
PATENTS | DESIGNS | TRADE MARKS
GEOGRAPHICAL INDICATIONS

Docket No 7015

Date/Time 05/06/2014 15:02:17

To
SHARANABASAVA

496, Udyog Vihar, Phase-III

User Code: sharan

Sr. No.	Ref. No./Application No.	App. Number	Amount Paid	C.B.R. No.	Fee Payment	Remarks
1	E-45/11/2014/KOL	612/KOL/2014	0	-----	Full	

Total Amount : ₹ 0
Amount in Words: Rupees Only

Print

Home About Us Contact Us

TH-1330_10610717

FORM-2

THE PATENTS ACT, 1970
THE PATENTS RULES, 2003

COMPLETE SPECIFICATION

Composition and Method for Dense Palladium Ceramic Composite Membrane Fabrication

Amrita Agarwal, Murali Pujari, Ramagopal Uppaluri & Anil Verma
Department Of Chemical Engineering
INDIAN INSTITUTE OF TECHNOLOGY GUWAHATI
GUWAHATI – 781039, ASSAM
INDIA

The following specification particularly describes and ascertains the nature of this invention and the manner in which it is to be performed

Applied Surface Science 320 (2014) 52–59

Contents lists available at ScienceDirect

Applied Surface Science

journal homepage: www.elsevier.com/locate/apsusc

A novel method of reducing agent contacting pattern for metal ceramic composite membrane fabrication

Amrita Agarwal, Murali Pujari, Ramgopal Uppaluri*, Anil Verma

Department of Chemical Engineering, Indian Institute of Technology Guwahati, Guwahati, –781039, Assam, India

ARTICLE INFO

Article history:
Received 24 June 2014
Received in revised form 4 September 2014
Accepted 6 September 2014
Available online 16 September 2014

Keywords:
Surfactant
Electroless plating
Reducing agent
Densification
Ceramic

ABSTRACT

Deliberating upon process modifications for surfactant induced electroless plating (SIEP), this article highlights the plating bath performance characteristics for two distinct reducing agent contacting modes (bulk and drop wise). Eventually, the effect of reducing agent concentration (50, 100, 200% excess) suitable for electroless plating bath for a nickel concentration of 0.08 mol/L was investigated. Finally, the compatibility of variation in nickel concentration (0.08–0.24 mol/L) with respect to variation in reducing agent concentration (50, 100, 200% excess) was investigated. LPSA, BET, FTIR, XRD, FESEM and nitrogen permeation experiments were used for surface and physical characterization. It was observed that for the bulk addition of reducing agent, the PPD values were 84.5% which increased to 89.3% for dropwise addition case. Thus the optimal combinations of SIEP process parameters were identified as 0.08 mol/L of nickel metal solution concentration with 100% excess drop-wise reducing agent. These conditions provided a plating rate of 5.5×10^{-5} mol/m^2 s, PPD of 89.3% and a metal film thickness of 15.7 μm respectively after 12 h of sequential plating.

1. Introduction

With the characteristic features of better corrosion and wear resistance, nickel electroless plating received significant industrial applications. The autocatalytic nickel electroless plating process suffers with the basic disadvantage of lower rates of deposition (1.5 μm h^{-1}) and hence rate transfer enhancements to supplement the regular electroless plating process have been addressed recently. These refer to membrane agitation [1], gas sparging [2], vacuum [3], sonication [4], hydrothermal [4] and surfactants [5].

Amongst these techniques, surfactant and sonication techniques are highly attractive from the perspective of ease of implementation and process scale up. Further, amongst these two, surfactant induced electroless plating is the most preferred due to lower energy requirements and cost. Conceptually, the usage of surfactant is beneficial in two ways. Firstly, in a surfactant induced electroless plating (SIEP) process, the surfactant reduces the interfacial tension between the generated gas bubble and plating solution which enables the generation of smaller bubbles on the surface and thus minimizes the pitting effect. Secondly, faster gas bubble removal from the surface (that is facilitated because of the generation of smaller bubbles and low interfacial tension), and cationic surfactants taking part in the chemical reaction due to active sites that participate in the plating reaction, promotes better plating characteristics [6–8].

For the fabrication of nickel-ceramic composite membranes [9], the primary emphasis is towards controlling the film characteristics to achieve the desired combinatorial parameters. For the SIEP process, while plating rates could be enhanced by increasing the concentrations of reducing agent, surfactant [10] and metal ions [11] in the plating solution, the quality of plating would significantly reduce at higher concentrations of these and an optimal combination exists that favors simultaneously achieving higher combinations of plating efficiency and pore densification. Further, higher concentration of reducing agent [12] is as well disadvantageous towards optimizing metal film characteristics.

The addition of reducing agent to an electroless plating process is similar to the current density utilized in an electroplating process. Conceptually, the plating behavior of an efficient SIEP process attempts to resemble that of the pulse electrodeposition technique, where the current density is highly programmed to achieve nano-structured metal deposition [13]. Considering the fact that electrodeposition techniques could not be efficiently applied for non-conducting surfaces, it is very important to conceive various process modifications to the surfactant enhanced electroless plating process to substantially improve both process and plating characteristics.

* Corresponding author. Tel.: +91 361 2582260; fax: +91 361 2582291.
E-mail address: ramgopalu@iitg.ernet.in (R. Uppaluri).

http://dx.doi.org/10.1016/j.apsusc.2014.09.036
0169-4332/

Nomenclature

A_m	Permeable area of the membrane, m^2
Q	Volumetric flow rate, m^3/s
P_2	Membrane pressure at permeate side, Pa
ΔP	Trans-membrane pressure drop, Pa
d_p	Average pore size, μm
(ε/q^2)	Effective porosity
J	Flux through the membrane, mol/m^2 s
$\bar{J}$	Average flux through the membrane, mol/m^2 s
i	Hour of nickel plating (as exponent)
$\bar{J}_0$	Average flux through the support, mol/m^2 s
$\bar{J}_i$	Average flux through the membrane after ith hour of nickel plating, mol/m^2 s
C_i	Initial concentration of Ni^{2+} in the plating solution, mol/L
C_f	Average Ni^{2+} solution concentration after plating, mol/L
x	Conversion
η	Plating efficiency, %
w_0	Dry weight of the membrane before plating, g
w_i	Dry weight of the membrane after ith hour of plating, g
w	Total amount of nickel originally available in the plating bath, g
n	Number of plating cycles
V_0	volume of plating solution in each plating cycle, L
M_{Ni}	Molecular weight of nickel metal, g/mol
ρ_{Ni}	Density of nickel metal, g/cm^3
$\bar{r}_i$	Plating rate, mol/L s
t_i	Time of plating for the ith hour, h
PPD	Percent pore densification, %
ELP	Electroless plating
CEP	Conventional electroless plating
SIEP	Surfactant induced electroless plating
SIEP-BR-BS	Surfactant induced electroless plating-bulk reducing agent-bulk surfactant
SIEP-DWR-BS	Surfactant induced electroless plating-dropwise reducing agent-bulk surfactant

It is well known that reducing agents such as hydrazine are heat sensitive and disintegrate within a short span of time, when they are brought in contact with the hot plating solution [12]. In addition to this, enhanced metal nucleation in the solution due to metal delamination from the substrate surface substantially contributes to poor metal deposition efficiency and the availability of excess hydrazine in the solution further deteriorates the quality of plating [12]. Along with these physical insights, it is further difficult to conceive the optimality of the contacting pattern of the reducing agent and ionic metal in a solution in the presence of a surfactant. Amongst several process alternatives, the controlled addition of reducing agent during SIEP process is an important option which did not receive research emphasis till date.

In the literature, while SIEP has been studied significantly for stainless steel supports and palladium deposition [14] with nickel inter diffusion barriers [15], SIEP studies towards nickel composite membranes have not been addressed for ceramic supports. Such studies are also required from a processing perspective as well, given the fact that stainless steel membranes are significantly expensive than ceramic membranes and the utilization of low cost ceramic membranes could pave the way for faster research commercialization and scale up. On the other hand, the plating characteristics of metal deposition on ceramic supports is distinct from metal (nickel/palladium) deposition on a metal (stainless steel) surface, owing to the fact that the plating rate is significantly influenced with the type of support and metal supports provide higher plating rate for Ni/Pd.

In summary, this work addresses two major objectives. Firstly, it elaborates upon the performance characteristics of SIEP processes supplemented with drop wise addition of the hydrazine as reducing agent. Secondly, it targets towards optimizing the quantity of the reducing agent and metal concentration in an SIEP process (in terms of % excess) for the optimal membrane fabrication. The bias towards the selection of optimal SIEP process parameters are maximum combinations of pore densification, conversions, plating rates and efficiency to achieve minimal metal film thickness.

2. Experimental

2.1. Raw materials

The raw materials used for the fabrication of ceramic membrane substrates are kaolin, feldspar, quartz, sodium carbonate, pyrophyllite, boric acid and sodium metasilicate. Kaolin was obtained from CDH Ltd., India; feldspar and pyrophyllite from National Chemicals, India; quartz from Research-lab Fine Chem Industries, India; sodium metasilicate from SD Fine-Chem Ltd., India and the other inorganic precursors (sodium carbonate and boric acid) were obtained from Merck Ltd., India. Composition of various above mentioned raw materials with their major functional attributes is presented in Table 1.

2.2. Membrane preparation and characterization

Laboratory fabricated circular ceramic substrates with a diameter of 36 mm and a thickness of 3.5 mm was used as supports in this work. The fabrication methodology consists of the following hierarchical steps: mixing of raw materials to make a paste; casting of the paste into circular moulds; drying of the raw discs; sintering; polishing of the membranes and ultrasonically cleaning. All membranes were prepared by sintering at 900 °C with a controlled heating/cooling rate (1.5 °C/min). The substrates were fabricated at pressure of 4.9 MPa using a hydraulic press (Make–Velan Engineering) using the dry compaction method. The sintered membrane support possessed a pore size d_p^{sup} and effective porosity (ε/q^2) of about 200 nm and 10–15% as evaluated from nitrogen permeation data respectively. Such lower combinations of pore size and porosity were opted because experimentally it has been reported that membranes with similar pore size and porosity are favorable for metal plating [16]. A detailed summary of the prepared membranes and the operating parameters are as listed in Table 2.

Surface and physical characterization were performed using several techniques. Laser particle size analysis (LPSA) (Make: Malvern; Model: Mastersizer 2000, UK) was carried out to evaluate the average particle size of the raw material. Fourier transform

Table 1
Composition of raw material along with their functional attributes.

Material	Composition (wt.%)	Functional attributes
Kaolin	40	Low plasticity and high refractory properties
Feldspar	15	Improves chemical and physical stability
Quartz	15	Mechanical and thermal stability
Na_2CO_3	10	Pore forming agent and colloidal agent
Pyrophyllite	10	Increased fired strength and reduced shrinkage
Boric acid	5	Colloidal agent and increases mechanical strength
Sodium metasilicate	5	Binding agent

Table 2
Membranes investigated along with variation of plating parameters.

Membrane no.	Reducing agent (%Excess)	Method of contacting	Nickel concentration (mol/L)	Abbreviated name
M_1	100	Bulk	0.08	SIEP-BR-BS
M_2	100	Drop wise	0.08	SIEP-DWR-BS
M_3	50	Drop wise	0.08	SIEP-DWR-BS
M_4	200	Drop wise	0.08	SIEP-DWR-BS
M_5	50	Drop wise	0.16	SIEP-DWR-BS
M_6	100	Drop wise	0.16	SIEP-DWR-BS
M_7	50	Drop wise	0.24	SIEP-DWR-BS
M_8	100	Drop wise	0.24	SIEP-DWR-BS

infrared spectroscopy (FTIR) analysis was conducted to record the characteristic peaks of various raw materials (Make: Shimadzu Corporation). The Brunauer–Emmett–Teller (BET) surface area and pore size of the support material was determined by N_2 adsorption desorption isotherm at 77 K by using a surface area analyzer (Make: Beckman-Coulter; Model: SA3100). X-ray diffraction (XRD) analysis of the inorganic substrate and metal membrane was conducted to evaluate the extent of phase transformations (Make: Bruker). Field emission scanning electron microscopic (FESEM) study (Make: Oxford; Model: LEO 1430VP, UK) was carried out to analyze the presence of possible defects and estimate the membrane pore size. The estimation of average membrane pore size (d_{sup}) from FESEM micrographs was carried out using ImageJ software. Room temperature nitrogen permeation experiments were conducted to quantify the extent of pore densification using the experimental setup fabricated by Bulasara et al. [11].

2.3. Electroless plating

Prior to electroless nickel plating the substrates were sensitized and activated with palladium seeds. The activation produced small Pd catalytic sites dispersed uniformly on the surface serving as the nuclei for electroless nickel deposition. The optimized electroless Ni plating bath composition (as shown in Table 3) consisted of nickel sulfate as a source of nickel, hydrazine hydrate as an electron source, trisodium citrate as a stabilizer, cetyltrimethylammonium bromide (CTAB) as the cationic surfactant and sodium hydroxide as a pH maintaining agent respectively. Plating characteristics were investigated at a loading ratio of 203 cm^2/L, plating bath temperature of 80 °C, pH of 10–12 and 1/2 h of plating time for one plating step.

The reduction of Ni^{2+} by reducing agent hydrazine hydrate in solution comprises of the following three reactions [17]:

$$2Ni^{2+} + N_2H_4 + 4OH^- = 2Ni \downarrow + N_2 \uparrow + 4H_2O \quad (1)$$

$$N_2H_4 = N_2 \uparrow + 2H_2 \quad (2)$$

$$3N_2H_4 = N_2 \uparrow + 4NH_3 \uparrow \quad (3)$$

In the above reactions, reaction (1) occurs on the activated substrate surface and is desired. However, reactions (2) and (3) which correspond to decomposition and disproportionation respectively occur primarily in the plating solution and are undesired reactions. These reactions follow from the heat sensitivity and instability of hydrazine at the conditions of the metal electroless plating.

Table 3
Typical composition of surfactant induced nickel electroless plating baths.

S. No.	Component	Formula	Amount/Conditions
1.	Nickel sulfate	$NiSO_4{\cdot}7H_2O$	0.08, 0.16, 0.24 mol/L
2.	Hydrazine hydrate	$H_2NNH_2{\cdot}H_2O$	50, 100, 200% excess
3.	Trisodium citrate	$Na_3C_6H_5O_7{\cdot}2H_2O$	0.2 mol/L
4.	Sodium hydroxide	NaOH	10–12 (pH)
5	Cetyltrimethylammonium bromide	$(C_{16}H_{33})N(CH_3)_3Br$	g/L

Therefore, bulk addition of hydrazine is bound to provide lower selectivities towards reaction (1) when compared to reaction (2) and reaction (3) and hence controlled addition of hydrazine to the metal electroless plating baths is anticipated to enhance the selectivities towards reaction (1). Thus with efficient contacting pattern for the reducing agent, the time period for one plating step has been reduced to 30 min which was not the case in our earlier work [8]. Thus, the efficacy of reducing agent contacting pattern has been investigated for the following cases:

(a) **SIEP-DWR-BS baths:** The SIEP baths were modified with drop wise addition of reducing agent (DWR) and bulk addition of the cationic surfactant (BS).
(b) **SIEP-BR-BS baths**: For these cases, SIEP baths were supplemented with bulk addition of reducing agent (BR) and bulk addition of the cationic surfactant (BS).

2.4. Evaluation of plating characteristics

Parameters involved in evaluating the performance assessment of nickel plating include average trans-membrane flux $\bar{J}$, plating inefficiency, average plating rate ($\bar{r}_i$), metal film thickness (δ) and percent pore densification PPD(%). Details with respect to the equations for evaluating the combinatorial plating characteristics are discussed elsewhere [8].

3. Results and discussion

3.1. Structural characterization:

The particle size distribution curve of the raw materials evaluated from LPSA indicated that the particle size varied from 0.955 to 34.674 μm, 1.259–39.811 μm, 0.822–15.31 μm, 1.905–52.81 μm and 0.955–316.28 μm for kaolin, quartz, feldspar, sodium carbonate and pyrophylite respectively.

FTIR analysis (shown in Fig. 1) indicates the existence of the characteristic peaks of kaolin for the raw material and after sintering of the raw material mixture the corresponding peaks were assigned to C—H, C=C, Si—O—Al and Si—O bonds as discussed earlier in details [8].

Nitrogen adsorption–desorption experiment at 77 K performed by using a surface area analyzer for the substrate material confirmed the presence of meso and macro pores with no micropores. Type III isotherm with H_3 hysteresis loop were observed (Fig. 2) that indicates slit-shaped pores according to IUPAC [18]. The inset graph shows the desorption Barrett–Joyner–Halenda (BJH) pore size distribution of the substrate material. The BET surface area of support is 4.130 m^2/g and total pore volume is 0.0325 mL/g with no micro pore volume.

Fig. 3 presents the XRD patterns of raw material mixture, sintered ceramic support, and the nickel membranes fabricated with SIEP-BR-BS and SIEP-DWR-BS baths. 100% reducing agent concentration were used to prepare these membranes. ICDD-JCPDS database was used for the phase analysis of the diffraction profile.

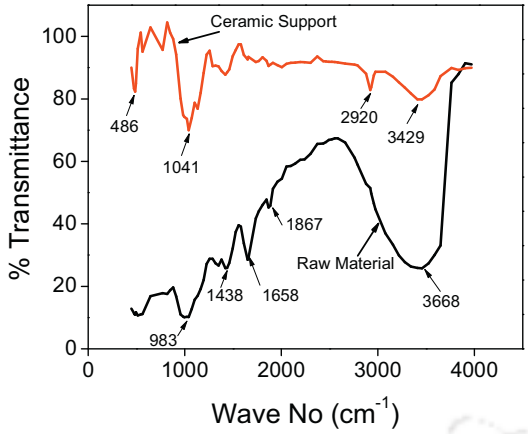

Fig. 1. FTIR spectral analysis of ceramic support and raw material.

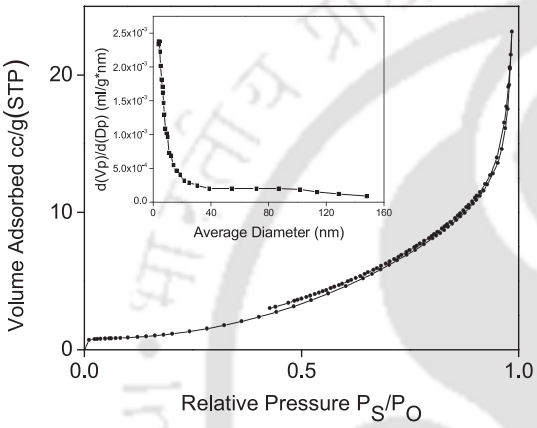

Fig. 2. Nitrogen adsorption–desorption isotherms of the substrate material. Inset: pore size distribution from BJH analysis.

As outlined in our earlier work [19], the XRD patterns for raw material mixture and sintered ceramic support (profiles A and B) in summary indicates: (a) the presence of phases for kaolin, quartz and sodium carbonate in the raw material mixture (b) the disappearance of the peaks corresponding to kaolin after sintering and (c) the appearance of nephiline phase after sintering.

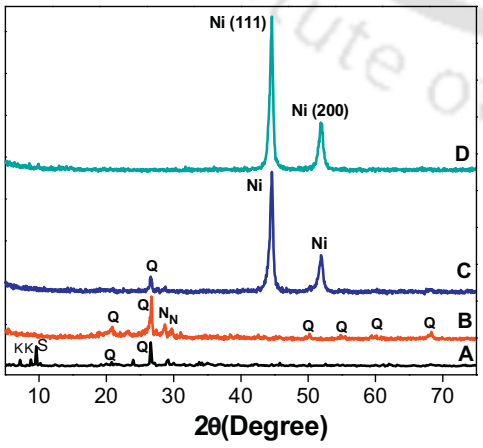

Fig. 3. XRD patterns for (i) A – raw material (ii) B – sintered support (iii) C – plating with bulk addition of reducing agent (iv) D – plating with drop-wise addition of reducing agent.
Where K – kaolin, S – sodium carbonate, Q – quartz, N – nephiline, Ni – nickel.

The metallic nickel peaks for electroless nickel plating with SIEP-BR-BS (profile C) and SIEP-DWR-BS baths (profile D) appeared at diffraction angle $2\theta = 44.5^\circ$ and 51.8° due to the diffraction of (1 1 1) and (2 0 0) plane [Pdf No 00-004-0850]. For plating with bulk wise addition of reducing agent it was observed that the peak intensity of quartz significantly decreased after nickel deposition due to plating of nickel on quartz particle thereby reducing the crystallinity of the quartz. But the quartz peak did not vanish completely suggesting poor densification and non-uniform plating. However this was not the case for nickel plating with drop wise addition of reducing agent. Diffraction profiles for drop wise addition of reducing agent (profile D) suggested simultaneous increase of nickel crystallinity as compared to profile C along with the formation of a uniform metal film. Thus from the XRD analysis it can be concluded that drop wise addition of reducing agent served better to promote uniformity of metal deposition on the substrate surface.

The surface FESEM micrographs of the ceramic support and the nickel layer deposited with an initial nickel sulfate concentration (C_i) of 0.08 mol/L are as shown in Fig. 4. It can be observed that well-developed nickel layers were existent for the membrane. Based on the ImageJ analysis of the FESEM image for the ceramic support, it was observed that the pores were distributed over wider pore size values and the average pore size of the support was found to be 300 nm which was close to that evaluated from nitrogen permeation (200 nm) respectively. FESEM images were in good agreement with XRD patterns which showed that dropwise addition of reducing agent gave better surface finish with agglomerates thereby providing the desired faster densification with lesser pinholes.

3.2. Efficacy of the contacting pattern of the reducing agent

Fig. 5 corresponds to the variation in the time dependent plating inefficiency and plating rate for SIEP-BR-BS and SIEP-DWR-BS baths during nickel electroless plating. The results presented in the figure correspond to the case of 0.08 mol/L nickel solution concentration, 100% excess reducing agent and 1.2 g/L of CTAB surfactant solution concentration. For a sequential nickel plating time of 12 h, the plating inefficiencies varied from 64 to 72% for the SIEP-BR-BS case (M_1), which reduced significantly to 46.9–52.2% SIEP-DWR-BS case (M_2). On the other hand, the average plating rate varied from 3.8 to 0.85×10^{-7} mol/L s for M_1 which enhanced to $5.7–0.94 \times 10^{-7}$ mol/L s for M_2 thus indicating that drop wise addition of the reducing agent enhances plating rate by about 1.5 times in comparison with the bulk addition case. Further for the plating time period in the range of 4–12 h, it was observed that the PPD for the M_1 membrane (SIEP-BR-BS) varied from 41 to 84.5%, which enhanced to 57.4–89.3% for the M_2 membrane (SIEP-DWR-BS). Hence, it can be inferred that the dropwise contacting pattern of the reducing agent reduced plating inefficiency and enhanced both plating rate and PPD, which are all desired features of an efficient ELP process.

The better performance of the SIEP-DWR-BS in comparison with the SIEP-BR-BS is due to the prolonged availability of electrons during the slow plating reaction in the former case due to continuous addition of the reducing agent, which favored better PPD. This indicates that during SIEP-DWR-BS, the removal of N_2 gas bubbles (reaction (1)) from the membrane surface did not provide significant delamination which in turn reduced metal nucleation in the solution (reactions (2) and (3)). On the other hand, during SIEP-BR-BS, the decomposition of hydrazine available at higher solution concentrations favored poor metal deposition on the membrane surface and greater metal nucleation in the solution.

The observed data trends for the SIEP-DWR-BS are in agreement with that provided by Yeung et al. [20] who also inferred that metal nucleation reduced with phase wise addition of the reducing agent.

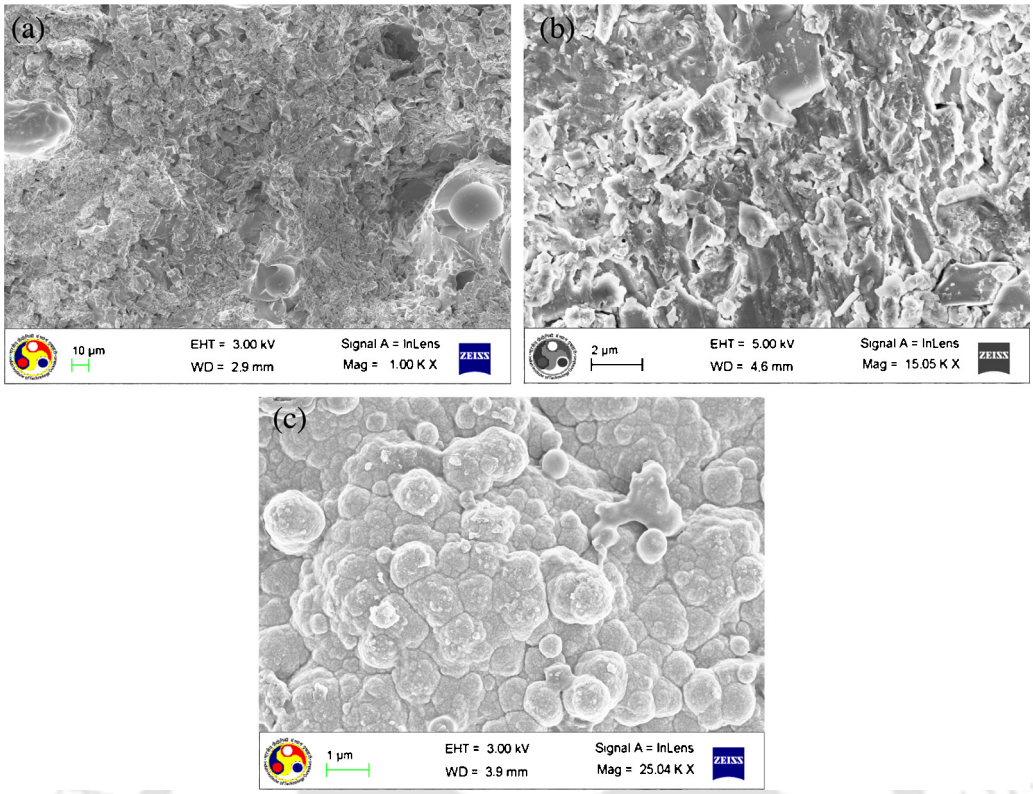

Fig. 4. Surface FESEM micrographs of (a) ceramic support (b) membrane with bulk addition of 100% excess reducing agent (c) membrane with drop wise addition of 100% excess reducing agent.

The next section elaborates upon the effect of excess reducing agent concentration for the SIEP-DWR-BS baths.

3.3. Optimality of reducing agent concentration

Fig. 6 illustrates the time dependent variation of nickel electroless plating characteristics namely plating inefficiency, plating rate, PPD and film thickness respectively for various cases of reducing agent concentration (50, 100 and 200% excess) with SIEP-DWR-BS baths. It was observed that, for 50% excess case (M_3), these parameters varied as 64–79.2% (plating inefficiency), 3.9–0.62 × 10^{-7} mol/L s (plating rate), 49.8–77.1% (PPD) and 7.3–10.6 μm (metal film thickness) respectively. Enhancing the reducing agent concentration to 100% excess (M_2) corresponds to the variation in these parameters as 46.9–52.2% (plating inefficiency), 5.7–0.94 × 10^{-7} mol/L s (plating rate), 57.4–89.3% (PPD) and 10.6–15.7 μm (film thickness). A further enhancement in the reducing agent concentration to 200% excess (M_4) corresponds to the variation in these parameters as 17–43.6% (plating inefficiency), 5.9–1.2 × 10^{-7} mol/L s (plating rate), 64.7–95% (PPD) and 10.9–20.2 μm (film thickness). For the case of 50% excess reducing agent, the nickel plating rate was low due to availability of less number of free electrons in the bath. This eventually resulted in lower metal deposition on the surface which could indicate an unstable nickel film. Thereby, the stronger bonding of the surfactant with the support could weaken the physical bonding of the metal and promote metal delamination [21], unwanted metal nucleation in the solution, and higher plating inefficiencies.

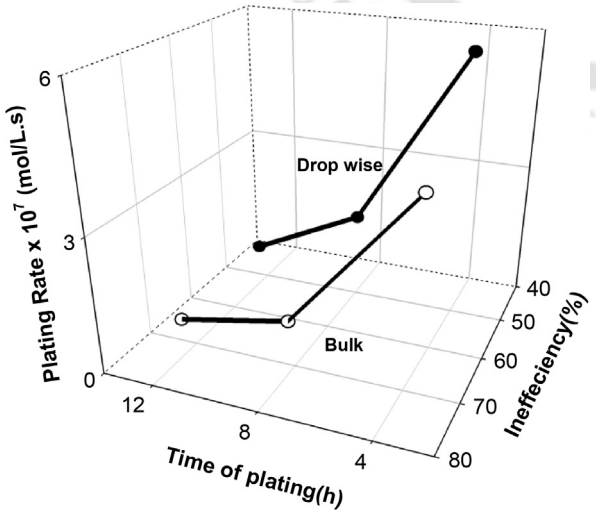

Fig. 5. A 3D graph showing time of plating vs. plating inefficiency vs. plating rate with 100% excess reducing agent (a) membrane with bulk addition of reducing agent (M_1) (b) membrane with drop wise addition of reducing agent (M_2).

However, for higher concentration of reducing agent (100% and 200% excess), nickel plating rates are significantly higher due to availability of greater number of free electrons for metal reduction in the surface. In such a scenario, the metal-support adhesion is high and the surfactant adsorption on the surface will not be able to promote pitting effect. Thereby, less metal nucleation in the solution occurs which translates into higher plating efficiencies.

The enhancement in plating efficiency with higher concentrations of reducing agent is indicative towards the complexity involved in the surface phenomena involved during SIEP. Typically in a conventional nickel electroless plating bath, higher concentrations of the reducing agent are not favorable to enhance the plating characteristics which is exactly opposite to the trends obtained in this work. Thus, the generalized rules of thumb that are often presented for regular electroless plating baths are not applicable for

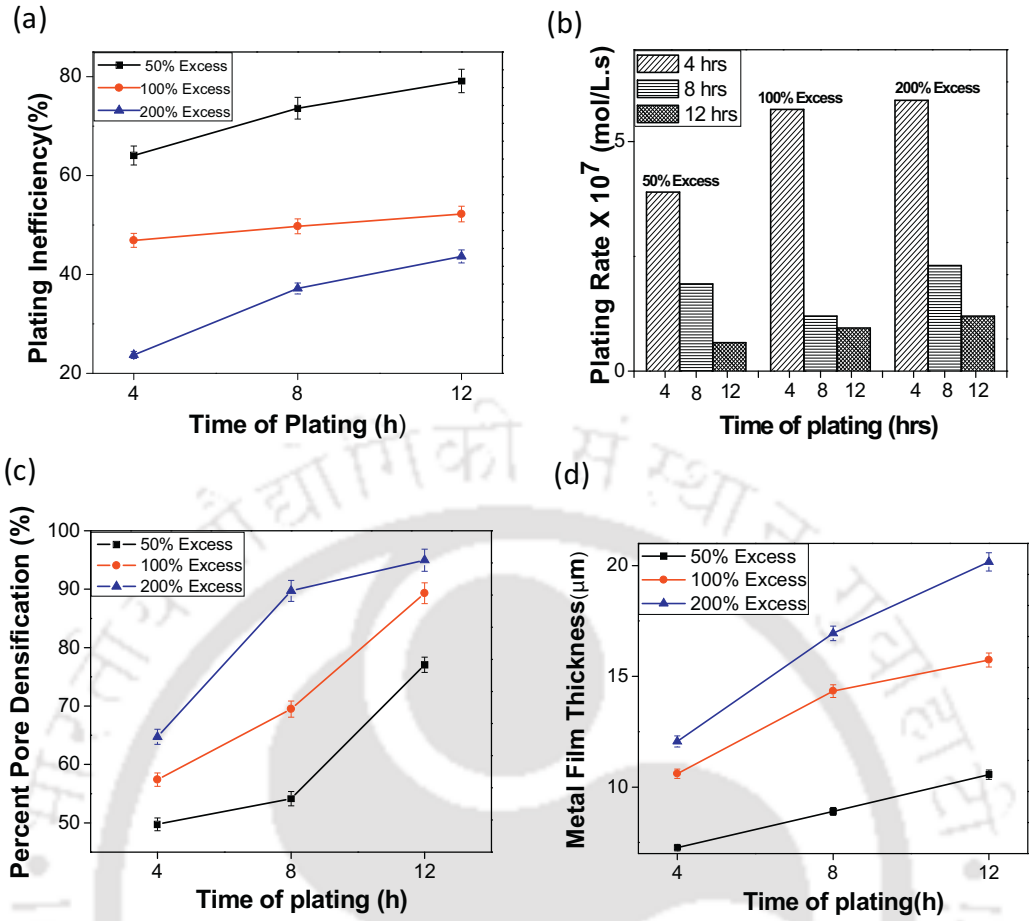

Fig. 6. For a nickel concentration of 0.08 mol/L variation of (a) plating inefficiency (b) metal plating rate (c) percent pore densification (PPD) (d) metal film thickness with variation in % excess of drop wise addition of reducing agent for different time of plating (M_2, M_3 and M_4).

the SIEP baths. The reduction of metal efficiency at lower reducing agent concentrations is solely attributed to the fact that for SIEP baths stronger metal-support adhesion is required to achieve desired plating characteristics. Thereby, these observations that have been verified at least twice indicate that the reducing agent concentration also needs to be studied with respect to its contribution towards the adhesion strength of the metal film during the nickel electroless plating.

With respect to the time dependency of several plating characteristic parameters, it can be observed for all cases, the variables namely plating inefficiency, PPD and thickness increased with increasing plating time. The film thickness was strongly affected with the variation in the concentration of reducing agent. It can be observed that the non-linearity in the variable variation is significant at highest concentration of the reducing agent (200% excess). An enhancement in the reducing agent concentration from 100 to 200% excess enabled significant enhancement in the film thickness by 22% with insignificant PPD enhancement of 5% after 12 h of plating. Therefore, it is apparent that 100% excess reducing agent concentration is the optimal choice due to the fact that the PPD variation is not significant for the case of 200% excess reducing agent concentration. It is anticipated that for the case of 100% excess reducing agent concentration, a further increment of plating time to 16 h gave a higher PPD (>94.9%) and lower metal film thickness (<20.2 μm). The reduction in the PPD at higher reducing agent concentrations (about 200% excess) is indicative to the fact that higher reducing agent concentrations do not favor pore densification and contribute to layering of films which is a highly undesired feature in the fabrication of dense metal composite membranes.

A comparison of observed plating characteristics with those available in the literature are presented as follows. Bulasara et al. [22] reported a plating rate of 7.6×10^{-6} mol/L s and a PPD of 91.1% for a high surfactant concentration (1.5 g/L) and a higher pore size of the support (275 nm). The optimal case in their work corresponds to a plating rate of 5.7×10^{-7} mol/L s and a PPD of 89.3% which is slightly lower than that reported by the authors, for the utilization of a support with a lower average pore size (200 nm) and lower surfactant concentrations (1.2 g/L) but with a controlled contacting pattern of the reducing agent. However, it shall be noted that the PPD calculation procedure reported in this work is better than that reported by Bulasara et al. [22], given the fact that they have evaluated PPD in terms of average pore size which is not the same as PPD evaluated with average flux.

3.4. Optimality of metal solution concentration

3.4.1. Plating in-efficiency tradeoffs

Table 4 summarizes the plating characteristics that correspond to various cases of nickel solution concentrations (0.08, 0.16 and 0.24 mol/L) and excess reducing agent concentrations (50, 100 and 200%). As presented, the plating inefficiencies for 0.08 mol/L nickel solution concentration varied from 64 to 79.2% for M_3 (50% excess), 46.9–52.2% for M_2 (100% excess), and from 17 to 43.6% for M_4 (200% excess). Similarly for 0.16 mol/L nickel solution concentration, plating inefficiencies varied from 48.1 to 54.6% for M_5 (50% excess), from 37.3 to 11.1% for M_6 (100% excess) and for 0.24 mol/L nickel solution concentration it varied from 68.5 to 82.8% for M_7 (50% excess) and 55.7–52.5% for M_8 (100% excess) respectively for 4–12 h

Table 4
Table showing a comparative study with variations in both process (metal and reducing agent concentration) and plating (inefficiency, rate, PPD, film thickness) parameters.

Reducing agent	50% excess			100% excess			200% excess		
Time of plating	4 h	8 h	12 h	4 h	8 h	12 h	4 h	8 h	12 h
Metal concentration	Plating inefficiency (%)								
0.08	64	73.6	79.2	46.9	49.7	52.2	17	37.2	43.6
0.16	48.1	51.5	54.6	37.3	33.4	11.1	–	–	–
0.24	68.5	78.6	82.8	55.7	54.2	52.5	–	–	–
	Plating rate $\times 10^7$ (mol/L s)								
0.08	3.9	1.2	0.62	5.7	1.9	0.94	5.9	2.3	1.2
0.16	5.5	2.4	1.4	6.7	2.5	1.3	–	–	–
0.24	11.2	3.4	1.8	12.9	5.6	3.4	–	–	–
	Percent pore densification (%)								
0.08	49.8	54.2	77.1	57.4	69.5	89.3	64.7	89.7	95.0
0.16	57.8	78.8	89.7	76	88	94.4	–	–	–
0.24	67.1	84.2	92.7	84.7	90	97.1	–	–	–
	Metal film thickness (μm)								
0.08	7.3	8.9	10.6	10.6	14.3	15.7	10.9	16.9	20.2
0.16	9.24	18.8	25.2	12.5	19	29.3	–	–	–
0.24	20.9	25.2	30.2	24.3	41.5	57.8	–	–	–

of nickel plating. This indicates that there exists an optimal metal solution concentration and excess reducing agent concentration that minimizes plating inefficiency. In general, all experimental data can be analyzed for five cases namely:

(a) **Case A:** Lower combinations of metal (0.08 mol/L) and reducing agent concentrations (50% excess).
(b) **Case B:** Moderately high metal concentration (0.16 mol/L) and lower reducing agent concentration (50% excess).
(c) **Case C:** Moderately high combinations of metal (0.16 mol/L) and moderate reducing agent concentration (100% excess).
(d) **Case D:** Higher metal concentration (0.24 mol/L) and moderate reducing agent concentration (100% excess).
(e) **Case E:** Moderate and high metal solution concentration (0.16 and 0.24 mol/L) and higher reducing agent concentration (200% excess).

The chemistry involving the interaction between surfactant, metal and reducing agent appears to be highly complex. For instance, when the nickel solution concentration is enhanced from 0.08 to 0.24 mol/L, it was observed that the plating inefficiency reduced from 49.7% (M_2) to 33.4% (M_6) which further increased to 54.2% (M_8) after 8 h of plating. Typically higher metal concentration enables higher combinations of plating rate, pitting, and nucleation and hence higher plating inefficiencies. Also, the variation in the reducing agent concentration alters the net amount of free electrons that are available for the reduction of metal ion both in the solution (unwanted) and on surface (desired).

The hypothesis for case A i.e. lower nickel solution concentration (0.08 mol/L) has already been addressed in our previous subsection. Further, for case B (0.16 mol/L, 50% excess) the plating inefficiency trends are in agreement with the trends observed for lower metal concentration. The only variation that was observed was in the reduction in the plating inefficiencies from 79.2% to 54.6%. This could be explained with the fact that at moderately higher metal concentration, the metal plating rate will be higher and surfactant adsorption to the support surface will not be able to control the surface bonding of the nickel metal, thereby reducing nucleation in solution and enhancing the plating efficiency.

Conceptually it is hypothesized that for a given metal and reducing agent concentration the plating inefficiency increases with time of plating. But for case C (0.16 mol/L Ni concentration and 100% excess reducing agent) it was observed that with time the plating inefficiencies decreased from 37.3% (4 h) to 11.1% (12 h). This is possibly due to compatibility of moderate concentrations of metal and reducing agent that favored metal deposition and adhesion on the support surface thereby minimizing metal delamination and eventually plating inefficiencies. Again for case D, (0.24 mol/L, 100% excess) it was observed that with time the plating inefficiencies decreased from 55.7% (4 h) to 52.5% (12 h) and the values were quite higher as compared to the previous case. This is due to the reason that at higher metal concentration the conversion of nickel ion to nickel metal is very fast due to the availability of large number of free electrons from the reducing agent [21]. Thus, faster metal deposition on the surface favors higher rates of metal delamination that enhances nucleation in the solution which has also been confirmed during the physical examination.

Lastly for case E (0.16 mol/L and 0.24 mol/L metal concentration, 200% excess reducing agent) data was not reported because of the fact that nickel precipitates were observed at the bottom and corners of the reaction vessel. At high concentrations of metal and reducing agents, the conversion of metal ion to metal on the substrate surface is very high. Thus the metal grains loosely adhered to the substrate provided maximum delamination from surface and metal nucleation in the solution and eventually higher plating inefficiency. At such higher metal conversions, the inability for surfactant to minimize nucleation and pitting and maximize PPD is evident due to the gas bubbles not being effectively removed from the substrate surface.

In summary, plating inefficiencies reduced with moderately high metal solution concentrations (0.16 mol/L) but not for higher metal concentrations (0.24 mol/L). This indicates the fact that the film stability and inefficient plating are strong functions of metal solution and reducing agent concentrations. Considering plating inefficiency as the sole tradeoff, the optimal case corresponds to 0.16 mol/L with 100% excess reducing agent that provided an inefficiency of 11.1% after 12 h of nickel plating.

3.4.2. Tradeoffs associated to membrane morphological parameters

In addition to the complexity in the plating inefficiency profiles, profiles for all other variables namely plating rate, PPD and metal film thickness increased with increasing metal solution and reducing agent concentrations. As presented in Table 4, the plating rates for 0.16 mol/L metal solution concentration varied from 5.5 to 1.4×10^{-7} mol/L s for M_5 (50% excess) and from 6.7 to 1.3×10^{-7} mol/L s for M_6 (100% excess). Similarly for a higher metal solution concentration of 0.24 mol/L the plating rate varied from 1.1 to 0.18×10^{-6} mol/L s for M_7 (50% excess) and from 1.3 to 0.34×10^{-6} mol/L s for M_8 (100% excess) respectively.

The efficient design of electroless plating process needs to visualize the maximum extent of pore densification with respect to minimum amount of metal required to densify the pores i.e. to achieve maximum PPD/δ value. It was observed that for 12 h of sequential deposition, for membrane M_2 (100% excess reducing agent and 0.08 mol/L metal solution concentration) the PPD was 89.3% with a metal film thickness of 15.7 μm, whereas for M_6 (100% excess reducing agent and 0.16 mol/L metal solution concentration) the PPD was 94.4% with a metal film thickness of 29.3 μm. Thus PPD/δ for M_2 is evaluated to be 5.7 whereas for M_6 it is 3.2 respectively. Thus for M_6, it was observed that for a little increment of PPD (5%) the metal film thickness increased 100% and therefore these conditions are not favorable from the process-product perspective. The insignificant enhancement in PPD with a significant enhancement in metal film thickness suggests the undesired feature of layering during membrane fabrication for the cases of moderate and higher metal concentrations. In conclusion, from the perspective of minimal metal film thickness for the desired PPD the optimal process parameters refer to lower nickel solution concentration (0.08 mol/L), moderate reducing agent concentrations (100% excess) along with suggested contacting pattern of the reducing agent in an SIEP process.

3.5. Conclusion

The process modification approach presented in this work can be used as a new methodology for the fabrication of dense nickel membranes with desired morphological parameters. The existing gap in the literature with respect to the role of reducing agent in affecting both nickel electroless process and membrane characteristics has been successfully addressed in this work. Several insights have been obtained with the combinatorial plating characteristics achieved for wider combinations of nickel solution (0.08–0.24 mol/L) and reducing agent (50–200% excess) which can be presented as follows:

1. The experiments successfully inferred that the time period of 1 h for a single plating step as reported in our earlier work [8,19] can be reduced by 50% by adopting SIEP-DWR-BS baths.
2. From the combinatorial perspectives of plating efficiency and PPD, the performance characteristics of SIEP-DWR-BS baths are significantly better than those obtained for SIEP-BR-BS.
3. The solution concentrations of lower nickel (0.08 mol/L) and reducing agent (100% excess) have been identified to be optimal from the perspective of the ratio of pore densification per unit metal film thickness.
4. The observed phenomena of lower plating efficiency with moderate nickel solution concentration (0.16 mol/L) and reducing agent (100% excess) needs further examination for the deposition of noble metals such as highly expensive metals such as Pd and Pt using ELP.
5. Based on the inferences drawn in this work as well as those presented in our earlier work for conventional (CEP), sonication assisted (SOEP) and surfactant induced (SIEP) ELP baths [8,19], the combinatorial plating characteristics of various baths is as per the following order: CEP-BR-BS < SOEP-BR-BS < SIEP-BR-BS < SIEP-DWR-BS.

The generalization of above inferences towards Pd composite membrane fabrication needs to be addressed in the near future. All in all, the addressed rigorous experimentation and methodology involving inexpensive nickel SIEP-DWR-BS baths provided several insights for the further improvement in the fabrication characteristics associated to low cost dense metal composite membranes.

Acknowledgments

This work is partially supported by a grant from the DST (Department of Science and Technology) (grant no. SR/S3/CE/070/2010) New Delhi. Any opinions, findings and conclusions expressed in this paper are those of the authors and do not necessarily reflect the views of DST, New Delhi. Special thanks to Central Instruments Facility (CIF) section of IIT Guwahati for analyzing our FESEM samples.

References

[1] M.E. Ayturk, Y.H. Ma, Electroless Pd and Ag deposition kinetics of the composite Pd and Pd/Ag membranes synthesized from agitated plating baths, J. Membr. Sci. 330 (2009) 233–245.
[2] O. Altinisik, M. Dogan, G. Dogu, Preparation and characterization of palladium plated porous glass for hydrogen enrichment, Catal. Today 105 (2005) 641–646.
[3] S.E. Nam, S.H. Lee, K.H. Lee, Preparation of a palladium alloy composite membrane supported in a porous stainless steel by vacuum electrodeposition, J. Membr. Sci. 153 (1999) 2163–2173.
[4] V.K. Bulasara, M.S. Abhimanyu, T. Pranav, R. Uppaluri, M.K. Purkait, Performance characteristics of hydrothermal and sonication assisted electroless plating baths for nickel–ceramic composite membrane fabrication, Desalination 284 (2012) 77–85.
[5] S. Ilias, M.A. Islam, Fabrication of Pd/Pd-alloy Films by Surfactant Induced Electroless Plating for H2 Separation from Advanced Coal Gasification Processes, Patent Application #20100068391 (USPTO assignment date: March 18, 2010).
[6] B.H. Chen, L. Hong, Y. Ma, T.M. Ko, Effects of surfactants in an electroless nickel–plating bath on the properties of Ni–P alloy deposits, Ind. Eng. Chem. Res. 41 (2002) 2668–2678.
[7] K. Zielinska, A. Stankiewicz, I. Szczygiel, Electroless deposition of Ni-P-nano-ZrO2 composite coatings in the presence of various types of surfactants, J. Colloid Interface Sci. 377 (2012) 362–367.
[8] A. Agarwal, M. Pujari, R. Uppaluri, A. Verma, Preparation, optimization and characterization of low cost ceramics for the fabrication of dense nickel composite membranes, Ceram. Int. 39 (2013) 7709–7716.
[9] S.K. Ryi, J.S. Park, S.H. Kim, S.H. Cho, J.S. Park, D.W. Kim, Development of a new porous metal support of metallic dense membrane for hydrogen separation, J. Membr. Sci. 279 (2006) 439–445.
[10] R. Elansezhian, B. Ramamoorthy, P.K. Nair, The influence of SDS and CTAB surfactants on the surface morphology and surface topography of electroless Ni–P deposits, J. Mater. Process. Technol. 209 (2009) 233–240.
[11] V.K. Bulasara, H. Thakuria, R. Uppaluri, M.K. Purkait, Effect of process parameters on electroless plating and nickel-ceramic composite membrane characteristics, Desalination 268 (2011) 195–203.
[12] Y.S. Cheng, K.L. Yeung, Effects of electroless plating chemistry on the synthesis of palladium membranes, J. Membr. Sci. 182 (2001) 195–203.
[13] K.J. Bryden, J.Y. Ying, Pulsed electrodeposition synthesis and hydrogen absorption properties of nanostructured palladium-iron alloy films, J. Electrochem. Soc. 145 (1998) 3339–3346.
[14] M.S. Islam, M.M. Rahman, S. Ilias, Characterization of Pd-Cu membranes fabricated by surfactant induced electroless plating (SIEP) for hydrogen separation, Int. J. Hydrogen Energy 37 (2012) 3477–3490.
[15] W.H. Lin, Y.C. Liu, H.F. Chang, Autothermal reforming of ethanol in a Pd-Ag/Ni composite membrane reactor, Int. J. Hydrogen Energy 35 (2010) 12961–12969.
[16] M. Kitiwan, D. Atong, Effects of porous alumina support and plating time on electroless plating of palladium membrane, J. Mater. Sci. Tech. 26 (2010) 1148–1152.
[17] Z. Li, C. Hun, Reduction of Ni^{2+} by hydrazine in solution for the preparation of nickel nano-particles, J. Mater. Sci. 41 (2006) 3473–3480.
[18] K.S.W. Sing, D.H. Everett, R.A.W. Haul, L. Moscou, R.A. Pierotti, J. Rouquerol, T. Siemieniewska, Reporting physisorption data for gas/solid systems with special reference to the determination of surface area and porosity, Pure Appl. Chem. 57 (1985) 603–619.
[19] A. Agarwal, M. Pujari, R. Uppaluri, A. Verma, Optimal electroless plating rate enhancement techniques for the fabrication of low cost dense nickel/ceramic composite membranes, Ceram. Int. (2013), http://dx.doi.org/10.1016/j.ceramint.2013.06.056.
[20] K.L. Yeung, S.C. Christiansen, A. Varma, Palladium composite membranes by electroless plating technique – relationships between plating kinetics, film microstructure and membrane performance, J. Membr. Sci. 159 (1–2) (1999) 107–122.
[21] N. Nwosu, A. Davidson, C. Hindle, M. Barker, On the influence of surfactant incorporation during electroless nickel plating, Ind. Eng. Chem. 51 (2012) 5635–5644.
[22] V.K. Bulasara, Ch.S.N. Mahesh Babu, R. Uppaluri, Effect of surfactants on performance of electroless plating baths for nickel-ceramic composite membrane fabrication, Surf. Eng. 28 (2012) 44–48.

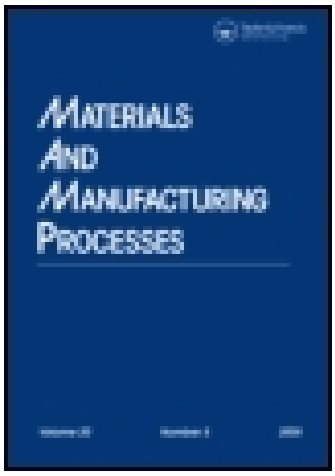

Materials and Manufacturing Processes
Publication details, including instructions for authors and subscription information:
http://www.tandfonline.com/loi/lmmp20

Efficacy of Palladium Solution Concentration on Electroless Fabrication of Dense Metal Ceramic Composite Membranes Coupled with Surfactant and Sonication

Amrita Agarwal[a], Murali Pujari[a], Ramgopal Uppaluri[a] & Anil Verma[a]
[a] Department of Chemical Engineering, Indian Institute of Technology Guwahati, Guwahati, Assam
Accepted author version posted online: 10 Nov 2014.

Efficacy of palladium solution concentration on electroless fabrication of dense metal ceramic composite membranes coupled with surfactant and sonication

Amrita Agarwal[1], Murali Pujari[1], Ramgopal Uppaluri[1], Anil Verma[1]

[1]Department of Chemical Engineering, Indian Institute of Technology Guwahati, Guwahati, Assam

Corresponding Author: Email: ramgopalu@iitg.ernet.in; ru.aissq@gmail.com

Abstract

This article addresses the effect of varying palladium solution concentration (0.005-0.015 mol/L) on the cost effective fabrication of dense palladium composite membranes. Laboratory fabricated clay (kaolin) based ceramic disc were used as substrate along with a modified electroless plating technique consisting of a coupled effect of ultrasound and surfactant. Further to increase the efficacy of the process controlled addition of reducing agent was opted for all baths. It was analyzed that the optimal concentration that provided higher plating efficiencies (95.9%), higher transport efficiency (41.3%), higher plating rates (1.5×10^{-4} mol/m^2.s), minimal total plating time (10.5 h) and maximum pore densification (99.7%) corresponds to 0.01mol/L.

KEYWORDS: Ceramic; Sonication; Surfactant; Electroless plating; Membrane

INTRODUCTION

With the rise of energy costs, membrane technology is growing up as an emerging field for the production of purified hydrogen due to continuous operation, scalability,

simplicity, modularity and reduced costs. Dense palladium composite membranes have been extensively studied due to their ability for higher H_2 separation capabilities.

The high cost of material and fabrication remains an important obstacle for commercialization, and drives research and innovation in membrane fabrication from certain perspectives. The significant reduction in dense Pd membrane cost can be targeted by (a) considering kaolin based ceramic membrane support (b) identifying and developing a rate enhanced Pd ELP process that utilizes minimal combinations of total plating time and total Pd precursor quantity.

Amongst all the support materials, ceramic membranes with their ability to endure high temperature and pressure conditions and lower cost make them a suitable option for industrial processes [1]. Further, amongst the ceramic membranes specifically natural clay based raw materials, kaolin is one of the cheapest membrane raw materials easily available in India.

The most important perspective for efficient fabrication of low cost palladium membranes is the usage of minimal metal concentration along with maximum utilization of the expensive metal. Fabrication efficacy should also take into account the amount of metal converted along with plating efficiency. Amongst the available literatures for dense palladium ceramic composite membrane fabrication, maximum of the studies are either directed towards high usage of palladium metal concentration or towards expensive fabrication technique.

Collins et al. in an U.S. Patent No. 5652020 A [1], adopted conventional electroless plating (CEP) at a Pd solution concentration of 0.03 mol/L to achieve 10 – 20 μm thick dense Pd composite membranes on tubular porous ceramic supports. Further, Rhoda Richard [2] in an U.S. Patent No. 3274022 A, adopted CEP process at a Pd solution concentration of 0.028 – 0.056 mol/L with asymmetric addition of dimethylhydrazine (concentration of 0.05 – 0.45 g/L) reducing agent.

Further, Ilias et al. [3] disclosed details with respect to CEP to achieve dense Pd ceramic membranes. For an alumina support pore size of 150 nm, the authors used a Pd solution concentration of 0.03 mol/L. Zhang Ke et al. [4] reported CEP supplemented with SDS anionic surfactant to be effective to achieve Pd composite membranes. On an α- alumina support of 270-280 nm average pore size, the authors used a Pd solution concentration of 0.189 mol/L to achieve a dense Pd metal film thickness of 2 μm after a total plating time of 8 – 12 h.

In a work by Islam et al. [5], the authors reported a Pd solution concentration of 0.015 mol/L and DTAB surfactant concentration of 4 CMC to achieve a dense Pd composite membrane. Based on the available literatures, one can conclude that higher Pd solution concentrations (0.03 – 0.28 mol/L) have been deployed to achieve dense Pd-alumina composite membranes in comparison with the Pd-stainless steel membranes (0.015 mol/L). The utilization of higher Pd solution concentrations for Pd ceramic composite membranes indicates that the raw material (especially Pd chemicals) cost is high. Further,

alumina substrate supports are always moderately expensive due to higher cost of alumina and sintering temperatures. Considering all these issues, the cost competitiveness of Pd ceramic composite membranes needs further research emphasis.

Several prominent fabrication techniques have been elaborated to achieve dense Pd composite membranes. Amongst all these techniques electroless plating (ELP) is particularly advantageous due to several promising features such as (a) simpler construction (b) ease to control process parameters (c) ability to achieve Pd deposition on non-conducting surfaces and low process cost. Thus, ELP appears to be the most relevant technique for the large scale cost effective fabrication of Pd composite membranes. Major limitations of the ELP process that require further research emphasis are slow metal deposition rates (1 – 1.5 µm) and lower process yield (10 – 25%).Thus to circumvent lower metal deposition rates (about 1 - 2 µm/h) and achieve better plating yield and efficiency, rate enhancement techniques are supplemented to the contemporary electroless plating.

Prominent rate enhancement techniques refer to stirring/agitation, vacuum, sonication [6] and surfactants [7]. Amongst the mentioned techniques, surfactant and sonication are two distinct rate enhancements to supplement Pd electroless plating for dense Pd membrane fabrication from the perspective of easy operatibilty, scalability and simplicity. The addition of a suitable surfactant (cationic) enables plating rate enhancement and achieves good surface finish due to the reduction of interfacial tension between the emanating gas bubbles and the membrane surface [7] whereas sonication promotes mass transport,

agglomeration of crystals and metal activation due to cavitation at the substrate-electrolyte surface [8].

Till date, there are no literatures available for coupled sonication and surfactant induced ELP (SSOEP) process for Pd ceramic composite membrane fabrication. In this regard, the efficacy of SSOEP process is highly relevant from the context of process operability, simplicity and scale up. Further, as major emphasis in the mentioned literatures is focused towards achieving dense Pd composite membrane, details with respect to optimal combinatorial plating characteristics have been only superficially mentioned in few prior articles. Given the fact that ceramics are non-conducting surfaces and plating will be more challenging and difficult on such surfaces, it would be an interesting research problem to investigate upon the role of optimal palladium solution concentration for dense Pd ceramic composite membrane fabrication using SSOEP baths.

MATERIALS AND METHODS

The ceramic substrates were fabricated using kaolin (40 wt%), feldspar (15 wt%), quartz (15 wt%), sodium carbonate (10 wt%), pyrophyllite (10 wt%), boric acid (5 wt%)and sodium metasilicate (5 wt%) in laboratory. The circular ceramic substrates were fabricated by the dry compaction method, details of which are discussed elsewhere. The ceramic substrates possesed a diameter of 36mm, thickness of 3.5mm, pore size in the range of 150-250nm and a porosity of 10-15% respectively.

The concentration of palladium solution is varied from 0.005 - 0.015 mol/L as shown in Table 1. The cationic surfactant used is cetyl trimethyl ammonium bromide (CTAB) at a solution concentration of 2 times its critical micelle concentration (CMC). Optimal cavitation strategy refers to sonication with an ultrasonic cleaning bath operated with degas mode of operation. Controlled (dropwise) addition of reducing agent (hydrazine hydrate) was used for all ELP baths. Thus for all experiments a coupled sonication and surfactant induced electroless plating (SSOEP) with dropwise reducing agent (DWR) and bulk surfactant (BS) addition i.e. SSOEP-DWR-BS baths were used for all the experiments. The optimality of SSOEP-DWR-BS baths with respect to other baths has been discussed elsewhere [9].

Parameters involved for evaluating the performance assessment of palladium plating include average trans-membrane flux $\bar{J}$, plating efficiency η , average plating rate ($\bar{r}_i$), percent pore densification PPD , conversion (x) and transport efficiency. Apart from transport efficiency all other calculations are similar to that described in details in our previous work [10].

Further transport efficiency is defined as the product of plating efficiency and conversion of the plating bath expressed as:

Transport efficiency = $\eta \times x$

RESULTS & DISCUSSIONS

Effect Of Pd Solution Concentration On The Combinatorial Pd Plating Characteristics For SSOEP Plating Baths

(A) PPD Profiles

Fig. 1 illustrates the time dependent variation of percent pore densification for variant Pd solution concentration. It has been evaluated that the time dependent PPD values varied from 19.5-96.3% (1.5-15h), 23.6- 99.7 % (1.5-10.5h) and 17.4-47.9% (1.5-6h) for a Pd solution concentration of 0.005, 0.01 and 0.015mol/L respectively. In general, as concentration increases, the PPD values should increase. But that is not always the case. The possible reason for reduction of PPD for a higher Pd solution concentration could be probably due to either insitu de-lamination of palladium film from the membrane surface or bulk precipitation [11]. Analyzing bath samples physically, the bulk precipitation of metal has been ruled out and insitu delamination is the most probable reason for the evaluated reduction in PPD. Therefore, there exists an optimal Pd solution concentration at which the desired process features could be achieved. From the evaluated PPD profiles, moderate Pd solution concentration of 0.01mol/L has been referred to be optimal in achieving higher PPD for the chosen total plating time.

(B) Plating Rate Profiles

Fig. 2 presents the effect of time dependent variation of average noble metal plating rate for a variation in Pd solution concentration. It has been evaluated that the plating rates varied from $1.19 – 0.66 \times 10^{-4}$(1.5-15h), $1.50 – 0.79 \times 10^{-4}$ (1.5-10.5h) and $1.60 – 0.81 \times 10^{-4}$ (1.5-6h) mol/m^2.s respectively for a Pd solution concentration of 0.005, 0.01 and 0.015mol/L. It can be observed that for a higher metal concentration of 0.015mol/L, the

plating rate were higher initially which reduced significantly at higher plating times. Such significant reduction in plating rate is an unfavorable feature of the SSOEP baths. In general, higher metal concentration corresponds to higher metal plating rate. But that might not always be the case. However, for a moderate Pd solution concentration of 0.01 mol/L, apart from the initial hour of plating, it was evaluated that the plating rates were higher during the entire plating period.

Hypothetically, higher concentration enhances plating rate. However, adhesion of the newly formed Pd film is dependent upon solid - liquid interface properties. While higher concentrations could enable higher metal deposition rates, they can significantly enhance metal delamination due to the shear stress induced by the faster evolution of gas bubbles [7]. In this regard, it should be noted that the usage of surfactant can only reduce but not eliminate shear stresses. Therefore, an optimal Pd solution concentration exists that provides highest combinations of plating rates and PPD.

(C) Efficiency Profiles

Fig. 3(a) and (b) illustrates the effect of Pd solution concentration on the time dependent variation of plating and transport efficiency for SSOEP baths. It can be observed that the plating efficiency varied from 81.6 -61% (1.5-15h), 95.9 - 60.6% (1.5-10.5h), 95.6-57.8% (1.5-6h) and the transport efficiency varied from 32.9 -18.1% (1.5-15h), 41.3-21.7% (1.5-10.5h), and 44-22.3% (1.5-6h) respectively for a Pd solution concentration of 0.005, 0.01 and 0.015mol/L. Higher transport efficiency could be achieved from two perspectives: In the first case, the plating efficiency could be high and bath conversions could be

moderate. In the second case, bath conversions could be high and plating efficiency could be low. Among these, the first case is desired and the second case is undesired. As illustrated in Fig. 3, for the SSOEP baths, higher Pd solution concentration (0.015mol/L) enabled the achievement of highest combinations of plating and transport efficiency during initial plating time. However, as time progressed a sharp decline in both the parameters illustrates incompatibility of the chosen higher metal concentration to achieve the desired process parameters in terms of PPD and plating rates. Thus, 0.01mol/L Pd solution concentration can be concluded to provide optimal combinations of process and membrane characteristics.

Literature Comparison

In a U.S. Patent by Collins and Way [1], the authors fabricated dense Pd tubular ceramic composite membranes by CEP process using a Pd solution concentration of 0.03 mol/L to achieve 10 – 20 μm metal film thickness. In another U.S. patent by Rhoda [2], the author fabricated dense Pd ceramic composite membranes by CEP process used a Pd solution concentration of 0.028 – 0.056 mol/L with asymmetric addition of dimethyl hydrazine (concentration of 0.05 – 0.45 g/L) reducing agent.

Further Ilias et al. [3] disclosed details with respect to CEP to achieve dense Pd ceramic membranes. For an alumina support pore size of 150 nm, the authors used a Pd solution concentration of 0.03 mol/L to achieve a dense metal film thickness of 12 μm. In similar context Zhang et al. [4] reported CEP supplemented with SDS anionic surfactant to be effective to achieve Pd composite membranes. On a α- alumina support of 270-280 nm

average pore size , the authors used a Pd solution concentration of 0.189 mol/L to achieve a dense Pd metal film thickness of 2 μm after a total plating time of 8 – 12 h.

Thus, this work clearly indicated that by modifying the plating process from CEP to SSOEP, many times lower palladium solution concentration could suffice for the fabrication of dense palladium ceramic composite membranes.

Lack of performance characteristics during composite membrane fabrication research is indicative to the fact that combinatorial plating characteristics has not been studied in details and this work elaborates on the same. One recent literature from our research group by Pujari et al. [12] elaborates on combinatorial plating characteristics of palladium on PSS supports. Their work reported a dense Pd membrane for SSOEP baths with a plating rate of 4.38×10^{-5} mol/m^2.s for a palladium solution concentration of 0.005mol/L and a surfactant concentration of 2 CMC. The plating rate in the present work is 7.9×10^{-5}mol/m^2.s for a palladium solution concentration of 0.01 mol/L and a surfactant concentration of 2 CMC. In the present work a similar surfactant and palladium concentration delivered a plating rate of 6.6×10^{-5}mol/m^2.s but with a PPD of 96.3%.

Thus it could be inferred that ceramic supports could deliver similar or higher plating rates than PSS supports for similar Pd precursor concentration but at the cost of higher plating time. In other words if similar plating time is to be used for both the supports that

the concentration of palladium ought to be doubled for ceramic supports as compared to PSS supports.

Membrane Characterization

(A) XRD Analysis

The XRD pattern for dense Pd ceramic membrane fabricated by coupled sonication and surfactant induced electroless plating using a palladium solution concentration of 0.01 mol/L are presented in Fig. 4. Phases of the diffraction profiles were analyzed using the ICDD-JCPDS database. It was analyzed that metallic Pd peaks appeared at diffraction angle 2θ= 40.1°, 46.6°, 68.1° , 82.1° and 86.6°due to the diffraction of (111), (200), (220), (311) and (222) plane [Pdf No 00-005-0681].The peaks clearly confirmed the presence of uniform palladium deposition after 10.5h of plating during coupled sonication and surfactant based electroless plating.

(B) FESEM Analysis

FESEM surface and cross sectional micrograph of Pd-ceramic composite membrane fabricated with SSOEP baths are shown in Fig. 5. Further Fig. 5(a) clearly indicates that the agitation caused by ultrasonic waves in a sonicator baths led to uniform dispersion throughout the substrate surface. Further Fig. 5(b) depicts the FESEM cross sectional image of the dense palladium membrane fabricated with a palladium solution concentration of 0.01 mol/L. It was observed that the palladium dense metal film thickness varied in the range of 10-12µm respectively.

Tradeoffs

Fig. 6 illustrates the tradeoffs associated with PPD/Plating rate Vs. PPD for SSOEP baths with variant Pd solution concentrations (0.005 – 0.015mol/L). Hypothetically, PPD/Plating rate is a measure to quantify the dominance of pore densification or layering. Higher value of PPD/Plating rate for similar time of plating signifies that the plating favors better PPD and lower metal layering. It has been evaluated that for a particular plating time (say 6h), both PPD and PPD/Plating rate values were higher for a Pd solution concentration of 0.01mol/L. Thus 0.01mol/L Pd solution concentration is the optimal concentration for the mentioned bath composition on porous ceramic supports. Thus, the results disclosed in this work indicate the potential of the SSOEP process to effectively achieve dense Pd ceramic composite membranes with lower palladium solution concentration.

CONCLUSIONS

The work is directed to a scalable low cost method for rapidly fabricating dense Pd membranes on porous kaolin based ceramic substrates. The critical aspects/findings of this work are:

(a) It utilizes a moderately low Pd solution concentration which refers to 0.01 mol/L.

(b) A unique optimal combination of sonication and surfactant as a potential rate enhancement to Pd electroless plating is the most sublime feature of the article.

(c) For the Pd ceramic composite membrane, SSOEP process involves best process characteristics that provides higher plating efficiencies (95.9%), higher transport

efficiency (41.3%), higher plating rates (1.5×10^{-4} mol/m^2.s), minimal Pd solution concentration (0.01 mol/L), lower surfactant concentration (2 CMC), minimal total plating time (10.5 h) and maximum pore densification (99.7%).

(d) The method is simple, fast, easy to use and scalable for large scale fabrication of Pd ceramic composite membranes.

(e) It provides good quality noble metal deposition (higher combinations of plating rate and PPD rate) on non-conducting porous surfaces.

ACKNOWLEDGEMENTS

This work is partially supported by a grant from the DST New Delhi. Any opinions, findings and conclusions expressed in this paper are those of the authors and do not necessarily reflect the views of DST, New Delhi.

REFERENCES

[1] Collins, J. P; Douglas Way J.; Hydrogen selective membrane. U.S. Patent No. 5652020 A.

[2] Rhoda Richard, N; Palladium deposition, U.S. Patent No. 3274022 A.

[3] Ilias, S.; Su, N.; Udo-Aka, U.I.; King, F.G.; Application of Electroless Deposited Thin-Film Palladium Composite Membrane in Hydrogen. *Separation Science and Technology* **1997**, *32*, 487-504.

[4] Zhang, K.; Huiyan, G. ; Zebao, R.; Yuesheng, L.; Yongdan, L.; Preparation of Thin Palladium Composite Membranes and Application to Hydrogen/Nitrogen Separation. *Chinese Journal of Chemical Engineering* **2007**, *15*, 643—647.

[5] Islam, M.A.; Ilias, S.; Characterization of Pd-Composite Membrane Fabricated by Surfactant Induced Electroless Plating (SIEP): Effect of Grain Size on Hydrogen Permeability, *Separation Science and Technology* **2010**, *45*, 1886-1893.

[6] Kathirgamanathan, P.; Ultrasound-assisted electroless deposition of copper onto and into microporous membranes for electromagnetic shielding. *Polymer* **1994**, *35*, 430–432.

[7] Chen, B.H.; Hong, L.; Ma, Y.H.; Ko, T.M.; Effects of surfactants in an electroless nickel – plating bath on the properties of Ni–P alloy deposits. *Industrial & Engineering Chemistry Research* **2002**, *41*, 2668–2678

[8] Mizukoshi, Y.; Takagi, E.; Okuno, H.; Oshima, R.; Maeda, Y.; Nagata, Y.; Preparation of platinum nanoparticles by sonochemical reduction of the Pt(IV) ions: role of surfactants. *Ultrasonic Sonochemistry* **2001**, *8*, 1-6.

[9] Agarwal, A.; Pujari, M.; Uppaluri, R.; Verma, A.; Efficacy of reducing agent and surfactant contacting pattern on the performance characteristics of nickel electroless plating baths coupled with and without ultrasound. *Ultrasonic Sonochemistry* **2014**, *21*, 1382–1391.

[10] Agarwal, A.; Pujari, M.; Uppaluri, R.; Verma, A.;Optimal Electroless Plating Rate Enhancement Techniques for the Fabrication of Low Cost Dense Nickel/Ceramic Composite Membranes. *Ceramics International* **2014**, *40*, 691–697.

[11] Nwosu, N.; Davidson, A.; Hindle, C.; Barker,M.; On the Influence of Surfactant Incorporation during Electroless Nickel Plating. *Industrial & Engineering Chemistry Research* **2012**, *51*(16), 5635 -5644.

[12] Pujari, M.; Agarwal, A.; Uppaluri, R.; Verma, A.;Effect of Surfactant Concentration and Loading Ratio on the Electroless Plating Characteristics of Dense Pd Composite Membranes, *Industrial & Engineering Chemistry Research* **2014**, *53*, 3105-3115.

Table 1. Composition of conventional palladium electroless plating baths.

S. No.	Component	Amount (mol/L)	Amount (mol/L)	Amount (mol/L)
1.	Palladium Chloride	0.005	0.01	0.015
2.	Hydrazine Hydrate (1M)	0.02	0.02	0.02
3.	Ethylene di-amine tetra acetic acid	0.04	0.08	0.12
4.	Liquor Ammonia (25%)	0.001	0.002	0.004

Figure 1. Time dependent variation of percent pore densification with variation in Pd solution concentration (0.005-0.015 mol/L) for SSOEP baths.

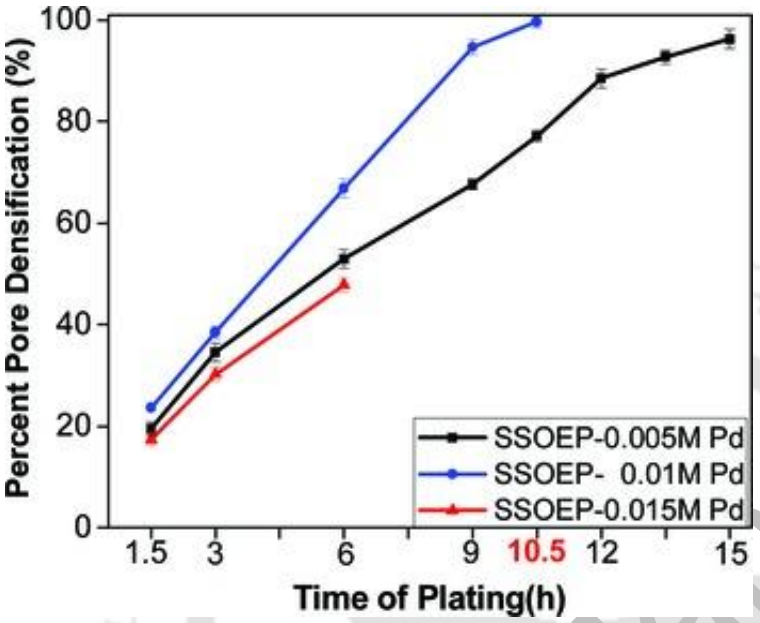

Figure 2. Variation of noble metal average plating rate for a variation in Pd solution concentration (0.005-0.015 mol/L) of SSOEP baths

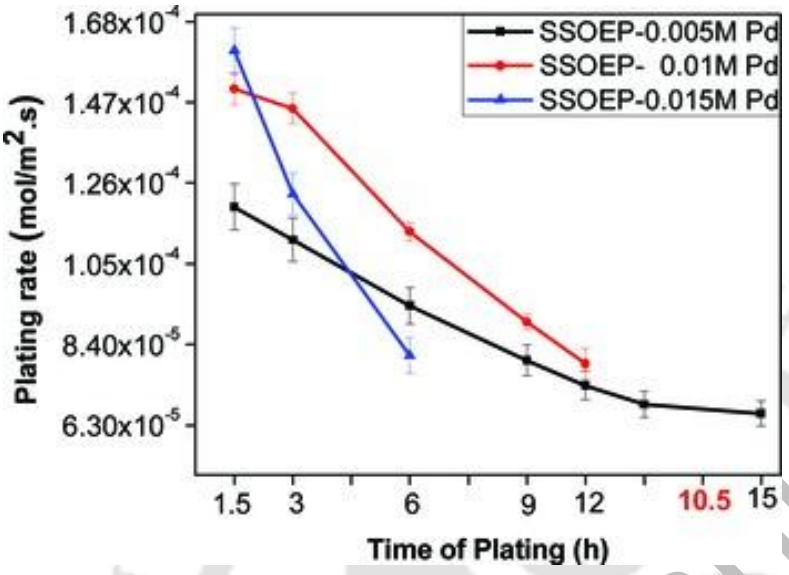

Figure 3(a) and (b). Time dependent variation of plating and transport efficiency for SSOEP baths for a variation in palladium solution concentration (0.005-0.015 mol/L)

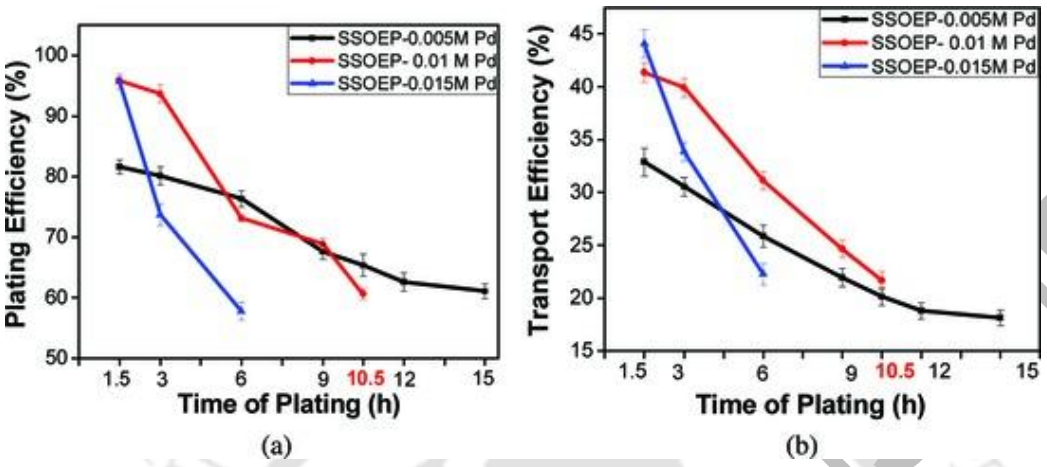

Figure 4. XRD profile of Pd-ceramic composite membrane fabricated using SSOEP baths

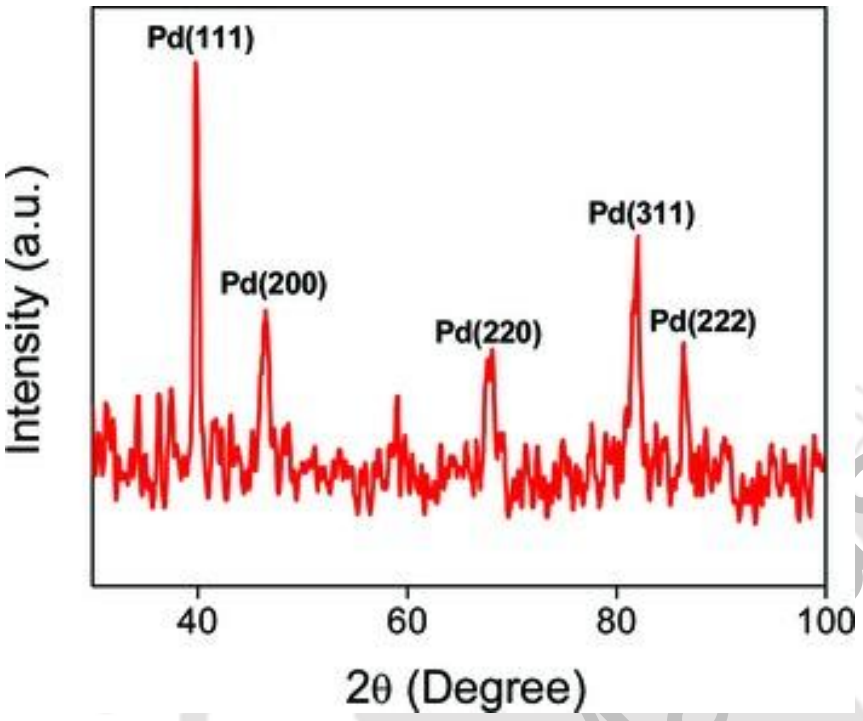

Figure 5. FESEM (a) surface (b) cross-sectional micrograph of Pd-ceramic composite membrane fabricated using SSOEP baths

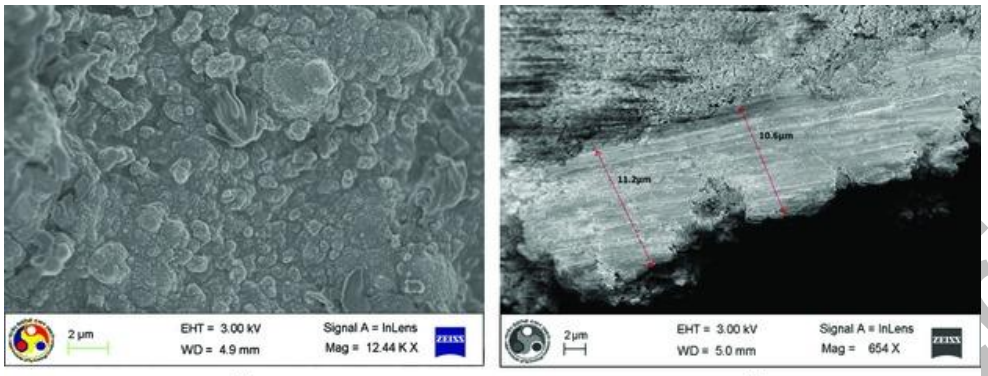

(a) (b)

Figure 6. PPD/Plating rate Vs. PPD tradeoffs for SSOEP baths at various Pd solution concentrations (0.005-0.015 mol/L)